

---

---

QUANTUM CRITICALITY IN THE  
HEAVY-FERMION SUPERCONDUCTOR  
CeCoIn<sub>5</sub>

---

---

by

Johnpierre Paglione

A thesis submitted in conformity with the requirements  
for the degree of Doctor of Philosophy  
Graduate Department of Physics  
University of Toronto

Copyright © 2005 by Johnpierre Paglione

---

---

## ABSTRACT

---

---

Quantum Criticality in the Heavy-Fermion Superconductor CeCoIn<sub>5</sub>

Johnpierre Paglione  
Doctor of Philosophy  
Graduate Department of Physics  
University of Toronto  
2005

The study of quantum phase transitions has received a large amount of attention owing to the fact that a range of anomalous properties appear to be linked to the occurrence of quantum fluctuations. CeCoIn<sub>5</sub> is a recently discovered heavy-fermion metal with an unconventional superconducting state below  $T_c = 2.3$  K and a range of properties unexplained by the conventional Fermi liquid theory of metals. As a member of the CeMIn<sub>5</sub> family (where M = Co, Ir or Rh), the anomalous transport, magnetic and thermodynamics properties of CeCoIn<sub>5</sub> are thought to arise from an antiferromagnetic instability which has yet to be identified.

This study reports measurements of heat and charge transport in CeCoIn<sub>5</sub>, as a function of temperature  $T$ , magnetic field  $H$  and orientation of current  $J$  with respect to the crystal axes, which have unearthed a host of incredible properties. These include the identification of a field-tuned quantum critical point (QCP) which coincides with the upper critical field of the superconducting state at  $H_{c2} = 5$  T. As evidenced by divergences of the  $T^2$  coefficients of both electrical and thermal resistivities in the field-induced Fermi liquid state, the nature of this QCP is further elucidated by the observed relation between  $\Delta H/T$  scaling and an anomalous  $T^{2/3}$  dependence of resistivity in the

high-field non-Fermi liquid regime of  $J \perp [001]$  transport. Additional measurements of antiferromagnetic CeRhIn<sub>5</sub> were also performed in order to shed light on the similarities and differences throughout this series of compounds.

As a function of current orientation, qualitatively different behaviour is observed both in temperature and field dependences of transport. Whereas the temperature dependence of resistivity evolves with field for  $J \perp [001]$  transport, it remains linear in temperature for the  $J \parallel [001]$  orientation, as observed in both the heat and charge channels. At the critical field, a test of the Wiedemann-Franz law in the  $T \rightarrow 0$  limit has revealed a stunning anisotropy: the Wiedemann-Franz law is obeyed by  $J \perp [001]$  currents, whereas a 27% violation occurs for  $J \parallel [001]$  currents. These observations suggest the existence of two distinct QCPs which influence correspondingly different conduction bands, highlighting the multi-band nature of quantum criticality in CeCoIn<sub>5</sub>.

---

---

## STATEMENT OF ORIGINALITY

---

---

The study of heavy-fermion materials has a long history as a popular subject of condensed matter physics which dates back almost thirty years. Although first reported in 1979, the presence of unconventional superconductivity in heavy-fermion systems has recently found a resurgence of interest owing to the record-breaking transition temperatures discovered in the high-temperature cuprate superconductors in 1986. Since then, the as-yet elusive physics of the cuprates has been suggested to share common ground with that of the heavy-fermion superconductors, since both systems exhibit magnetism closely tied to their superconducting states.

In this context, much effort has been spent on studying the effects of magnetic phase transitions which occur at absolute zero temperature, called quantum phase transitions, since they are often accompanied by the appearance of superconductivity. This thesis is aimed at studying such phenomena in CeMIn<sub>5</sub>, a system of materials which were discovered only recently in 2000, yet have received a stunning amount of attention owing to a plethora of unconventional normal and superconducting state properties. Although a number of publications have reported a wide range of experimental results on this system, detailed characterizations of heat and charge transport at high magnetic fields and low temperatures have not been reported. Thus the motivation behind the current study is to shed light on the non-Fermi liquid and quantum critical properties of the 115 system by providing a detailed account of the anomalous transport behaviour, thus supplying an important contribution to the study of these subjects in the context of this and other systems.

In summary, this thesis presents a comprehensive study of the unconventional physics of the 115 system, in the forms of superconductivity, magnetism and quantum criticality as probed through low temperature transport properties. In the course of this study, a number of unexpected and fascinating observations have been made which find no counterpart in existing literature. These include:

1. a strong effect of spin fluctuations on electronic thermal transport, as demonstrated in CeRhIn<sub>5</sub>;
2. a field-induced quantum phase transition in CeCoIn<sub>5</sub> which *exactly* coincides with the upper critical field for superconductivity;
3. both verification *and* violation of the Wiedemann-Franz law in CeCoIn<sub>5</sub> as a function of current orientation at the quantum critical point - a truly new and eminent discovery.

None of these observations have been studied in any detail previous to this work, with the latter two unearthing completely new phenomena which find no explanation within the current theoretical framework of quantum criticality. As a result of these observations, we were the first to report the existence of a field-induced quantum phase transition in CeCoIn<sub>5</sub>, distinguishing it from the *zero-field* quantum criticality often cited throughout the current set of publications. The last item, which is the most significant result of this study, highlights the first evidence of a “violation anisotropy” of the long-standing law of Wiedemann and Franz. This observation finds no similarity to any previous studies of quantum critical systems or any other material in general.

All experimental aspects of this study were performed by myself, primarily with the aid of Makariy Tanatar but also in conjunction of all other members of the research group of Louis Taillefer. Experiments were performed using samples provided by a collaboration with Cedomir Petrovic (Brookhaven National Laboratory) and Paul Canfield (Ames Laboratory). The various projects presented in and related to this thesis have been summarized in a number of manuscripts which have been either submitted or accepted for publication. These are listed:

- ”Field-induced quantum critical point in CeCoIn<sub>5</sub>,” Johnpierre Paglione, M.A. Tanatar, D.G. Hawthorn, Etienne Boaknin, R.W. Hill, F. Ronning, M. Sutherland, Louis Taillefer, C. Petrovic, P. C. Canfield. Phys. Rev. Lett. **91**, 246405 (2003).
- ”Field-induced quantum critical point in CeCoIn<sub>5</sub>,” Johnpierre Paglione, M.A. Tanatar, D.G. Hawthorn, Etienne Boaknin, R.W. Hill, F. Ronning, M. Sutherland, Louis Taillefer, C. Petrovic, P. C. Canfield. Physica C, **408-410**, 705 (2004).

- "Heat transport as a probe of electron scattering by spin fluctuations: the case of antiferromagnetic CeRhIn<sub>5</sub>," Johnpierre Paglione, M.A. Tanatar, D.G. Hawthorn, R.W. Hill, F. Ronning, M. Sutherland, Louis Taillefer, C. Petrovic, P.C. Canfield. Submitted to Phys. Rev. Lett. (cond-mat/0404269)
- " $T^{2/3}$  resistivity and the field-tuned quantum critical point in CeCoIn<sub>5</sub>," Johnpierre Paglione, M.A. Tanatar, D.G. Hawthorn, E. Boaknin, R.W. Hill, F. Ronning, M. Sutherland, Louis Taillefer, C. Petrovic, P.C. Canfield. Submitted to Phys. Rev. Lett. (cond-mat/0405157)
- "Unpaired electrons in the superconducting state of heavy-fermion CeCoIn<sub>5</sub>," M.A. Tanatar, Johnpierre Paglione, D.G. Hawthorn, E. Boaknin, R.W. Hill, F. Ronning, M. Sutherland, Louis Taillefer, C. Petrovic, P.C. Canfield. (unpublished)

All of these papers are a direct result of this study and were written primarily by myself, Makariy Tanatar and Louis Taillefer, together with the participation of all other co-authors.

---

---

## ACKNOWLEDGEMENTS

---

---

After spending many days (and more nights) compiling this work, there are numerous individuals that deserve an acknowledgement for their contribution to its completion.

First and foremost, I would like to thank my supervisor, Louis Taillefer, for providing me with an incredible academic experience that finds no counterpart in any previous endeavours I have followed. His leadership and guidance throughout my graduate career remain unparalleled, and the wealth of experience and knowledge that I have absorbed will aid me in all future directions. Also, my Master's supervisor John Perz provided an excellent welcome to my graduate career.

I also would like to acknowledge the continuously evolving research group of Prof. Taillefer that I have been a member of for the past five years. With a beginning in ultrasound research, I am grateful for the excellent technical guidance and teachings of Andrew MacFarlane, Cyril Proust and Christian Lupien, who helped launch my efforts at becoming a low temperature experimentalist. Also, the continual aid (and distractions) of Etienne Boaknin, Dave Hawthorn and Mike Sutherland have elevated the joys of graduate life toward the undergraduate level of fun. (I would especially like to thank Etienne for pulling us back to the dock...) Finally, without the professional and technical expertise of Rob Hill, Shiyan Li, Filip Ronning and Makariy Tanatar, I would not have been able to complete this project with such quality and quantity. I especially acknowledge Makariy for continuously “leak-checking” both our experimental equipment and our ideas! He is certainly the main contributor to this project.

There are a host of professors, post-docs and students which have greatly enhanced my research experience throughout the years, most notably in the context of the Canadian Institute for Advanced Research which has provided numerous opportunities for interaction and collaboration. At the University of Toronto, I have enjoyed many fruitful discussions with Profs. Allan Griffin, Hae-Young Kee, Yong-Baek Kim, Mike Walker and John Wei, along with many laughs from Prof. Bryan Statt, who will be missed by many.

In addition, I would like to thank Mike Smith for putting up with endless questions, and our collaborators Cedomir Petrovic and Paul Canfield for supplying the most essential component of this project - the amazingly pure crystals!

I would like to acknowledge the National Sciences and Engineering Research Council of Canada (NSERC), the Walter Sumner Foundation, the Ontario Graduate Scholarship Program and the University of Toronto for providing the financial means to proceed through graduate school.

Finally, I would like to thank my many friends in both physics (Etienne, Mike, Dave, Christian, Zahra, Peter, Barry, Amit, Jessica, Yasser, Caroline, Patrick, The Grads, Kalen, Claire) and other vices (Kites, Tone-Dog, Agostino, Giovan', Carla, MacGregs29, CK, Cakes, RJ, Juan Valdez, Scobie, DoubleTrouble, Mar'anator, the Rock, Randall-Pink, Gord-o, and many more...including Rolf) for the fun and games. Thanks to my brother and sister for putting up with my endless plight, and to "coffee girl" for distracting me. And last, but most of all, thanks to my parents for giving me the means and the will, and showing me what is most important in life.

*shine on you crazy diamond*

---

---

## CONTENTS

---

---

ABSTRACT	ii
STATEMENT OF ORIGINALITY	iv
ACKNOWLEDGMENTS	vii
<b>1 INTRODUCTION</b>	<b>1</b>
1.1 Heavy-Fermion Materials . . . . .	3
1.1.1 Heavy Fermi Liquids . . . . .	3
1.1.2 Superconductivity . . . . .	5
1.1.3 Non-Fermi Liquid Behaviour . . . . .	6
1.2 Quantum Phase Transitions . . . . .	8
1.2.1 Introduction . . . . .	8
1.2.2 Theories . . . . .	11
<b>2 BACKGROUND</b>	<b>16</b>
2.1 Transport Theory . . . . .	16
2.1.1 Electrical Conductivity . . . . .	16
2.1.2 Thermal Conductivity . . . . .	19
2.2 Comparing Heat and Charge Transport . . . . .	21
2.2.1 $T = 0$ : Wiedemann-Franz Law . . . . .	21
2.2.2 $T > 0$ : Inelastic Scattering . . . . .	23
2.2.3 Electron-Electron Scattering . . . . .	25
2.3 QCP Theory Predictions . . . . .	26
2.3.1 Charge Transport . . . . .	27
2.3.2 Wiedemann-Franz Law . . . . .	28

<b>3 CEMIN<sub>5</sub> FAMILY</b>	<b>29</b>
3.1 Crystal Structure . . . . .	30
3.2 Ce(Co,Ir,Rh)In <sub>5</sub> Alloys . . . . .	31
3.3 Electronic Structure . . . . .	32
3.4 Thermodynamic Properties . . . . .	35
3.4.1 Upper Critical Fields . . . . .	35
3.4.2 Specific Heat . . . . .	36
3.5 Magnetic Properties . . . . .	37
3.5.1 Susceptibility . . . . .	38
3.5.2 Spin Resonance and Neutron Scattering . . . . .	39
3.6 Transport Properties . . . . .	40
3.6.1 Resistivity . . . . .	40
3.6.2 Thermal Conductivity . . . . .	41
<b>4 EXPERIMENTAL TECHNIQUES</b>	<b>43</b>
4.1 Sample Preparation . . . . .	43
4.1.1 Etching and Cleaving . . . . .	43
4.1.2 Contact Methods . . . . .	45
4.2 Cryogenic Techniques . . . . .	47
4.2.1 <sup>4</sup> He and <sup>3</sup> He Refrigeration . . . . .	48
4.2.2 Dilution Refrigeration . . . . .	50
4.2.3 Thermometry . . . . .	52
4.3 Transport Measurements . . . . .	54
4.3.1 Electrical Resistivity . . . . .	54
4.3.2 Thermal Conductivity . . . . .	59
<b>5 CERHIN<sub>5</sub>: PROBING SPIN FLUCTUATIONS</b>	<b>65</b>
5.1 Thermal Conductivity . . . . .	65
5.2 Transport and Spin Disorder . . . . .	67
5.3 Comparing Heat and Charge Transport . . . . .	68
5.3.1 Vertical Scattering . . . . .	69
5.3.2 Lorenz Ratio and e-e scattering . . . . .	70
5.3.3 Fluctuation Regime . . . . .	71
5.4 Conclusions . . . . .	72

<b>6 CECoIn<sub>5</sub>: FIELD-TUNED QUANTUM CRITICALITY</b>	<b>74</b>
6.1 Magnetoresistance . . . . .	75
6.1.1 Temperature Dependence . . . . .	75
6.1.2 Field Dependence . . . . .	77
6.2 Field-Induced Fermi Liquid State . . . . .	79
6.2.1 Divergent Scattering at $H^* = H_{c2}$ . . . . .	79
6.3 $H$ - $T$ Phase Diagram ( $J \perp [001]$ ) . . . . .	81
6.3.1 $H_{c2}$ Transition and MR Crossover . . . . .	81
6.3.2 Power Law Evolution . . . . .	83
6.3.3 $\Delta H/T$ Scaling . . . . .	85
6.4 Nature of the field-induced QCP . . . . .	88
6.4.1 Thermal Transport in the FL Regime . . . . .	88
6.4.2 Wiedemann-Franz Law . . . . .	90
6.4.3 Kadowaki-Woods Ratio . . . . .	97
6.5 Conclusions . . . . .	99
<b>7 CECoIn<sub>5</sub>: MULTI-BAND EFFECTS</b>	<b>101</b>
7.1 Inter-Plane Charge Transport . . . . .	102
7.1.1 Residual Resistivity . . . . .	102
7.1.2 Magnetoresistance . . . . .	103
7.1.3 Two-Component Conductivity . . . . .	106
7.2 Inter-Plane Thermal Transport . . . . .	110
7.2.1 Wiedemann-Franz Law . . . . .	112
7.3 Discussion . . . . .	116
7.3.1 Scattering Anisotropy . . . . .	117
7.3.2 Spin fluctuations . . . . .	118
7.3.3 WF Law Violation . . . . .	120
7.3.4 Multi-Band Quantum Criticality . . . . .	123
7.4 Conclusions . . . . .	123
<b>8 CONCLUSIONS</b>	<b>126</b>
<b>A CECoIn<sub>5</sub>: ADDITIONAL ANALYSIS</b>	<b>129</b>
A.1 Orbital MR: $\omega_c\tau > 1$ Limit . . . . .	129
A.2 Breakdown of $\Delta H/T$ Scaling . . . . .	130

A.3	Transport in $\text{Ce}_{1-x}\text{La}_x\text{CoIn}_5$	131
A.3.1	Field-Induced QCP in $\text{Ce}_{0.90}\text{La}_{0.10}\text{CoIn}_5$	131
A.3.2	First-Order Phase Transition	132
A.3.3	La-doping Phase Diagram	133
<b>B</b>	<b>CERHIN<sub>5</sub>: ADDITIONAL ANALYSIS</b>	<b>136</b>
B.1	Low Temperature Magnetoresistance	136
B.2	Ambient-Pressure Superconductivity	137
<b>C</b>	<b>THERMAL CONDUCTIVITY: CONSIDERATIONS</b>	<b>140</b>
C.1	Phonon Conductivity	140
C.2	Contact Considerations	143
C.2.1	Test Experiment	143
C.2.2	Coupled Resistor Model	144
C.2.3	Contact Effects in $\text{CeCoIn}_5$	147
	<b>BIBLIOGRAPHY</b>	<b>149</b>

---

---

## FIGURES AND TABLES

---

---

### FIGURES

2.1	Lorenz ratio in vanadium . . . . .	24
3.1	$P$ - $T$ phase diagram of CeIn <sub>3</sub> . . . . .	30
3.2	Crystal structure of CeMIn <sub>5</sub> . . . . .	31
3.3	Ce(Co,Ir,Rh)In <sub>5</sub> alloy phase diagram . . . . .	32
3.4	Fermi surfaces of CeCoIn <sub>5</sub> . . . . .	33
3.5	Field dependence of $m^*$ in CeCoIn <sub>5</sub> . . . . .	34
3.6	$H$ - $T$ critical field phase diagrams of CeCoIn <sub>5</sub> . . . . .	35
3.7	Specific heat of CeMIn <sub>5</sub> . . . . .	36
3.8	Evolution of $\gamma_0$ with pressure in CeRhIn <sub>5</sub> . . . . .	37
3.9	Susceptibility and magnetization in CeCoIn <sub>5</sub> . . . . .	38
3.10	Resistivity of CeMIn <sub>5</sub> . . . . .	40
4.1	CeCoIn <sub>5</sub> sample (photo) . . . . .	46
4.2	Copper block sample mount . . . . .	47
4.3	<sup>3</sup> He– <sup>4</sup> He phase diagram . . . . .	50
4.4	Schematic of <sup>3</sup> He/ <sup>4</sup> He dilution fridge . . . . .	51
4.5	Schematic of the thermal conductivity setup . . . . .	59
4.6	Schematic of heater and thermometer design . . . . .	61
4.7	Thermal conductivity of Ag wire . . . . .	64
5.1	Thermal conductivity of CeRhIn <sub>5</sub> . . . . .	66
5.2	Thermal and electrical resistivity of CeRhIn <sub>5</sub> . . . . .	68
5.3	Vertical scattering in CeRhIn <sub>5</sub> . . . . .	69
5.4	Temperature dependence of Lorenz ratio in CeRhIn <sub>5</sub> . . . . .	70
5.5	Power law fit of resistivity of CeRhIn <sub>5</sub> . . . . .	72

6.1	Resistivity of CeCoIn <sub>5</sub> up to 16 T.	75
6.2	Magnetoresistance of CeCoIn <sub>5</sub> .	76
6.3	Low temperature magnetoresistance of CeCoIn <sub>5</sub> .	77
6.4	Divergence of $T^2$ resistivity coefficient in CeCoIn <sub>5</sub> .	79
6.5	MR crossover in $H - T$ phase diagram of CeCoIn <sub>5</sub> ( $J \perp [001]$ ).	82
6.6	Resistivity power law evolution in CeCoIn <sub>5</sub> ( $J \perp [001]$ ).	83
6.7	Power law evolution in $H-T$ phase diagram of CeCoIn <sub>5</sub> ( $J \perp [001]$ ).	84
6.8	$\Delta H/T$ scaling analysis of resistivity in CeCoIn <sub>5</sub>	86
6.9	Normal state thermal conductivity of CeCoIn <sub>5</sub> .	89
6.10	Normal state Lorenz ratio of CeCoIn <sub>5</sub> .	91
6.11	Lorenz ratio comparison between CeCoIn <sub>5</sub> and CeRhIn <sub>5</sub> .	93
6.12	Vertical scattering component in CeCoIn <sub>5</sub> .	94
6.13	Field dependence of Lorenz ratio of CeCoIn <sub>5</sub> .	95
6.14	Kadowaki-Woods ratio in CeCoIn <sub>5</sub> .	98
7.1	Charge transport anisotropy of CeCoIn <sub>5</sub>	102
7.2	Magnetoresistance of CeCoIn <sub>5</sub> ( $J \parallel [001]$ )	104
7.3	Longitudinal and transverse MR of CeCoIn <sub>5</sub> ( $J \parallel [001]$ )	105
7.4	Two-component conductivity analysis ( $J \parallel [001]$ )	107
7.5	Effect of impurities on $T^2$ component of $J \parallel [001]$ transport	110
7.6	Inter-plane thermal transport of CeCoIn <sub>5</sub> ( $J \parallel [001]$ )	111
7.7	Field dependence of normal state thermal transport in CeCoIn <sub>5</sub>	112
7.8	Electrical and thermal resistivities of CeCoIn <sub>5</sub> at 5.3 T and 10 T ( $J \parallel [001]$ )	113
7.9	Lorenz ratio of CeCoIn <sub>5</sub> at 5.3 T and 10 T ( $J \parallel [001]$ )	114
7.10	Comparison of residual resistivities in CeCoIn <sub>5</sub> ( $J \parallel [001]$ )	115
7.11	Comparison of transport in CeCoIn <sub>5</sub> to CeNi <sub>2</sub> Ge <sub>2</sub>	119
A.1	Orbital magnetoresistance of CeCoIn <sub>5</sub> .	130
A.2	Effect of disorder on resistivity power law.	131
A.3	Field-induced Fermi liquid state in Ce <sub>0.90</sub> La <sub>0.10</sub> CoIn <sub>5</sub>	132
A.4	$H-T$ phase diagram of Ce <sub>0.90</sub> La <sub>0.10</sub> CoIn <sub>5</sub>	133
A.5	Effect of La doping on order of $H_{c2}$ transition in Ce <sub>1-x</sub> La <sub>x</sub> CoIn <sub>5</sub>	134
A.6	$H-T-x$ phase diagram of Ce <sub>1-x</sub> La <sub>x</sub> CoIn <sub>5</sub>	134
B.1	Resistivity of CeRhIn <sub>5</sub> in field	137

B.2	Resistivity field sweeps of CeRhIn <sub>5</sub>	138
B.3	Superconducting transition in CeRhIn <sub>5</sub>	139
C.1	Phonon analysis of Ce <sub>0.98</sub> La <sub>0.02</sub> CoIn <sub>5</sub>	141
C.2	Phonon analysis of Ce <sub>0.90</sub> La <sub>0.10</sub> CoIn <sub>5</sub>	142
C.3	Contact resistance effects in YBa <sub>2</sub> Cu <sub>3</sub> O <sub>6.95</sub>	143
C.4	Coupled resistor model of low- <i>T</i> transport.	145
C.5	Effect of contact resistance on $\kappa$ measurements in CeCoIn <sub>5</sub>	148

## TABLES

3.1	Lattice parameters of CeMIn <sub>5</sub>	31
4.1	Resistance thermometer properties	53

## INTRODUCTION

---

---

Dating back thousands of years to the discoveries of gold and copper, the study of metals is one of the oldest disciplines of modern civilization. In the past 100 years, the discovery of a plethora of fascinating physical phenomena in solid-state materials has led not only to practical and technological endeavours of obvious importance, but also to a physical understanding of some of the most fundamental facets of our world.

An empirical law discovered in 1853 by Wiedemann and Franz, which stated that the ratio of electrical to thermal conductivities is the same in all metals [1], was one of the first quantitative reports to question the inner nature of metallic materials. This was proposed well before any significant understanding of conduction was known, but would nevertheless lay the foundation of our current understanding of metals. One of the first attempts to directly explain the passage of electrical currents in metals was made by Weber in 1875. But it was the subsequent discovery of the electron by J. J. Thomson in 1897 that provided the path to not only our current understanding of metals, but also to the current interpretations of the fundamental structure of all matter.

Soon after, much effort went into explaining the behaviour of electrons in a solid, with the first successful theoretical explanation of the Wiedemann-Franz law by Drude in 1900, in terms of a classical gas of electrons. The advent of quantum mechanics played a crucial role in advancing this interpretation, leading to corrections of transport theory by Sommerfeld and Bloch in 1928. At this point, the general properties of metals could be understood in terms of a set of quantum mechanical particles which obey Fermi statistics, but do not experience any interactions beyond the classical ideal gas model. Although quite successful, it was not obvious how the presence of presumably strong interactions could be neglected - *i.e.* how do  $\sim 10^{23}$  negatively-charged particles sharing the confined space of a crystal lattice of positively-charged ions behave as an essentially non-interacting gas of particles? This remained a mystery for some time.

One of the most amazing discoveries of the 20<sup>th</sup> century was that of superconductivity

in mercury by Kamerlingh-Onnes in 1911. This phenomenon is an incredible macroscopic example of quantum mechanics which would be fully explained only decades later by Bardeen, Cooper and Schrieffer with the infamous BCS theory of superconductivity [2]. One of the crucial tenets of BCS theory, which explains a ground state drastically different from that of an ideal gas, involves a phenomenological theory put forth by L. D. Landau in 1957 called Fermi liquid (FL) theory [3]. This theory presented a new way of thinking about the strong interactions present in a system,<sup>1</sup> introducing the notion of “quasiparticles” and elementary excitations as the correct description of the underlying strongly interacting system of particles.

The conventional picture of metals is now based on FL theory (see *e.g.* Ref. [4]), which in essence explains why the low energy physics of interacting electron systems can be treated as that of essentially free electrons. The quite amazing result of this theory was that the charge carriers in a metal, now considered as quasiparticles, can be treated as *non-interacting* particles with the effects of interaction “buried” within renormalized quantities. For instance, the density of quasiparticle states (and hence the specific heat) has the same form as for an ideal gas, but with an *effective mass*  $m^*$  replacing the bare electron mass. Furthermore, Landau’s approach applies not only to electrons in a metal, but includes more complex excitations such as phonons.<sup>2</sup>

With such a successful treatment of the complex interactions in a conductive metal, it is no wonder that intense effort has been directed at trying to understand why and how FL theory fails. There have been great successes in describing the reason for this failure in some cases, such as in the quantum hall effect (see *e.g.* Ref. [6]) or the Luttinger liquid (see *e.g.* Ref. [7]), but numerous examples [7] of so-called “non-Fermi liquid” (NFL) systems remain. The most well-known example to date is that of the high-temperature cuprate superconductors discovered in 1986 by Bednorz and Müller [8]. These materials, which fail to be explained by BCS theory, continue to puzzle theorists and experimentalists alike with astonishingly high transition temperatures and peculiar NFL behaviour.

This study focuses on a recently discovered series of compounds commonly referred to as the “115” family. With the general formula  $\text{CeMIn}_5$ , where M=Co, Ir or Rh, the ground state of these systems can be fine-tuned between magnetic order, superconductivity and a coexistence of the two. As a result, a plethora of anomalous properties

---

<sup>1</sup>Landau’s original motivation was in fact to explain the properties of liquid  ${}^3\text{He}$ .

<sup>2</sup>See *e.g.* Ref. [5] for a description of how the notion of quasiparticles can be used to describe crystal lattice excitations as “phonon” particles.

are found throughout this series due to another strong deviation from FL theory, the quantum phase transition. As will be discussed, these compounds present an opportune chance to systematically study the NFL behaviour both theoretically and experimentally, providing the hope of explaining yet another general set of strongly correlated electron systems that fail to be understood within the current set of conventional condensed matter physics principles.

The remainder of this chapter will review the general properties of the class of systems to which the 115 series belongs, and will introduce the concept of a quantum phase transition. A review of both conventional transport theory and some of the recent theoretical work attempting to understand NFL behaviour is provided in Chapter 2, followed by a review of the current set of theoretical ideas and experimental studies pertaining to the 115's in particular, found in Chapter 3. After an explanation of the experimental techniques used in this study is provided in Chapter 4, we will present experimental results on studies of both CeRhIn<sub>5</sub> (Chapter 5) and CeCoIn<sub>5</sub> (Chapters 6-7), with pertinent discussions and conclusions provided in each chapter and in the final section.

## 1.1 Heavy-Fermion Materials

Twenty-five years ago, Landau's quasiparticle description of interacting particle systems was to be tested by the discovery of so-called heavy-fermion (HF) metals, or materials in which strong interactions would seem to push the idea of renormalization to the limit. These materials typically contain  $f$  electrons of actinide or rare earth elements (*i.e.* Ce, U or Yb atoms) together with lighter elements that contribute lower-orbital electrons. Owing to their peculiar properties, these systems have been studied intensively and a number of early reviews on a handful of “benchmark” HF materials have summarized their properties extensively (see *e.g.* Refs. [9, 10]).

### 1.1.1 Heavy Fermi Liquids

At high temperatures, the properties of HF systems tend to be dictated by a weakly interacting set of magnetic moments of the  $f$  electrons that coexist with light (mass  $\sim m_0$ )  $s$  and  $d$  conduction electrons. However, upon decreasing temperature a peculiar interaction between the moments and the conduction electrons tends to set in, giving rise to a normal (*i.e.* FL), antiferromagnetic (AFM) or superconducting ground state that exhibits properties drastically different than in simple metals [9]. For instance, in the low-temperature “normal” state of HF systems, the electronic specific heat is typically

orders of magnitude larger than that found in ordinary metals. Also, de Haas-van Alphen (dHvA) oscillations are highly temperature-dependent, suggesting very large cyclotron masses, and an anomalously large magnetic susceptibility does not show saturation until extremely low temperatures.

Amazingly, Landau's quasiparticle picture seems to hold in the normal state of HF systems. The first known material to exhibit heavy-fermion properties well-described by FL theory is CeAl<sub>3</sub>. Below  $\sim 1$  K, Andres *et al.* observed 1) a linear  $T$  dependence of specific heat with a coefficient  $\gamma = 1620 \text{ mJ/mol K}^2$ , 2) a magnetic susceptibility  $\chi$  that has very little temperature variation, and 3) a resistivity  $\rho$  well-described by  $\rho = \rho_0 + AT^2$ , where  $\rho_0$  is the residual resistivity and  $A = 35 \mu\Omega \text{ cm/K}^2$  [11]. Such properties suggest that quasiparticles with effective masses exceeding  $100\times$  that of the bare electron mass  $m_0$  can be considered as dictating both the thermodynamic and transport properties of such HF systems. However, note that the application of FL theory to such systems is not straightforward [9], due to such factors as intrinsic anisotropy, strong spin-orbit coupling, and significant non-quasiparticle contributions to the static susceptibility.

The behaviour of HF systems has commonly been associated with single-impurity Kondo systems, where a dilute amount of magnetic impurities sit in a simple-metallic matrix. These systems typically display local-moment behaviour at high temperatures, followed by a “screening” of the impurity spins by the conduction electrons which results in a *logarithmic increase* in the scattering rate as  $T \rightarrow 0$  [12].<sup>3</sup> The physics of HF systems is thought to be captured within some extension of Kondo physics which accounts for strong deviations from the dilute-impurity picture, including interactions between the moments themselves, among many other considerations.<sup>4</sup> A *competition* between Kondo screening of a dense array of local moments and RKKY<sup>5</sup> antiferromagnetism was first proposed by Doniach to connect the magnetic and heavy-electron behaviour found throughout these systems [14]. In some cases (*e.g.* CeCu<sub>6</sub> [15]), there is indeed an onset of long-ranged AFM order between the *f* moments at low temperatures. Since these *f* moments in HF systems are either “weighing down” the conduction electrons (perhaps becoming somewhat itinerant themselves), ordering antiferromagnetically or placing the

<sup>3</sup>Note that the low temperature properties of the Kondo effect can be understood in a (local) Fermi liquid framework - see Ref. [7].

<sup>4</sup>See Refs. [7, 9, 12] for a discussion of the complications of this approach, as well as an extensive review by Coleman [13].

<sup>5</sup>Named after Ruderman, Kittel, Kasuya and Yosida, this is a magnetic interaction between local-moment spins mediated by conduction electrons (see *e.g.* [13] for a review).

system somewhere between these somewhat well-defined ground states, it is not surprising that instabilities can arise, as will be discussed below.

### 1.1.2 Superconductivity

The occurrence of either a heavy mass FL or magnetic ground state in HF systems is not surprising, considering the presence of moments of order  $1 \mu_B$  per  $f$ -electron, which can either interact and order magnetically or be screened by the conduction electrons via a Kondo-type mechanism [12]. However, the most surprising phenomenon, as stated by Fisk *et al.* [9], is the occurrence of *superconductivity* in the presence of these moments, since conventional superconductivity is readily destroyed by the addition of magnetic impurities [16]. This was the first indication that superconductivity in HF materials did not comply with conventional BCS theory.

The first case of HF superconductivity was discovered twenty-five years ago in the compound  $\text{CeCu}_2\text{Si}_2$  [17]. At the transition temperature  $T_c = 0.5$  K, the enormous specific heat discontinuity, together with the observation of a resistive transition and bulk Meissner effect, were the first definitive proof that heavy electrons were indeed able to pair and result in the observed bulk superconducting state. This was further proof of the credibility of the quasiparticle description of the HF state. However, as noted, HF superconductors also exhibit properties that do not follow BCS theory, and hence are considered as part of the family of unconventional superconductors believed to be mediated by a mechanism other than the electron-phonon interaction. For instance, power laws in specific heat in both  $\text{UPt}_3$  and  $\text{UBe}_{13}$  are indicative of an unconventional superconducting gap structure containing zeroes in the gap amplitude [9, 18].

Because HF superconductors tend to be on the verge of magnetic order, it has long been thought that *magnetically-mediated* superconductivity is a prime candidate to explain the anomalous pairing state that many of these materials exhibit [19]. For instance, the most extensively studied HF superconductor,  $\text{UPt}_3$ , is thought to have an unconventional spin-triplet pairing state mediated by spin fluctuations.<sup>6</sup> This type of superconductivity seems to frequently nucleate around the point where a magnetic transition is driven to  $T = 0$  by some external tuning parameter, and is thus a probable result of superconductivity mediated by spin fluctuations. Two benchmark examples were demonstrated by Mathur *et al.* in the cases of  $\text{CeIn}_3$  and  $\text{CePd}_2\text{Si}_2$ , both systems

---

<sup>6</sup>See [18] for a thorough review of the superconducting state of  $\text{UPt}_3$ .

with antiferromagnetic order which, when driven to  $T = 0$  upon application of pressure, gives way to a superconducting state [19]. With a common connection between unconventional superconductivity and magnetic instabilities in Ce and U compounds,<sup>7</sup> much effort has recently gone into trying to describe the physics of the quantum phase transition in an attempt to fully understand the mechanism of this unconventional superconductivity. But it is also now understood that a strong departure from FL theory is another aspect of these systems which presents even greater challenges to the current levels of understanding in condensed matter physics.

### 1.1.3 Non-Fermi Liquid Behaviour

Although Landau's quasiparticle picture is successful in describing the ground state of some HF systems, this seems to be the exception rather than the rule. In the last few decades, over fifty different  $d$ - or  $f$ -electron systems have been shown to exhibit physical properties that do not find explanation within a FL picture [20]. These so-called NFL systems are widely considered as a new class of materials in which the treatment of strong correlations between electrons requires new theoretical ideas that go beyond the weakly interacting quasiparticle picture.<sup>8</sup>

The first conclusive evidence for NFL behaviour in a HF system was discovered in low temperature measurements of the so-called Kondo alloy  $\text{Y}_{1-x}\text{U}_x\text{Pd}_3$  [21]. In their study, Seaman *et al.* reported anomalous temperature dependences of both thermodynamic and transport quantities which did not conform to FL theory. Subsequently, a systematic study of a handful of  $f$ -electron systems - including  $\text{Y}_{1-x}\text{U}_x\text{Pd}_3$ ,  $\text{Th}_{1-x}\text{U}_x\text{Pd}_2\text{Al}_3$  and  $\text{UCu}_{3.5}\text{Pd}_{1.5}$  - was used to identify a list of “common” NFL properties, suggesting the existence of a new class of strongly correlated electron systems [22, 23]. Many more materials have since been added to this list, and a wider range of such common NFL properties has been identified [20].

#### *Properties*

Of course, the general label “NFL” encompasses a broad range of possible behaviour. However, a number of common properties have been recognized to exist in many of these systems, as shown in low temperature resistivity, specific heat and susceptibility

---

<sup>7</sup>Interestingly, a superconducting state has yet to be discovered in any of the Yb compounds!

<sup>8</sup>A huge amount of literature on this subject has been summarized in a recent comprehensive review by Stewart - see Ref. [20].

measurements. For example, some of the hallmark experimental signatures associated with this class of materials include:

- non-quadratic temperature dependence of transport (*i.e.*  $\Delta\rho \sim T^n$  where  $n < 2$ ).
- non-Curie-like susceptibility (*i.e.*  $\chi \sim f(T)$ )
- non-saturating electronic specific heat (*i.e.*  $C/T \sim \gamma(T)$  where  $\gamma \neq \text{const.}$ )

As suggested by Stewart, this classification strongly depends on experimental evidence obtained over a significant range (*i.e.* over a decade) of temperature which reaches an adequately low value. For example, the FL behaviour of CeAl<sub>3</sub> only appears below  $\sim 0.3$  K [11], whereas other systems exhibit NFL behaviour down to the lowest measured temperatures without any sign of a magnetic phase transition or a crossover to FL behaviour.

A more intriguing phenomenon involving scaling was also identified as an important aspect of the NFL nature of these systems. For instance, measurements of the imaginary component of the dynamical susceptibility  $\chi''(\omega, T)$  in UCu<sub>5-x</sub>Pd<sub>x</sub> were the first to show the existence of  $\omega/T$  scaling [24]. Such behaviour is completely inconsistent with a FL ground state since it implies that the only energy scale in the system is temperature itself, as opposed to the dominant Fermi energy in a FL.

### Models

Since most NFL systems possess some aspect of local-spin physics, it is not surprising that numerous models have been proposed that are centered around extensions of the single-impurity Kondo effect. For instance, the “multichannel” Kondo model proposed by Nozières and Blandin [25] is a generalization the original Kondo effect to include more than one orbital degree of freedom of the conduction electrons (*e.g.* multi-band). This model can be solved exactly in the limit of dilute magnetic impurities, resulting in definite NFL properties.<sup>9</sup> However, its relevance to real systems is not as direct as that of the concentrated limit, which is much more difficult to solve exactly. Nevertheless, some success has been had in matching experimental observations to predicted quantities of *e.g.* the two-channel Kondo lattice case (see *e.g.* Ref. [26]).

Other approaches have studied the effects of *disorder* in Kondo physics. The so-called “Kondo disorder” model proposed by Bernal *et al.* imposed the assumption of

---

<sup>9</sup>See Ref. [20] and references therein for a review of various approaches.

a disorder-induced range of characteristic (Kondo) temperatures to exist in the system [27, 28], thereby allowing the persistence of unquenched local spins to remain down to low temperatures, resulting in NFL behaviour. In relation to this, it was also recognized [28] that thermodynamic quantities in a disordered system can be dominated by the existence of rare, strongly-coupled magnetic clusters - a situation known as a Griffith's phase - leading to further predictions of measurable quantities. Such a model may be most relevant to systems in which a spin glass structure is the most likely source of NFL behaviour [20].

## 1.2 Quantum Phase Transitions

The models described above have shared some success in describing NFL behaviour, but have failed to capture all common attributes which exist across a broad range of materials with varying classifications. For example,  $T$ -linear transport behaviour has been observed in both highly disordered and extremely clean, stoichiometric materials [20]. Thus, the observation of similar properties in both chemically substituted and stoichiometric HF materials is suggestive of a more general underlying mechanism for NFL behaviour.

One of the more promising avenues of exploration in NFL physics lies in efforts to explain the properties of systems which possess a zero-temperature, or *quantum* phase transition. It seems that consistent NFL behaviour appears in proximity to such a transition - whether invoked by disorder, pressure, doping, magnetic field, etc. - and so the quantum nature of the fluctuations surrounding such a transition is widely believed to be the source of novel NFL behaviour in a plethora of systems.

### 1.2.1 Introduction

A classical phase transition between *e.g.* an ordered and an unordered phase occurs when the free energy of a system becomes non-analytic - *i.e.* a singularity occurs in thermodynamic quantities as functions of the external parameters. Based on the Ehrenfest scheme, such transitions are either *first-order* or *continuous*, depending on the continuity of the free energy derivatives. For example, the classical water-ice transition is first-order, since a latent heat is required to drive the abrupt transition between the two phases, whereas the commonly demonstrated example of liquid and vapour phases of carbon dioxide becoming indistinguishable at  $T = 31^\circ \text{ C}$  and  $P = 73 \text{ atm}$  is an example of a continuous transition with no latent heat released. When a continuous transition is approached, thermally-excited fluctuations of the order parameter cause a smooth evolution from one

phase to another as the temperature is changed, and hence the transition is considered to be *driven* by thermal fluctuations [29].

First proposed by Hertz over three decades ago, the idea of a quantum phase transition involves a continuous transition that occurs at absolute zero temperature - *i.e.* without any thermal fluctuations present - as a function of some external parameter other than temperature [30]. Whereas classical phase transitions are driven only by thermal fluctuations and hence freeze into a fluctuationless ground state at  $T = 0$ , quantum fluctuations are non-zero due to the Heisenberg uncertainty principle. At  $T = 0$ , quantum fluctuations develop long range correlations in both space and time [31], and hence can drive very interesting and diverse phase transitions which give rise to a plethora of interesting properties.<sup>10</sup>

Directly at the continuous  $T = 0$  transition between the two phases, called the *quantum critical point* (QCP), a divergence in the length and time scales occurs as the transition temperature (*e.g.* the Neél temperature  $T_N$  in an antiferromagnet) is tuned to zero. Unlike classical transitions, where universal quantities (*e.g.* critical exponents) are completely independent of quantum mechanics,<sup>11</sup> the critical behaviour of  $T = 0$  transitions will depend on the quantum mechanical properties of the system [32].<sup>12</sup> However, analogies can be made between classical and quantum models.<sup>13</sup> For instance, just as dimensionality plays a central role in determining the robustness of universality in classical systems,<sup>14</sup> it also plays an analogous role in determining the nature of quantum phase transitions [34], and so critical exponents are important parameters to characterize in order to understand what properties of a QCP, if any, are universal.

Of course, experiments probe the properties of a system at small but finite temperatures, so it may seem needless to study the  $T = 0$  properties of a QCP. However, the physics of the so-called “quantum critical region” (finite-temperature region above the QCP) is controlled by the QCP itself, with temperature being the largest energy scale of the system in this region [32]. As suggested by Coleman, one of the key challenges is

<sup>10</sup>A comprehensive study of quantum phase transitions can be found in Ref. [31].

<sup>11</sup>This is true even for phases with properties (*e.g.* transition temperature) completely governed by quantum mechanics - *i.e.* a superconducting phase transition [32].

<sup>12</sup>Upon approaching  $T = 0$ , the critical long-wavelength fluctuations of the order parameter must involve quantum mechanical statistics since thermal fluctuations are no longer fast enough to destroy the quantum coherence [30].

<sup>13</sup>The use of dimensionally-equivalent classical models can provide tractable methods of calculation which are applicable to their quantum mechanical counterparts [31].

<sup>14</sup>For example, the same critical exponent is observed for both a liquid-gas transition and a ferromagnetic transition [33].

to study the new class of universal excitations which exist in this regime, which exhibits common physical properties in a number of systems [20].

In reality, quantum phase transitions are “tuned” by changing quantities - such as pressure, chemical composition or magnetic field - that couple directly to the dynamics of the system. For example, applying external pressure to a crystal can change the lattice density and hence affect the bandwidth, density of states, etc. In HF systems, the large effective masses translate to small bandwidths which are easily tunable in this way, so the effective screening ability of the conduction electrons can be changed to push the system toward a magnetic instability associated with the  $f$ -electron moments. As mentioned previously, the competition between RKKY-mediated magnetism and Kondo screening was first proposed as a mechanism to explain the general behaviour of HF systems. This competition between energy scales has been captured in the well-known Doniach phase diagram, which suggests that a  $T = 0$  transition can indeed occur between the two ends of the spectrum (*i.e.* where the energy scales of antiferromagnetism and Kondo screening are degenerate). It was not immediately appreciated that this transition could be continuous, but experimental studies [15, 35, 36, 37, 38] have since shown otherwise.

The most well-studied HF material to exhibit quantum critical behaviour is the  $\text{CeCu}_{6-x}\text{Au}_x$  system [15, 39, 40, 41, 42, 43]. The ground state of this material can be tuned, by substituting gold atoms for copper, from HF (paramagnetic) at  $x = 0$  to antiferromagnetic at  $x > 0.1$ .<sup>15</sup> Hence, a QCP associated with the suppression of  $T_N$  to  $T = 0$  occurs at the critical gold concentration of  $x = 0.1$ . At this concentration, the hallmark NFL properties -  $C/T \sim -\log(T)$ ,  $\Delta\rho \sim T$  and  $\chi \sim 1 - \sqrt{T}$  - appear to dominate a significant range of temperature which extends down to the lowest measured values [39]. Interestingly, in addition to chemical tuning (*i.e.* changing  $x$ ), the critical behaviour in  $\text{CeCu}_{6-x}\text{Au}_x$  can also be tuned with applied pressures or magnetic fields [40]. This is an excellent example of the way in which different external parameters can be used to tune criticality, allowing systematic studies to be performed. Note, however, that in this particular case different critical behaviour is observed (*i.e.* the NFL properties show different  $T$ -dependences) depending on whether the system is tuned via pressure or field [40]. This may be due to a number of reasons, including the fact that applied hydrostatic pressure is isotropic while applied fields are not, in addition to the fact that magnetic fields also break time-reversal symmetry. However, the recently studied HF sys-

---

<sup>15</sup>The substitution of Au for Cu expands the lattice spacing, thus decreasing the hybridization of the Ce  $f$ -electrons with the conduction band [15].

tem  $\text{YbRh}_2\text{Si}_2$  indeed shows similar critical behaviour when the QCP is reached by either field-tuning [44] or changing lattice density (substituting Ge for Si) [38], suggesting that a magnetic field can indeed be used to effectively probe criticality in such systems. In essence, one must be careful in treating different tuning parameters on common ground when analyzing critical behaviour.

### 1.2.2 Theories

In many HF systems, the source of NFL behaviour seems to stem from the interplay between the local moment magnetism and conduction electrons found in these materials. A range of interpretations have been proposed to account for this behaviour, including local moment compensation via the Kondo effect, nearness to a quantum phase transition, disorder effects, valence fluctuations, etc.<sup>16</sup>

Here we are concerned with proposals of NFL behaviour stemming from a QCP, which is a largely unsolved problem. There are two main classes<sup>17</sup> of QCP theories which have received considerable theoretical attention: the spin-density wave (SDW) and local QCP scenarios.<sup>18</sup> These have been categorized [46], respectively, as the weak-coupling and strong-coupling approaches to a QCP which separates a heavy-mass (paramagnetic) FL phase from an antiferromagnetically ordered phase.

#### *Spin-Density Wave Scenario*

The weak coupling approach, commonly referred to as Hertz-Millis or spin-fluctuation theory, begins with a heavy FL and treats the QCP as a spin-density wave instability of the Fermi surface. In this scenario, the mutual interaction between damped spin fluctuations and inelastically scattered quasiparticles can be loosely considered as the Bragg diffraction of electrons from quantum fluctuations in the spin density [47]. Renormalization-group methods [30, 48] and extensions thereof [49, 50] have been used to integrate out the fermions from the problem to allow analytical calculations to be performed. Hence, the conduction electrons are assumed not to participate in the critical dynamics, only providing extra channels into which the critical spin fluctuations can decay. The only critical modes are thus the long-wavelength fluctuations of the magnetic order parameter

---

<sup>16</sup>See Refs. [7, 13, 20] for a survey of various theories.

<sup>17</sup>There is also a phenomenological extension of Landau's scaling formalism - so-called *hyperscaling* analysis [45] - which is reviewed by Stewart [20].

<sup>18</sup>A number of excellent papers by Coleman *et al.* have detailed the differences in the current theories on NFL behaviour in HF systems - see Refs. [13, 34, 46, 47].

(paramagnons). This is also referred to as a *Gaussian* quantum critical theory, which predicts a simple mean-field behaviour for physical properties [51].

The *self-consistent renormalization* (SCR) model [52] is an approximation to the Hertz-Millis theory which was constructed to deal with critical behaviour in itinerant magnetic systems. This phenomenological theory considers the collective modes of excitations (rather than the excitations themselves) by assuming a form of the dynamical susceptibility that is singular at the magnetic ordering wavevector. Its main strength lies in the ability to provide a number of analytically-derived predictions for experimentally measurable quantities - such as specific heat and transport (see *e.g.* Ref. [20] - which, in the low-temperature limit, are equivalent to those of the Hertz-Millis model.

Unfortunately, both the Hertz-Millis and SCR models do not consider the effects of disorder. Hlubina and Rice were the first to recognize the importance of *other* scattering mechanisms in the calculation of transport quantities using the Hertz-Millis model. In their so-called “hot-spot” model [53], they recognized the fact that only small portions of the Fermi surface (connected by the magnetic ordering wavevector) are affected by spin fluctuations, resulting in highly anisotropic scattering from spin waves. Hence, in the  $T \rightarrow 0$  limit scattering will be dominated by parts of the Fermi surface *not* affected by spin fluctuations, and a recovery of FL behaviour (*i.e.*  $\Delta\rho \sim T^2$ ) is expected for 3D fermions interacting with 3D spin fluctuations. This was later extended [19, 49, 54] to include the effect of 2D fluctuations, where a finite *area* of the Fermi surface becomes hot, thereby increasing the effect of disorder in favoring isotropic scattering and reducing the temperature at which FL recovery is expected.<sup>19</sup>

The essential aspects of the weak-coupling approach include 1) the development of a magnetic instability in momentum space, and 2) the fact that a FL ground state is underlying all observable behaviour (*i.e.* a fundamental breakdown of the quasiparticle picture is not expected to occur). The first aspect, in the framework of SCR theory, has been shown to well-describe experimental results in both CeRu<sub>2</sub>Si<sub>2</sub> [36] and CeNi<sub>2</sub>Ge<sub>2</sub> [37, 55, 56]. The second aspect can be tested, for example, by checking the validity of the Wiedemann-Franz law in the  $T \rightarrow 0$  limit, which was indeed shown to hold in the case of CeNi<sub>2</sub>Ge<sub>2</sub> [56].

---

<sup>19</sup>The effects of disorder are considered in great detail by Rosch within a semiclassical approach using a Boltzmann equation - see Ref. [50].

### Local QCP Scenario

The strong-coupling approach treats a HF system as a Kondo lattice of local moments and approaches the QCP from the magnetically ordered phase, with composite bound states forming between conduction electrons and local moments. This interpretation treats the QCP as essentially a breakdown of the Kondo effect - where the Kondo energy scale reaches zero and complete screening is no longer possible. Since it is *local* fluctuations (*e.g.* dynamics of local moments) which play the dominant role, a FL description is not possible and hence this is very different than the spin-density wave approach discussed above. This approach has been pursued not only to improve the assumptions of the weak-coupling theory (*i.e.* including electronic excitations in the critical dynamics), but also to explain experimental evidence which points to a breakdown of the Gaussian picture. For example, an absence of momentum dependence of the spin damping at the QCP in  $\text{CeCu}_{6-x}\text{Au}_x$  [15] suggests that the NFL behaviour arises from spacially-local critical excitations.<sup>20</sup> More recently, critical behaviour in  $\text{YbRh}_2\text{Si}_2$  has been shown to exhibit properties which do not coincide with predictions of either the 2D or 3D SDW scenario [38].

The local QCP theory proposed by Si *et al.* suggests that the dynamical spin susceptibility has anomalous frequency and temperature dependences throughout the momentum space of the Brillouin zone, and is hence locally singular [51]. This model stems from the ideas of Doniach [14], who suggested that the Kondo interaction can overcome the RKKY interaction and lead to complete screening of the local moments. However, in the local QCP picture the presence of critical spin fluctuations, with the help of the RKKY interaction, prevents a complete screening of the local moments at the QCP. Therefore, in addition to long-wavelength critical fluctuations of the magnetic order parameter, the interaction of conduction electrons with *unscreened* local moments also contributes a critical degree of freedom, and hence the electrons directly participate in the critical behaviour.

The essential aspect of the local QCP picture is the real-space destruction of the composite bound states between conduction electrons and local moments, which relies strictly on the existence of 2D spin fluctuations [51]. In the same framework, Si *et al.* found that the presence of 3D spin fluctuations results in a *finite* Kondo energy scale at the

---

<sup>20</sup>The presence of  $\omega/T$  scaling in  $\text{CeCu}_{6-x}\text{Au}_x$  is also a significant departure from the Gaussian picture [15] - see Ref. [51] for a comprehensive discussion.

QCP [51], leading to complete screening of the local moments and hence the presence of quasiparticles which do not participate in the dynamics - as in the SDW scenario discussed above. The question of why quantum critical HF systems such as  $\text{CeCu}_{6-x}\text{Au}_x$  and  $\text{YbRh}_2\text{Si}_2$  should favor quasi-2D spin fluctuations when their electronic structure is highly 3D, as posed by Coleman [34], is a significant challenge to the true applicability of this strong-coupling approach.

### Other Proposals

There are a few other recent and interesting ideas about the nature of the QCP which separates a heavy FL from a local-moment magnetic state. These involve a fractionalization of the electron into separate spin and charge excitations - a break-up of the quasiparticle picture - at the QCP, which gives rise to the NFL behaviour.

Senthil *et al.* have recently proposed a model of weak magnetism [57] which claims that the local moments in HF systems do not participate at all in the Fermi surface construction. Rather, magnetic order is a resultant instability of a new nonmagnetic state which is separated by the conventional FL state by a QCP. This picture is somewhat similar to the local QCP picture described above, but suggests that a similar destruction of the Kondo effect can occur at this QCP in the presence of 3D spin fluctuations [57]. Their model predicts a jump in the volume of the Fermi surface at the QCP, associated with the transition between the conventional FL state and the *fractionalized* FL state. This fractionalized state includes a small Fermi surface of conduction electrons, but also a set of coexistent exotic excitations - a form of spin-charge separation [57].

Similar ideas have been proposed by Coleman *et al.*, who also suggest that HF quantum criticality is a 3D phenomenon [34, 47]. The idea of “spinorial magnetism” [47, 58] suggests that the heavy quasiparticle would decay into a charge-neutral “spinon” and a spinless, charge  $e$  fermion - a form of spin-charge separation similar to that proposed to occur in the high- $T_c$  cuprates [59]. In the case of HF systems, this may occur as a result of pre-formed Kondo singlets that never become coherent directly at the QCP [60]. This scenario has even been suggested to occur over a finite range of critical tuning (*i.e.*  $T = 0$  NFL behaviour over an *extended* range of the external tuning parameter) [61].

Coleman has suggested [34] that a stringent test of the nature of a QCP would involve a measurement of the Hall constant as the system is tuned from the paramagnetic (HF) and antiferromagnetic ground states. Because both of the above scenarios involve a drastic change in the Fermi surface at the QCP, abrupt changes in the Hall coefficient - including

a jump or even a sign change - would be expected [34]. Such an observation would be contrasted to the expectation from the SDW picture, which predicts a continuous change as the system is tuned through the QCP.

## BACKGROUND

---

---

This chapter provides some background theory regarding the interpretation of heat and charge transport in both conventional and unconventional systems. After giving a brief review of the standard interpretations of transport and their expected low temperature behaviour in conventional metals, a summary of ideas involving the usefulness of comparing heat and charge transport quantities will be given. Finally, we will review the currently available predictions of NFL behaviour arising from a quantum critical point.

### 2.1 *Transport Theory*

The measured conductivity of a material can be a complicated quantity, being composed of different contributions which can be collectively or separately influenced by numerous scattering mechanisms, but it remains one of the most sensitive probes of phase transitions and can at least give a qualitative interpretation of the electronic nature of a material (*i.e.* metal, insulator or semiconductor) and its electronic structure (*i.e.* anisotropy). Furthermore, because the conductivity is coupled, via scattering, to various entities of interest (*e.g.* spins, phonons, impurities, etc.), its measurement can be used as a probe of the dependence of such entities on external parameters such as temperature and magnetic field. Here we will discuss both electrical and thermal conductivity, which are intimately related through the Wiedemann-Franz law but can also behave quite differently, as discussed below.

#### 2.1.1 *Electrical Conductivity*

The Drude model of metallic conduction remains as the most simple and useful interpretation of transport properties. It neglects any complex interactions between conduction electrons and ions in a solid and applies the rules of kinetic theory to a simple “gas” of free charge carriers. According to Ohm’s law, the electrical conductivity  $\sigma$  is defined as

the proportionality factor between a current density  $\mathbf{j}_e$  and an electric field  $\mathbf{E}$  as  $\mathbf{j}_e = \sigma \mathbf{E}$ .<sup>1</sup> With a number of assumptions [62], Drude expressed this proportionality constant as

$$\sigma = \frac{ne^2\tau}{m}, \quad (2.1)$$

where  $n$  is the electronic density,<sup>2</sup> and  $e$  and  $m$  are the charge and mass, respectively, of the electron. In this way, the only unknown parameter needed to describe the conductivity is the parameter  $\tau$ , which can be considered as the time between collisions, or *scattering time*. Although this treatment assumes a completely free and independent electron gas, FL theory has justified why such an assumption in fact works by encapsulating interaction effects into a renormalized mass  $m^*$  and continuing on with the assumption of non-interacting electrons, as shown in semiclassical calculations [62].

In a real metal, of course, the assumptions of the Drude model are far from correct. Conduction electrons can scatter not only between themselves, but from lattice ions, impurities, defects, and many other complicated entities. However, a relaxation-time approximation [62] can be taken for these collision processes, and assuming that the presence of each process does not alter the way in which the others function, the total rate of collisions will be the sum of that due to each process acting alone. This is known as Matthiessen's rule,

$$\frac{1}{\tau} = \frac{1}{\tau_1} + \frac{1}{\tau_2} + \dots, \quad (2.2)$$

which asserts that the total resistivity  $\rho = 1/\sigma$  is simply the sum of resistivities due to each process. This is most useful in distinguishing between different scattering processes present in a material which, for instance, follow different temperature dependencies.

Because it is difficult to calculate scattering amplitudes, exact numerical values of resistivities resulting from various scattering processes are not obtainable. However, order of magnitude values, and more importantly, temperature dependencies of various scattering processes are calculable by solving the kinetic equation [5]. The exact values for each scattering rate can then be extracted from experiment.

The *residual* resistivity  $\rho_0$  of a material arises due to scattering from lattice defects such as impurities, dislocations and vacancies, and can be shown [5] to be temperature-independent using a hard-sphere model. Thus, since any crystal lattice contains imperfections of this sort, this scattering mechanism is always expected to be present and can

---

<sup>1</sup>Although  $\mathbf{E}$  and  $\mathbf{j}_e$  need not be parallel, we will only discuss the isotropic case where  $\sigma$  is a constant.

<sup>2</sup>This is in relation to the density of states at the Fermi surface  $N(E_F) = \frac{3n}{2E_F} = \frac{3n}{m^*v_F^2}$ , where  $E_F$  and  $v_F$  are the Fermi energy and velocity, respectively.

be extracted from the low-temperature limit - *i.e.*  $\rho \rightarrow \rho_0$  at  $T \rightarrow 0$ . One exception to this rule involves the presence of *magnetic impurities* in a crystal. In this case, the conduction electrons will tend to *screen* the spins of the impurities as a result of the Kondo effect (see *e.g.* Ref. [12]), leading to a logarithmic increases of scattering with decreasing temperature.

Even if a metal were ideally pure and free of defects, thermal lattice vibrations provide an intrinsic source of scattering, even for Bloch electrons in a perfect periodic lattice. The semiclassical model predicts an *electron-phonon* scattering rate that can vary between  $T^3$  and  $T^5$  at temperatures  $T \ll \Theta_D$ , depending on Umklapp processes [62]. This is usually the dominant scattering process in normal metals, and has been studied in depth (see *e.g.* Refs. [5, 62, 63, 64]).

### *Electron-Electron Scattering*

Another type of “intrinsic” scattering involves interactions between the electrons (quasiparticles) themselves. In a Fermi liquid, this type of scattering will include electrons with energies lying within  $k_B T$  of  $E_F$ , and so the number of potential scatterers will be  $\sim k_B T \times N(E_F)$ , where  $N(E_F)$  is the density of states. Because the number of vacant states within  $k_B T$  of  $E_F$  will be the equivalent amount, the probability for *electron-electron* (e-e) scattering, and hence the scattering rate, will be proportional to  $(k_B T \times N(E_F))^2$  [63]. In simple metals, the magnitude of this scattering rate is usually dominated by that of electron-phonon scattering, and is therefore hard to observe experimentally. However, in transition and HF metals, the high density of states at the top of the *d*- or *f*-bands can greatly increase the probability of e-e scattering since the density of levels in the final state is much greater.<sup>3</sup> In these cases, e-e scattering can easily become the dominant temperature-dependent scattering mechanism, giving rise to a resistivity of the form

$$\rho = \rho_0 + AT^2. \quad (2.3)$$

The observation of this form of resistivity in a number of transition metals has brought about a large number of studies involving e-e scattering (see *e.g.* Refs. [66, 67, 68, 69, 70]), and is considered an important signature of quasiparticles in a Fermi liquid.

There are a number of models considering an *s* band of conduction electrons scattering

---

<sup>3</sup>In a model of scattering between a light *s* band and a heavy *d* band, for example, the *s-d* transitions will involve an initial small density of states (*s*-band) and a final, much heavier density of states (*d*-band) - see *e.g.* Ref. [65].

from a heavier band, via a direct Coulomb interaction (*i.e.* number density fluctuations of the heavier band [70]), or a spin interaction (*i.e.* spin-density fluctuations of the heavier band [69, 71, 72]) with the electrons of the heavier band. Although qualitatively different, each mechanism still involves an interaction between electrons and hence still gives rise to a  $T^2$  dependence of the scattering rate.

### Kadowaki-Woods Ratio

As shown above, the coefficient  $A$  of the resistivity due to e-e scattering is roughly proportional to the square of the electronic density of states, and so one can imagine a relation to the electronic specific heat coefficient  $\gamma_e = C_e/T$ , which is proportional to the density of states as well (see Eqn. (2.6) below). Such a relation between  $A$  and  $\gamma_e$  is expected *e.g.* for an e-e Coulomb interaction mechanism [70]. The so-called Kadowaki-Woods (KW) ratio  $A/\gamma^2 = 10 \mu\Omega \text{ cm mol}^2 \text{ K}^2/\text{J}^2$  [73], which is an empirical quantity observed in a plethora of systems ranging from elemental metals to HF compounds,<sup>4</sup> suggests that this relation is far more universal. This implies that, whatever the mechanism of e-e scattering, the magnitude of its scattering rate (*i.e.*  $A$  coefficient) is a direct measure of the (squared) density of states.

#### 2.1.2 Thermal Conductivity

In the same manner as  $\sigma$  is the proportionality between a charge current and an applied electric field, the *thermal conductivity*  $\kappa$  is the proportionality between a heat current  $\mathbf{j}_q$  and an applied temperature gradient  $\nabla T$ , following  $\mathbf{j}_q = -\kappa \nabla T$ .<sup>5</sup>

Whereas electrical conduction is determined by charge carriers alone, the thermal conduction in a material is in principle determined by contributions from all mobile entities able to achieve an excited state, and hence “carry” entropy. Thus, the total thermal conductivity is the sum of the conductivities of all heat carriers,

$$\kappa = \kappa_e + \kappa_{ph} + \dots, \quad (2.4)$$

where  $\kappa_e$  is due to electrons and  $\kappa_{ph}$  is due to phonons.<sup>6</sup>

---

<sup>4</sup>For example, in the HF compound CeAl<sub>3</sub>,  $\gamma = 1620 \text{ mJ/mol K}^2$  and  $A = 35 \mu\Omega \text{ cm}$  [11], giving a KW ratio  $A/\gamma_e^2 = 13 \mu\Omega \text{ cm mol}^2 \text{ K}^2/\text{J}^2$  which is very close to the universally observed value.

<sup>5</sup>From herein, the temperature gradient will be discussed as a discrete value in accord with experimental quantities - *i.e.*  $\Delta T = T^+ - T^-$ .

<sup>6</sup>In practice, electrons and phonons are the prominent heat carriers in a solid, but other carriers, such as magnons, spinons, etc. can contribute as well - see *e.g.* Ref. [74] for an example of magnon heat transport.

Each heat carrier, in turn, will participate in various scattering processes and hence follow Matthiessen's rule. For instance, the scattering of phonons can involve other phonons (Umklapp processes), electrons, point defects, sample boundaries, dislocations, etc. [63]. As can be seen, the presence of multiple scattering mechanisms in addition to multiple carriers can make any reasonable extraction of separate quantities from an experiment hopeless. However, in a high purity metal  $\kappa_e$  usually exceeds  $\kappa_{ph}$  by orders of magnitude (especially at low temperatures), making an observation of the electronic conduction feasible.

### *Electronic Conductivity*

Applying the Sommerfeld theory of metals (*i.e.* inserting quantum (Fermi) statistics into the Drude model) to the free electron gas results in an expression for the electronic thermal conductivity determined by the specific heat  $C_e$ , Fermi velocity  $v_F$  and mean free path  $l_e = v_F \tau_e$ . This is given by

$$\kappa_e = \frac{1}{3} C_e v_F^2 \tau_e = \frac{1}{3} C_e v_F l_e, \quad (2.5)$$

where the specific heat,

$$C_e = \frac{\pi^2}{3} N(E_F) k_B^2 T = \pi^2 k_B^2 \frac{n}{m^* v_F^2} T, \quad (2.6)$$

is linear in temperature. Thus, in a normal metal one expects  $\kappa_e \sim T$ , assuming a temperature-independent mean free path.<sup>7</sup>

### *Lattice Conductivity*

In most metals, a measurable phonon contribution is indeed present, but its low- $T$  conductivity is also usually dictated by one dominant scattering process so a simple temperature dependence can be expected in certain cases. Debye theory predicts a  $T^3$  dependence for the lattice specific heat, and so an estimation of  $\kappa_{ph}$  can be made using kinetic theory (similar to  $\kappa_e$  above) if the *phonon* mean free path  $l_{ph}$  is known. When  $l_{ph}$  is not limited by certain scattering processes, it eventually reaches the length of typical experimental sample sizes (*e.g.* 1 mm), and so *boundary scattering* becomes the dominant process [63]. In this case,  $l_{ph}$  is the sample width, which is  $T$ -independent so  $\kappa_{ph} \sim T^3$ .<sup>8</sup> In the presence of a high concentration of conduction electrons, phonon-electron scattering will

---

<sup>7</sup>This is indeed achieved in the elastic (*e.g.* impurity) limit, when  $\rho \rightarrow \rho_0$ .

<sup>8</sup>This power can be less than cubic in certain cases - see *e.g.* Ref. [75].

dominate, resulting in  $l_{ph} \sim 1/T$  due to the number of electrons available for scattering ( $\sim k_B T$ ), and so in this case  $\kappa_{ph} \sim T^2$  [63]. For a thorough review of phonon heat conduction mechanisms, see *e.g.* Chapter 2 of Ref [76].

## 2.2 Comparing Heat and Charge Transport

Although one can proceed to examine experimental data with a basic notion of how to interpret thermal and electrical conductivities in the hope of identifying the relevant scattering processes in a metal, the inability to compare precise experimental magnitudes to theoretical predictions limits the usefulness of this approach. However, a comparison between the two quantities can often circumvent this problem since integral elements common to both thermal and electrical currents often cancel when *e.g.* taking their ratio, thus allowing precise comparisons to calculated quantities.

It is well known that metals are good conductors of both electricity and heat. Given the fact that heat and charge transport in a metal involve essentially the same carrier, namely the electron, it is not surprising that the two quantities are proportional. The Wiedemann-Franz (WF) law states that electrical and thermal conductivities of metals are not independent quantities, but are in fact related by the ratio

$$\frac{\kappa}{\sigma T} = L, \quad (2.7)$$

where the *Lorenz number*  $L$  is approximately the same in all metals. This law was first discovered empirically in 1853 by Wiedemann and Franz [1], who showed it to hold in a range of metals at room temperature. An explanation of this observation was proposed by Drude in 1900, who (ironically) mistakenly reported a value for  $L$  which was twice the correct prediction of the Drude model, thus agreeing with experiment.

The true disagreement was later shown to be a consequence of the use of classical statistics in the Drude model, and was corrected by Sommerfeld with the application of the Fermi-Dirac distribution. Sommerfeld's value for the Lorenz number,  $L_0 \equiv \frac{1}{3} \left( \frac{\pi k_B}{e} \right)^2 = 2.44 \times 10^{-8} \text{ W } \Omega \text{ K}^{-2}$ , is obtained from the expressions for electrical (Eqn. (2.1)) and thermal (Eqn. (2.5)) conductivities, together with the Sommerfeld specific heat for a free electron gas (Eqn. (2.6)).

### 2.2.1 $T = 0$ : Wiedemann-Franz Law

The robustness of the WF law has been studied in great detail, and the assumptions taken in the Sommerfeld theory have been tested in various studies. For instance, Chester and

Thellung have verified the Sommerfeld result with the most general derivation, assuming non-interacting electrons (obeying Fermi-Dirac statistics), an isotropic system and an elastic scattering mechanism, but have also showed it to hold for any strength of scattering [77]. Subsequently, this result was also shown to hold in anisotropic systems and under strong magnetic fields [78], under all levels of disorder, including weak and strong localization regimes [79, 80], and for arbitrary band structure [62].

In essence, the WF law is expected to be valid for *any system*<sup>9</sup> which supports heat and charge transport governed by mobile carriers of charge  $e$  which obey Fermi-Dirac statistics and experience strictly elastic scattering. Thus, in the elastic scattering limit,<sup>10</sup> where no energy is lost in collision processes, the WF law can be considered a simple result of the fact that the *same* quasiparticles are responsible for both energy and charge transport, and is thus considered to be one of the most robust signatures of Landau's Fermi liquid (FL) theory. In this light, an investigation of the WF law in the  $T \rightarrow 0$  limit is considered a stringent test of the quasiparticle interpretation of electronic systems.

The extent of validity of the WF law has been shown to far exceed theoretical treatments, as determined by numerous experiments. For instance, it has not only been verified in a plethora of simple metals [67, 68, 81, 82, 83, 84], alloys [69, 85] and compounds [86], but also in strongly correlated systems such as the HF materials CeAl<sub>3</sub> [87], UPt<sub>3</sub> (normal state) [88] and UCu<sub>5</sub> [89], the 2D systems Sr<sub>2</sub>RuO<sub>4</sub> [90], NbSe<sub>2</sub> [91] and Na<sub>x</sub>CoO<sub>2</sub> [92], and systems displaying NFL behaviour such as CeCu<sub>6</sub> [41], CeNi<sub>2</sub>Ge<sub>2</sub> and CeRu<sub>2</sub>Si<sub>2</sub> [56].

In the high- $T_c$  cuprate superconductors, where the validity of the quasiparticle picture is one of the fundamental questions concerning the ground state of these anomalous materials, several tests of the WF law have been performed. The WF law has indeed been observed to hold in overdoped Tl<sub>2</sub>Ba<sub>2</sub>CuO<sub>6- $\delta$</sub>  [93] and La<sub>2- $x$</sub> Sr <sub>$x$</sub> CuO<sub>4</sub> [94], as expected considering the FL-like properties that exist on the overdoped side of the phase diagram. In the field-induced normal state of optimally-doped Bi<sub>2+ $x$</sub> Sr<sub>2- $x$</sub> Cu<sub>2</sub>O<sub>6+ $\delta$</sub> , Bel *et al.* observed a Lorenz number  $L = 1.3 \pm 0.2L_0$  [95], which slightly exceeds the WF law expectation but is not a substantial violation. The most drastic deviation from the WF expectation was observed in optimally-doped Pr<sub>2- $x$</sub> Ce <sub>$x$</sub> CuO<sub>4</sub> [96]. Hill *et al.* observed

---

<sup>9</sup>This is not true for strictly 1D systems, such as Luttinger liquids.

<sup>10</sup>This is the  $T \rightarrow 0$  in any system, but can occur at a finite temperature where an elastic scattering mechanism dominates (*e.g.* where resistivity becomes temperature-independent due to dominant impurity scattering),

two qualitatively different violations of the WF law in the field-induced normal state: 1) an apparent *absence* of heat conductivity ( $L \rightarrow 0$ ) as  $T \rightarrow 0$ , and 2) an *excess* heat conductivity ( $L \simeq 2L_0$ ) above 0.3 K. The first observation may be due to an extrinsic effect.<sup>11</sup> The second case, however, is believed to be intrinsic and may be similar to the observations in  $\text{Bi}_{2+x}\text{Sr}_{2-x}\text{Cu}_2\text{O}_{6+\delta}$  by Bel *et al.*.

An excess heat conductivity in the elastic limit, although unprecedented, is not a completely unexpected observation in strongly correlated systems thought to deviate from FL theory. For example, spin-charge separation theories (see *e.g.* Ref. [59]) suggest that electrons can fractionalize into charge-neutral spin-carrying fermions (spinons) and charged bosons (chargons), in which case the heat-carrying fermions would not partake in charge transport: an added contribution to thermal transport from exotic Fermionic excitations would cause  $L(0) > L_0$  [57].

One of the most daunting questions about quantum criticality is in regard to the ground state excitations that seem to dictate the anomalous finite-temperature properties: does the integrity of the quasiparticle survive the strong interactions responsible for the  $T = 0$  phase transition, or does a new state of matter emerge ( see *e.g.* Ref. [34])? A study of the WF law is an ideal test of this question, providing strict constraints on any theoretical explanation of the exotic properties that surround a quantum phase transition. This is the main focus of the current study, and will be revisited in the subsequent chapters regarding quantum criticality in  $\text{CeCoIn}_5$ .

### 2.2.2 $T > 0$ : Inelastic Scattering

At higher temperatures, deviations from the WF law are expected in any metal [62, 63, 64, 65]. This is a result of the difference in the effect of *inelastic scattering* processes on energy and charge transport. This anisotropy arises from the fundamentally different electron distributions that are set up in the cases of 1) an electric field and 2) a thermal gradient. In the first case, the whole electronic  $\mathbf{k}$ -space distribution is shifted entirely so that an excess of electrons are directed in a particular momentum direction, and hence a charge current flows. In the second case, there is (normally) no net current flow, and so the electronic  $\mathbf{k}$ -space distribution remains symmetric about  $k = 0$  but with a shift in

---

<sup>11</sup>The observed violation of the WF law in  $\text{Pr}_{2-x}\text{Ce}_x\text{CuO}_4$  in the  $T \rightarrow 0$ , which involves an absence of observable electronic heat conduction, may be due to the effect of electron-phonon decoupling as discussed in Ref. [97]. The same type of violation was observed in  $\text{La}_{2-x}\text{Sr}_x\text{CuO}_4$  [94] and in  $\text{CeCoIn}_5$ , the latter of which is shown in Appendix C.2 to be an experimental artifact, and not an intrinsic  $T = 0$  violation of the WF law.

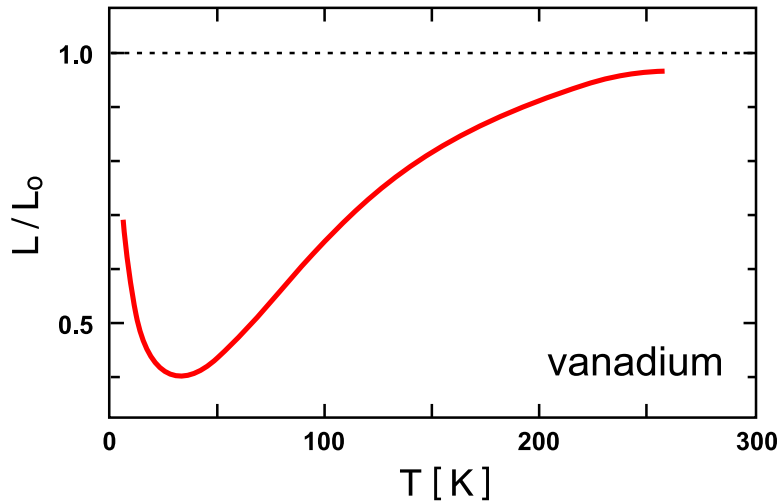


Figure 2.1: Normalized Lorenz ratio  $L/L_0$  measured in pure vanadium (from Ref. [83]).

the direction of thermally-excited electrons. Thus, a scattering event can affect the two currents much differently depending on the angle and energy change that occurs in the process.

In the case of a spherical Fermi surface, a scattering event degrades a charge current ( $j_e$ ) and a heat current ( $j_q$ ) by the following amounts [69]:

$$\Delta j_e \approx - \frac{k_F}{m^*} e (1 - \cos\theta) \quad (2.8)$$

$$\Delta j_q \approx - \frac{k_F}{m^*} [ (E - \mu) (1 - \cos\theta) + \hbar\omega \cos\theta ] \quad (2.9)$$

where  $e$  is the electron charge and  $\mu$  the chemical potential. The electron has initial velocity  $\hbar k_F/m^*$  and energy  $E$ , and sees its direction deflected by an angle  $\theta$  and its energy changed by an amount  $\hbar\omega$ . For elastic scattering ( $\hbar\omega = 0$ ), both currents are degraded in the same way, namely by a change in momentum direction, and one obtains the Wiedemann-Franz law, or  $L = L_0$ . But for inelastic scattering ( $\hbar\omega \neq 0$ ), the two currents begin to differ and the behaviour of  $L$  will strongly depend on the scattering angle. Thus, a measurement of the Lorenz number reveals information about the nature of scattering processes involving the two types of transport.

As a conceptual example of the effects of inelastic scattering, let us consider the case of electron-phonon scattering. At low temperatures, only long-wavelength (small- $\mathbf{q}$ ) phonons are thermally excited so small-angle collision processes occur between phonons and electrons which involve an energy transfer of order  $k_B T$ , and hence degrade  $j_q$ . But these collisions do not strongly influence  $j_e$  because the velocity of the scattered

electron is not reversed, so an anisotropy develops between the two currents so that  $L(T) < L_0$ . Conversely, high energy phonons which are excited at high temperatures ( $T > \Theta_D$ , where  $\Theta_D$  is the Debye temperature), can contribute to large-angle scattering of electrons, affecting both  $j_e$  and  $j_q$  so that  $L(T) \simeq L_0$ .<sup>12</sup> Thus, in a normal metal one would expect the WF law to hold at both low temperatures, due to impurity scattering, and high temperatures, due to large-angle phonon scattering. As shown in Fig. (2.1), this is indeed observed experimentally in vanadium, for example, where  $\Theta_D \simeq 390$  K [62].<sup>13</sup>

For inelastic scattering (finite  $\hbar\omega$ ), the two terms in Eqn. (2.9) lead to two contributions to the thermal resistivity  $w_e \equiv L_0 T / \kappa$ , such that  $w_e = w_{\text{hor}} + w_{\text{ver}}$  [72], but only the first type of scattering process enters in  $\rho$ , so that  $\rho(T) = w_{\text{hor}}(T)$ . These two scattering processes are sometimes referred to as “horizontal” and “vertical” processes, resulting, respectively, from changes in the direction of the electron wavevector and energy [69, 72]. Many years ago, it was recognized by Kaiser that the *difference* between experimentally measured thermal and electrical resistivities  $\delta(T) \equiv w_e(T) - \rho(T)$  can give access to the vertical component (*i.e.*  $\delta(T) = w_{\text{ver}}$ ) [72], and hence information about the characteristic temperature at which vertical scattering dissolves can be extracted from experiment. In the case of electron-phonon scattering, this temperature is merely  $\Theta_D$ , above which phonons no longer have enough energy to scatter electrons through the “thermal layer” (*i.e.*  $k_B T$ ) and become effectively *elastic*. But other scattering mechanisms, such as that of electrons scattering from fluctuating local moments, will have their own characteristic energy scale which can be extracted in this way, as will be shown in Chapter 5 for the case of CeRhIn<sub>5</sub> and Chapter 6 for the case of CeCoIn<sub>5</sub>. Finally, note that both terms in  $w_e$  involve weighted integrals over  $\mathbf{q}$  and  $\omega$  of the fluctuation spectrum:  $w_{\text{hor}}$  is weighted by  $\mathbf{q}^2$ , while  $w_{\text{ver}}$  is weighted by  $\omega^2$ . Thus, comparing the two gives access to the  $\mathbf{q}$  and  $\omega$  dependence of scattering.

### 2.2.3 Electron-Electron Scattering

In conjunction with investigations of the resistivity due to e-e scattering (*i.e.*  $\Delta\rho = AT^2$ ), a number of studies have considered the effect of e-e scattering on the electronic contribution to thermal conductivity (see *e.g.* Ref. [69]), and hence calculations of the resultant

---

<sup>12</sup>Note that phonon energies are also limited to values  $k_B\Theta_D$ , so scattering is effectively *elastic* in addition to large-angle when  $T > \Theta_D$ .

<sup>13</sup>Another example involving pure silver, for which  $\Theta_D \simeq 215$  K [62], is shown in Fig. (4.7).

Lorenz ratio due to e-e scattering  $L_{ee}/L_0$  have been performed. Early calculations by Bennett *et al.*, motivated by the complex band structure of transition metals, used a two-band model of conductive  $s$  electrons scattered by heavier  $d$  electrons to predict that  $L_{ee}/L_0$  should be nearly temperature-independent and in the range from  $\sim 0.4$  (for small-angle scattering) to  $\sim 0.65$  (for isotropic scattering) [66]. Herring also predicted that the assumption of a complicated, multi-band system can actually simplify the collision integral, leading to an approximate calculated universal value of  $L_{ee}/L_0 \sim 0.65$  in the absence of impurity scattering [98], and  $L_{ee}/L_0 \sim 0.55$  in the presence of strong impurity scattering (see Ref. 29 in [69]).

In practice, a ratio  $L_{ee}/L_0 \simeq 0.4\text{--}0.6$  is characteristic of most metals [67], from elemental Ni, where  $L_{ee}/L_0 \simeq 0.4$  [68], to the heavy-fermion compound UPt<sub>3</sub>, where  $L_{ee}/L_0 \simeq 0.65$  [99].<sup>14</sup> By assuming the dominant inelastic scattering mechanism is due to e-e interactions and incorporating residual scattering processes, the finite-temperature Lorenz ratio in a FL is thus expected to proceed as

$$\frac{L}{L_0} = \frac{\rho_0 + AT^2}{w_0 + BT^2} \quad (2.10)$$

where we have incorporated the residual resistivities for charge ( $\rho_0$ ) and heat ( $w_0 \equiv L_0 T / \kappa_0$ , where  $\kappa_0/T \equiv \lim_{T \rightarrow 0} \kappa/T$ ), and the e-e scattering coefficients for charge ( $A$ ) and heat ( $B \equiv (w - w_0)/T^2$ ). In this sense, the value of  $L_{ee}/L_0$  can be extracted directly from experiment by the determination of the ratio of  $T^2$  resistivity coefficients  $A/B$ , and a plot of the experimental Lorenz ratio will show a crossover from impurity-dominated scattering ( $L/L_0 \rightarrow \rho_0/w_0 = 1$  at  $T \rightarrow 0$ ) to e-e scattering ( $L/L_0 \rightarrow A/B \simeq 0.5$  at  $T \rightarrow \infty$ ). Of course, this is for the ideal case where e-e scattering dominates all other inelastic scattering mechanisms. The systems to be discussed in this study only show a finite range of FL (e-e scattering) behaviour (if any) before crossing over to a different scattering mechanism, so  $L/L_0 = A/B$  is only expected to be observable through a finite range of temperature, as will indeed be shown in the following chapters.

## 2.3 QCP Theory Predictions

A review of the relevant QCP theories was given in Section 1.2.2 without any reference to the various predictions that have been made regarding NFL transport properties. Although the nature of NFL behaviour arising around a QCP is not well understood, a

---

<sup>14</sup>There are some exceptions, such as tungsten and platinum, which both have a ratio  $L_{ee}/L_0 \leq 0.1$  [67].

number of quantitative predictions have been made which can be compared to experiment.

### 2.3.1 Charge Transport

The SDW or mean-field theory of quantum phase transitions has produced a number of analytically-derived predictions of the  $T$ -dependence of resistivity, susceptibility and specific heat at low temperatures [30, 48, 52].<sup>15</sup> For resistivity, all  $T$ -dependencies are predicted to follow a power law smaller than that of e-e scattering in a FL - *i.e.*  $\Delta\rho \sim T^n$  with  $n = 1 - 5/3$ , depending on the physical dimension of the system and the dynamical critical exponent (*i.e.* ferromagnetic or antiferromagnetic). Moriya's SCR theory has the same predictions as Hertz-Millis theory for AFM systems, which expect  $n = 1$  for 2D and  $n = 3/2$  in a 3D system.

As discussed, the consideration of realistic scattering mechanisms in the SDW model brings about the “hot spot” mechanism, which suggests that any observation of NFL behaviour will eventually lose out to FL behaviour at low but experimentally accessible temperatures [53]. Rosch [54] and Paul *et al.* [49] have extended this approach to consider 2D spin fluctuations in a 3D system, giving the prediction of  $T$ -linear resistivity which can dominate the (underlying) FL behaviour for a given disorder level [49]. Rosch has further considered the effects of disorder on the NFL behaviour in great detail, showing that resistivity can indeed display greatly varying (and temperature-dependent) power laws ( $n = 1 - 2$ ) depending on the amount of disorder [50]. In essence, Rosch’s predictions show that disorder effects must be carefully considered before relating observed power laws to any specific theory.

At present, there are no specific calculations of transport properties in the local QCP picture. However, note that the “hot spot” mechanism essentially becomes extreme in this scenario (the entire Fermi surface is affected by the local fluctuations) so that NFL behaviour is expected to dominate transport to  $T = 0$  at a QCP [100]. Note also that in this picture the change in the volume of the Fermi surface is expected to affect the residual resistivity as a system is tuned through its QCP [100].

---

<sup>15</sup>See Ref. [20] for a comprehensive summary of these predictions for both ferromagnetic and antiferromagnetic fluctuations in both two- and three-dimensional systems.

### 2.3.2 Wiedemann-Franz Law

A calculation of the Lorenz ratio in the SCR framework was presented by Kambe *et al.* in the context of studies on CeNi<sub>2</sub>Ge<sub>2</sub> [56]. Because the SDW picture essentially assumes an underlying FL ground state, the WF law is expected to hold for  $T \rightarrow 0$ . This was calculated using the materials parameters of CeNi<sub>2</sub>Ge<sub>2</sub> and plotted for differing magnitudes of the ordering wavevector, showing a subtle variation in  $L/L_0$  of up to  $\sim 20\%$  from the WF expectation at higher temperatures (*i.e.*  $\sim 1$  K for the case of CeNi<sub>2</sub>Ge<sub>2</sub>).

The only other known prediction for the WF law was made by Senthil *et al.* for the case of a fractionalized FL state [57]. In this picture, charge conduction proceeds as in the normal FL state, but heat conduction would have an additional contribution from gapless spinons, thus causing the Lorenz ratio to be *in excess* of the WF law expectation at  $T \rightarrow 0$  [57].

---

---

# 3

---

---

## CEMIN<sub>5</sub> FAMILY

---

---

The discovery of the 115 system of compounds has brought a wealth of interesting phenomenon to the hands of experimental and theoretical physicists. The opportunity to study novel forms of magnetism, superconductivity and quantum critical phenomenon in extremely clean and stoichiometric materials has already motivated a large array of experimental data on these materials to be produced. In this chapter, a brief review of experimental data and theoretical conclusions is given, focusing on the properties relevant to our study.

The rich physics garnered in the 115 system of compounds finds its roots in the discovery of pressure-induced superconductivity in the so-called "parent" compound CeIn<sub>3</sub>, a material of simple cubic crystal structure which develops commensurate AFM order with  $\mathbf{Q}=[111]$  below  $T_N = 10.1$  K, albeit with a reduced moment of  $0.4 \mu_B$ . The ordering temperature in CeIn<sub>3</sub> can be driven to absolute zero by increasing applied pressure to  $P_c \simeq 26$  kbar, where superconductivity appears below  $T_c \simeq 200$  mK [19, 101], as shown in Fig. (3.1). The observed NFL properties (*e.g.*  $\Delta\rho(P_c) \propto T^{1.5}$ ) and behavior of  $T_N$  with pressure as a tuning parameter, together with a comparison to similar behavior found in CePd<sub>2</sub>Si<sub>2</sub>, led Mathur *et al.* to postulate that these systems possess magnetically-mediated superconductivity [19]. It is thought that such a superconducting phase can be enhanced by simultaneously increasing the bandwidth of the magnetic relaxation spectrum and decreasing the dispersion along one crystal axis via a reduced dimensionality.

In this light, it was not surprising that superconductivity was quickly discovered in a tetragonal version of CeIn<sub>3</sub>, namely CeRhIn<sub>5</sub> [102]. In this system, where the Ne  l temperature can also be reduced via applied pressure, superconductivity also appears above a critical pressure, but in this case with  $T_c = 2.1$  K, an order of magnitude larger than in CeIn<sub>3</sub>. This immediately prompted further searches for superconductivity in other quasi-2D variants of the cubic "parent" compound CeIn<sub>3</sub>, and led to the discovery of superconductivity at *ambient* pressure in CeIrIn<sub>5</sub> [103] and subsequently in CeCoIn<sub>5</sub>.

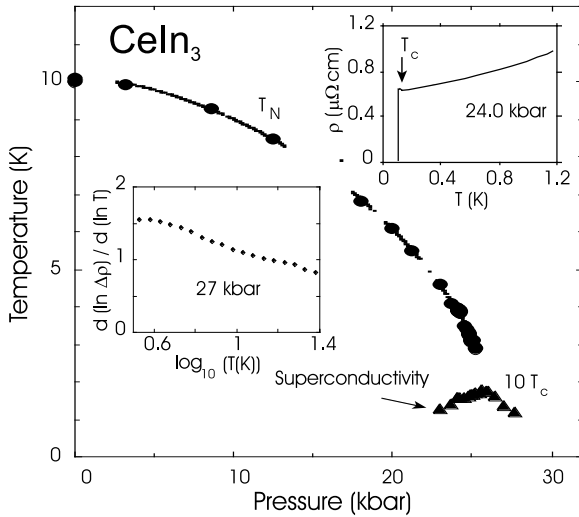


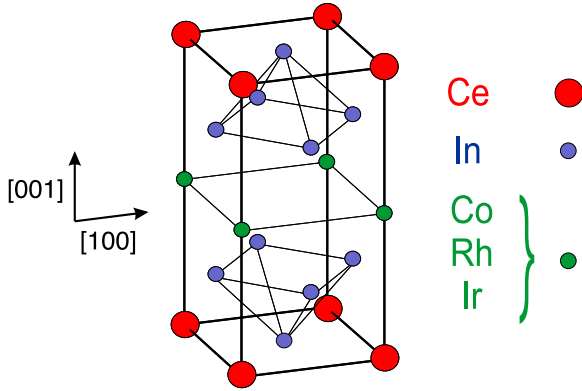
Figure 3.1: ( $P$ - $T$ ) phase diagram of CeIn<sub>3</sub> (from [19]).

[104]. These initial discoveries have motived further study of the general system CeMIn<sub>5</sub>, where M=Co, Ir, Rh and their alloys.

Superconductivity was recently discovered in PuCoGa<sub>5</sub> [105], a material with the same crystal structure as the 115's but with Pu and Ga in place of Ce and In, respectively, resulting in a transition temperature  $T_c = 18.5$  K which is *two orders of magnitude* larger than in CeIn<sub>3</sub>. Although the relation between these systems is not straightforward, it is widely believed that similar physics dictates the behavior throughout this general “115” series of compounds. The relationship between the Ce- and Pu-115 systems is being actively pursued and is only noted here.

### 3.1 Crystal Structure

CeMIn<sub>5</sub> has a primitive tetragonal HoCoGa<sub>5</sub> crystal structure that is composed of alternating layers of CeIn<sub>3</sub> and MIn<sub>2</sub> stacked sequentially along the [001] axis, as shown in Fig. (3.2). The lattice parameters are given in table (3.1), along with superconducting and magnetic transition temperatures. Although it is not presently clear what role dimensionality plays in determining the varying ground states in CeMIn<sub>5</sub>, a linear correlation between  $T_c$  and the anisotropy ratio  $c/a$  of lattice constants has been highlighted [106], suggesting a roughly consistent increase of the pairing potential with decreasing dimensionality. Furthermore, neutron powder diffraction experiments show that distortions of the CeIn<sub>3</sub> cuboctahedra are more apparent in CeCoIn<sub>5</sub> and CeIrIn<sub>5</sub> than in CeRhIn<sub>5</sub>, being qualitatively different in CeCoIn<sub>5</sub> [107]. This, together with the  $c/a$  vs.  $T_c$  re-

Figure 3.2: Crystal structure of CeMIn<sub>5</sub>.

	CeIn <sub>3</sub>	CeRhIn <sub>5</sub>	CeIrIn <sub>5</sub>	CeCoIn <sub>5</sub>
a [Å]	4.689(2)	4.652	4.688	4.614
c [Å]	-	7.542	7.515	7.552
c/a	1	1.621(1.624)	1.610	1.637
T <sub>c</sub> [K]	(0.2)	(2.1)	0.4 <sup>†</sup>	2.3
T <sub>N</sub> [K]	10.1	3.8	-	-

Table 3.1: Lattice parameters and transition temperatures of CeMIn<sub>5</sub> at ambient pressure and under applied pressure (values in brackets) as described in the text. Data is taken from [108], except for CeRhIn<sub>5</sub> (2.5 GPa) data which is from [109] (<sup>†</sup>bulk superconducting transition).

lation and the striking similarities between the superconducting states of CeCoIn<sub>5</sub> and CeRhIn<sub>5</sub> under pressure, certainly suggests an important connection between structural and electronic properties throughout this system. This is also reflected in the electronic band structure, as discussed below.

### 3.2 Ce(Co,Ir,Rh)In<sub>5</sub> Alloys

The ability to grow single-phase crystals of Ce(Rh,Ir,Co)In<sub>5</sub> alloys has allowed much insight into the competing and/or coexisting phases that exist in admixtures of the base compounds. Pagluso *et al.* were the first to map out such a phase diagram, revealing the rich interplay between superconducting and magnetic ground states in the 115 system, as shown in Fig. (3.3). This phase diagram immediately highlights the existence of QCPs which lie adjacent to the pure compounds in the alloying series, and are almost certainly responsible for many of the NFL properties in the 115 system, as will be discussed

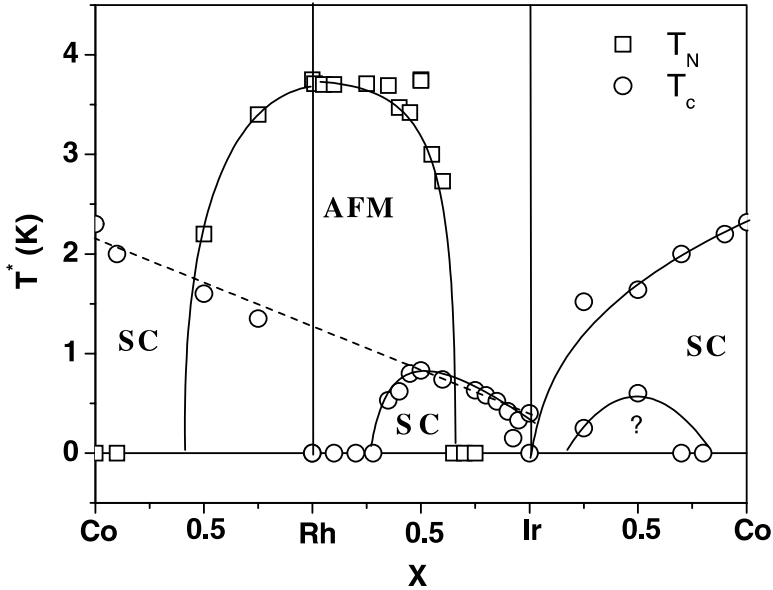


Figure 3.3: Ce(Co,Ir,Rh)In<sub>5</sub> alloy phase diagram (from [106]).

throughout this study.

### 3.3 Electronic Structure

The question of how structural dimensionality translates to the electronic properties of CeMIn<sub>5</sub> has been partially addressed by both band structure calculations and experimental studies of the Fermi surface as measured through the de Haas-van Alphen (dHvA) effect. In this system, an important aspect of the strong correlations that give rise to such interesting physics is in regard to the nature of the 4f electrons of the Ce ions: as shown in Section 3.4. large specific heat coefficients throughout the 115 series demonstrate the presence of heavily-renormalized *f*-electrons, but do not demonstrate how these electrons participate in conduction. In other words, are they itinerant or localized, and how does each picture relate to the different ground states throughout the 115 series?

A comparison between detailed dHvA measurements and band structure calculations has allowed a refinement of the understanding of the evolution of the electronic structure in the 115 series. In comparing measured dHvA cyclotron frequencies and their angular dependence on field orientation to band structure predictions, it is generally accepted that the Fermi surfaces in CeMIn<sub>5</sub> consist of multiple quasi-2D and 3D sheets associated with four to five bands crossing the Fermi level. The existence of quasi-2D sheets has been directly observed through the angular dependence of dHvA oscillations in a number

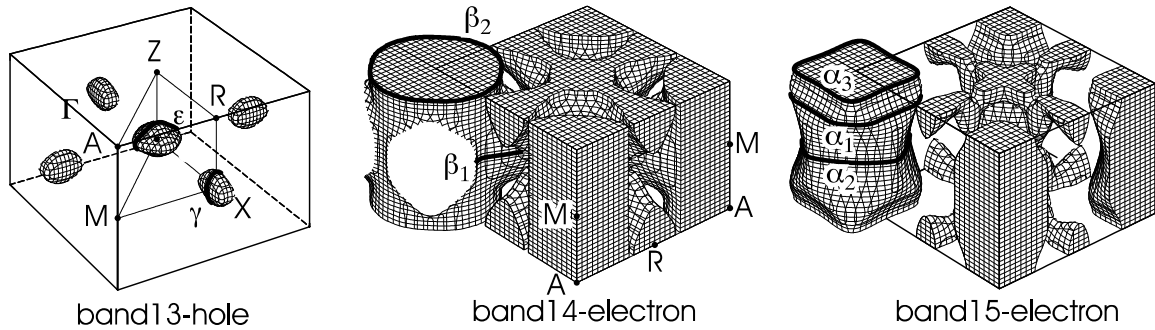


Figure 3.4: Fermi surfaces of CeCoIn<sub>5</sub>, with various observed cyclotron orbits shown. The center of the Brillouin zone is centered at the  $\Gamma$  point (from [111]).

of experiments [110, 111], and measured frequencies map on to various orbits quite well [111, 112].

Calculations using the relativistic linear augmented-plane-wave method in the *itinerant* 4f electron picture have shown that the Fermi surfaces for CeCoIn<sub>5</sub> and CeIrIn<sub>5</sub> are almost identical, as constructed from two electron and two hole bands crossing the Fermi energy [112].<sup>1</sup> These surfaces consist of multiple sheets associated with each band, taking the form of small 3D pockets, quasi-2D “monsters” and cylindrical geometries as shown in Fig. (3.4). Most predicted cyclotron orbits have been observed experimentally, but a number of frequencies have not been accounted for in either theory or measurement.<sup>2</sup> The cyclotron mass  $m^*$  can be determined from the temperature dependence of the dHvA signal amplitude associated with each orbit, and is expected to be quite large in HF systems. Observed values of  $m^*$  range up to  $\sim 6m_0$  for CeRhIn<sub>5</sub> [110],  $\sim 30m_0$  for CeIrIn<sub>5</sub> [113] and  $\sim 100m_0$  for CeCoIn<sub>5</sub> [111], where  $m_0$  is the free electron mass.

The enhanced cyclotron mass was studied as a function of magnetic field by tracking various orbits through the superconducting and field-induced normal states in CeCoIn<sub>5</sub> [111]. Amazingly, a number of orbits exhibit a large mass increase as fields are lowered toward  $H_{c2}$  of either orientation (see Section 3.4), as shown in Fig. (3.5). The “ $\beta$ ” orbits, associated with the quasi-2D sheets shown in Fig. (3.4), show the most divergent behavior, but smaller mass enhancement is also seen in the “ $\alpha$ ” orbits associated with the cylindrical sheets. The “ $\epsilon$ ” orbit, associated with the small 3D hole pockets of band-13, displays a field-independent value which is also observed deep into the superconducting

<sup>1</sup>The study of Maehira *et al.* also concluded that any differences between CeCoIn<sub>5</sub> and CeIrIn<sub>5</sub> must arise on a small energy scale that would not affect the band structure calculation (*i.e.* crystal field effects).

<sup>2</sup>This is especially true in CeRhIn<sub>5</sub>, where an abundance of frequencies have been observed [110].

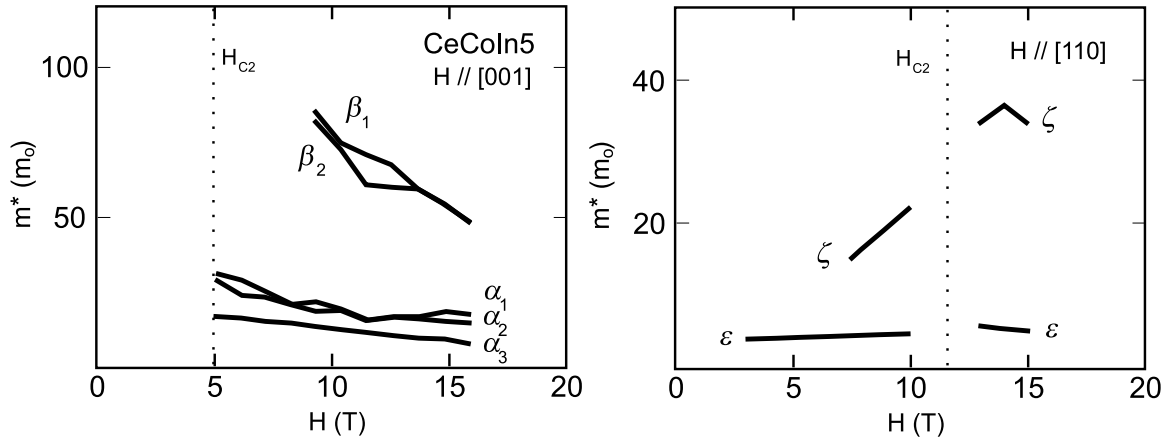


Figure 3.5: Field dependence of  $m^*$  in CeCoIn<sub>5</sub> (from [111]).

state, down to  $\sim 0.2H_{c2}$  [111].<sup>3</sup> Note that a recent study by McCollum *et al.* has shown that a marked deviation from conventional Lifshitz-Kosevich behaviour, usually used to extract effective mass values, occurs down to the lowest measured temperatures in CeCoIn<sub>5</sub> [115]. This behaviour suggests that the field dependence of  $m^*$  is not simple and may contain a complicated multi-component dependence.

In the case of CeRhIn<sub>5</sub>, initial investigations [116] concluded that the Fermi surfaces were very similar to those of CeIrIn<sub>5</sub>, but a number of subsequent experiments have questioned the itinerant character of the  $f$  electrons. A direct comparison [110] of the angular dependence of various dHvA frequencies has shown that the measured Fermi surface of CeRhIn<sub>5</sub> is more comparable to that of LaRhIn<sub>5</sub> (which has no  $f$  electron character due to the absence of Ce) than to that of CeCoIn<sub>5</sub>, thus leading Shishido *et al.* to conclude that the contribution of the  $4f$  electrons to the volume of the Fermi surface in CeRhIn<sub>5</sub> is negligibly small. Furthermore, photoemission studies have shown both itinerant [117] and localized [118] behavior in CeIrIn<sub>5</sub> (although both studies were performed at high temperatures of  $\sim 30$  K, so it is not clear how this reflects the ground state). Calculations using density functional theory [119] suggest that the  $f$  electrons are on the border between localization and itinerancy in all 115's. The most convincing evidence was found in a dHvA study of Ce<sub>x</sub>La<sub>1-x</sub>RhIn<sub>5</sub> [120], which showed that diluting the Ce lattice does not have any significant effect on the observed cyclotron orbits. This indicates that the  $f$  electrons in CeRhIn<sub>5</sub> are truly localized, in line with the conclusions

<sup>3</sup>Although such behavior in other type-II superconductors has been associated with vortex-state physics [114], the survival of the dHvA signal down to such low fields cannot be dismissed as a simple vortex state effect.

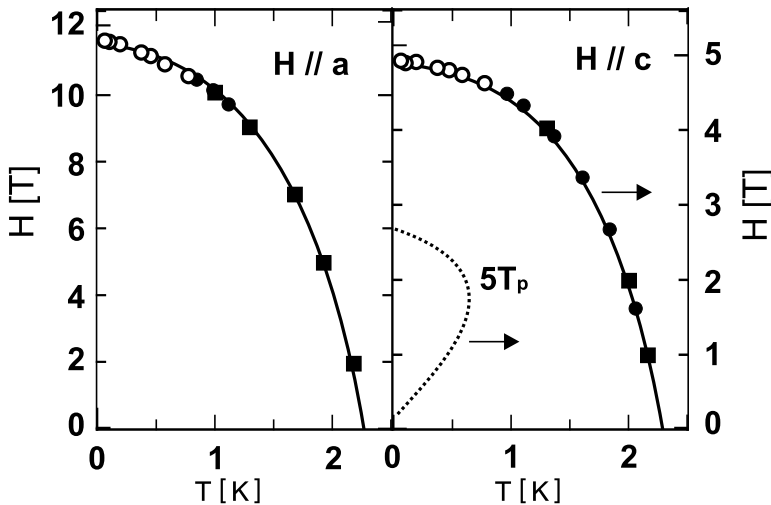


Figure 3.6:  $H$ - $T$  critical field phase diagrams of CeCoIn<sub>5</sub> for both  $H \parallel a$  and  $H \parallel c$  orientations. Circles and squares denote  $H_{c2}$  from magnetization data. Open circles denote first-order transition. Dotted line indicates the position of hysteresis peaks observed in magnetization at temperatures  $T_p$  (from [122]).

of Shishido *et al.*.

Finally, note that the pressure dependence of the dHvA signals in CeRhIn<sub>5</sub>, as it is driven into a superconducting state very similar to that in CeCoIn<sub>5</sub> (at ambient pressure), shows a large increase in  $m^*$  toward values similar to those found in CeCoIn<sub>5</sub> [121]. This is yet another comparable feature between the superconducting states in each system.

### 3.4 Thermodynamic Properties

#### 3.4.1 Upper Critical Fields

As shown in Fig. (3.6), a DC magnetization study [122] has mapped the position of the upper critical field  $H_{c2}$  of CeCoIn<sub>5</sub> for both  $H \parallel a$  and  $H \parallel c$  orientations. Estimates of the orbital limiting field for each orientation, as obtained from the slope of  $H_{c2}$  at  $T_c$ , are much greater than the observed values indicating that  $H_{c2}$  is strongly suppressed in CeCoIn<sub>5</sub> by Pauli paramagnetism. The factor of  $\sim 2$  anisotropy of  $H_{c2}$  with respect to field orientation has been attributed to the anisotropy in the electronic system [110, 123]. In addition, an anomalous peak effect in magnetization has been observed [110, 123] in the superconducting state at low temperatures and near  $\sim 2$  T, and remains unexplained.

The most striking characteristic of  $H_{c2}$  is the presence of a *first-order* transition below  $\sim 1$  K for both field orientations, as observed in magnetization [122, 123], specific heat, thermal expansion and magnetostriction [124], and most readily in thermal conductivity

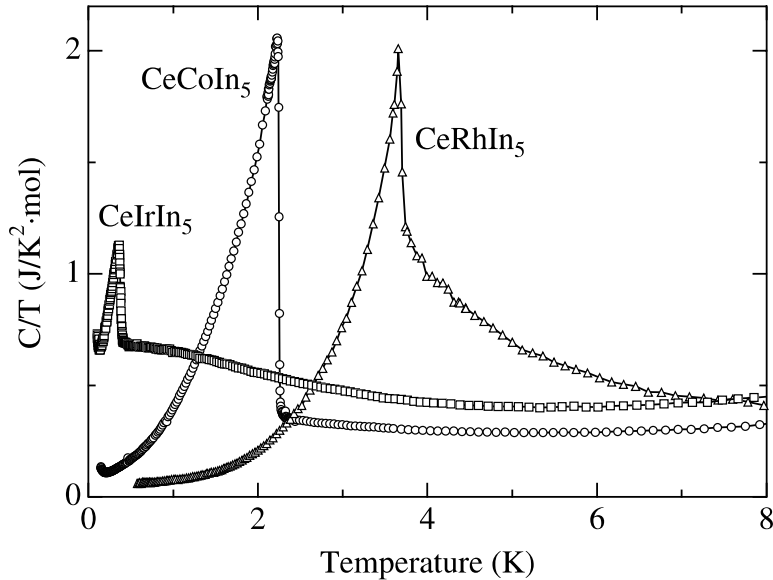


Figure 3.7: Specific heat of CeMIn<sub>5</sub> (from [110]).

measurements [125]. A first-order transition is predicted to occur in the Pauli paramagnetically limited superconducting state (See *e.g.* Ref. [122] and references therein), but this behavior has also been linked to the possible presence of a Fulde-Ferrel-Larkin-Ovchinnikov (FFLO) phase [122, 123, 126, 127].

### 3.4.2 Specific Heat

As shown in Fig. (3.7), there are distinct specific heat anomalies at the transition temperatures of each compound in the 115 series, occurring at  $T_c$  for CeCoIn<sub>5</sub> and CeIrIn<sub>5</sub>,<sup>4</sup> and at  $T_N$  for CeRhIn<sub>5</sub>, all indicating the bulk nature of these transitions.<sup>4</sup>

The specific heat jump at the superconducting transition can be related to the BCS weak-coupling gap, which predicts a value of  $\Delta C/\gamma T_c = 1.43$ . The jump in CeIrIn<sub>5</sub> and CeCoIn<sub>5</sub> was found to be 0.76 and 4.5, respectively [110], being slightly small in the first case and very large in the second case as compared to the BCS prediction. The large value of  $\Delta C/\gamma T_c$  may indicate strong coupling, but another scenario was suggested involving coupling between the superconducting order parameter and fluctuating magnetic moments [129]. At lower temperatures, power laws observed in the superconducting state of both CeCoIn<sub>5</sub> and CeIrIn<sub>5</sub> [130] are part of a number of observations suggesting unconventional superconductivity with a nodal structure.

<sup>4</sup>Although a zero-resistance state is observed at 1.2 K [103], the bulk superconducting transition in CeIrIn<sub>5</sub> only occurs at 0.4 K. This bulk  $T_c$  is also known to *increase* with applied pressure [128].

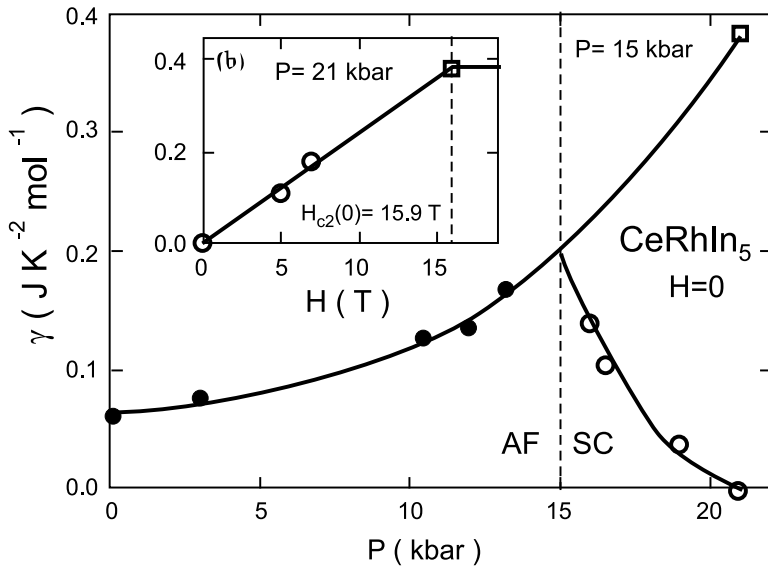


Figure 3.8: Evolution of  $\gamma_0$  with pressure in CeRhIn<sub>5</sub> (from [133]).

Evidence for the anomalous dichotomy of magnetic and superconducting electrons was shown in a number of studies. In a study of CeRh<sub>1-x</sub>Ir<sub>x</sub>In<sub>5</sub> alloys, Pagluso *et al.* have shown that the total magnetic entropy, as extracted from low temperature specific heat measurements, does not change as a function of alloying (*i.e.*  $x$ ) [131]. This behaviour was also observed in CeRh<sub>1-x</sub>Co<sub>x</sub>In<sub>5</sub> alloys [132], indicating that throughout the 115 system *the same 4f electrons form both AFM and SC ground states*. This behavior was most convincingly shown in a pressure study on CeRhIn<sub>5</sub> [133], where the ambient pressure AFM ground state can be gradually transformed into a superconducting state, passing through a coexistent region as the pressure is increased. As shown in Fig. (3.8), the residual electronic component  $\gamma_0$  shows a smooth evolution from one state to the other, with the fraction of electrons involved in Cooper pairing steadily increasing with pressure.

### 3.5 Magnetic Properties

The long-range magnetic order that appears in CeRhIn<sub>5</sub> at ambient pressure can be continuously tuned away, either by alloying (Fig. (3.3)) or pressure (Fig. (3.8)). Thus it is not surprising to find large susceptibilities in CeCoIn<sub>5</sub> and CeIrIn<sub>5</sub>, which appear to be on the verge of long-ranged order. The magnetic properties of the 115 series have been somewhat well-characterized, but not completely mapped out. However, because all members of this series are closely related, one can draw a number of conclusions based on available data.

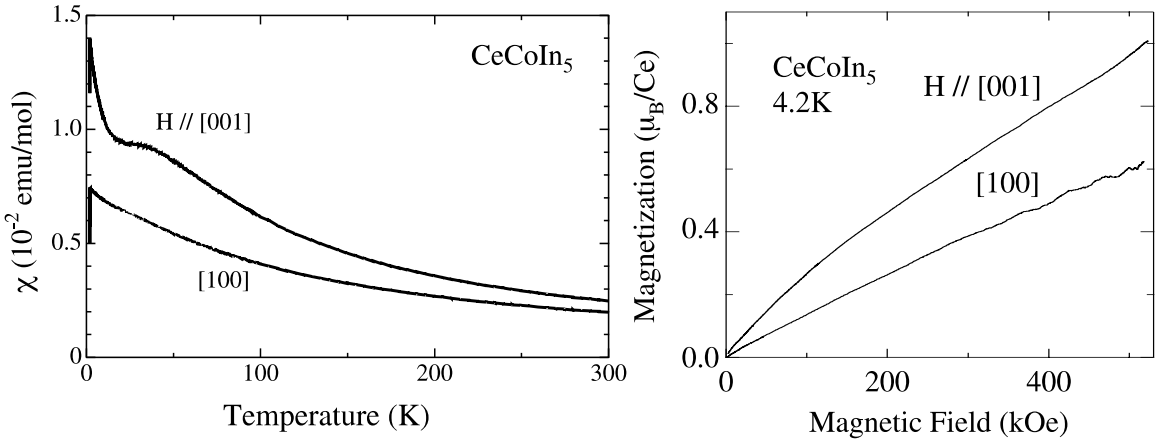


Figure 3.9: Susceptibility and magnetization in CeCoIn<sub>5</sub> (from [110]).

### 3.5.1 Susceptibility

The susceptibility  $\chi(T)$  of CeCoIn<sub>5</sub> is shown in Fig. (3.9), along with magnetization  $M(H)$  in high fields. As a function of temperature,  $\chi(T)$  shows an anisotropy depending on field orientation, showing a continuous increase for  $H \perp [001]$  and a sign of saturation below  $\sim 50$  K for  $H \parallel [001]$  (the latter being somewhat typical of a HF metal). However, below  $\sim 25$  K the susceptibility for  $H \parallel [001]$  continues to increase down to where it abruptly changes due to the onset of superconductivity at  $T_c$ . Similar anisotropic behaviour is observed in CeIrIn<sub>5</sub> (although less pronounced) [103, 134], whereas a maximum in  $\chi(T)$  is observed near 8 K in CeRhIn<sub>5</sub> for both field orientations [102, 134], with a decrease at lower temperatures.

Above the shoulder at  $\sim 50$  K,  $\chi(T)$  in CeCoIn<sub>5</sub> and CeIrIn<sub>5</sub> is well-described by the effects of crystalline electric fields based on a 4f-level scheme [110, 122, 135], and the shoulder itself may be due to the onset of coherence of the Kondo lattice [136] (also observed in resistivity - see below). But the continual *increase* below 25 K finds no explanation from either of these phenomena - it has largely been classified as a NFL effect arising from the proximity of a QCP [20]. Note that the same shoulder is also observed in higher fields, but with a suppression of the increase below 25 K [122], suggesting that the low temperature behaviour may indeed be attributed to *quantum critical fluctuations which can be suppressed by field*. In this scenario, the absence of the shoulder in  $H \perp [001]$  data may be an indication of the anisotropy of spin fluctuations. Clearly, more studies of  $\chi(T)$  are required, especially in high fields and low temperatures (where superconductivity is suppressed).

Finally note that the continual increase of magnetization of CeCoIn<sub>5</sub> up to  $\sim 50$  T

is similar to that observed in CeIrIn<sub>5</sub> [134], showing no obvious sign of field-induced ferromagnetic (FM) order. Similar behaviour is also observed in CeRhIn<sub>5</sub>, but with signs of saturation at the highest fields (near  $\sim 50$  T) [134]. The absence of saturation in  $M(H)$  until at least  $\sim 50$  T suggests that the strength of AFM correlations is strong in all three compounds, even in the absence of long-range AFM order.

### 3.5.2 Spin Resonance and Neutron Scattering

Nuclear magnetic resonance (NMR) experiments [137] probing the spin relaxation rate  $1/T_1$  of the planar In(1) nuclei have been used to probe the low frequency spin dynamics of CeCoIn<sub>5</sub>. Curro *et al.* have shown that  $1/T_1$  is dominated by *local* fluctuations of the Ce moments above  $\sim 40$  K, and influenced by a momentum- and temperature-dependent component of fluctuations below. This latter component was associated with the presence of *itinerant* Ce 4f (heavy) electrons. Furthermore, the temperature dependence of  $1/T_1$  at low temperatures suggests that the AFM fluctuations are 2D in nature [137]. A similar conclusion was drawn by Kawasaki *et al.* using both NMR and nuclear quadrupole resonance (NQR) measurements on both the In and Co nuclei [138], which suggest that in-plane magnetic correlations are stronger than out-of-plane correlations in CeCoIn<sub>5</sub>.

NQR measurements [139] on the In nuclei of CeRhIn<sub>5</sub> were of the first to show that the AFM order which onsets below  $T_N = 3.8$  K is consistent with a helical spiral structure of the Ce moments that is incommensurate with the crystal lattice. This was definitively confirmed by neutron scattering measurements, which identified the AFM incommensurate ordering wavevector  $Q = [1/2, 1/2, 0.297]$  [140]. Above the ordering temperature, both NMR [137] and neutron scattering [140] measurements suggest that the AFM correlations which result in the ordered state below  $T_N$  are anisotropic, but 3D in nature (as opposed to the more 2D nature of correlations in CeCoIn<sub>5</sub>).

The evolution of the incommensurate nature of magnetic ordering in CeRhIn<sub>5</sub> has been investigated using neutron scattering of both CeRhIn<sub>5</sub> [141] and its two-layer version Ce<sub>2</sub>RhIn<sub>8</sub> [142]. In the former, the pitch of the spiral wavevector was shown to be essentially insensitive to pressure up to the applied pressure that destroys magnetic order and invokes superconductivity [141], suggesting that pressure does not gradually change the nature of magnetic order, but rather induces an abrupt change in the magnetic interaction of the Ce moments. In the latter, a neutron scattering study of Ce<sub>2</sub>RhIn<sub>8</sub> has shown that the AFM order which sets in below  $T_N = 2.8$  K is commensurate with an ordering wavevector  $Q = [1/2, 1/2, 0]$  [142]. Furthermore, the field-temperature phase

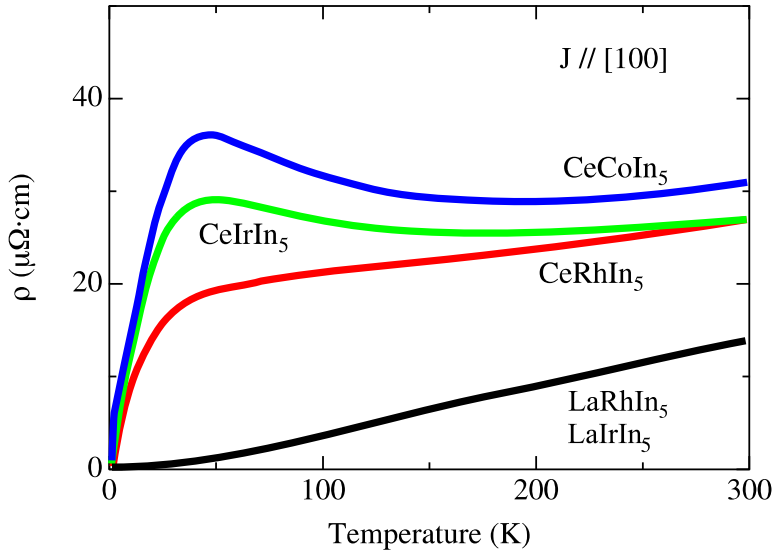


Figure 3.10: Resistivity of CeMIn<sub>5</sub> (from [110]).

diagram of CeRhIn<sub>5</sub> displays a rich behavior as a function of applied field, with at least three separate phases identified by specific heat transitions which appear to be very similar in both CeRhIn<sub>5</sub> and Ce<sub>2</sub>RhIn<sub>8</sub> [143].

## 3.6 Transport Properties

Although the study of transport is the main focus of this study, a brief review of resistivity in zero applied field and pressure is given here. Fig. 3.10 shows a comparison of the temperature dependence of resistivity in all 115 compounds, together with two of the non-magnetic analogs (where La is completely substituted for Ce).

### 3.6.1 Resistivity

The resistivity of the La compounds shows conventional metallic behaviour: quadratic  $T$ -dependence indicative of a FL regime at low temperatures, and linear  $T$ -dependence at higher temperatures (above  $\sim 50$  K) as expected for phonon scattering [62]. The low residual resistivities - 0.01 and 0.04  $\mu\Omega \cdot \text{cm}$  in LaIrIn<sub>5</sub> and LaRhIn<sub>5</sub>, respectively [110] - indicate the extremely low level of impurities in these compounds, which is quite astonishing for ternary systems.

As shown in Fig. (3.10), the resistivity of the Ce compounds exhibits different behaviour, with little or no  $T$ -dependence near room temperatures followed by a peak and/or dramatic decrease upon cooling. This form is typical of HF systems, and is generally

attributed to a crossover between incoherent scattering at high temperatures and the development of a coherent HF state at lower temperatures. The so-called *coherence peak* near  $T_{\text{coh}} \simeq 45$  K in all of the 115 compounds<sup>5</sup> can be associated with this crossover.

An analysis of this crossover behaviour in both transport and specific heat has been done in a study by Nakatsuji *et al.*, where the dilution of magnetic Ce ions by La (non-magnetic analog) allows one to study the nature of intersite interactions by dilution of the “Kondo lattice” [136]. This study concluded that all energy scales in CeCoIn<sub>5</sub> are well separated, associating the lowest energy scale with a Kondo temperature  $T_K = 1.7$  K and  $T_{\text{coh}} \simeq 45$  K with the intersite AFM coupling energy scale. The evolution of the Kondo lattice properties were further analyzed using a *two-fluid* description [144], indicating that the single-site Kondo impurities undergo a condensation into a HF state at low temperatures. Interestingly, this study concluded that this condensation remains incomplete, leaving 5% and 10% of the “Kondo gas” uncondensed (*i.e.* unscreened) in CeIrIn<sub>5</sub> and CeCoIn<sub>5</sub>, respectively. The impact of this interpretation on the low temperature properties remains unclear.

### 3.6.2 Thermal Conductivity

Two thermal conductivity studies have been performed on these systems. A low temperature study by Movshovich *et al.* concluded that an unconventional superconducting gap with line nodes is present in both CeIrIn<sub>5</sub> and CeCoIn<sub>5</sub> based on the existence of power law behaviour in  $\kappa(T)$  in the superconducting state (zero field) [130]. A subsequent study by Izawa *et al.* measured  $\kappa(T)$  as a function of magnetic field rotation within the basal plane of CeCoIn<sub>5</sub> [125]. This study revealed a fourfold symmetry of  $\kappa$  in the basal plane, which was concluded to be the result of a superconducting gap with nodes along the  $(\pm\pi, \pm\pi)$  directions. In addition, this study also revealed the first evidence of a first-order superconducting transition (as discussed above) below 1.0 K, as revealed by a jump in  $\kappa(H)$  at  $H_{c2}$ .

Although the current study is not concerned with the specific nature of the superconducting state of CeCoIn<sub>5</sub>, it is important to note that there are some conflicts found in these studies. First, a recent study [145] of specific heat as a function of magnetic field rotation within the basal plane of CeCoIn<sub>5</sub> has also found a clear fourfold oscillation of the specific heat which is consistent with the observation of a fourfold symmetry in the

---

<sup>5</sup>There is no absolute maximum in CeRhIn<sub>5</sub>, but strong curvature near  $T_{\text{coh}}$  is evident. Furthermore, the application of hydrostatic pressure shows that a peak emerges near  $T_{\text{coh}} \simeq 30$  K [102].

thermal conductivity study of Izawa *et al.* [125]. However, the conclusions about the location of gap nodes from each study are in conflict, with a 45° offset between the two proposed symmetries. This discrepancy is unresolved, but may be a result of the presence of a group of *uncondensed* carriers in the superconducting state of CeCoIn<sub>5</sub> [146]. Second, the residual electronic thermal conductivity  $\kappa_0/T$  of CeCoIn<sub>5</sub> measured by Movshovich *et al.* in zero field [130] is many times smaller than that observed in two other studies [125, 146]. Since this quantity is a measure of the contribution of nodal quasiparticles (see *e.g.* Ref. [75]), its value has a significant impact on the determination of the nature of the superconducting gap. It is currently thought [146] that the anomalously low residual value observed by Movshovich *et al.* may be due to an extrinsic effect similar to that believed to cause the observed [96]  $T \rightarrow 0$  WF law violation in the cuprate superconductor Pr<sub>2-x</sub>Ce<sub>x</sub>CuO<sub>4</sub> - see Ref. [97] and Appendix C.2 for a discussion of this effect.

## EXPERIMENTAL TECHNIQUES

---

---

The experimental techniques used to obtain the data presented in this thesis involved careful, systematic measurements of heat and charge transport spanning temperatures down to 25 mK and magnetic fields up to 18 T. These experiments were performed using a variety of commercial and custom electronics, apparatus and software, incorporating and building on a wealth of prior knowledge and fine-tuning due to the work of various graduate students and postdoctoral fellows working with the same equipment.

In this chapter, a detailed report of procedures followed in sample preparation for transport experiments will be given, followed by a brief summary of the techniques and apparatus utilized. For comprehensive information on the standard techniques and equipment that have been developed and used in the Taillefer group, the reader is referred to the dissertations of E. Boaknin [76] and C. Lupien [147].

### 4.1 *Sample Preparation*

The most crucial aspect of any condensed matter experiment is of course the specimen on which experiments are performed. Through the course of this study, a procedure has been developed to prepare small, oriented single-crystal samples (provided by the crystal grower) for standard four-wire transport measurements, optimizing the sample geometry for low noise and maximizing the sample-wire contact conductance. This procedure, involving isolating a proper specimen, optimizing its geometry and attaching proper measurement wires, is reported below.

#### 4.1.1 *Etching and Cleaving*

The growth of 115 single-crystal specimens, performed in an In flux, was reported in detail elsewhere [104]. This procedure typically produces a growth of well-separated, faceted platelets (with large area surface parallel to the [001] crystal axis) with a characteristic

size  $3\text{ mm} \times 3\text{ mm} \times 0.1\text{ mm}$ , but small, rectangular parallelepiped-shaped crystals also grow.<sup>1</sup>

Proper size platelets are usually simple to isolate from a growth batch, either by etching an intergrowth complex to separate, or by mechanically separating specimens with tweezers. Once isolated, samples can be either cleaved or polished to attain a proper geometry (*i.e.* long and slim, with large separation between voltage contacts): for  $J \parallel [100]$  or  $J \parallel [110]$  geometry, platelet specimens are cleaved if necessary; for  $J \parallel [001]$  geometry, the polishing of a cube is necessary since  $[001]$  axis-oriented platelets do not grow readily. Samples must then be etched in acid to remove excess In flux from the surfaces,<sup>2</sup> and cleaned as described below.

#### *Preparation Procedure:*

- Remove appropriate size platelet or cube from intergrowth complex (etching or polishing<sup>3</sup> a large intergrowth complex if necessary).
- Cleave to appropriate geometry by using sharp, straight razor blade pressed to flat sample on glass slide and “tapping” with light weight to induce cleave.
- Etch sample in bath of pure or diluted<sup>4</sup> HCl for 60 min or until visibly free of In flux on surface.
- Wash thoroughly with ethanol several times to remove any remnant HCl.
- Prepare for wire/contact application immediately.

---

<sup>1</sup>Rather large cube-type specimens ( $\sim 1\text{ cm}^3$ ) have been grown that appear to be single crystals, most readily for the case of CeRhIn<sub>5</sub>. Note that these are typically composed of inner intergrowths, and proper polishing and investigation was performed to verify single growth samples were used in this study.

<sup>2</sup>Care must be taken to remove excess In from the surface of samples, since it can contaminate resistivity measurements (*i.e.* by shorting out a portion of the surface impedance below the superconducting transition temperature of In ( $T_c \approx 3\text{ K}$ )).

<sup>3</sup>These crystals can be readily polished with  $\sim 1000$  grit SiC paper by securing a specimen to a proper polishing jig with Loctite 404 adhesive and/or Crystalbond mounting adhesive, and subsequently detaching it by dissolving in acetone.

<sup>4</sup>For CeCoIn<sub>5</sub>, use pure concentration; for CeRhIn<sub>5</sub>, use  $\sim 50\%$  H<sub>2</sub>O dilution and shorter time interval because of stronger reaction

### 4.1.2 Contact Methods

Four-wire contacts were made to each sample using either 25  $\mu\text{m}$  or 50  $\mu\text{m}$  pure Ag or annealed<sup>5</sup> Pt wire, depending on sample size, attached with a conductive adhesive. Due to the high conductivity of these materials, a highly conductive contact between sample and probe wire is required to minimize 1) self-heating effects in low- $T$  resistivity measurements, and 2) electron-phonon decoupling in low- $T$  thermal conductivity measurements (see Appendix C.2). Several contact methods were attempted, resulting in a range of contact resistances ( $R_c$ ) measured at low temperatures. Methods resulting in  $R_c \simeq 0.5\text{-}1 \Omega$  included the following:

- Attach wires with Dupont 4929N Ag conductive paint.
- Au evaporation of contact pads; attach wires with Ag paint.
- Epo-Tex H20E Ag epoxy cured<sup>6</sup> at  $\sim 100^\circ\text{C}$  for  $\sim 24$  hrs.
- pure Ga metal (does not “wet” to sample surface very well).
- In-Ga eutectic/alloy with Ag paint for mechanical stability.

A typical prepared sample size of  $\sim 1 \text{ mm} \times 0.2 \text{ mm} \times 0.1 \text{ mm}$  results in typical sample resistances of  $< 10 \text{ m}\Omega$  at low temperatures for CeCoIn<sub>5</sub> and even less for CeRhIn<sub>5</sub>.<sup>7</sup> Because of this, the contact-making methods quoted above result in a contact-to-sample resistance ratio that is much too high for proper thermal transport measurements below 1 K (for a detailed comparison of this effect, see Appendix C.2). To improve this situation, another method was utilized involving soldering the Ag wires to samples using pure indium,<sup>8</sup> resulting in  $R_c \simeq 5 \text{ m}\Omega$  at low temperatures. Because In is one of the formula units in the CeMIn<sub>5</sub> system, this method provides a completely natural and compatible contact between probe wires and sample, and is described below.

<sup>5</sup>Annealing Pt wire under a flame increases its malleability, thus reducing the danger of damaging contacts during sample manipulation.

<sup>6</sup>Note that the low melting point of indium does not allow the proper curing temperatures for this epoxy to be achieved without causing degradation of the sample - the maximum allowable curing temperature was found to be  $\sim 200^\circ\text{C}$ .

<sup>7</sup>Due to the extremely high conductivity of CeRhIn<sub>5</sub> at low temperatures, a special sample was prepared to extend over 4 mm in length, thus increasing the absolute resistance and facilitating both heat and charge transport measurements.

<sup>8</sup>In wire used for high-vacuum seals is adequate.

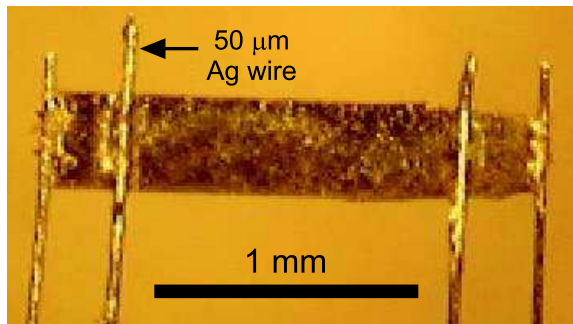


Figure 4.1: CeCoIn<sub>5</sub> sample with In-soldered leads.

### Soldered Contacts

After etching specimens in HCl, a small amount of aggressive flux<sup>9</sup> is applied to contact areas before soldering to improve “wetting” and to help control the flow of melt. To solder the wire leads to these areas, a fine-tipped soldering iron is utilized, controlling its temperature to  $\sim 200^{\circ}\text{C}$ .<sup>10</sup> A small amount of indium is first used to coat the tip of each Ag wire, which is subsequently positioned to touch the sample at the (flux-wetted) contact area. By gently applying heat to the lead wire close to (but not directly on) the sample, either by direct contact with the iron or through a small “indium tip” extension of the iron tip, the lead wire is then soldered to the sample under close visual monitor. After all leads are soldered, the sample should sit in a bath of ethanol for  $\sim 30$  min to dissolve any residual soldering flux.

As in the case of bad electrical contacts (Section C.2), there is some concern about using a superconducting material to solder the probe wires to the sample, since a (*s*-wave) superconductor is a perfect thermal (electronic) insulator at zero temperature. Although this method can complicate the interpretation of zero-field measurements at the lowest temperatures, the majority of results presented in this study involve measurements in magnetic fields well above that of the critical field of pure indium. In the case of zero-field (superconducting state) measurements, the effect of this method was tested by sweeping the magnetic field through a small range, from negative to positive, through  $H = 0$ .

### Geometric Factor

After contacts are made, a sample’s geometric factor  $\alpha = A/L$  (where  $A$  is the cross-sectional area and  $L$  is the length between voltage contacts) is measured using a high

<sup>9</sup>Kester 2164 water soluble soldering flux.

<sup>10</sup>The melting point of pure In is  $156.6^{\circ}\text{C}$ .

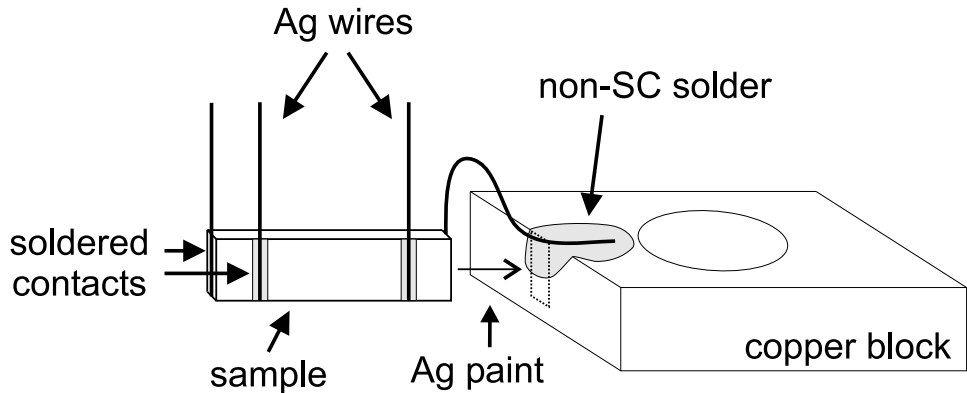


Figure 4.2: Copper block sample mount.

precision optical microscope and ruled length standard (with  $20\ \mu\text{m}$  divisions). The value of  $L$  was obtained by averaging the distances between outside and inside edges of voltage pads, and the error estimated by the width of the pads (typically  $50 - 100\ \mu\text{m}$ ). The error associated with  $A$  was, for most cases, dictated by the resolution of the ruler observable under the microscope, which is  $\pm 0.004\ \text{mm}$ . The errors in  $\alpha$  ranged from 5 - 15%, but for almost all samples studied the typical error in this measurement was 10%.

### Sample Mounting

For all low temperature measurements, samples with four-wire contacts were mounted on small Cu blocks for easy positioning and compatibility with the various cryogenic tails. To achieve a good thermal and electrical contact between the sample and Cu block (and subsequently the experimental stage), the “ground” lead of the sample can be attached to the block using either non-superconducting solder or Ag epoxy, as shown in Fig. (4.2). After attaching and positioning the sample next to the block, a small amount of Ag paint can then be applied between the sample and block to improve mechanical stability and reduce vibration.

## 4.2 Cryogenic Techniques

The concept of cooling an experiment to liquid He temperatures is rather simple: the use of a liquid cryogen (*i.e.*  $^4\text{He}$ ) makes it fairly straightforward to carry out an experiment at the constant temperature of the cryogen’s boiling point<sup>11</sup> by simply submersing an experiment in the liquid. The next step, which involves adjusting the temperature either

<sup>11</sup>For example, at ambient pressure the boiling points of  $^4\text{He}$  and nitrogen are 4.2 K and 77 K, respectively.

above or below this boiling point, involves either heating or cooling the experiment from this fixed point. In practice, controlling the temperature of an experiment involves manipulating a subtle interplay between cooling power, heating power and thermal links between these sources/sinks, the experiment and the room temperature environment. For more information on low temperature techniques, including cooling methods, cryogenic engineering, etc., see [148, 149, 150, 151].

The experiments for this study were performed in a number of different cryostats, including a custom  $^4\text{He}$  “dipper” system ( $1.5\text{ K}$ ), and three Oxford Instruments systems, including a *Heliox*  $^3\text{He}$  cryostat ( $0.3\text{ K}$ ) and two *Kelvinox*  $^3\text{He}/^4\text{He}$  dilution refrigerators (models 300 and 400;  $40\text{ mK}$  and  $25\text{ mK}$ , respectively). Resistivity measurements were performed in all cryostats, covering a temperature range  $25\text{ mK} < T < 300\text{ K}$ , whereas thermal conductivity measurements were performed using one dilution fridge for  $50\text{ mK} < T < 4\text{ K}$ , and the dipper fridge for  $1.5\text{ K} < T < 100\text{ K}$ . Below, a brief review of cryogenic techniques will be presented, focusing on the systems used in this study. For more detailed information on these particular systems and the procedures involved in conducting experiments, please see [76, 147].

#### 4.2.1 $^4\text{He}$ and $^3\text{He}$ Refrigeration

The most straightforward method of controlling temperature involves placing an experiment inside a vacuum-pumped container and submersing the assembly into liquid  $^4\text{He}$ . If the vacuum can system is properly designed, a weak thermal link between experiment and surrounding environment (cryogen) can provide a slow cooling rate upon submersion, and an experimental quantity (*e.g.* resistivity, which requires a measurement time on the order of seconds) can be measured while continuously cooling the experiment toward  $4.2\text{ K}$ . It is possible to cool below this temperature by pumping on the cryogen bath, which reduces the vapor pressure of the cryogen by effectively removing the more energetic particles. A more efficient method is to pump on a small volume of cryogen liquid contained in an enclosure which is part of the cryostat (*i.e.* isolated from the main bath). This is the basis for the cryostat designs discussed below.

##### $^4\text{He}$ Dipper Cryostat ( $1.5\text{ K} < T < 300\text{ K}$ )

This cryostat utilizes a simple design [152] which allows for efficient cooling and a fast turn-around time. The procedure involves submersing or “dipping” a small, vacuum-pumped assembly into a large bath of liquid  $^4\text{He}$  (contained in a large storage dewar),

and controlling the temperature through the use of an attached heater and a  $^4\text{He}$  cooling stage. This stage utilizes a “1 K pot,” or a continuous fill  $^4\text{He}$  pot which is pumped on using an external pumping line in order to reduce the pressure, and hence the temperature of the liquid inside the pot down to  $\sim 1.5 \text{ K}$ .<sup>12</sup>

This technique is often used as an initial cooling stage in more elaborate cryostats, as discussed below (*e.g.* see Fig. (4.4)), but in this case it is the coldest point of the assembly. Hence, the experiment<sup>13</sup> is placed on a highly conductive copper “tail” which is attached directly to the 1 K pot,<sup>14</sup> and temperature control is achieved by balancing the cooling power of the pot and the heating power of a resistance heater placed on the pot. The dipper is also very suitable for higher temperature experiments, since the simple design allows for a slow and steady cooling rate to be achieved from room temperature down to  $\sim 10 \text{ K}$  - see Section 4.3.

### $^3\text{He}$ Heliox Cryostat ( $0.3 \text{ K} < T < 300 \text{ K}$ )

A  $^3\text{He}$  system uses the same concept as discussed previously, but achieves much lower temperatures by reducing the pressure of a volume of  $^3\text{He}$  liquid. Temperatures down to  $\sim 300 \text{ mK}$  can be achieved due to the different weight and statistics of the  $^3\text{He}$  isotope. Because  $^3\text{He}$  is much more rare than  $^4\text{He}$ , it is also much more expensive, so these systems typically entail a closed-cycle pumping system. In the case of the Heliox fridge, the closed-cycle system uses an adsorption pumping system, which cycles the  $^3\text{He}$  between a “ $^3\text{He}$  pot” and a gas-adsorbing volume, or “sorb,” using intermediate  $^4\text{He}$  cooling stages. Temperature control is obtained via control of the pumping pressure (by controlling the sorb temperature) and by using a resistance heater placed on the  $^3\text{He}$  pot; this is an automated process which is controlled by computer software.

By condensing and then pumping on the  $^3\text{He}$  pot, stable temperatures are obtained in the range  $0.3 \text{ K} < T < 2 \text{ K}$ . For the range  $2 \text{ K} < T < 20 \text{ K}$ , it was found empirically that the best temperature control is achieved by utilizing an additional resistance heater placed directly on the sorb assembly and maintaining the sorb temperature<sup>15</sup> at  $\sim 20 \text{ K}$  throughout the experiment.

<sup>12</sup>The temperature of this stage can reach lower values if more pumping power is utilized, but a limit is set by the characteristics of the continuous fill action.

<sup>13</sup>This particular design is modular so as to allow the interchange of various stage designs optimized for either resistivity or thermal conductivity measurements.

<sup>14</sup>Designs also exist where an experiment is submersed directly in the cryogen liquid, but the need for thermal isolation of the sample is crucial in *e.g.* a thermal conductivity experiment.

<sup>15</sup>This involves overriding the automatic control of the sorb by simply disconnecting the installed heater.

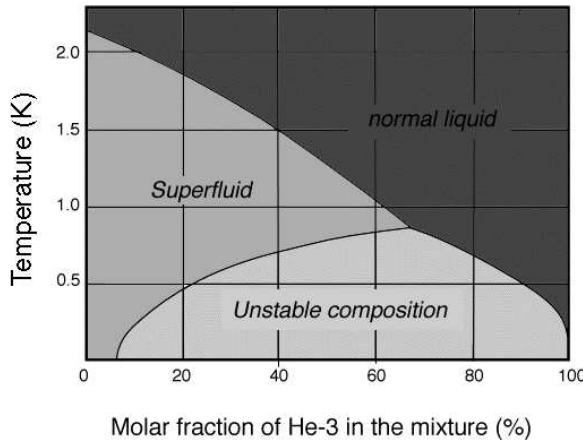


Figure 4.3:  $^3\text{He}$ – $^4\text{He}$  phase diagram.

#### 4.2.2 Dilution Refrigeration

Although  $^3\text{He}$ – $^4\text{He}$  dilution refrigeration is more complicated than the methods described above, it is able to achieve base temperatures near  $\sim 10 \text{ mK}$ . This is made possible by exploiting the characteristics of a mixture of  $^3\text{He}$  and  $^4\text{He}$  atoms at low temperatures: due to their differing quantum statistics, such a mixture will separate into a concentrated  $^3\text{He}$  phase and a dilute phase (containing 6.6%  $^3\text{He}$ ), as shown in Fig. (4.3). Because the dilute mixture is unstable for any concentrations above 6.6%, the removal of any  $^3\text{He}$  from this mixture will effectively drive the temperature down along the phase boundary between the superfluid and unstable regions, theoretically to absolute zero.<sup>16</sup>

The dilution fridge setup, shown in Fig. (4.4), utilizes this property to achieve cooling by continuously removing  $^3\text{He}$  atoms from the dilute phase, thus forcing a flow of atoms from the concentrated phase to cross the phase boundary and keep the mixture in equilibrium. Because this process requires energy, heat will be taken from the mixture which sits in the mixing chamber, and the walls of the chamber will cool. In order to make this process continuous, the fridge is designed to circulate the mixture in a closed-cycle pumping system which removes He from the mixing chamber and then reintroduces it.<sup>17</sup> Thus, very low temperatures can be maintained indefinitely while the circulation process is continued.

Conventional operation of the dilution fridge, as explained elsewhere [147, 149], is quite

<sup>16</sup>Practical limitations, including the Kapitza resistance between liquids and solids, place a lower limit on the ultimate temperature that is reached in any real fridge design, but temperatures of 20–25 mK can be routinely achieved.

<sup>17</sup>Careful design of heat exchangers ensures that heating from this process is minimized.

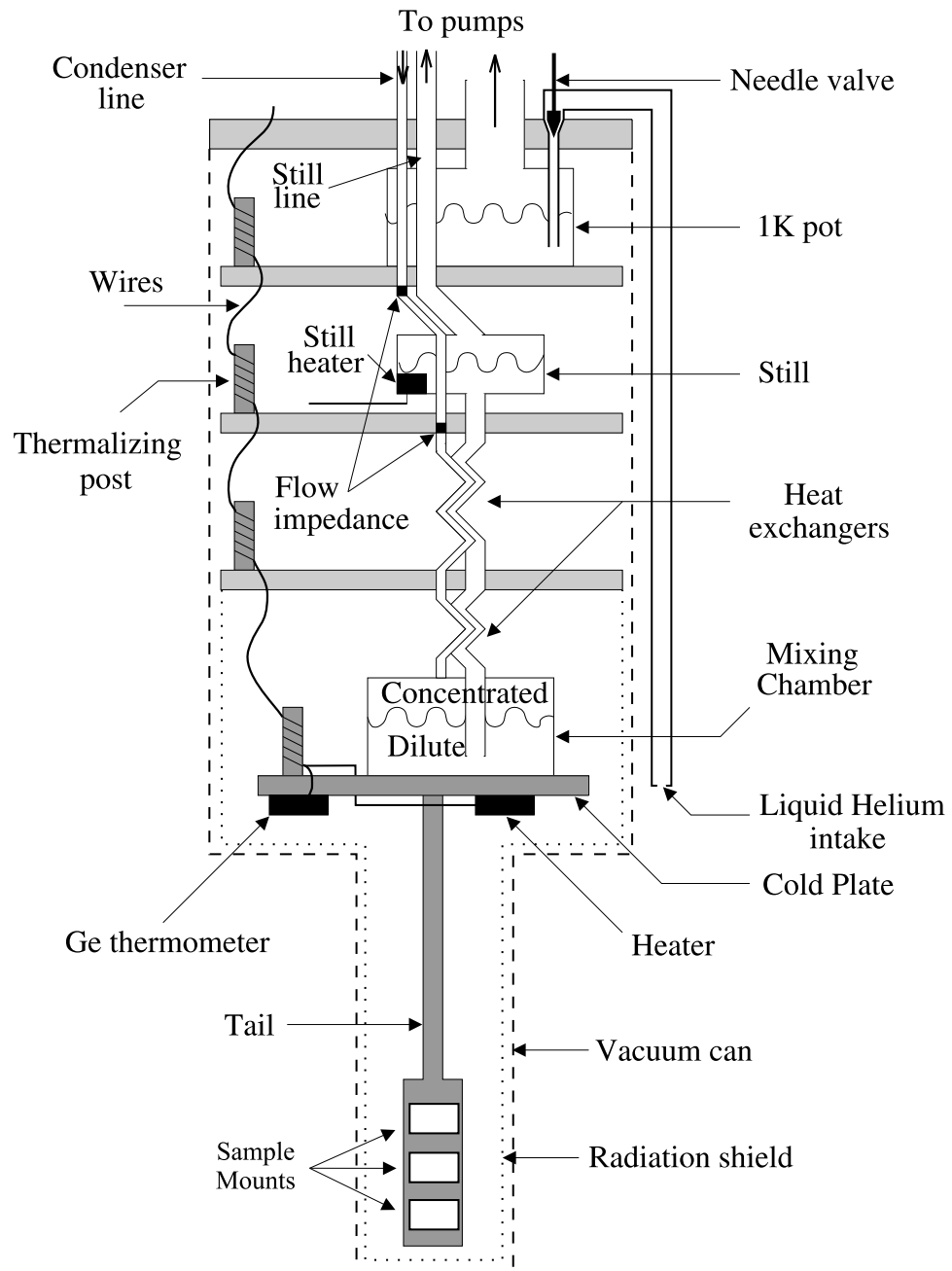


Figure 4.4: Schematic of  $^3\text{He}/^4\text{He}$  dilution fridge (not to scale; adapted from [147]).

simple once the circulation process has been started: temperature control is achieved by applying heat to the mixing chamber as described previously, and the fridge can be operated in this manner up to  $\sim 1$  K. For the purposes of this study, it was often more practical to extend measurements in the dilution fridges to temperatures above 1 K. This involved implementing a few non-standard techniques to operate the fridges above stable circulation mode temperatures, as described below.

#### *“One-Shot” Mode ( $1 \text{ K} < T < 2 \text{ K}$ )*

Above 1 K, stable temperatures can be achieved by stopping circulation and pumping on the mixture in a manner similar to the operation of a 1 K pot. Because circulation is stopped, this process is irreversible and experiments must be performed upon warming the mixing chamber through this temperature range.

#### *High- $T$ Mode ( $T > 2 \text{ K}$ )*

For temperatures above  $\sim 2$  K, the mixing chamber temperature is comparable to the temperature of the intermediate 1 K pot cooling stage, and so the best temperature control is achieved by simply operating the fridge as a  $^4\text{He}$  system; in this mode, the 1 K pot provides the cooling power. Since the thermal link between the 1 K pot and the mixing chamber (and essentially the tail) is intentionally made poor for low temperature (circulation) operation, it is necessary to trap a small portion of mixture (approx. 50 mbar) in the mixing chamber assembly to participate as exchange gas. This procedure provides adequate temperature control up to above 6 K.

### *4.2.3 Thermometry*

For precise low temperature measurements, it is imperative to have good control of the temperature variations of the cryostat, but the accuracy of an experiment that relies on temperature variations of a certain quantity obviously relies on an accurate knowledge of the temperature itself. Although there are many elaborate thermometry techniques available to the low- $T$  experimentalist (see *e.g.* [149], chapter 8), the temperature range and accuracy necessary in this study are well satisfied by employing various resistance thermometers. The reference thermometers used throughout this study are summarized in table (4.1).

Each cryostat system utilized a dedicated temperature controller to measure its reference thermometer and control its heater. The Kelvinox 400 and Heliox fridges employed Oxford Instruments ITC 503 and FemtoPower systems, respectively, while the Dipper

Thermometer	Serial	T Range [K]	R Range [ $\Omega$ ]	Calibration	Cryostat
Ge	GR-200A-30	0.035-4	75k-20	Lakeshore <sup>a</sup>	Kelvinox 300
RuO <sub>2</sub>	H23	0.025-4	150k-2k	Oxford	Kelvinox 300
RuO <sub>2</sub>	L15	0.025-6.5	50k-2k	Oxford	Kelvinox 400
Cernox 1030	X14651	0.3-300	50k-50	in-house <sup>b</sup>	all
Cernox 1050		1.5-300	100k-50	Lakeshore	Dipper
Carbon glass		1.5-300	(500)	Oxford	Heliox
RuO <sub>2</sub>		0.3-1.5	20k-2k	in-house <sup>c</sup>	Heliox

<sup>a</sup> Original calibration; re-calibrated using Oxford RuO<sub>2</sub> (H23).

<sup>b</sup> Lakeshore CX-1030 chip resistors calibrated using Dipper Cernox (1050) and Oxford RuO<sub>2</sub> (L15).

<sup>c</sup> Phillips SMD precision chip resistor model RC12H calibrated using Oxford RuO<sub>2</sub> (H23).

Table 4.1: Resistance thermometers used for temperature measurement in the various cryostats.

used a Lakeshore DRC-93 controller and the Kelvinox 300 used a Lakeshore Model 340 controller.

#### *Temperature Stability and Accuracy*

The most obvious concern about performing proper cryostat measurements is in regard to the accuracy and level of precision of the temperature at which measurements are performed. The temperature accuracy is dictated by the accuracy of the thermometer calibration and the accuracy of its resistance measurement (described below). The Oxford-calibrated RuO<sub>2</sub> thermometers are quoted as having an accuracy which depends on temperature as follows:  $\pm 5$ , 10 and 30 mK for ranges  $50 \text{ mK} < T < 150 \text{ mK}$ ,  $150 \text{ mK} < T < 1.5 \text{ K}$  and  $1.5 \text{ K} < T < 4.2 \text{ K}$ , respectively.<sup>18</sup> The temperature calibration of each fridge thermometer is routinely checked against those of standard calibrated thermometers which are kept for this purpose.<sup>19</sup> Therefore, the temperature accuracy is known to approximately  $\pm 5\%$  for all temperatures up to 4 K, and to a much better value at higher temperatures.

The precision is dictated by the temperature stability. At low temperatures, both

<sup>18</sup>Note that these values are the common accuracy values for fully calibrated RuO<sub>2</sub> sensors used routinely by Oxford Instruments - the true accuracy is most likely much better than quoted since calibrations for each thermometer have been compared to each other.

<sup>19</sup>The Ge thermometer is used because of its high reproducibility, but is checked yearly against an Oxford-calibrated RuO<sub>2</sub> which is not thermally cycled very often.

dilution fridges routinely attain a temperature stability of approximately 0.1% (*e.g.* about 0.1 mK at  $T = 50$  mK), which is easily measurable given sensitivities of  $\sim 10^5$  Ω/K of *e.g.* a Ge thermometer in this temperature region.<sup>20</sup>

### 4.3 Transport Measurements

The key technique that is essential to both thermal and electrical conductivity measurements performed in this study is the measurement of sample and thermometer resistances. In the case of electrical conductivity, this primary measurement directly gives the quantity of interest. A thermal conductivity measurement, on the other hand, requires a slightly more complicated analysis of thermometer resistances in conjunction with the control of a heat source to attain the quantity of interest. These techniques will be summarized below.

Depending on the temperature range under study, data was collected using one of the various cryostats, either upon (uncontrolled) cooling or  $T$ -controlled warming.<sup>21</sup> For high temperature resistivity, the most practical method of measurement involved using the Dipper, evacuated<sup>22</sup> and inserted into a He dewar to achieve a slow cool from room temperature to  $< 10$  K, which occurs over a time scale of  $\sim 12$  hours. For lower  $T$  measurements, resistivity was measured using either the Heliox or Kelvinox cryostats by first cooling to base temperature and then sequentially stepping up the temperature, recording resistance data at each (fixed) temperature.

Most low- $T$  resistivity measurements were performed in the Kelvinox 400 fridge, using a multiplexed 6-sample technique, and occasionally in the Kelvinox 300 by using the thermal conductivity setup with an in-situ resistivity attachment.<sup>23</sup>

#### 4.3.1 Electrical Resistivity

Electrical resistance measurements were performed using a standard, four-wire measurement technique where a charge current  $I$  flows into and out of a sample via two wires ( $I^+$  and  $I^-$ ), and a potential difference  $\Delta V$  is measured across the sample via two additional

---

<sup>20</sup>See Ref. [76] for a thorough examination of temperature stability in the Kelvinox 300 fridge.

<sup>21</sup>Thermal conductivity measurements require measurements to be made at a stable temperature for an extended time, so they must be performed by controlling the cryostat temperature (*i.e.* upon warming).

<sup>22</sup>A high vacuum of  $\sim 10^{-5}$  Torr is adequate for both slow-cooling and temperature-controlled measurements.

<sup>23</sup>This in-situ method was used to enable a proper test of the Wiedemann-Franz law by removing sample-field orientation concerns - see Section 6.4).

wires ( $V^+$  and  $V^-$ ). For sample resistivity, the measured resistance  $R$  is converted to resistivity  $\rho$  units based on the geometry of the sample using  $\rho = \alpha R$  (with  $\alpha$  defined in Section 4.1.2).

In practice, there are a number of experimental considerations in performing a low temperature resistivity measurement. The most common items include sample thermalization, excitation current, self-heating, RF interference/heating, and grounding issues. These will be discussed below.

### *Resistance Bridge*

The use of an AC resistance bridge measurement technique allows for accurate, low-noise measurements to be performed without strenuous efforts. The accuracy is a result of the bridge technique, where the measured resistance is compared to a known reference resistance. The optimization of signal-to-noise ratio is due to the use of an AC lock-in technique, which minimizes the extraneous effects of  $1/f$  noise, mains and other higher frequency interference, and thermal interference.<sup>24</sup> Furthermore, the required AC (RMS) excitation current is much less than for a DC measurement, thus reducing self-heating effects.

This study employed a Linear Research LR-700 AC resistance bridge, operated at a fixed frequency of 16 Hz.<sup>25</sup> The LR-700 was equipped with a LR-720-8 multiplexing unit, which provides the ability to measure up to eight separate four-wire resistance measurements sequentially with the same bridge. This multiplexing unit was essential in taking parallel resistivity measurements of up to six samples mounted together on the Kelvinox 400 fridge, and for performing parallel thermal conductivity measurements of up to three samples mounted together on the Kelvinox 300 fridge (where the resistance of two thermometers per sample is measured - see Section 4.3.2).

The quoted accuracy of the LR-700 is  $\pm 0.005\%$  for the excitation ranges used in this study. The achievable precision for a  $10\text{ m}\Omega$  resistance measurement is  $0.0015\%$  when using  $1\text{ mA}$  of excitation current,<sup>26</sup> and for a  $1\text{ k}\Omega$  resistance it is  $0.003\%$ . However, the measurable scatter in all low temperature resistance measurements is far larger than these values, and so other sources of error dominate the actual precision of our

<sup>24</sup>Thermopower effects, where extrinsic DC voltages are created due to the presence of thermal gradients across dissimilar metallic lead elements, can lead to errors in a low temperature DC resistance measurement.

<sup>25</sup>Low AC frequencies are used to reduce the effect of lead capacitance.

<sup>26</sup>Note that this excitation current is about an order of magnitude larger than that used in this study.

measurements, as discussed below.

### Grounding

All measurement leads were shielded from pickup of spurious electromagnetic fields by using either twisted pair (in the cryostat) or coaxial cables (room temperature stages) throughout the experimental setup. The shield of each cable was grounded to earth, together with the cryostat, storage dewar, and all electronics, avoiding the creation of ground loops wherever possible. For thermal conductivity measurements, a Faraday cage was employed to minimize external RF signal interference.

During a resistance measurement, the LR-700 bridge automatically grounds the  $I^-$  lead at the measurement unit. For this reason, and for the sake of preemptive troubleshooting, all leads were usually floated at the tail position and electrically grounded at the room temperature distribution panel.<sup>27</sup> For resistivity measurements, sample isolation was achieved by placing a thin layer of Kapton insulating film between the sample mounting block and tail (except for certain cases as discussed below).

### Self-Heating

At low temperatures, the effect of Joule (*i.e.*  $I^2R$ ) heating can raise the true temperature of a sample to above the cryostat (tail) temperature, and hence contaminate a temperature-dependent measurement. This “self-heating” effect can easily be tested for by checking for any excitation current dependence of the measured resistance at the base temperature of the cryostat. Typically, excitation currents of 0.1 mA were used to measure sample resistances on the order of 10 m $\Omega$ , equating to a heating power of  $\sim 0.1$  nW. Considering the cooling power of *e.g.* the Kelvinox 400 (*i.e.*  $\sim 400\mu\text{W}$ ), this does not seem to be a concern unless a weak thermal link exists between sample and experiment stage, in which case a sample can easily incur self-heating. This situation can occur if there is a large thermal boundary or “Kapitza” resistance<sup>28</sup> between the sample and tail introduced by electrical isolation, but can be avoided by simply providing good electrical contact between the sample (copper block) and tail. For the most conductive samples (*i.e.* CeRhIn<sub>5</sub>), higher excitation currents were necessary to obtain the same noise levels, so the “floating” configuration was not used and the  $I^-$  lead was grounded at the tail position in order to minimize self-heating.

<sup>27</sup>This was found to minimize spurious capacitive charging effects resulting from the electrical switching action of the ground in the multiplexing unit.

<sup>28</sup>This phenomenon occurs due to the acoustic mismatch between two materials [153],

### *Field Measurements*

The three He dewars used for the cryostats are all equipped with superconducting magnets capable of reaching either 15 T or 18 T. The two dilution fridge dewar magnets make use of a compensated field zone, in which the sensitive reference thermometry is placed to avoid the complications of magnetoresistance. The Heliox magnet is equipped with an Oxford Instruments PS 120 power supply (115 A current for 18 T field), while the Kelvinox 400 magnet is equipped with a newer model - Oxford Instruments IPS 120.

Both magnet systems produce magnetic fields which are controllable to 1 mT increments. Because of the superconducting nature of the solenoids, the drift in field is very small (unmeasurable). However, the large fields routinely used in experiments can cause a small residual magnetization to remain trapped in the magnet structure, even after removing any current from the solenoid. To prevent this from affecting low-field measurements, a field-zeroing procedure is used before every experiment, where the field is systematically ramped from positive to negative to remove the residual field.

A more important concern, especially for large-field experiments, is with respect to sample-field alignment. In this study, all samples were mounted on cryostat tails and aligned with respect to the tail's orientation using an optical microscope. An estimate of the error in sample alignment in this procedure, together with small deviations of tail alignment with respect to the field direction, gives  $\pm 2^\circ$  as a conservative value.

### *Data Acquisition*

LabView data acquisition VIs were designed to acquire data from the resistance bridge and control the experiment by interfacing with the temperature controller and magnet power supply, all through a standard IEEE-488 (GPIB) interface. Custom LabView VIs were constructed (for both dilution fridges) to allow in-situ data averaging and simultaneous acquisition of sample and thermometer resistances. For the multiplexed 6-sample measurement, an acquisition program was designed to use the following sequence:

- set new temperature or field value.
- log temperature adjustment by tracking resistance of first sample and independent thermometer(s) (up to three).
- measure resistance of first sample and thermometer(s) for a set number of itera-

tions.<sup>29</sup>

- compute average of measurement values and record results to file.
- repeat sequence for each subsequent sample and then repeat process for a new temperature or field.

By allowing the close monitor of temperature stability, this sequence allows for the optimization of temperature stabilization times and necessary averaging, thus minimizing measurement times. Also, this sequence improves upon previous methods by allowing the simultaneous measurement of thermometer temperatures and sample resistances throughout the averaging process (rather than simple before/after temperature measurement), allowing subsequent investigation of temperature stability for each data point.

#### Measurement Error

Once checks are made to ensure that the proper resistance (*i.e.* the actual sample resistance) is being measured, the error in accuracy, dictated by the capabilities of the LR-700 bridge, is far lower than all other sources of error in this measurement. Thus, the error in a measured resistance value is dominated by the level of precision in our experimental setup.<sup>30</sup>

As stated, the achievable precision of the measurement electronics is far greater than that dictated by the measured range of scatter. It is suspected that the main causes of measurement scatter are from systematic error sources such as mechanical vibration and electrical noise. The effects of vibration on resistance measurements at low temperatures are mainly due to vibration-induced heating. This effect can be easily tested and minimized, but unfortunately cannot be completely eliminated due to the nature of the cryostat operation (mechanical pumps, however isolated, are still physically connected to the cryostat). Electrical noise can have various origins, including high frequency RF heating and interference, and is minimized using various techniques as described above (*i.e.* shielding and grounding).

The scatter in resistance values is largest (due to limitations in excitation current) at the lowest temperatures, reaching typical levels of  $\sim 1\%$  in almost all sample resistance

---

<sup>29</sup>This usually involved a sequence of 5-15 acquisitions of data values, each of which were already a digital average calculated by the bridge itself over a continuous 3-second measurement interval.

<sup>30</sup>For resistivity measurements, the error in geometric factor determination is the dominant source of error in attainable accuracy. As stated previously, this error is typically  $\sim 10\%$  in the samples used in this study.

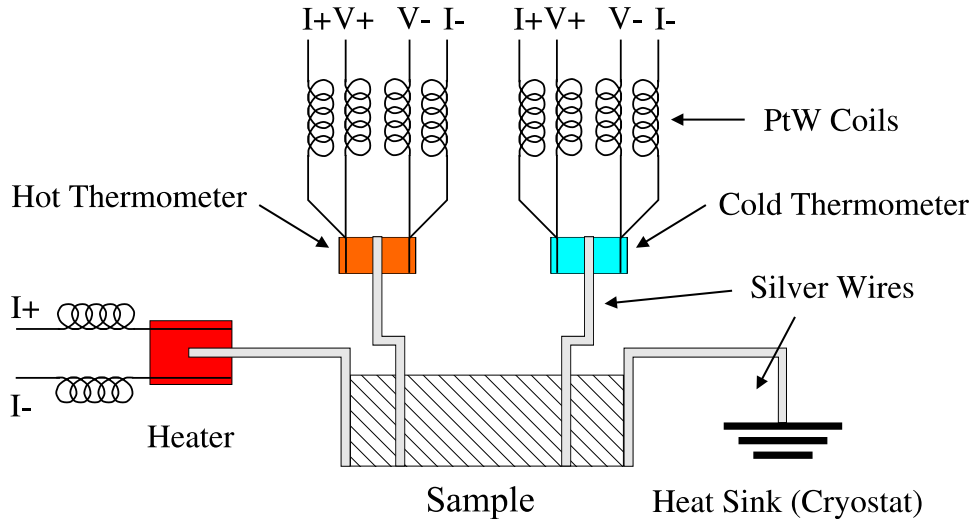


Figure 4.5: Schematic of the thermal conductivity setup.

measurements in this study. To minimize these sources of random error, significant signal averaging is done in all measurements to the level required by each experiment. Furthermore, in measurements with a high amount of scatter, more data points - *i.e.* as a function of temperature - were taken to improve statistics.<sup>31</sup>

Finally, the best test of the accuracy of our resistance measurements can be made by testing the WF law on a common metal, thereby testing both thermal and electrical transport measurements simultaneously. This will be discussed in the next section.

### 4.3.2 Thermal Conductivity

All thermal conductivity measurements incorporated a standard DC, steady-state technique which is analogous to the four-wire resistivity measurements described above. In this case, a heat current  $\dot{Q}$  is sent through the sample, setting up a temperature gradient  $\Delta T$  across the sample which is measured with two separate thermometers (*i.e.* for  $T^+$  and  $T^-$ ). The thermal conductivity is then calculated, using the geometric factor  $\alpha$ , as  $\kappa = \frac{\dot{Q}}{\alpha \Delta T}$ . This quantity can be measured either as a function of swept temperature at set field, or of swept field at a set temperature. For the sake of brevity, a brief review of the low- $T$  measurements performed in the Kelvinox system will be given. The details of thermal conductivity measurements using the Dipper cryostat are given elsewhere [76]

### Experimental Setup

The generic setup is shown schematically in Fig. (4.5). A heat current is supplied by the Joule heating of a resistive heater and the temperature gradient is measured via two resistive thermometers. In practice, the required quantities,  $\dot{Q}$  and  $\Delta T$ , are obtained by calculating the power of the heater and temperatures of the two thermometers, respectively. For the first, a heat current  $\dot{Q} = I_h^2 R_h$  is generated by supplying a controlled electrical current  $I_h$  through a known resistance  $R_h$ . For the second, the temperature of each thermometer is obtained by converting their measured resistances using a calibration (see below). Hence, a precise determination of these quantities requires two wires for supplying  $I_Q$ , and four wires for measuring each thermometer resistance, totaling ten wires for a complete measurement.

The most important aspect of a heat transport measurement is thermal isolation. Ideally, perfect isolation of the sample, heater and thermometers results in an exact determination of the thermal conductance. Realistically, some contact to each element is unavoidable due to simple mounting requirements and attachment of measurement wires. By the choice of proper materials, a careful direction of heat paths and minimization of heat leaks, the error in measurement of the true conductance is greatly reduced. In the designs used here, the main approach is to employ highly conductive paths between heater, sample, thermometers and ground only, and highly resistive mechanical and electrical measurement elements. For instance, as shown Fig. (4.5), highly conductive paths are achieved by using high purity silver wires, and electrical contacts to the thermometers and heater are achieved through highly resistive coils ( $R > 100 \Omega$ ) made with  $25 \mu\text{m}$  diameter PtW wire,<sup>32</sup> thus maximizing thermal isolation of each element.<sup>33</sup>

As shown in Fig. (4.6), a detailed schematic of the thermometers and heaters used in the dilution fridge reveal that great care was taken to ensure that each thermometer was thermally coupled as best as possible to the sample, while maintaining the best possible isolation from the surrounding environment. Likewise, the design of the heaters was motivated by the same concerns. The mechanical support for all elements, employing a thin Kapton film “clothes line” suspension design, is described elsewhere [76].

<sup>31</sup>See, for example, the case of CeRhIn<sub>5</sub> in Appendix B.2.

<sup>32</sup>Model 479 Pt (92% Pt and 8% W) from Sigmund Cohn Corporation.

<sup>33</sup>For the present designs, heat leaks have been carefully studied [76], and found to affect measured values of thermal conductance to at most a few percent.

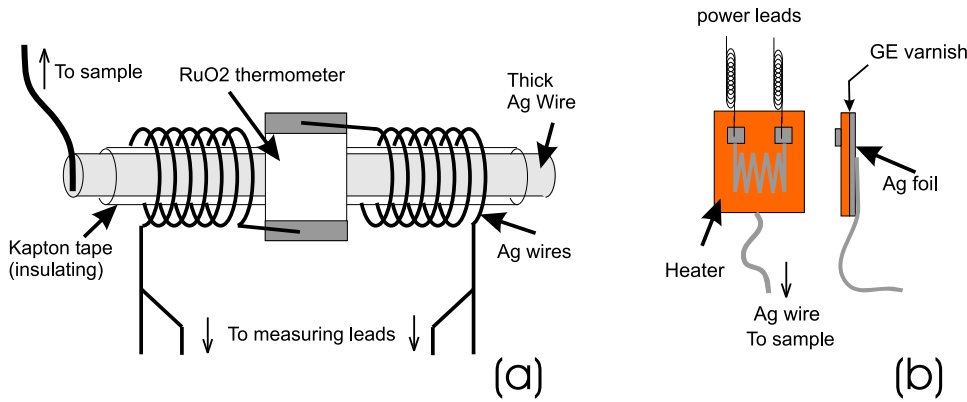


Figure 4.6: Detailed schematic of heater and thermometer elements (not to scale; adapted from [76]).

### Measurement Technique

Measurements in the Kelvinox 300 involved a multiplexed setup capable of measuring three samples simultaneously (in immediate sequence for each temperature or field step), from 40 mK to above 4 K, in fields up to 15 T.

The sequence of a  $T$ -sweep measurement involves a two-step process, followed at each temperature step. First, the resistance of each thermometer ( $T^+$  and  $T^-$ ) is first measured *without* an applied heat current ( $\dot{Q} = 0$ ) and hence at a temperature equal to the cryostat's temperature, providing an in-situ calibration. This method removes any concerns of calibration problems from *e.g.* magnetoresistance of thermometers under large magnetic fields, since the calibration is taken from a reference thermometer which resides in a field-compensated zone of the cryostat. The thermometers, which are RuO<sub>2</sub> resistors,<sup>34</sup> were measured using an LR-700 bridge as described above. Next, a heat current is applied and the thermometer resistances are measured. The controlled heat current is applied via controlling  $I_h$  with a commercial current source<sup>35</sup>, and sourcing it through a 10 k $\Omega$  resistance heater constructed of commercial strain gauges,<sup>36</sup> as shown in Fig. (4.6).

### Field Measurements

Note that all measurements involving applied magnetic fields were performed in the dilution fridges, which both incorporate *field-compensated* zones in their magnet designs.

<sup>34</sup>RuO<sub>2</sub> thick film surface mount chips from Dale Electronics.

<sup>35</sup>Keithley model 220 (0.5 nA precision) and 224 (0.5 $\mu$ A precision).

<sup>36</sup>Model SR-4, Type FSM-A6306S-500-S13C strain gauges from BLH Electronics, Inc. were used, since their resistances (5000  $\Omega \pm 1\%$ ) have negligible temperature and magnetic field dependence.

This allows placement of thermometry in a region where any applied fields are cancelled by a compensating applied field. This is especially important in the calibration routine for in-field measurements: although the sample thermometers used do display magnetoresistance, they were continuously calibrated using thermometry placed in the field-compensated zone.

Field-sweep measurements at constant temperature were performed in a similar way, where a continuous heat current was applied while incrementally stepping the field value, but bypassing the thermometer calibration step. Thermometer temperatures were then obtained from calibrations taken during temperature sweep measurements.

### *Data Acquisition*

LabView data acquisition VIs were designed, as described previously, to acquire thermometer resistances from the resistance bridge, to set heater current values with the current sources and to set and read the reference temperature with a Lakeshore temperature controller. For the multiplexed 3-sample measurement, an acquisition program was designed to use the following sequence, beginning with no applied heater current:

- set new temperature or field value.
- log all thermometer resistances (two per sample) sequentially for a specified number of iterations.
- measure resistance values, average and record to file.
- set heater current using estimated value of thermal conductivity.
- log all thermometer resistances sequentially for a specified number of iterations.
- measure resistance values, average and record to file.
- record heater current values (from instrument) to file.
- repeat process for a new temperature or field.

In this procedure, the value of heat current is set using an estimate of the thermal conductivity of each sample. The current setup dictates the amount of heat current to be applied based on the estimate, which is a polynomial function of either temperature or field, the geometric factor and the requested thermal gradient  $\Delta T$ , which is usually set

to be approximately 5% of the sample temperature (taken as the average of  $T^+$  and  $T^-$ ). Although the first attempt at such an estimate may be far from correct, the software was designed in a way as to allow adjustments of these parameters during the measurement.

### Measurement Error and Testing

Error determination in heat transport measurements is much more complicated than that in charge transport measurements, since in addition to errors associated with resistance measurements, considerations such as heat losses, thermometer calibrations and accuracy of heater current supply must be taken into account. All of these sources of error have been taken into consideration [76], and the experimental setup has been optimized to minimize the error from each source. Again, the precision of this measurement is dominated by random, systematic errors associated with resistance measurements (*i.e.* of thermometers), and can be determined by performing an optimized experiment and examining the data scatter. As shown in Fig. (4.7), a test measurement of a specimen of highly conductive silver wire demonstrates the high precision of the dilution fridge setup, as reflected in a scatter of less than 3% in the measured thermal conductivity. Furthermore, measurements of the electronic insulator  $\text{La}_2\text{CuO}_4$  [154] confirm the absence of a linear term of  $\kappa(T)$  in the  $T \rightarrow 0$  limit to within  $3 \mu\text{W K}^{-2} \text{ cm}^{-1}$ , giving an indication of the achievable resolution of our measurement.

A fundamental test of the accuracy of thermal conductance<sup>37</sup> measurements is obtained by measuring both heat and charge conductance in a sample and comparing their ratio directly to the Wiedemann-Franz law expectation (see Section 2.2.1). In this way, the error associated with determination of the geometric factor of the sample in question is irrelevant,<sup>38</sup> and the accuracy of both measurements can be tested directly. As a standard test, the electrical and thermal conductivity of a specimen of highly conductive silver wire was measured in both the dipper and the dilution fridge, allowing a check of the Wiedemann-Franz law to be performed over a large range of temperatures. The accuracy of measurements performed in the  ${}^4\text{He}$  cryostat is confirmed in comparing heat and charge transport by plotting the Lorenz ratio (see Section 2.2.1), which approaches

---

<sup>37</sup>The accuracy of thermal conductivity, as in resistivity measurements, is again limited by geometric factor determination.

<sup>38</sup>Ideally, geometric factors are equal for both measurements, but note that there is a possibility that a slight difference in *e.g.* voltage contact separation is possible depending on the nature of the contacts. For instance, the finite width of a voltage pad may be effectively shorted out for a charge transport measurement (relative to sample), but averaged over its width for heat transfer in a thermal transport measurement, resulting in *e.g.* a slight deviation from the WF law expectation.

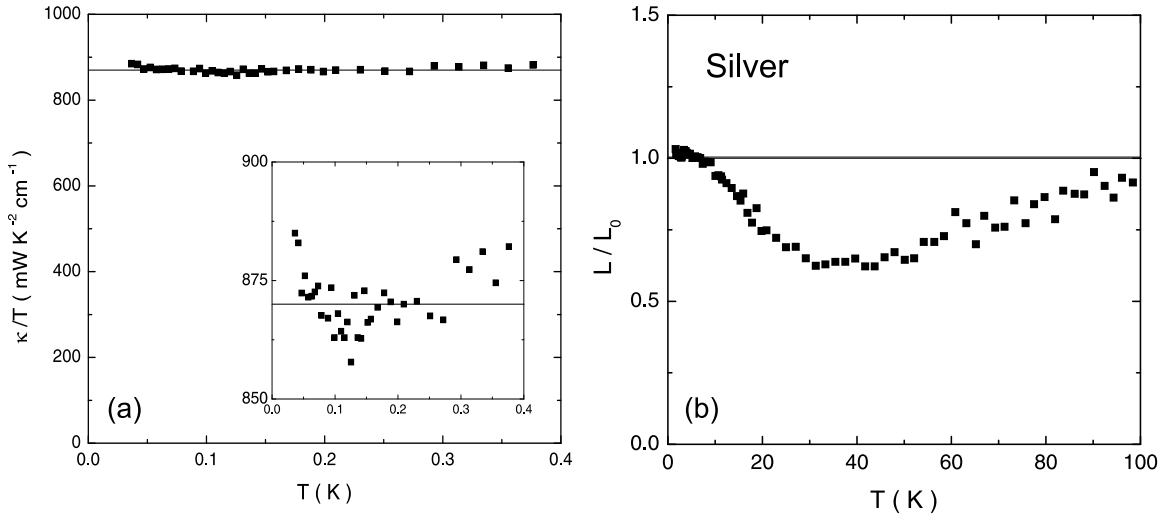


Figure 4.7: Test experiment on pure Ag wire, showing (a) thermal conductivity measured using the dilution refrigerator setup, with an inset highlighting the 3% scatter in precision, and (b) the Lorenz ratio measured from 1.5 to 100 K in the  ${}^4\text{He}$  cryostat. The Wiedemann-Franz law is obeyed at low temperatures and  $L$  falls below  $L_0$  at higher temperatures, as expected in a metal (from [76]).

unity to within experimental precision at both low and high temperatures. (For further tests of the apparatus and methods used, see Ref. [76].)

The accuracy of the dilution fridge setup used in this study has been well tested in a number of other studies: agreement of the WF law in the  $T \rightarrow 0$  limit has been observed in  $\text{Tl}_2\text{Ba}_2\text{CuO}_{6-\delta}$  [93],  $\text{LuNi}_2\text{B}_2\text{C}$  [86],  $\text{NbSe}_2$  [91],  $\text{Na}_{0.7}\text{CoO}_2$  [92] and  $\text{Sr}_3\text{Ru}_2\text{O}_7$ . The agreement found in this series of samples is quite amazing, considering the varying parameters found in the different studies (*i.e.* sample size, resistance, type of contacts and nature of transport). In some cases, agreement with the WF expectation to the level of 1% has been achieved [93], showing that the accuracy of heat transport measurements performed with the equipment and methods utilized in this study can approach that of resistance measurements, which are precision-limited. Therefore, except for the most extreme cases,<sup>39</sup> the error in thermal conductance is also precision-limited and determined by *e.g.* the statistical error (scatter) of each experiment.

<sup>39</sup>In highly resistive samples, for example, heat losses can become considerable and must be carefully considered. However, there are no samples of such a nature in this study.

## CeRhIn<sub>5</sub>: PROBING SPIN FLUCTUATIONS

---

---

The anomalous properties of the 115 system of compounds are widely thought to be caused by the influence of spin fluctuations which arise due to the close proximity of magnetic ground states. For instance, in CeCoIn<sub>5</sub> the observed NFL behavior and unconventional superconductivity were first attributed to the possible proximity to a QCP and the presence of magnetically-mediated pairing, respectively [104]. As discussed in Section 3.2, alloying studies have shown that CeCoIn<sub>5</sub>, CeRhIn<sub>5</sub> and CeIrIn<sub>5</sub> are all closely related systems which seem to share common ground states. Being the most well-characterized material of the three to date, with an incommensurate AFM ground state below  $T_N = 3.8$  K [140], CeRhIn<sub>5</sub> may exhibit the key magnetic characteristics relevant to describing the physics of the quantum critical behaviour throughout the 115 system.

In this chapter, we begin the analysis of experimental results with a detailed study of heat and charge transport in CeRhIn<sub>5</sub>, a well-characterized material in which spin fluctuations dominate the scattering of electrons. This chapter reports two compelling observations: 1) the thermal resistivity perfectly tracks the magnetic entropy, revealing that spin fluctuations are exactly as effective in scattering electrons as they are in disordering moments; 2) the difference between thermal and electrical resistivities provides a direct measure of the characteristic energy of the fluctuation spectrum.

All measurements in this chapter were performed using the same four contacts, with currents applied in the basal plane of the tetragonal crystal structure.

### 5.1 Thermal Conductivity

The extremely high quality of the crystals used in this study was confirmed by the observation of a remarkably low residual resistivity,  $\rho_0 = 0.037 \pm 0.001 \mu\Omega \text{ cm}$ ,<sup>1</sup> which is an order of magnitude lower than previously reported [102]. This value was confirmed

---

<sup>1</sup>The uncertainty in  $\rho_0$ , obtained from a non-linear least-squares fit to the data, includes the  $\pm 4\%$  error in geometric factor.

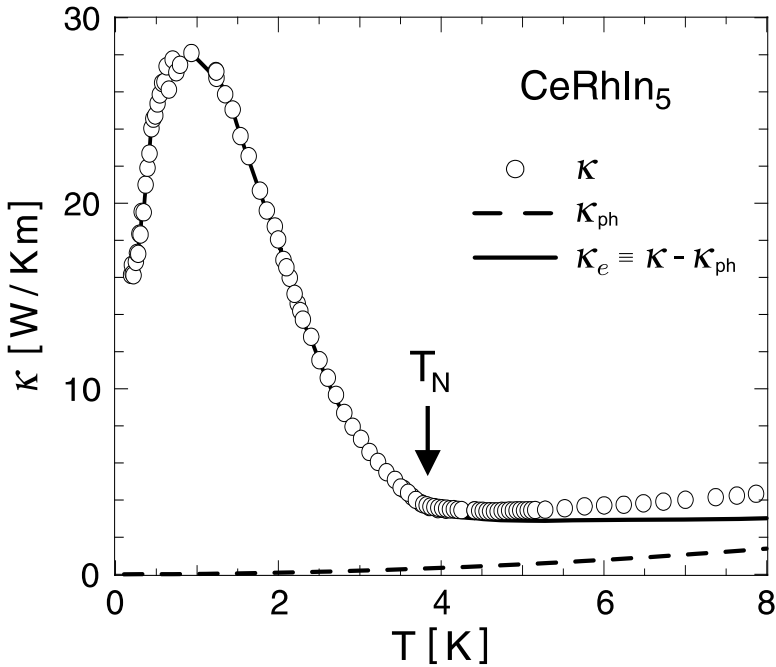


Figure 5.1: Temperature dependence of the thermal conductivity of CeRhIn<sub>5</sub>, for a current in the basal plane. Open circles are raw data ( $\kappa$ ), the dashed line is the estimated phonon conductivity ( $\kappa_{ph}$ ), and the solid line is the electronic contribution ( $\kappa_e \equiv \kappa - \kappa_{ph}$ ).

by measurements performed on two different samples possessing an order of magnitude difference in geometric factors (*i.e.* cross-sectional area to length ratio), which yielded equivalent results.<sup>2</sup> Also, the low residual resistivity is in fact comparable to that of the non-magnetic analog LaRhIn<sub>5</sub>, where  $\rho_0 = 0.04 \mu\Omega \text{ cm}$  [110], again indicating the remarkable ease in which these systems grow into single crystals of high quality. With such low impurity scattering levels, a comprehensive study of electronic thermal conductivity is greatly facilitated since a) the electronic component of  $\kappa$  dominates all other channels of conduction (including phonon transport) over a wide range of temperature, and b) the behaviour of inelastic scattering can be observed to low temperatures, as will be discussed below.

The temperature dependence of the thermal conductivity of CeRhIn<sub>5</sub> is shown in fig. (5.1), where a phonon subtraction (see Appendix C.1) has been used to obtain the electronic contribution  $\kappa_e$ . Upon cooling,  $\kappa_e$  increases dramatically below the onset of AFM order at  $T_N$ , such that  $\kappa_e/T$  grows by a factor of 60. This is due to the freezing out of magnetic fluctuations upon entering the ordered state, and is quite similar to the

<sup>2</sup>To enable an adequate signal-to-noise ratio in performing transport measurements, the long sample with dimensions  $\sim 4 \times 0.1 \times 0.05 \text{ mm}$  was utilized in the measurements reported below.

increase in  $\kappa_e/T$  observed below  $T_c$  in the superconducting state of CeCoIn<sub>5</sub> [130], which can be attributed to the suppression of magnetic fluctuations [137, 155].<sup>3</sup> Note that an abrupt *increase* in  $\kappa/T$  is also observed at temperatures much lower than  $T_N$ , near  $\sim 200$  mK. This signature, together with similar observations in charge conductivity, suggest the presence of a superconducting transition in CeRhIn<sub>5</sub> that occurs at ambient pressure, as shown and explained in detail in Appendix B.2. Since this observation is not the subject of the current chapter, the remainder of discussion and analysis deals with data above the apparent superconducting transition temperature.

## 5.2 Transport and Spin Disorder

In order to explore the connection between magnetic fluctuations and transport in detail, we compare the thermal resistivity  $w_e(T) \equiv L_0 T / \kappa_e(T)$  (in units of  $\rho$ ) to two other quantities: the magnetic entropy  $S_{\text{mag}}(T)$  and the electrical resistivity  $\rho(T)$ .

In Fig. (5.2),  $w_e(T)$  is seen to perfectly track  $S_{\text{mag}}(T)$ , calculated from specific heat measurements by Hegger *et al.* [102], over a wide range of temperature ( $0 < T < 2 T_N$ ). Such a relation,  $w_e(T) \propto S_{\text{mag}}(T)$ , has to our knowledge never been discovered before. Many years ago, Fisher and Langer pointed out that the same spin-spin correlation function enters in the calculation of both the magnetic energy of a metal and the relaxation time associated with scattering of electrons by spin fluctuations, so that the temperature derivative of the resistivity  $d\rho/dT$  should vary as the magnetic specific heat  $C_{\text{mag}}$  near  $T_N$  [157]. This predicted correlation was roughly confirmed in subsequent measurements on the antiferromagnet PrB<sub>6</sub>, for example, where a sharp peak was observed in both  $d\rho/dT$  and  $C_{\text{mag}}(T)$  at  $T_N = 6.9$  K [158].

The same approximate correlation ( $d\rho/dT \propto C_{\text{mag}}$ ) was recently pointed out in the case of CeRhIn<sub>5</sub> by Bao *et al.* who, moreover, directly showed it to originate from the magnetic correlation function, measured with neutron scattering [140]. Fig. (5.2) reveals that in CeRhIn<sub>5</sub> the best correlation is in fact between *scattering rate* and *entropy* ( $w_e \propto S_{\text{mag}}$ ), rather than  $d\rho/dT \propto C_{\text{mag}}$ . Moreover, it holds much better for heat transport than for charge transport, presumably because charge conductivity involves a much stronger angular weighting of fluctuations (in favour of high- $\mathbf{q}$ ) than heat conductivity, while entropy involves none.

---

<sup>3</sup>Similar behaviour is also observed in the high- $T_c$  cuprate superconductors (see, *e.g.* Ref. [75]), where the increase in thermal conductivity observed below  $T_c$  can be attributed to the same effect [156]

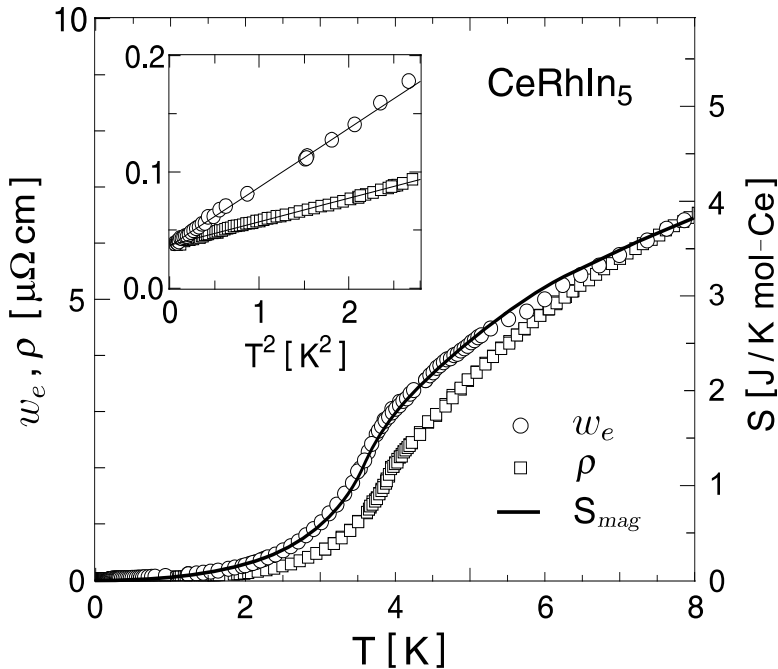


Figure 5.2: Temperature dependence of electronic thermal resistivity  $w_e$  (circles) and electrical resistivity  $\rho$  (squares). These are compared to the magnetic entropy  $S_{mag}$  (line), obtained from published specific heat data [102]. Inset: low-temperature data as a function of  $T^2$ . Lines are linear fits.

### 5.3 Comparing Heat and Charge Transport

We further explore the role of magnetic fluctuations in scattering conduction electrons by comparing in detail the two resistivities, both through their difference, defined as  $\delta(T) \equiv w_e(T) - \rho(T)$  and shown in Fig. (5.3), and through their ratio, defined as the normalized Lorenz ratio  $L(T)/L_0 \equiv \rho(T)/w_e(T)$  and shown in Fig. (5.4).

In the elastic regime, one obtains the Wiedemann-Franz law, as indeed confirmed in CeRhIn<sub>5</sub> at  $T \rightarrow 0$ :  $w_e(T) = \rho(T)$  (see inset Fig. (5.2)), or  $L(T) = L_0$  (see Fig. (5.4)). In the inelastic regime, as explained in Section 2.2.2, the difference  $\delta(T)$  can give access to the so-called “vertical” component of scattering, which involves only changes in energy, while the ratio  $L(T)$  involves a mixture of both vertical and horizontal components. Model calculations by Kaiser have extended the temperature range of previous work [69] considering the scattering of conduction electrons off fluctuating local moments. These calculations show that the effect of vertical processes is greatly reduced (eventually to zero) as the temperature increases above  $T_{SF}$ , the characteristic temperature of the spin fluctuations, since these fluctuations then have insufficient energy to scatter electrons through the thermal layer (width of the Fermi function) [72]. This effect is well-known

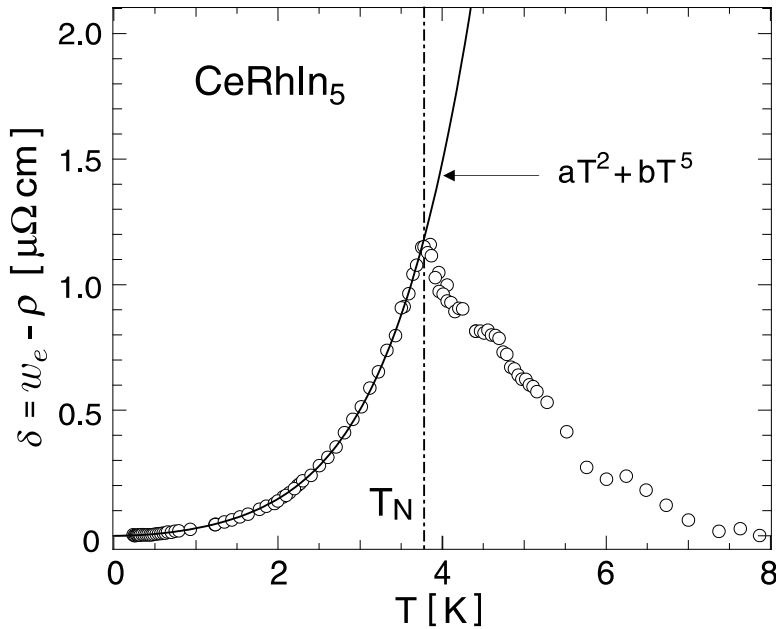


Figure 5.3: Difference between thermal ( $w_e \equiv L_0 T / \kappa_e$ ) and electrical ( $\rho$ ) resistivities:  $\delta(T) \equiv w_e(T) - \rho(T)$ . The vertical dash-dotted line marks the Néel temperature  $T_N$ . Note how abruptly the onset of static AFM order cuts off the growth in  $\delta(T)$  with decreasing temperature. Note also that  $\delta(T)$  vanishes above  $T \simeq 8$  K, revealing that temperature has by then exceeded the characteristic energy of magnetic fluctuations. The solid line is a fit to  $aT^2 + bT^5$  below  $T_N$ .

in the case of phonon scattering where  $L \rightarrow L_0$  ( $\delta(T) \rightarrow 0$ ) when  $T > \Theta_D$ , where  $\Theta_D$  is the Debye temperature, characteristic of the lattice fluctuations. Thus one can see that  $\delta(T)$  can be used to determine  $T_{\text{SF}}$  while  $\rho(T)$  by itself typically cannot. In this light, let us now examine the behaviour of  $\delta(T)$  and  $L(T)$  in CeRhIn<sub>5</sub>.

### 5.3.1 Vertical Scattering

In Fig. (5.3),  $\delta(T)$  is seen to exhibit two key features: 1) it vanishes for  $T > 8$  K; 2) it drops abruptly below  $T_N$ . The first feature reveals the sharp contrast between horizontal and vertical scattering processes, which respectively cause  $w_{\text{hor}}(T) = \rho(T)$  to increase steadily with increasing temperature, but  $w_{\text{ver}}(T) = \delta(T)$  to decrease (beyond  $T_N$ ). In analogy with phonon scattering (see Section 2.2.2), we use the fact that  $\delta \rightarrow 0$  at  $T > 8$  K to claim that the characteristic fluctuation energy in CeRhIn<sub>5</sub> is of the order of 8 K. Actual calculations, along the lines of those by Kaiser [72] but with an appropriate fluctuation spectrum, are needed to be more specific, but note that  $\mathbf{q}$ -dependent magnetic correlations observed by neutron scattering in CeRhIn<sub>5</sub> do have a characteristic energy less than 1.7 meV (18 K) and they develop below 7 K [140].

Having established a new signature of magnetic scattering in metals, namely the

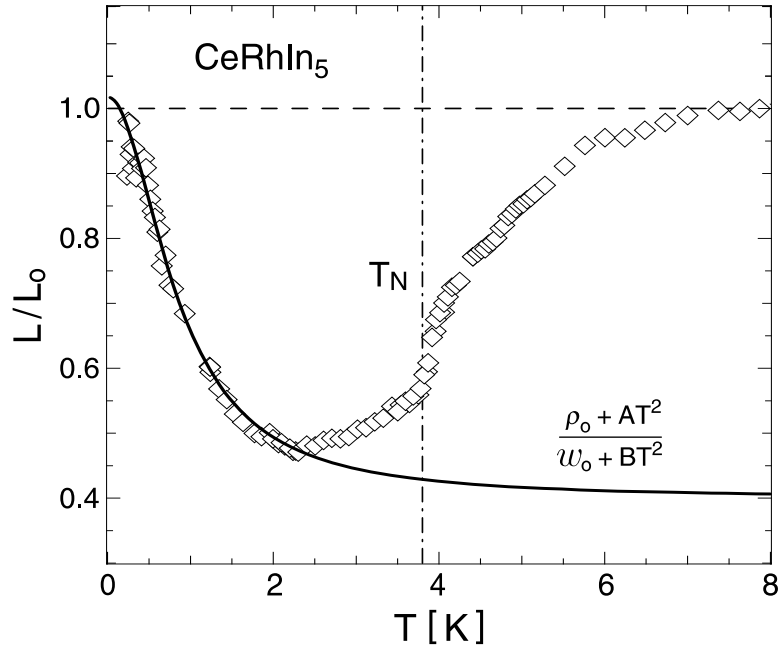


Figure 5.4: Temperature dependence of normalized Lorenz ratio,  $L(T)/L_0 \equiv \kappa_e/L_0\sigma T = \rho(T)/w_e(T)$ . The solid line is a fit to the Fermi-liquid expression,  $L/L_0 = (\rho_0 + AT^2)/(w_0 + BT^2)$ .

criterion  $\delta(T) \rightarrow 0$  at  $T = T_{SF}$ , we can now imagine, for example, using a measurement of  $\delta(T)$  to track the evolution of the fluctuation spectrum as one approaches a QCP.<sup>4</sup>

The second, rather dramatic, feature of Fig. (5.3) is the fact that the rise in  $\delta(T)$  with decreasing  $T$  is interrupted abruptly by the onset of static AFM order at  $T_N$ . Indeed, immediately below  $T_N$ ,  $\delta(T)$  drops rapidly, with a dependence which is well described<sup>5</sup> by  $\delta(T) = w_{\text{ver}}(T) = aT^2 + bT^5$ . Let us look at both terms in turn.

### 5.3.2 Lorenz Ratio and e-e scattering

As shown in the inset of Fig. (5.2), a  $T^2$  dependence is observed in CeRhIn<sub>5</sub> for both resistivities below  $\sim 1.5$  K:  $\rho = \rho_0 + AT^2$  and  $w_e = w_0 + BT^2$ , with  $A = (2.1 \pm 0.1) \times 10^{-2} \mu\Omega \text{ cm}/\text{K}^2$  and  $B = (5.1 \pm 0.2) \times 10^{-2} \mu\Omega \text{ cm}/\text{K}^2$  extracted from linear least-squares fits to the data. The magnitude of  $A$  is quite small compared to other heavy-fermion metals such as CeAl<sub>3</sub> [11], but in fact the ratio of  $A$  to the electronic specific heat coefficient  $\gamma_0 = 56 \text{ mJ/K}^2/\text{mol Ce}$  [143] yields a Kadowaki-Woods ratio ( $A/\gamma_0^2 =$

<sup>4</sup>This is the focus of Section 6.4.2, where the evolution of  $T_{SF}$  in CeCoIn<sub>5</sub> is tracked as a function of applied field.

<sup>5</sup>Data for  $T < T_N$  was fit to the form  $\delta(T) = aT^2 + bT^p$ , where  $a$ ,  $b$  and  $p$  are free parameters, resulting in  $a = 2.9 \times 10^{-2} \mu\Omega \text{ cm}/\text{K}^2$ ,  $b = 1.0 \times 10^{-3} \mu\Omega \text{ cm}/\text{K}^p$  and  $p = 5.0 \pm 0.5$ .

$6.7 \mu\Omega \text{ cm mol}^2 \text{ K}^2/\text{J}^2$ ) that lies on the universal line for heavy-fermion compounds [73].

The fact that  $B > A$  reflects the importance of vertical processes and low- $\mathbf{q}$  scattering, which can result in an angular distribution of scattering that affects heat and charge transport differently (see Section 2.2.2). In this so-called Fermi-liquid regime, we therefore have  $\delta(T) \sim T^2$  and  $L/L_0 = (\rho_0 + AT^2)/(w_0 + BT^2)$  (solid line in Fig. (5.4)), so that the *inelastic* Lorenz ratio is constant:  $L_{\text{in}}(T) \equiv (\rho(T) - \rho_0)/(w_e(T) - w_0) = A/B = 0.41 \pm 0.01$ .<sup>6</sup> Quantitatively, the precise value of  $L_{\text{in}}$  is sensitive to the angular distribution of scattering over the Fermi surface, but is always  $\approx 0.5$  for any type of e-e scattering process (see Section 2.2.3).

A specific calculation based on a two-band screened Coulomb interaction model of *s*-electrons from a spherical Fermi surface scattered by *d*-electrons from a cylindrical surface (originally applied to the transition metal Re) gives a value  $L_{\text{in}} = 0.4$  [69], which is very similar to the value observed in our experiments on CeRhIn<sub>5</sub>.<sup>7</sup> Finally, recall (Section 2.1.1) that the scattering of electrons from localized spin fluctuations also yields a  $T^2$  dependence of the resistivity and a ratio  $A/B$  in the range 0.3-0.6, depending on the angular distribution of scattering [69, 72].

### 5.3.3 Fluctuation Regime

The  $T^5$  term in  $\delta(T)$  below  $T_N$  is a distinctive property of vertical scattering in the ordered state. It survives all the way up to  $T_N$ , but then abruptly goes away beyond that temperature (see Fig. (5.3)). The impact of broken symmetry is dramatic, first and foremost because of a suppression of spin fluctuations caused by a change in the fluctuation spectrum. (This is perhaps due to the opening of a gap, suggested by an activated dependence of specific heat on temperature [143], although no obvious exponential dependence is seen in  $\delta(T)$ .) That suppression is reflected in  $\rho(T)$  as well, but it leads to a different temperature dependence in the case of horizontal scattering:  $\Delta\rho(T) = AT^2 + cT^6$ , as shown by the fit<sup>8</sup> in Fig. (5.5).

---

<sup>6</sup>Note that, similar to the Lorenz number, the error on this value is independent of errors associated with the geometric factor and is determined by statistical errors associated with fitting  $A$  and  $B$  (*e.g.* linear fits in inset of Fig. (5.2)).

<sup>7</sup>The comparison of our result for CeRhIn<sub>5</sub> to this specific calculation is justified given the presence of light, spherical 3D pockets and heavy, quasi-2D cylindrical sheets in the Fermi surface [116], but a more specific calculation using quantities specific to CeRhIn<sub>5</sub> would be useful.

<sup>8</sup>Data for  $T < T_N$  was fit to the form  $\Delta\rho(T) = AT^2 + cT^p$  by fixing the value of  $A$  (extracted previously) and floating the coefficient  $c$  and power  $p$  of the second term, resulting in  $c = 4.2 \times 10^{-4} \mu\Omega \text{ cm}/\text{K}^p$  and  $p = 6.0 \pm 0.1$ .

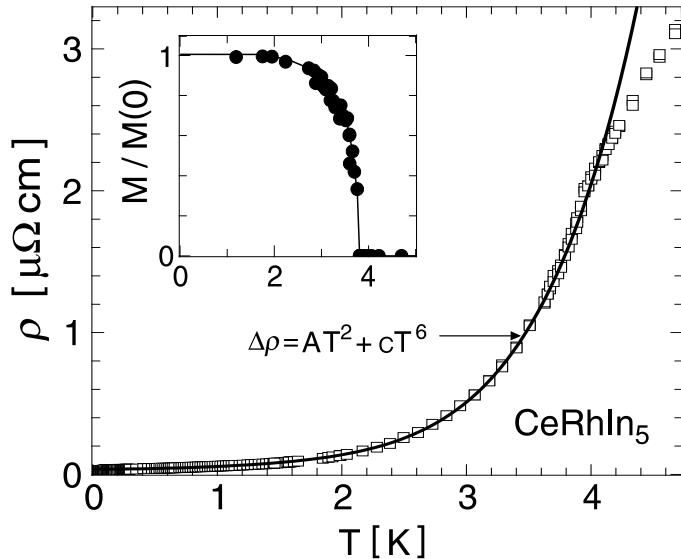


Figure 5.5: Power law fit of resistivity of CeRhIn<sub>5</sub>. Inset shows AFM order parameter obtained from sublattice magnetization (from Ref. [140]).

This difference in power law contains information on the nature of magnetic fluctuations in the ordered state. In this respect, it would be interesting to correlate these power laws with another measure of spin fluctuations: the drop in the sub-lattice magnetization  $M(T)$ . This quantity is a measure of the AFM order parameter that appears below  $T_N$ , and was observed in both neutron diffraction [140] and <sup>115</sup>In nuclear quadrupole resonance [139] measurements to display a  $T$ -dependence that is much more rapid than the mean field expectation ( $\sim (1 - T/T_N)^{1/2}$ ). This may be due to the presence of a multicritical phase transition at  $T_N$  [137], as suggested by the rich field dependence of the CeRhIn<sub>5</sub> phase diagram [143].

## 5.4 Conclusions

In conclusion, we have shown that the dual measurement of heat and charge transport in a metal with magnetic scattering can be used to probe the  $\mathbf{q}$  and  $\omega$  dependence of spin fluctuations and their effect on electron scattering. Our study on the test material CeRhIn<sub>5</sub> reveals a number of interesting features:

- the thermal resistivity is directly proportional to the magnetic entropy;
- the difference between heat and charge transport vanishes above 8 K – a result which can be used to obtain the characteristic energy of the fluctuation spectrum;

- the inelastic Lorenz ratio is equal to 0.4 at low temperature - a direct measure of the angular distribution of scattering;
- the onset of AFM order yields a clean  $T^5$  dependence in the thermal resistivity due to vertical scattering ( $\omega^2$  weighting) and a  $T^6$  dependence in the electrical resistivity due to horizontal scattering ( $\mathbf{q}^2$  weighting).

Detailed calculations based on the known fluctuation spectrum of CeRhIn<sub>5</sub>, measured by magnetic neutron scattering, would be very useful in further exploring all of this information. The following chapter, which explains a similar study of the normal state of CeCoIn<sub>5</sub> as a function of magnetic field, will use a similar approach to see how the characteristic energy scale of spin fluctuations behaves as the field-induced QCP is approached.

---

---

6

---

---

## CeCoIn<sub>5</sub>: FIELD-TUNED QUANTUM CRITICALITY

---

---

The peculiar magnetic properties of CeCoIn<sub>5</sub> are determined by the magnetic moments of Ce<sup>3+</sup> ions and by conduction electrons. As mentioned in Section 3.6.1, systematic studies of Ce<sub>1-x</sub>La<sub>x</sub>CoIn<sub>5</sub> alloys have shown that the energy scales associated with the relevant magnetic interactions are all well separated,<sup>1</sup> and that the dominance of direct intersite interactions below the coherence peak temperature  $T_{\text{coh}} \approx 45$  K gives rise to pronounced two-dimensional antiferromagnetic (AFM) correlations [136]. Although long-range magnetic order is not present in CeCoIn<sub>5</sub> [159], the close proximity of this system to AFM order [155] results in an abundance of spin fluctuations which lead to behaviour that is notably different from that expected in the Landau Fermi liquid (FL) model. Examples of NFL behavior in CeCoIn<sub>5</sub> include a logarithmic increase of the electronic specific heat coefficient on cooling [135, 160, 161], an enhancement of the effective mass at low temperatures and its strong field dependence, as seen in dHvA measurements [110] and microwave conductivity [162] experiments, and a magnetic susceptibility that does not saturate at low temperatures [104].

This chapter discusses heat and charge transport measurements of CeCoIn<sub>5</sub>, for magnetic fields directed along the [001] axis ( $H \parallel [001]$ ) and currents directed in the basal plane ( $J \perp [001]$ ). In this orientation, the strong dependence of transport properties in CeCoIn<sub>5</sub> on magnetic field gives rise to 1) a change in sign of magnetoresistance, 2) a peculiar evolution of power laws, and, most importantly, 3) the ability to suppress quantum fluctuations as a function of field. By performing a systematic study of transport throughout the field-induced normal state, we construct an  $H$ - $T$  phase diagram which reveals a number of important characteristics of quantum criticality in this system. In the next chapter, this diagram will be compared and contrasted with that for the  $H \parallel [001]$  and  $J \parallel [001]$  orientation.

---

<sup>1</sup>The first CEF excited state ( $\Delta \approx 200$  K) is well above the temperatures considered here [136].

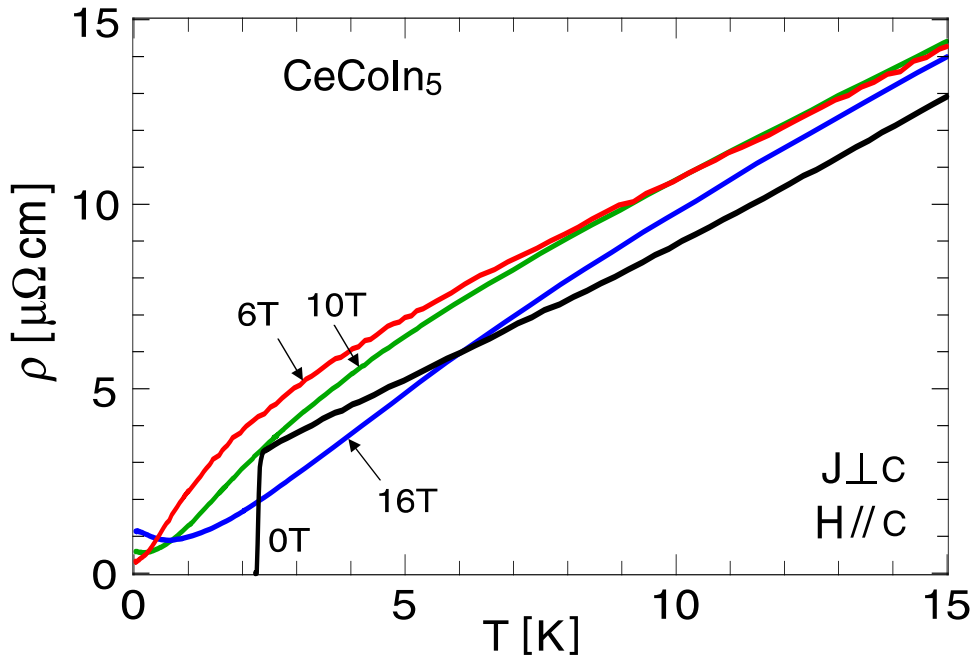


Figure 6.1: Resistivity of CeCoIn<sub>5</sub> up to 16 T.

## 6.1 Magnetoresistance

As shown in Chapter 5, the scattering behaviour in the 115 systems is dominated by spin fluctuations, and so the transport quantities, such as electrical and thermal conductivity, are reflective of the behaviour of the underlying spin spectrum. Hence, the field dependence of transport is a direct probe of the field dependence of the fluctuations. In this section, the characteristics of the magnetoresistance (MR), both as a function of temperature (at constant fields) and field (at constant temperatures), will be discussed in detail.

### 6.1.1 Temperature Dependence

As reported in Section 3.6.1, the zero-field resistivity of CeCoIn<sub>5</sub> exhibits a slight increase upon cooling from room temperature, followed by a crossover to metallic behaviour below  $T_{\text{coh}} \simeq 45$  K, as is seen in many heavy-fermion systems [10, 20]. As shown in Fig. 6.1,  $\rho(T)$  displays a linear temperature dependence below  $\sim 10$  K which persists down to  $T_c = 2.3$  K. Because  $T$ -linear resistivity has been observed in many systems which lie at or close to a QCP [20, 34], this behaviour quickly prompted the conclusion that CeCoIn<sub>5</sub> also lies very close to a QCP at ambient pressure and zero magnetic field [104].

Above 30 K, the MR in CeCoIn<sub>5</sub> is negligibly small up to 16 T, whereas notable MR

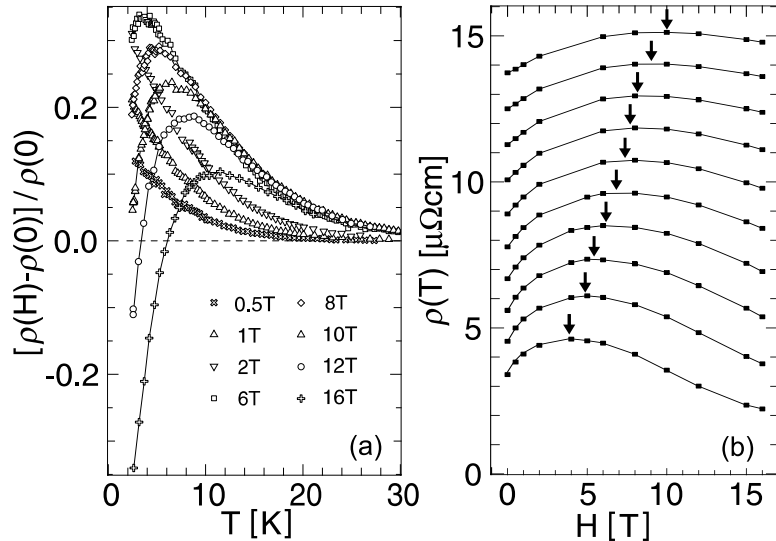


Figure 6.2: Resistivity of CeCoIn<sub>5</sub> under various fields, shown (a) as magnetoresistance versus temperature, normalized to zero field resistivity, and (b) versus applied field, as isotherms for  $T = 16, 14.5, 13, 11.5, 10, 8.5, 7, 5.5, 4$  and  $2.5$  K from top to bottom (lines are guides to the eye and are not offset). The arrows indicate the position of the crossover from positive to negative MR with increasing field for each temperature.

begins to develop below 30 K, as shown in Fig. 6.2(a). A large MR begins to occur at relatively small fields, as shown by a  $\sim 10\%$  increase in the resistivity near  $T_c$  at a field of only 0.5 T, which continues to increase up to  $\sim 6$  T. This peculiar dependence is reflected in the drastic deviation from the  $T$ -linear dependence of  $\rho(T)$  observed at  $H = 0$ . For instance, the 6 T curve (Fig. 6.1) displays a notable deviation from linearity below  $\sim 5$  K and decreases on cooling to a value much lower than the residual resistivity inferred from a linear extrapolation of  $\rho(T, H = 0)$  to  $T = 0$ . By 16 T, the downturn in  $\rho(T)$  shifts to much higher temperatures, as evidenced by the large negative MR below  $\sim 5$  K.

As can be seen in Fig. 6.1, a curvature begins to develop in  $\rho(T)$  at very low temperatures and fields above  $\sim 6$  T, reminiscent of the  $T^2$  dependence of resistivity characteristic of a FL regime. The development of  $T^2$  resistivity was also seen in CeCoIn<sub>5</sub> under applied pressure, where a jump in the exponent of  $T$  from linear to quadratic occurs near 2 GPa [163]. This curvature indeed follows a quadratic temperature dependence and is strongly field-dependent, as will be discussed in Section 6.2.

The behaviour of MR in CeCoIn<sub>5</sub> can be compared and contrasted to that observed in the two closely related 115 materials. In CeIrIn<sub>5</sub>, no significant MR has been observed between 50 mK and 5 K at ambient pressure [103], which is very different than the behaviour of CeCoIn<sub>5</sub> for  $J \perp [001]$  but is intriguingly similar to the MR observed in

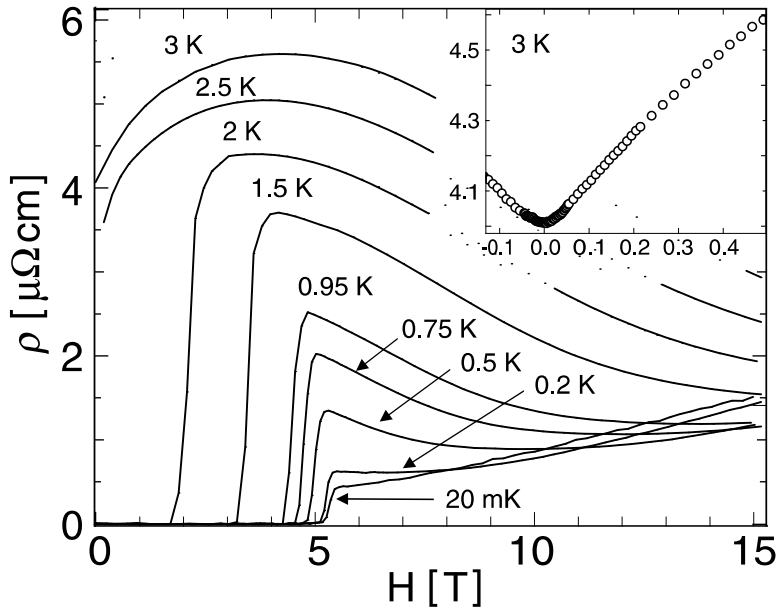


Figure 6.3: Low temperature magnetoresistance of CeCoIn<sub>5</sub>, highlighting the large orbital MR at low  $T$  and high  $H$ . Inset shows the anomalous linear behaviour of MR at low fields.

CeCoIn<sub>5</sub> for  $J \parallel [001]$ , which is the topic of Chapter 7. In CeRhIn<sub>5</sub>, a very large positive MR is observed at ambient pressure [164], which is also reported in Appendix B. The strong field dependence of transport in CeRhIn<sub>5</sub>, which is an extremely clean system, is indicative of the influence of field on the static or fluctuating spin structure, which may be a common phenomenon shared by both CeRhIn<sub>5</sub> and CeCoIn<sub>5</sub>.

### 6.1.2 Field Dependence

The field dependence of  $\rho$ , plotted at constant  $T$  values in Fig. 6.2(b), reveals the development of a *crossover in the sign of MR*, from positive to negative, with increasing field and temperature, being most prominent just above the superconducting state transition. Tracked from  $\sim 16$  K down to temperatures just above  $T_c$ , this MR crossover is a clear indication of a field-induced change in character of the spin fluctuations residing in this system. The qualitative shape of these  $\rho(H)$  curves is notably different from that expected for weak-field orbital MR (*i.e.*  $\Delta\rho \sim H^2$ ) [165], while at high fields the MR becomes negative. Both of these facts, together with the dominance of magnetic scattering observed in CeRhIn<sub>5</sub>, encourage us to consider an unconventional magnetic origin to the observed MR behaviour.

Taking into account the connection commonly made between zero-field  $T$ -linear resistivity and AFM spin fluctuations [20], this conclusion is natural. The initial increase of

$\rho$  with field could originate from an increase of spin disorder. Although positive MR is unexpected in Kondo systems,<sup>2</sup> an increase of  $\rho$  with field is indeed observed in systems with AFM order [44, 164], and in systems approaching a coherent FL state [167]. In CeCoIn<sub>5</sub>, there is no evidence for long-range AFM order [159]. However, notable AFM correlations are observed below  $T_{coh}$ , and so it is natural to associate the increase of spin disorder with a suppression of AFM correlations.

The presence of a large external field is expected to have a strong influence on AFM spin fluctuations. For example, an NMR/NQR study [138] of the effect of field on the spin fluctuation spectrum in CeCoIn<sub>5</sub> has suggested that AFM fluctuations are easily suppressed by field. In YbRh<sub>2</sub>Si<sub>2</sub>, NMR measurements have shown a crossover from AFM fluctuations at low fields to ferromagnetic (FM) fluctuations at high fields [168]. Furthermore, recent neutron scattering experiments [169] on CeCoIn<sub>5</sub> suggest that field-induced (*i.e.* field-polarized) FM order does develop at high fields. Clearly, the polarization of spins by increasing field strength should eventually lead to a field-aligned state, as was indeed observed in the case of YbRh<sub>2</sub>Si<sub>2</sub> [44]. Therefore, a crossover to negative MR should occur at progressively increasing fields at higher temperatures, as observed.

As shown in the inset of Fig. 6.3, the normal state, low-field MR displays a notable range of *linear field dependence*, reproduced in negative field by sweeping through  $H = 0$ . This behaviour, showing positive MR quite different from the usual  $\sim H^2$  dependence observed at such low fields in conventional metals, is also certainly not the  $H$ -linear MR often observed in the  $\omega_c\tau \gg 1$  limit.<sup>3</sup> The origin of linear MR has been suggested by a number of calculations, for example in systems with both small FS pockets and small carrier masses [170], or in Kondo lattice systems [171]. But the reason of its presence in this system is not clear. Curiously, similar linear behaviour is observed in CeRhIn<sub>5</sub> in the same field and temperature range (see Section B), suggesting a direct relation between  $H$ -linear MR and AFM fluctuations. In CeCoIn<sub>5</sub>, the anomalous  $T$ - and  $H$ -linear resistivity present at low fields may indeed be associated with proximity to a zero-field QCP of AFM origin [50]. However, as will be shown below, this low-field behaviour seems to be *unrelated* to the fluctuations associated with a QCP which resides at higher fields.

---

<sup>2</sup>In an system with Kondo impurities, an applied field reduces incoherent Kondo scattering, resulting in negative magnetoresistance. See, for example, Ref. [166]

<sup>3</sup>The  $\omega_c\tau > 1$  limit, where  $H$ -linear MR is expected in normal metals [165], is indeed achieved in CeCoIn<sub>5</sub>, but only at much higher fields - see Section 6.2.

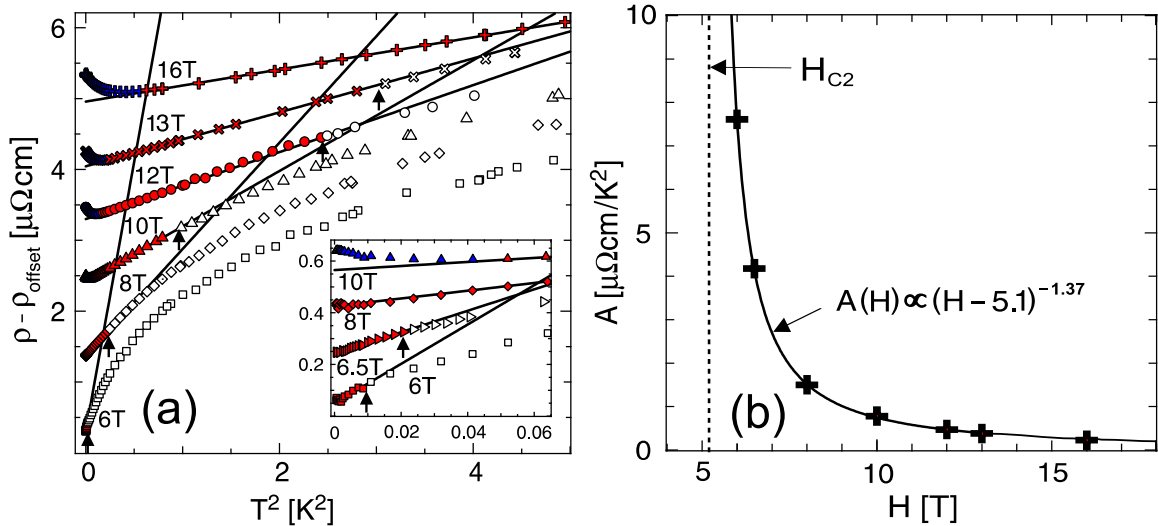


Figure 6.4: (a) Low temperature resistivity of CeCoIn<sub>5</sub> plotted vs.  $T^2$  for several magnetic fields, with an inset zooming on the lowest temperatures (data sets are offset for clarity in both figures). The solid lines are linear fits to the data points shown in red, showing the behaviour of the quadratic-term coefficient (slope) under applied field, with arrows indicating the upper limit ( $T^*$ ) of the temperature range of  $T^2$  behaviour. The blue data points indicate the occurrence of an upturn in  $\rho(T)$  due to orbital effects, as explained in the text. (b) Field dependence of the quadratic coefficient  $A$  of  $\rho(T)$  (solid line is a fit of the data points (+) to the displayed formula).

## 6.2 Field-Induced Fermi Liquid State

This section will focus on the FL ground state which is reached at fields  $H > H_{c2}$ . The strong electron-electron scattering present in this regime is shown to decrease with increasing field, and, moreover, to actually diverge close to the upper critical field for superconductivity. This is the first evidence of a *field-tuned* QCP in CeCoIn<sub>5</sub>.

### 6.2.1 Divergent Scattering at $H^* = H_{c2}$

A close analysis of our 6 T data at low temperatures reveals a narrow but clearly distinguishable range of  $T^2$  behaviour below ~100 mK, highlighted in a plot of  $\rho$  vs.  $T^2$  in Fig. 6.4(a). This range gradually becomes wider and more apparent with increasing field, as determined by a linear least squares fit to each data set.<sup>4</sup> As shown by the linear fits in Fig. 6.4(a), the upper limit of the  $T^2$  temperature range, signified by a characteristic temperature  $T^*$ , increases with field and extends to at least 2.5 K by  $H=16$  T.

<sup>4</sup>The procedure used to fit each curve is similar to that utilized in Ref. [172], where the range of  $T^2$  behaviour, and hence the best fit, is determined by varying the range of fit until the minimum  $\chi^2$  error is found.

Simultaneously, at the lowest measured temperatures, a small *upturn* in  $\rho(T)$  starts to develop above  $\sim 8$  T and continues to grow upon further field increase,<sup>5</sup> which can also be seen in the low temperature field sweeps.<sup>6</sup> This upturn (and positive MR at the lowest temperatures) is attributed to the achievement of the  $\omega_c\tau > 1$  limit, and is discussed in Section A.1.

The slope of the fitted  $\rho$  vs.  $T^2$  curves in Fig. 6.4(a) - *i.e.* the coefficient  $A$  of the  $T^2$  term in  $\rho = \rho_0 + AT^2$  - is a measure of the strength of electron-electron interactions, notoriously high in HF materials. As is clear from the fits,  $A$  tends to decrease with increasing field. As shown in Fig. 6.4(b), the field dependence of  $A$ , or  $A(H)$ , displays *critical* behaviour best fitted<sup>7</sup> by the function  $A \propto (H - H^*)^{-\alpha}$ , with parameters  $H^* = 5.1 \pm 0.2$  T and  $\alpha = 1.37 \pm 0.1 \simeq 4/3$ .<sup>8</sup>

The field-induced recovery of a FL regime in CeCoIn<sub>5</sub>, as expressed by the emergence of a  $T^2$  resistivity component, exhibits a distinct similarity to the behaviour observed in several other systems. In Sr<sub>3</sub>Ru<sub>2</sub>O<sub>7</sub> and CeRu<sub>2</sub>Si<sub>2</sub>, a field-induced anomaly in resistivity is associated in both cases with a change from predominantly AFM to FM fluctuations [173]. In U<sub>0.9</sub>Th<sub>0.1</sub>Be<sub>13</sub>, a system close to a superconducting phase, the evolution of  $A(H)$  and  $T^2$  resistivity with field [172] both bear a close resemblance to that found in this study. In YbRh<sub>2</sub>Si<sub>2</sub>, critical behaviour in  $A(H)$  was observed in proximity to a field-induced QCP associated with a second-order AFM transition, with a critical exponent  $\alpha = -1$  that is similar to the value obtained for CeCoIn<sub>5</sub> [44].

All of the aforementioned systems exhibit critical behaviour in resistivity when approaching some critical field value  $H^*$ . However, what is unique (and intriguing) about CeCoIn<sub>5</sub> is the fact that  $H^*$  is very close to  $H_{c2}(0)$ , which points to the existence of a *QCP coincident with the superconducting transition at  $T = 0$* . The question is whether this coincidence is essential or accidental. In the latter case, the critical behaviour would originate from proximity to an ordered phase (and transition) other than the supercon-

<sup>5</sup>The appearance of this upturn prompted the selection of a lower bound in the  $T^2$  fits, requiring a slight modification of the fitting routine. Nevertheless, since this effect is confined to very low temperatures and high fields, it does not hinder the observation of  $T^2$  resistivity.

<sup>6</sup>For instance, at 20 mK the positive MR observed at all fields ( $H > H_{c2}$ ) shown in Fig. 6.3 is quite different than the (negative) field dependence observed at higher temperatures.

<sup>7</sup>This and all subsequent fits were performed using a non-linear least squares fit routine following the Marquardt algorithm.

<sup>8</sup>Error bars were determined from  $\chi^2$  values obtained in the fit to the critical form by assuming an equal weight on all values of  $A(H)$ . The statistical error on the values of  $A(H)$  (determined from the linear fits of  $\rho$  vs.  $T^2$ ; not shown) is  $\pm 8\%$  at 6 T and much smaller at higher fields. This excludes the absolute error from determination of the geometric factor (since it is equal for all values).

ducting state (and in fact would be masked by superconductivity). In this respect it is interesting to recall the compelling evidence that the  $H_{c2}$  transition in CeCoIn<sub>5</sub> is first-order below  $\sim 1$  K for all field orientations (see Section 3.4). This suggests that critical behaviour of the kind observed here, which is usually associated with a second-order phase transition brought to absolute zero, is not caused by the vicinity of the superconducting state itself. Rather, it is tempting to propose that the quantum critical behaviour observed in CeCoIn<sub>5</sub> is associated with a zero-temperature transition of magnetic origin, much as is the field-induced transition from AFM to field-aligned state in YbRh<sub>2</sub>Si<sub>2</sub> [44]. Further evidence for the non-superconducting fluctuations scenario will be discussed in light of thermal conductivity measurements in Section 6.4.1.

### 6.3 $H$ - $T$ Phase Diagram ( $J \perp [001]$ )

Based on our charge transport analysis, we have constructed a phase diagram of the  $H$ - $T$  plane which reveals a number of key elements relating to both the superconducting and normal states. As shown in Figs. 6.5 and 6.7, we have separated these elements to focus on each of them individually, as discussed in each section below.

#### 6.3.1 $H_{c2}$ Transition and MR Crossover

As shown in Fig. 6.5, a phase diagram can be constructed from a) the experimentally determined ranges of  $T^2$  behaviour at low temperatures, and b) the crossover observed in the sign of MR at higher temperatures. It is apparent that the MR crossover line approaches the  $H_{c2}$  transition and meets it at a finite temperature, so that below  $\sim 1$  K the domain of negative MR is directly adjacent to the SC domain. In fact, the position where this line impinges on the superconducting transition line, at  $\sim 1$  K, coincides with the first-order to second-order tricritical point of  $H_{c2}$  [122, 123, 124, 125], as discussed in Section 3.4. Although many studies have suggested that this tricritical point is connected with the endpoint of the FFLO phase, a recent study by Radovan *et al.* has concluded that the FFLO phase begins below  $T_{\text{FFLO}} = 0.35$  K, *i.e.* much lower than that of the tricritical point [127].

Surprisingly, the MR crossover line in Fig. 6.5 strongly resembles that determined by torque magnetometry [123] for  $H \parallel [110]$ , where a jump in torque associated with the first-order  $H_{c2}$  transition below  $\sim 1.4$  K was traced well into the normal state (up to  $\sim 25$  K), indicative of a metamagnetic transition. Although no such anomaly was found above  $T_c$  for  $H \parallel [100]$  or  $H \parallel [001]$ , and subsequent magnetization measurements did

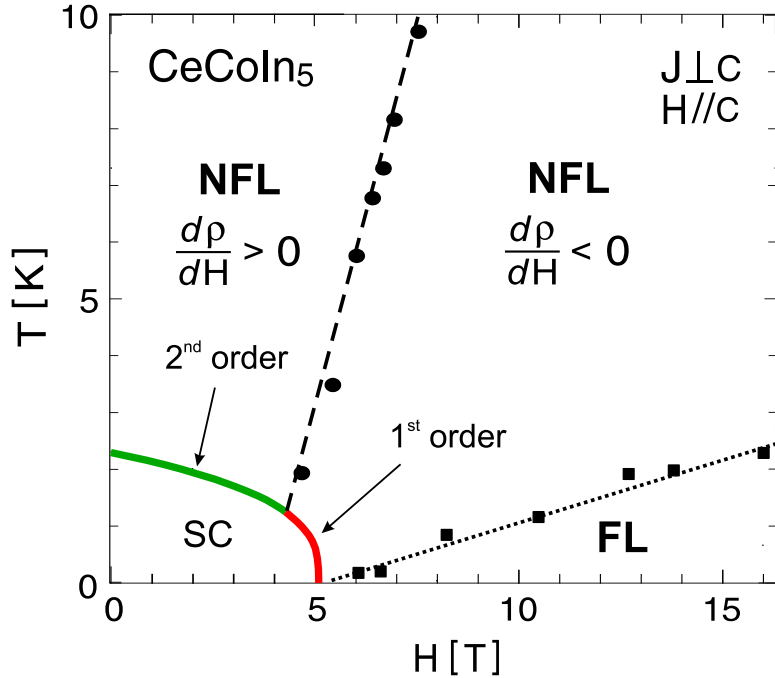


Figure 6.5:  $H - T$  phase diagram of CeCoIn<sub>5</sub> determined from resistivity measurements, including the upper bound of  $T^2$  resistivity (squares), the position of the MR maximum (circles), and  $H_{c2}$  (solid line, separated into two sections indicating the change from second-order (green) to first-order (red) with increasing field). The dotted line indicates the crossover boundary between FL and NFL regimes, and the dashed line indicates the crossover between negative and positive MR regimes, as explained in the text.

not reproduce this result [122], the sensitivity of torque measurements may highlight the importance of the  $H \parallel [110]$  orientation, perhaps associating it with the spin polarization of a sheet of Fermi surface [123].

The similar behaviour observed in both MR and torque measurements further suggests the possible existence of a magnetic order parameter, where the direct observation of a transition may be complicated by many factors, including the multi-band nature of conductivity. In any case, the coincidence between the metamagnetic transition, MR crossover line and the tricritical point suggests that its position is more closely connected to this system's proximity to magnetism, rather than the FFLO state itself. The origin of the tricritical point remains to be shown, but a study of the evolution of MR crossover behaviour and the tricritical point with Ce-site dilution (*i.e.* Ce<sub>1-x</sub>La<sub>x</sub>CoIn<sub>5</sub>) may provide the strongest link yet between these phenomena - see Appendix A.3.

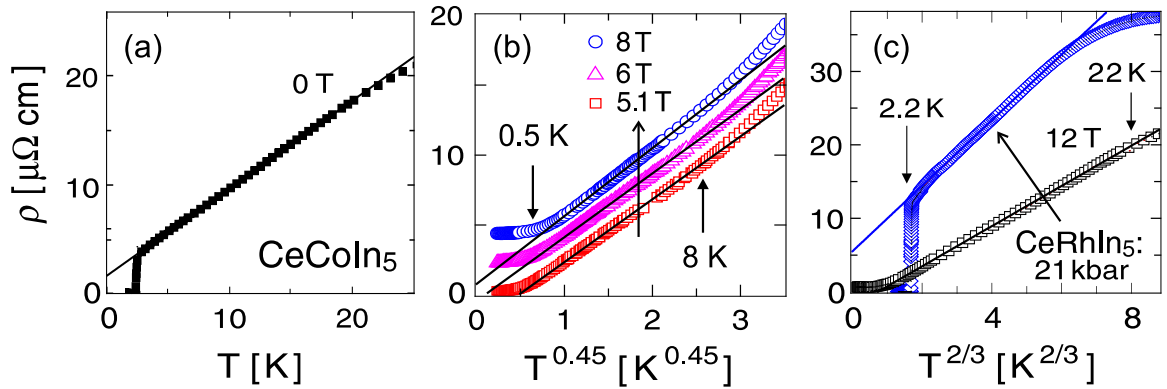


Figure 6.6: In-plane resistivity of CeCoIn<sub>5</sub> plotted (a) vs.  $T$  at 0 T, (b) vs.  $T^{0.45}$  at 5.1, 6 and 8 T, and (c) vs.  $T^{2/3}$  at 12 T, together with resistivity data for CeRhIn<sub>5</sub> at 0 T and 21 kbar applied pressure (from Ref. [102]).

### 6.3.2 Power Law Evolution

A systematic analysis of the power law behaviour of  $\rho(T)$  in the NFL regime (*i.e.*  $\Delta\rho \propto T^n$ ) shows that the zero-field  $T$ -linear temperature dependence undergoes a *qualitative* change with increasing field: the shape of  $\rho(T)$  begins to deviate from linearity, and *sub- $T$ -linear* power laws (*i.e.*  $n < 1$ ) develop over a sizable range spanning more than a decade in temperature. As shown by the linearity of the  $\rho$  vs.  $T^n$  curves in Fig. 6.6, this power law evolves from  $n = 1$  at zero field to  $n = 2/3$  at high fields. The range of validity is over one decade in all cases: *e.g.* from  $T_c = 2.3$  K to  $\sim 20$  K in  $H = 0$ , and from  $T^* = 1 - 2$  K to  $\sim 25$  K in  $H \geq 12$  T.

The evolution of this power law exponent through the  $H$ - $T$  plane is highlighted in Fig. 6.7. Typically, the phase diagrams of systems tuned through a QCP are characterized by a single power law of  $\rho(T)$  throughout the NFL regime [19, 20, 38, 50, 174, 175]. In CeCoIn<sub>5</sub>, the evolution of the exponent  $n$ , from linear to sub-linear with increasing field, is unusual. Furthermore, it is non-monotonic, with the smallest value observed in a small region near the critical field (shaded area in Fig. 6.7), where  $n \simeq 0.45$  between  $\sim 0.5$  K and  $\sim 8$  K at 5.1 T (see Fig. 6.6(b)). Although this is the strangest power law reported here, note that the same value ( $n \simeq 0.45$ ) is also observed for longitudinal transport (*i.e.* for  $H \parallel J$ ) near  $H_{c2} \simeq 13$  T - see Fig. (7.3), and that the MR crossover appears to be centered near this field for both orientations.

The field evolution of the transport power law, together with the MR crossover, are indicative of competing energy scales, and may indeed be a consequence of the presence of two QCPs. For example, a scenario involving two distinct QCPs has recently been

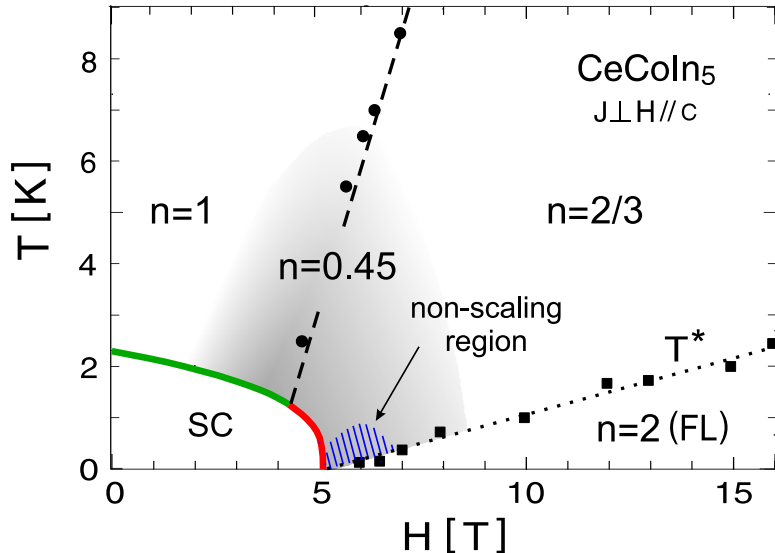


Figure 6.7:  $H$ - $T$  phase diagram of CeCoIn<sub>5</sub>, with evolution of the exponent  $n$  (in  $\Delta\rho \propto T^n$ ) observed in the non-Fermi liquid regime above the superconducting (SC) and Fermi liquid (FL) states. The dotted line indicates the FL-NFL crossover at  $T^*$  (squares are data points marking the end of the FL ( $n = 2$ ) regime). The dashed line indicates the crossover from positive (at low  $H$ ) to negative (at high  $H$ ) magnetoresistance (circles are data points marking the peak in  $\rho$  vs.  $H$ ). The shaded area is a crossover region where neither of the well-defined power laws ( $n = 1$  at low  $H$  and  $n = 2/3$  at high  $H$ ) are observed, and the hatched area indicates the region where  $\Delta H/T$  scaling fails, as explained in the text.

identified in the HF superconductor CeCu<sub>2</sub>Si<sub>2</sub>, where competing magnetic and mixed-valence states give rise to two separate superconducting phases as a function of lattice density [176]. In the case of CeCoIn<sub>5</sub>, the two QCPs may involve two distinct groups of carriers (*i.e.* different Fermi surfaces), an idea which will be elaborated upon in Chapter 7.

Aside from hints of competing criticality in the power law evolution of  $\rho(T)$ , a *sub-linear* value of the power law exponent is itself quite intriguing. For instance, a  $T$ -linear (*e.g.* in YbRh<sub>2</sub>Si<sub>2</sub> [175]) or  $T^{3/2}$  (*e.g.* in MnSi [174] and CeIn<sub>3</sub> [19]) dependence of  $\rho(T)$  have become standard indications of NFL behaviour arising from a QCP, and some success has been had in describing such power laws with spin fluctuation theories [30, 48, 50, 52] (see Section 2.3). For example, a linear  $T$  dependence - one of the hallmarks of electron behaviour in cuprates - is obtained for AFM fluctuations in two dimensions [49, 54].

Recently, a *downward curvature* in (*i.e.* a sub-linear  $T$  dependence of)  $\rho(T)$  has appeared in several systems on the verge of magnetic order. For instance, the resistivity of both URu<sub>2</sub>Si<sub>2</sub> [177] and YbAgGe [178] exhibit such behaviour in their field-induced NFL regimes, and that of Na<sub>*x*</sub>CoO<sub>2</sub> has been described with a  $\sim T^{2/3}$  power law [179]. Such

a strong  $T$  dependence finds no explanation by any of the standard theories of quantum criticality, and has gone largely unnoticed.

It is therefore instructive to compare CeCoIn<sub>5</sub> to its close cousin CeRhIn<sub>5</sub>, an antiferromagnet with  $T_N = 3.8$  K. Under an applied pressure of 21 kbar, CeRhIn<sub>5</sub> develops a superconducting state [102], with a  $T_c$  similar to that of CeCoIn<sub>5</sub> but with a zero-field resistivity that is *not* linear in temperature. Rather, as shown in Fig. 6.6(c), CeRhIn<sub>5</sub> displays a  $T^{2/3}$  dependence, with a prefactor and temperature range that are comparable to that of CeCoIn<sub>5</sub> at high field.

Although this common behaviour occurs in different regions of phase space for the two materials (*i.e.* at different pressure and field values), it is worth noting that the  $T^{2/3}$  dependence in CeRhIn<sub>5</sub> exists in a region where this system is on the verge of developing long-range AFM order [141]. The observation of a similar power law in Na<sub>x</sub>CoO<sub>2</sub> [179], a compound seemingly unrelated but close to a spin-density wave instability, suggests that the 2/3 exponent may be characteristic of a more general set of systems close to an ordering instability.

In addition to the apparent empirical connection between sub-linear power laws and proximate magnetic order, there are indications that such power laws may in fact be calculable. It has been suggested that when several bands cross the Fermi surface, Umklapp-type scattering may enforce the same  $T$ -dependence in  $\rho$  as the  $\omega$  dependence in the single-particle self-energy (Ref. [7], pg. 351). It is thus tempting to relate the  $T^{2/3}$  behaviour to an  $\omega^{2/3}$  dependence of the imaginary part of the fermionic self-energy, which was obtained in some recent calculations considering various Fermi liquid instabilities [180]. More theoretical work is needed in order to understand how sub-linear power laws can arise from various mechanisms, and how these relate to the system at hand.

### 6.3.3 $\Delta H/T$ Scaling

In order to help elucidate the origin of the  $T^{2/3}$  resistivity, as well as the true role of magnetic field as a tuning parameter, it is necessary to understand the relationship between the relevant energy scales:  $H$  and  $T$ . In Fig. 6.8, we show that for  $H \geq 8$  T, the resistivity data can be scaled as a function of  $\Delta H^\gamma/T$  (where  $\Delta H = H - H^*$ ) with an exponent  $\gamma = 1.0 \pm 0.02$ .<sup>9</sup> This relationship, which spans both the FL and

---

<sup>9</sup>The scaling exponent was determined by varying the exponent and minimizing the resultant mean of the average residual values for each data set ( $T$ -sweep at each field) as determined by their difference from the 8 T data set across the overlapping temperature range. The error in this value was estimated as one standard deviation from the minimum value.

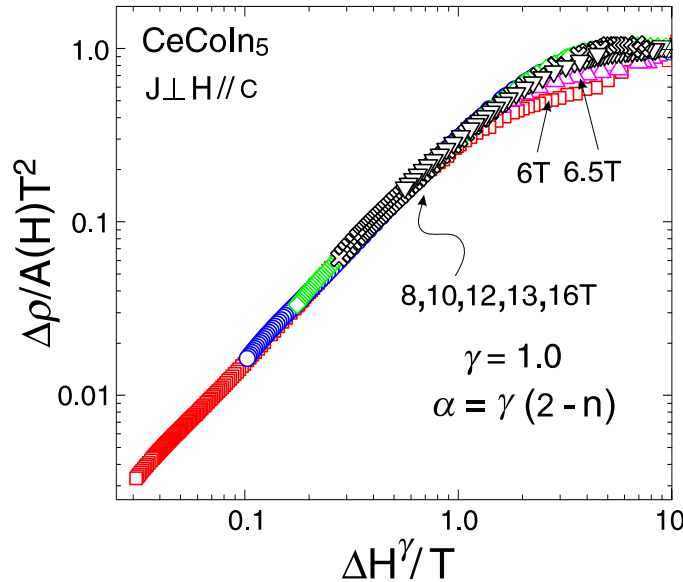


Figure 6.8: Scaling analysis of resistivity in the normal state of CeCoIn<sub>5</sub>, as a function of  $\Delta H \equiv (H - H^*)$  and  $T$ . The linear scaling, with  $\gamma = 1.0$ , confirms the direct relation between the exponent  $\alpha = 4/3$  of the diverging e-e coefficient  $A(H) \propto (H - H_A^*)^{-\alpha}$  in the FL regime and the power  $n = 2/3$  of the  $T$ -dependent resistivity  $\Delta\rho \propto T^n$  in the NFL regime. A small region of non-scaling behavior is highlighted at low temperatures for 6 and 6.5 T, and is described in the text.

NFL regimes, indicates that upon crossing  $T^*$  the dominant energy scale is transferred from temperature to magnetic field, confirming that  $\Delta H$  is indeed the relevant quantum critical tuning parameter.

The significance of this scaling is realized by considering the  $T$ - and  $H$ -dependent resistivity to include a function  $f(\Delta H^\gamma/T)$  which describes scattering in both FL and NFL regimes - *i.e.*  $\Delta\rho = A(H, T)T^2 = f(\Delta H^\gamma/T) \times A(H)T^2$ . The limits of this function (in the FL and NFL regimes) must obey experimental observations, imposing the relation  $\alpha = \gamma(2 - n)$  between the critical exponent  $\alpha$ , the resistivity power law exponent  $n$  and the scaling exponent  $\gamma$ . This can be shown as follows:

- For  $T \ll \Delta H$  (FL regime),  $\Delta\rho = A(H)T^2$  and  $f(\Delta H^\gamma/T) \rightarrow \text{constant}$ .
- For  $T \gg \Delta H$  (NFL regime),  $f(\Delta H^\gamma/T) \rightarrow (\Delta H^\gamma/T)^\lambda$  (since  $\Delta\rho \sim T^n \sim A(H)T^2 \times (\Delta H^\gamma/T)^\lambda$  for some arbitrary exponent  $\lambda$ ) and so the exponent  $n$  must obey the relation  $n = 2 - \lambda$ . In this limit, the field-dependent component of  $\Delta\rho$  (*i.e.*  $A(H) \times (\Delta H^\gamma)^\lambda$ ) must remain self-consistent. Since we know  $A(H) \sim \Delta H^{-\alpha}$ , this immediately identifies the restriction  $\alpha = \gamma(2 - n)$ .

Therefore, the scaling exponent  $\gamma = 1.0$  is shown to reveal  $\alpha = 4/3$  and  $n = 2/3$  as two

aspects of the same critical behaviour: respectively, the  $H$  dependence in the FL regime and the  $T$  dependence in the NFL regime. We can thus conclude that the anomalous  $T^{2/3}$  high-field transport behaviour is *directly related* to the field-induced QCP at  $H^*$ .

Recently, field-tuned quantum criticality was established in the AFM compound YbRh<sub>2</sub>Si<sub>2</sub>, where the zero-field Néel temperature  $T_N = 70$  mK can be driven to zero by applying a field of  $H^* = 0.66$  T. As this QCP is approached, the scattering cross-section is found to diverge as  $A(H) \propto (H - H^*)$  [38]. Although its critical exponent (*i.e.*  $\alpha = 1$ ) and NFL power law (*i.e.*  $n = 1$ ) differ from those of CeCoIn<sub>5</sub>, this system also exhibits linear  $\Delta H/T$  scaling of resistivity (*i.e.*  $\gamma = 1$ ). This is reflected in both systems as a *linear* field dependence of  $T^*$  (*i.e.*  $T^*(H) \propto \Delta H$ , as seen in Fig. 6.6), and was shown to be a universal property of YbRh<sub>2</sub>(Si<sub>1-x</sub>Ge<sub>x</sub>)<sub>2</sub> (observed in both  $x = 0$  and  $x = 0.05$  compounds). Moreover, this linear relationship was also observed in the scaling of specific heat, leading Custers *et al.* to conclude that the reported break-up of the FL in YbRh<sub>2</sub>Si<sub>2</sub> involves the entire Fermi surface [38].

In CeCoIn<sub>5</sub>, specific heat data was shown to follow a peculiar form of  $\Delta H/T$  scaling in the range  $6$  T  $< H < 9$  T, where the data can be scaled by first subtracting the critical field data [161]. Although the reported thermodynamic scaling exponent is different from that obtained here, one must be cautious in comparing these values. First, there is only 1 T of overlap between the field ranges of scaling in the two experiments. Second, the FL-NFL crossover behaviour is qualitatively different for the two quantities: in contrast to the strictly  $T^2$  dependence of  $\rho(T)$  seen down to 6 T,  $C/T$  does not show the complete saturation characteristic of a FL regime until above  $\sim 8$  T [161]. Intriguingly, this is precisely the same range (*i.e.*  $H < 8$  T and  $T < 1$  K) where resistivity deviates from the scaling function, as highlighted in Fig. 6.8 for fields below 8 T.

The deviations observed near the critical field - from  $\Delta H/T$  scaling in transport and from saturation of  $C/T$  in specific heat - could be a consequence of competing fluctuations, as suggested previously, or an effect of disorder (see Section A.2). Considering the multi-band nature of CeCoIn<sub>5</sub>, it is not surprising to see such subtle differences between transport and thermodynamic quantities, whose properties are dominated by light- and heavy-mass carriers, respectively. Furthermore, if scaling is breaking down closest to the QCP in one quantity, there is no particular reason to expect parallel behaviour in the other. In any case, it may be more instructive, for instance, to compare these quantities more directly via the Kadowaki-Woods relation, as will be shown in Section 6.4.3.

## 6.4 Nature of the field-induced QCP

With a connection between the  $T^{2/3}$  resistivity and the field-induced QCP firmly established, we now attempt to shed further light on the nature of this unusual QCP by comparing heat and charge transport. One of the main questions about quantum criticality is whether the Wiedemann-Franz (WF) law is obeyed at the QCP: does the quasiparticle picture really underlie the so-called NFL behavior observed at finite temperatures, or do new exotic excitations occur as a result of the strong interactions? In CeCoIn<sub>5</sub>, we have the advantage of being able to tune the criticality using magnetic field, allowing us to probe the zero-temperature limit and the WF law while smoothly approaching and retreating from the QCP with minimal systematic error. As discussed in Chapter 5, the comparison of heat and charge at higher temperatures can also unveil useful information about the inelastic scattering processes involved in the observed NFL behaviour, which will be shown.

This section will focus on a set of heat and charge transport data (for  $H \parallel [001]$ ,  $J \perp [001]$ ) obtained from the *same sample* of CeCoIn<sub>5</sub> in a “double-run” experiment.<sup>10</sup> This procedure was specially designed to avoid disturbing the sample-field orientation and to use the same contacts to measure both  $\rho(T)$  and  $\kappa(T)$ , thus ensuring a proper comparison between the two quantities. A final comparison between transport and specific heat, via the Kadowaki-Woods relation, will be made at the end of the section.

### 6.4.1 Thermal Transport in the FL Regime

The normal state ( $H > H_{c2}$ ) thermal conductivity of CeCoIn<sub>5</sub> is shown in Fig. 6.9(a) as  $\kappa/T$  vs.  $T$ . Upon cooling,  $\kappa/T$  increases in all fields, and shows a divergent behavior as the field is decreased toward  $H_{c2} = 5$  T, without any tendency toward saturation.<sup>11</sup> This behaviour is reminiscent of specific heat measurements [161], which shows a logarithmic temperature dependence at  $H_{c2}$  which does not saturate down to the lowest measured temperatures. The unusual shape of  $\kappa/T$  is also different from previous observations in HF systems, and it reflects the combination of the relatively weak elastic scattering (*i.e.* small  $\rho_0$ ), and the strong inelastic scattering (*i.e.* divergent behaviour of  $A(H)$ ) that appears in these compounds.

---

<sup>10</sup>The same results were reproduced in a second sample measured in the same way.

<sup>11</sup>No indication of a superconducting transition was observed in  $\kappa(T)$  down to 5.1 T, which is not any different than data at 5.25 T.

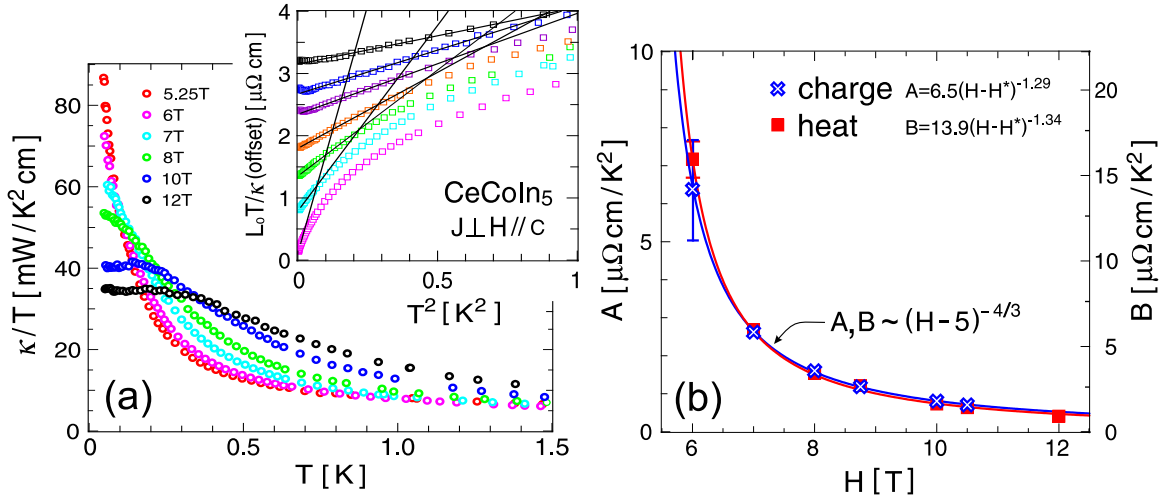


Figure 6.9: (a) Normal state thermal conductivity of CeCoIn<sub>5</sub>. Main plot:  $\kappa/T$  [mW/K<sup>2</sup>cm] vs  $T$  [K] for applied fields 5.25T, 6T, 7T, 8T, 10T, 10.5T, and 12T. Inset: linear fits of the thermal resistivity  $L_0 T / \kappa$  vs.  $T^2$  for applied fields of 6, 7, 8, 8.75, 10, 10.5 and 12 T (bottom to top). The data is offset for clarity. (b) Field dependence of the  $T^2$  Fermi-liquid coefficients of charge ( $A$ ) and heat ( $B$ ) transport, with line fits as shown and described in the text.

Charge transport data for this sample<sup>12</sup> was analyzed in the same manner as discussed in Section 6.2 to obtain the  $T^2$  resistivity range and coefficient as a function of field. For this data, the divergence of  $A(H)$  is characterized by fit parameters  $H_A^* = 5.0 \pm 0.1$  T and  $\alpha = 1.29 \pm 0.1$ , thus reproducing the previous result to within experimental error.<sup>13</sup> In the inset of Fig. 6.9(a), the thermal data is plotted<sup>14</sup> as  $w_e \equiv L_0 T / \kappa_e$  vs.  $T^2$ , in a way convenient for comparison with resistivity (as done in Section 5.2). In this plot, the slope  $B$  represents the contribution of e-e scattering to thermal transport, analogous to the  $A$  coefficient. This plot reveals a strong  $T^2$  contribution to the thermal resistivity (*i.e.* in  $w_e = w_0 + BT^2$ ), characteristic of a FL regime at high fields, with a temperature range that decreases rapidly as the field is decreased toward  $H_{c2}$ .<sup>15</sup>

The field dependence of  $B$  is plotted in Fig. 6.9(b) together with that of  $A$ , both determined using the same fitting procedure. It is readily apparent that  $B(H)$  possesses the *same critical field dependence* as  $A(H)$ . Specifically,  $B$  is best fitted by a function  $B(H) \propto (H - H_B^*)^{-\beta}$  with parameters  $H_B^* = 5.0 \pm 0.2$  T and  $\beta = 1.34 \pm 0.1$ , so that

<sup>12</sup>This sample is from a different growth than the one analyzed in Section 6.2 (*i.e.* Fig. 6.4).

<sup>13</sup>The critical fit was also done in the same manner as above. Note that the statistical error in  $A(H)$  (determined from the linear fits of  $\rho$  vs.  $T^2$ ) has a maximum value of  $\pm 5\%$  for this particular sample.

<sup>14</sup>Although a phonon contribution was subtracted in the same manner described previously (Section 5.1), it is in fact negligible below  $\sim 1$  K.

<sup>15</sup>Note that the FL-NFL crossover temperature for thermal transport is found to be *lower* than for charge transport ( $T^*$ ) at a given field.

$H_A^* = H_B^* = H_{c2}$  and  $\alpha = \beta$  to within error. Therefore,  $A(H)$  and  $B(H)$  differ only by a *field-independent* factor,  $A/B = 0.47 \pm 0.05$ ,<sup>16</sup> which is a value typical of e-e scattering in metals, as observed and discussed for the case of CeRhIn<sub>5</sub> (Section 5.3.2).

Although the coefficients  $A$  and  $B$  describe scattering in the FL regime, their dependence on  $\Delta H$  is an *intrinsic* connection to the QCP: a comparison between the two quantities reflects the nature of the fluctuations responsible for the field-dependent scattering, and hence contains information on the nature of the quantum phase transition itself. The parallel behaviour of heat and charge transport, as evidenced by a constant  $A/B$  ratio, certainly seems to rule out critical fluctuations of a superconducting nature, as these two conductivities generally tend to differ most severely in the presence of superconducting correlations (*i.e.* charge conductivity becomes much higher than thermal conductivity).

Rather, this behaviour, together with the similarities to CeRhIn<sub>5</sub> discussed above, points to critical fluctuations of a magnetic origin. For instance, if FM fluctuations are present, inelastic scattering of electrons involves a wavevector  $\mathbf{q} = 0$ , so a strong difference between the scattering of heat and charge should be observed both in the  $T$ -dependence [64] and in the distance  $\Delta H$  to the QCP (since  $\Delta H/T$  scaling connects the two). On the contrary, large- $\mathbf{q}$  scattering from AFM fluctuations is expected to degrade currents of heat and charge in a similar way, as shown for the case of CeRhIn<sub>5</sub> in Chapter 5. In CeCoIn<sub>5</sub>, the constant  $A/B$  ratio is suggestive of dominant large- $\mathbf{q}$  scattering, and hence AFM fluctuations associated with the field-tuned QCP.

#### 6.4.2 Wiedemann-Franz Law

We can gain further insight into the nature of fluctuations in CeCoIn<sub>5</sub> by analyzing the ratio of heat to charge conductivities, or the Lorenz number  $L(T) = \rho(T)/w_e(T)$ . In Fig. 6.10 we plot the Lorenz ratio normalized to that expected by the WF law,  $L = L_0$ , for magnetic fields up to 12 T, with a phonon correction applied to the thermal data.<sup>17</sup> It is immediately apparent that  $L(T)$  approaches the WF law expectation at low and high temperatures, with strong deviations visible at intermediate temperatures. We will discuss each of these regions below.

<sup>16</sup>Statistical error associated with determination of coefficients of  $A(H)$  and  $B(H)$ .

<sup>17</sup>A phonon contribution was subtracted from  $\kappa(T)$  in the same manner as described previously in Section 5.1 - see Appendix C.1 for details.

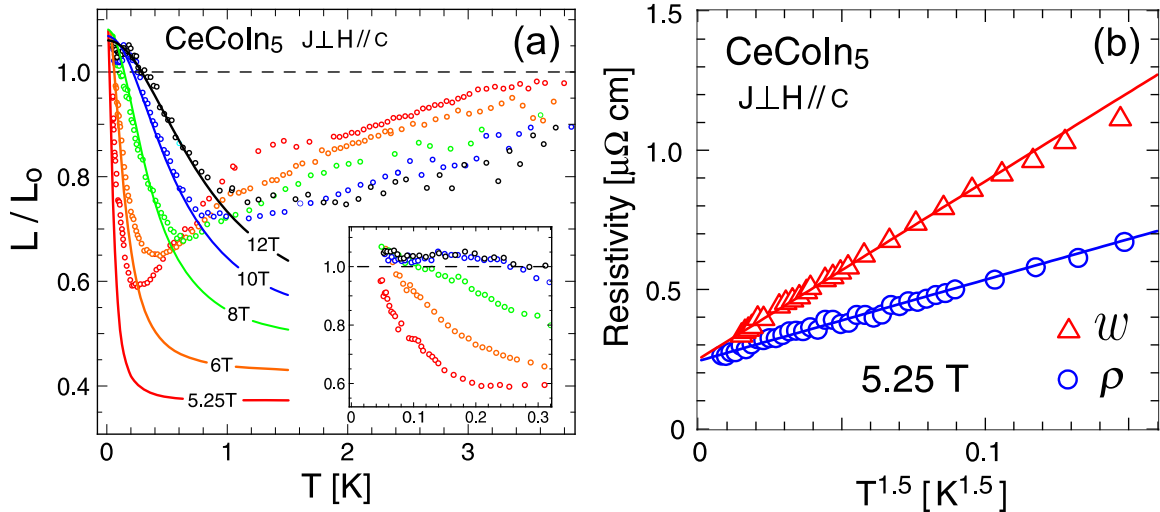


Figure 6.10: (a) Normal state Lorenz ratio of CeCoIn<sub>5</sub> for  $J \perp [001]$  and various fields  $H \parallel [001]$ , shown as a function of temperature and normalized to the WF law expectation. The solid lines are fits to the Fermi-liquid expression,  $L/L_0 = (\rho_0(H) + A(H)T^2)/(w_0(H) + B(H)T^2)$ , for each field as indicated. Inset: zoom of low temperature data. (b) Plot of electrical ( $\rho$ ) and thermal ( $w$ ) resistivity at the critical field as a function of  $T^{1.5}$ .

$T \rightarrow 0$  (elastic limit):

At the lowest temperatures, the data for all fields tend toward  $L(0) = L_0$ , to within systematic experimental error.<sup>18</sup> As shown in Fig. (6.10)(b), the agreement of the WF law nearest to the critical field (5.25 T) can be seen directly in  $T \rightarrow 0$  extrapolations of  $\rho(T)$  and  $w(T)$ . Linear fits<sup>19</sup> of each quantity yield residual resistivity values that differ by only 2%, which is within the statistical error<sup>20</sup> associated with each fit. This observation verifies that the WF law is indeed satisfied closest to the field-induced QCP as  $T \rightarrow 0$  for  $J \perp [001]$  transport, ruling out the possible existence of exotic Fermionic excitations (e.g. spin-charge separation), where an added contribution to thermal transport would cause  $L(0) > L_0$  [57]. Thus, Landau's quasi-particle picture seems to be valid for transport in the basal plane, and no detectable breakdown of FL theory occurs at the field-induced

<sup>18</sup> There is a  $\pm 2\%$  error associated with the interpolation fitting (of resistivity) required to plot the Lorenz ratio, in addition to the scatter associated with each set of data. A systematic  $\sim 5\%$  positive deviation from  $L = L_0$  at  $T \rightarrow 0$ , although within scatter, is most likely a geometric factor effect: thermal transport is not hindered by sample defects in the same manner as charge transport. The observation of this trend in various samples, together with a lack of field dependence allow us to rule out any intrinsic origin of this observation.

<sup>19</sup>The best power law fit to the low temperature portion of each data set yielded a  $T^{1.5}$  dependence. Although merely used to attain the best extrapolation to  $T = 0$  at this point, the significance of this temperature dependence will be discussed in Chapter 7.

<sup>20</sup>Fits to each quantity yield  $\rho_0 = 0.245 \pm 0.003 \mu\Omega \text{ cm}$  and  $w_0 = 0.250 \pm 0.003 \mu\Omega \text{ cm}$  (excluding error associated with the geometric factor, which is 11% for this sample).

QCP. Although this conclusion is drawn from data taken at 5.25 T, which is slightly above the critical field value of 5 T, thermal transport data taken at 5.1 T (which is the closest possible field to  $H_{c2}$  without any indication of superconductivity)<sup>21</sup> is identical to that taken at 5.25 T. This excludes the possibility that the measurements at 5.25 T are not representative of the behaviour at the true critical field of 5 T.<sup>22</sup>

$0 < T < T^*$  (FL regime):

Upon increasing  $T$ , the data at all fields quickly deviate below  $L = L_0$ , most notably at the lowest field of 5.25 T. This drop is accounted for by the *crossover* from dominant elastic ( $L/L_0 \rightarrow 1$ ) to inelastic ( $L/L_0 \rightarrow A/B$ ) e-e scattering, as discussed in Section 2.2.3. In this case, the  $T^2$  scattering terms have a (divergent) field dependence, so Eqn. (2.10) is written as

$$L/L_0 = \frac{\rho_0(H) + A(H)T^2}{w_e(H) + B(H)T^2}, \quad (6.1)$$

which includes the field dependence of the  $T^2$  coefficients and residual resistivities.<sup>23</sup> As shown by the solid lines in Fig. 6.10, the field evolution of  $L/L_0$  in the FL regime is testament to the increasing strength of inelastic scattering - *i.e.* magnitude of  $A$  ( $B$ ) relative to  $\rho_0$  ( $w_0$ ) - upon approach to the field-induced QCP at  $H_{c2}$ . This behaviour results in an unprecedented 40% deviation from the WF expectation in 5.25 T field at only 200 mK. Amazingly, the WF law is recovered at lower temperatures as stated previously, highlighting the *extremely small* energy scales involved in this system.

As highlighted in Fig. 6.11, the initial decrease in  $L(T)$  of CeCoIn<sub>5</sub> in 10 T is in fact quite similar to that of CeRhIn<sub>5</sub>. Despite the  $\sim 40$  times smaller  $A$  coefficient of CeRhIn<sub>5</sub> ( $0.8 \mu\Omega\text{cm}/\text{K}^2$ ), the large difference in residual resistivities equates to a comparable ratio of elastic-to-inelastic scattering strengths, and hence a similar crossover behavior which can be attributed to e-e scattering in both cases. The more abrupt deviation from the FL expectation in CeCoIn<sub>5</sub> at higher temperatures is a result of the difference in spin fluctuation energy scales, as will be discussed below.

<sup>21</sup>Charge resistivity at 5.1 T showed indications of superconductivity, and hence a proper comparison between heat and charge could not be made at this field.

<sup>22</sup>Further evidence, which includes an observed violation of the WF law at 5.3 T for  $J \parallel [001]$ , will be given in the next chapter.

<sup>23</sup>The residual resistivity is approximately linear in field (*i.e.*  $\rho_0(H) \sim H$ ) up to 18 T, but is also affected by orbital MR, making its field dependence highly dependent on sample-field orientation (see Appendix A.1); this is the main reason for performing heat and charge measurements on a sample who's position was undisturbed between runs.

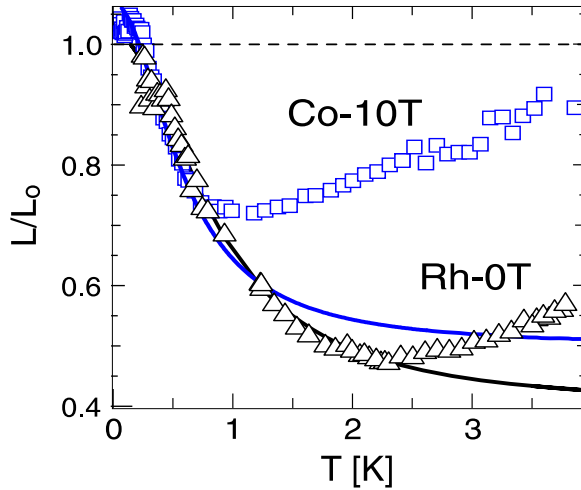


Figure 6.11: Comparison between the Lorenz ratio of CeCoIn<sub>5</sub> at 10 T and CeRhIn<sub>5</sub> at 0 T, showing similar evolution with field. The solid lines are fits to the Fermi-liquid expression  $L/L_0 = (\rho_0 + AT^2)/(w_0 + BT^2)$ , as described in the text.

#### $T > T^*$ (NFL regime):

In the FL regime, the influence of spin fluctuations is thought to be “buried” within the field dependence of the FL coefficients: hybridization of the  $f$  electrons with the conduction band results in a renormalized effective mass that increases (diverges) toward the QCP. Above  $T^*$ , this is no longer the case, and the angular distribution of electron-spin fluctuation scattering should be directly observable through  $L(T)$ . At 5.25 T, where there is no observable FL regime,  $L(T)$  appears to lie above the predicted FL expectation (*i.e.* using  $\Delta H = 0.15$  T in Eqn. (6.1)) at all measured temperatures as seen in Fig. 6.10. Presumably, the 5.25 T data are coincident with this line at only the lowest temperatures, increasing above it at or below the lowest observable temperatures. As the field is increased (and hence the  $T$ -range of FL behaviour), this *increase* of  $L(T)$  above the FL expectation begins to occur at successively increasing temperatures with increasing field, suggestive of a crossover in the scattering anisotropy (between heat and charge) that is concordant with the FL-NFL crossover.

Above this crossover, the Lorenz ratio smoothly recovers toward the WF expectation at higher temperatures. This can be interpreted as the effect of large- $\mathbf{q}$  scattering, or prominent AFM fluctuations which play a *direct* role in electron scattering processes. This behavior is comparable to that observed in the correlated spin fluctuation regime of CeRhIn<sub>5</sub>, where an abrupt increase in  $L(T)$  above  $T_N$  is attributed to a sudden change in

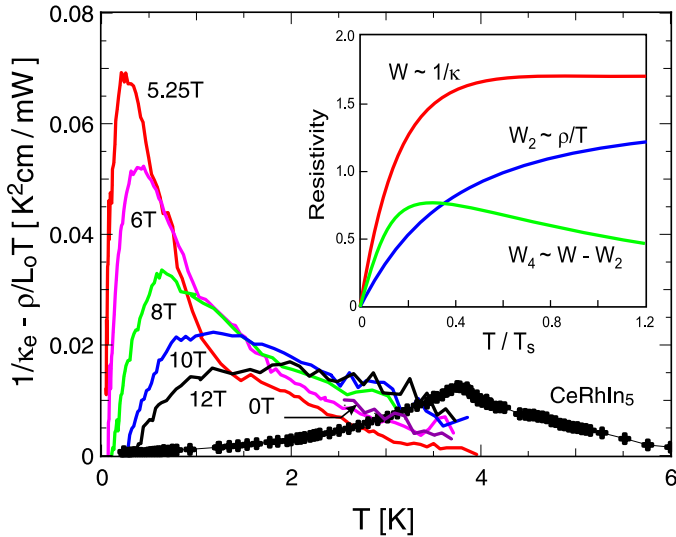


Figure 6.12: Vertical scattering component  $W_{\text{ver}}$  in CeCoIn<sub>5</sub> plotted for various fields, with a comparison to that of CeRhIn<sub>5</sub> at 0 T. Inset shows a theoretical calculation of scattering rate components in a system with local (unordered) fluctuating moments (from Ref. [72]), as described in the text.

the fluctuation spectrum.<sup>24</sup> The absence of finite-temperature order in CeCoIn<sub>5</sub> removes any sharp feature, but the similar increase in  $L(T)$  - above  $\sim T_N$  in CeRhIn<sub>5</sub> and  $\sim T^*$  in CeCoIn<sub>5</sub> - tempts one to assign a similar fluctuation spectrum to each, where the direct influence of fluctuations is “frozen out” below a well-defined temperature which signals the onset of long-range order in one case, and heavy renormalization in the other. In any case, this behaviour puts strong constraints on any theory attempting to explain the quantum critical phenomena in CeCoIn<sub>5</sub>.

These considerations can be taken further by comparing heat and charge transport in a different way. As discussed in Section 5.3.1, the vanishing of so-called “vertical” processes (*i.e.*  $L \rightarrow L_0$ ) in CeRhIn<sub>5</sub> was associated with a characteristic fluctuation energy scale of order  $T_{\text{SF}} \sim 8$  K. By analogy, in CeCoIn<sub>5</sub> this scale steadily decreases with field as  $H \rightarrow H^*$ , reaching  $\sim 4$  K at 5.25 T. This also can be seen by plotting the vertical component directly, as obtained by the difference between thermal and charge resistivities, or  $W_{\text{ver}} \equiv 1/\kappa - \rho/L_0 T$ ,<sup>25</sup> as shown in Fig. 6.12. In contrast to the case of CeRhIn<sub>5</sub>, where the onset of long-range AFM order imposes a sharp anomaly in  $W_{\text{ver}}$

<sup>24</sup>An increase above the FL expectation in CeRhIn<sub>5</sub> is observed at temperatures lower than  $T_N$ , occurring in fact very near the point where a  $T^6$  component in transport becomes observable at  $\sim 2$  K, and can be accounted for by this crossover.

<sup>25</sup>This quantity differs from the quantity  $\delta(T)$  discussed in Section 5.3.1 by a factor of  $L_0 T$ , allowing a direct comparison to available theory.

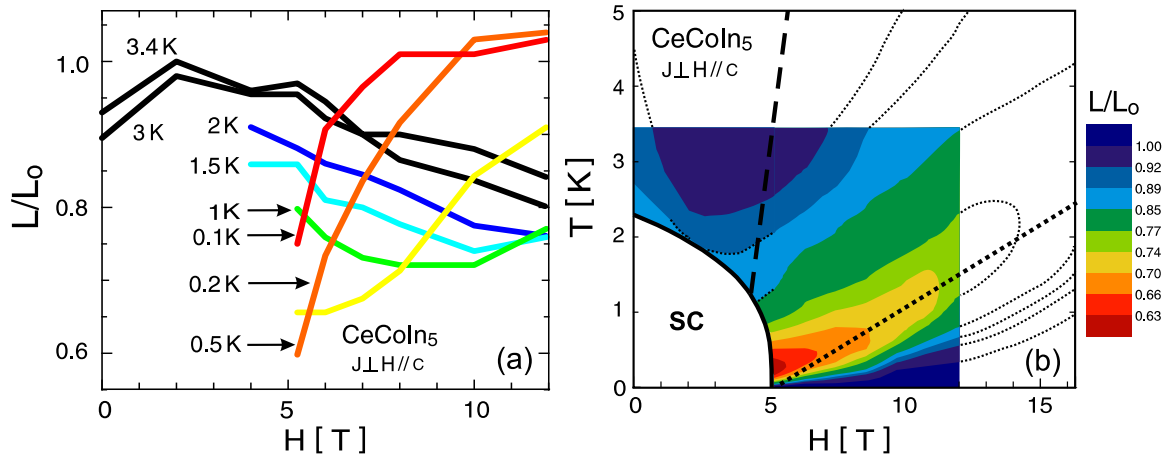


Figure 6.13: (a) Normal state Lorenz ratio of CeCoIn<sub>5</sub> for  $J \perp [001]$  and  $H \parallel [001]$ , normalized to the WF law expectation and shown for various temperatures as a function of field. (b) Contour plot of normalized Lorenz ratio data on the  $H$ - $T$  plane, with values of  $L/L_0$  as indicated in the legend. The thick dotted and dashed lines are the  $T^*$  and MR crossover lines, respectively (from Fig. 6.5). Thin dotted lines indicate estimated contours where data is absent, and are guides to the eye.

directly at the ordering temperature  $T_N$ , the absence of long-range order in CeCoIn<sub>5</sub> results in a smooth temperature dependence, as can be seen for all temperatures and fields measured. For instance, the increase from zero, maximum and subsequent decrease of  $W_{\text{ver}}$  in CeCoIn<sub>5</sub> at 12 T upon increasing temperature are all of the same magnitude as that in CeRhIn<sub>5</sub>, but occur without any sharp anomaly.

Because CeCoIn<sub>5</sub> is on the verge of AFM order, this temperature dependence can be directly compared to theoretical calculations which consider the scattering of electrons from locally-fluctuating moments in a system on the verge of magnetic order [72], in a manner as discussed in Section 2.2.2. Although actual calculations including the appropriate fluctuation spectrum for CeCoIn<sub>5</sub> are needed to be more specific, it is interesting to note that the qualitative shape of  $W_{\text{ver}}$  in CeCoIn<sub>5</sub> is strikingly similar to the same quantity ( $W_4$ ) calculated by Kaiser and shown in the inset of Fig. 6.12. Furthermore, it is apparent that there is a strong field dependence. Although analogous to the discussion about the recovery of the WF expectation in the Lorenz ratio at higher temperatures (*i.e.*  $T_{\text{SF}} \sim 4$  K), the comparison of  $W_{\text{ver}}$  to  $W_4$  from Kaiser's calculation directly shows the evolution of the energy scale  $T_{\text{SF}}$  with field as the system is tuned toward the field-induced QCP:  $T_{\text{SF}}$  finds its lowest value *closest to the critical field*, increasing for both lower and higher fields.

Finally, in Fig. 6.13(a) we show the field dependence of  $L$ , or  $L(H)$ , transcribed from

the  $T$ -sweep data. It is apparent that  $L(H)$  *decreases* with field at higher temperatures, which may seem to indicate a rising influence of small- $q$  scattering processes, and hence field-induced FM correlations at large fields. Although this conclusion would be in line with observations of a tendency toward field-induced FM order in high fields [169], one must recall the behaviour of both the e-e scattering (solid lines in Fig. 6.10) and the characteristic fluctuation energy scale  $T_{SF}$  as a function of field: both suggest that the return to the WF expectation ( $L \rightarrow L_0$ ) will happen at increasing temperatures and fields. Therefore, the field dependence of the Lorenz ratio remains consistent with prior observations: namely, the presence of dominant AFM fluctuations.

Note that a *maximum* in  $L(H)$  at 3.5 K is observable at or below 2 T, which can be seen more clearly in the contour plot of  $L(H, T)/L_0$  drawn onto the  $H$ - $T$  phase diagram shown in Fig. 6.10(b). This behaviour is roughly consistent with the observations of Bel *et al.* which show that the Nernst effect in CeCoIn<sub>5</sub> produces a particularly strong signal in the same range of field and temperature [181].<sup>26</sup> Furthermore, there is an approximate correlation between the evolution of maximum and minimum values of  $L/L_0$  with the MR crossover and the FL-NFL crossover, respectively. In any case, the fact that the WF law is most readily observed at this small, but non-zero field must be of consequence for any theory which describes the angular distribution of inelastic scattering (*i.e.*  $A/B \simeq 1$ ) for  $T$ -linear transport, and may again hint at the effect of competing energy scales.

#### *Comparison to other systems*

The ability to study the WF law at a QCP depends crucially on the relative magnitudes of elastic and inelastic contributions. In CeNi<sub>2</sub>Ge<sub>2</sub>, a material thought to lie very close to a QCP at ambient pressure, the observation of a small decrease ( $\sim 10\%$ ) from  $L/L_0 = 1$  at finite  $T$  has been ascribed to an increased scattering of heat from inelastic quantum critical spin-fluctuation contributions [56]. Such a small deviation from  $L = L_0$  at finite  $T$ , presumably expected to be much larger at a QCP, may be due to a relatively large impurity concentration, as suggested by a  $3\times$  larger value of  $\rho_0$ , or conversely a weaker inelastic scattering strength, which could suggest that this system is actually further away from the critical point than expected.

A similar study of the HF compound CeCu<sub>6</sub> has reported the observation of the WF law at the  $T \rightarrow 0$  limit (down to 50 mK), with a slight increase of  $L(T)$  at higher

---

<sup>26</sup>The study of Bel *et al.* involved measurements down to 2.5 K, and so further comparisons are not possible.

temperatures (above  $\sim 200$  mK) [41]. Even though the inelastic scattering strength in CeCu<sub>6</sub> at zero field is enormous (*i.e.*  $A \simeq 100 \mu\Omega\text{cm}/\text{K}^2$ ), the apparent absence of an expected *decrease* of  $L(T)$  may be due to a relatively large residual resistivity (*i.e.*  $\rho_0 \simeq 10 \mu\Omega\text{cm}$ ), thus making any phonon contribution non-negligible. This conclusion is corroborated by a subsequent experiment on a cleaner sample ( $\rho_0 \simeq 5 \mu\Omega\text{cm}$ ), which showed a  $\sim 15\%$  decrease in  $L(T)$  at  $\sim 300$  mK from the WF expectation [42].

Since it is known that CeCu<sub>6</sub> can be tuned closer to an AFM QCP with doping (*e.g.* CeCu<sub>6-x</sub>Au<sub>x</sub>) [39], stronger inelastic effects may be expected closer to the QCP. Unfortunately, chemical doping unavoidably introduces impurities, thus increasing the relative elastic scattering and presumably making a study of the WF law even more difficult. Both of these systems highlight the advantage (and fortuity) of studying the WF law in CeCoIn<sub>5</sub>, an extremely clean system with a QCP that can be tuned using a non-invasive parameter.

#### 6.4.3 Kadowaki-Woods Ratio

In many quantum critical systems, an essential investigation into the nature of the observed singular behaviour involves a comparison between transport and thermodynamic quantities. More precisely, a comparison of the  $T^2$  resistivity coefficient ( $A$ ) to the electronic specific heat coefficient ( $\gamma_0$ ), known as the Kadowaki-Woods (KW) ratio ( $A/\gamma_0^2$ ), can help discriminate between various models of quantum criticality (see *e.g.* Refs. [38, 47]).

The critical behaviour of  $A(H)$  in CeCoIn<sub>5</sub> would lead us to expect a divergence of  $\gamma_0(H)$  somewhere close to  $H_{c2}$ . A recent study by Bianchi *et al.* of specific heat as a function of field ( $H \parallel [001]$ ) in the normal state has indeed shown divergent (logarithmic) behaviour of  $\gamma_0$  at the same critical field ( $H^* = H_{c2}$ ), as shown in Fig. 6.14(a) [161]. In this study, a FL regime was also recovered at higher fields, as indicated by a saturation of  $\gamma(T)$  at the lowest temperatures. This suggests that properties of the field-tuned QCP are at least qualitatively similar in both transport and thermodynamic properties.

To compare these quantities in more detail, we can compare the measured KW ratio to the universal value of  $a_0 \equiv 10 \mu\Omega \text{ cm mol}^2 \text{ K}^2/\text{J}^2$  [73]. In the FL regime, the values of the  $A$  coefficient for various fields (Fig. 6.4(b)) can be compared to the value of  $\gamma_0$  from extrapolated estimates of the measured specific heat [161]. In doing so, one obtains a value of  $A/\gamma_0^2$  in the range  $\sim 2.4 - 3.0 \mu\Omega \text{ cm mol}^2 \text{ K}^2/\text{J}^2$  for fields between 6 and 9 T, which is  $\approx 0.35a_0$ , a value observed in numerous HF systems (see, *e.g.* Ref. [182]).

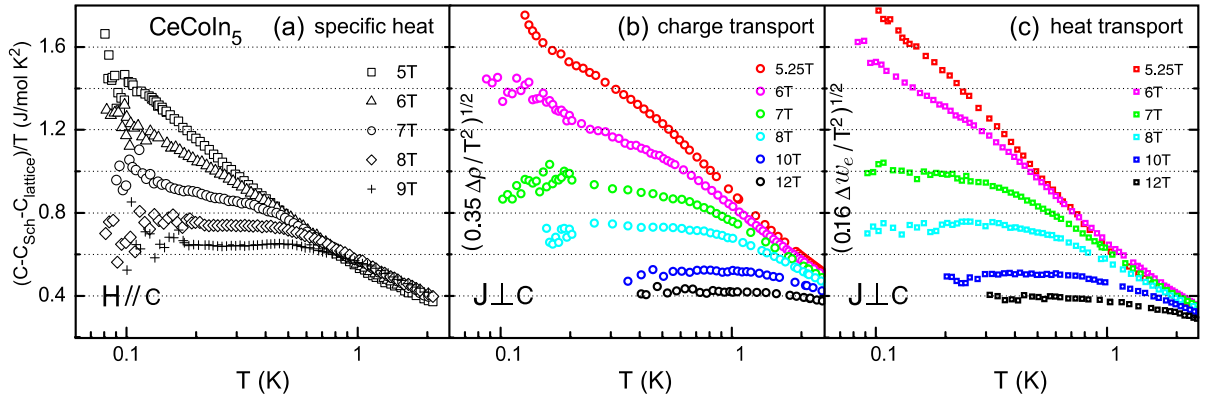


Figure 6.14: Comparison of Kadowaki-Woods ratio ( $A/\gamma_0^2$ ) quantities in CeCoIn<sub>5</sub> for fields  $H \geq H^*$ : evolution of (a) electronic specific heat  $\gamma(T)$  (from Ref. [161]), and the equivalent quantities in (b) charge transport and (c) heat transport, as explained in the text.

One can go a step further and investigate the KW ratio in the NFL regime by comparing the temperature-dependent quantities  $\gamma(T) = C(T)/T$  and  $A(T) = \Delta\rho(T)/T^2$ . This comparison was done in the vicinity of the field-induced QCP in YbRh<sub>2</sub>Si<sub>2</sub> [38], where a deviation from the (temperature-independent) universal value at low temperatures provided the main evidence for a breakdown of the composite fermion picture directly at the QCP. We have compared these quantities in CeCoIn<sub>5</sub> by plotting specific heat data measured by Bianchi *et al.* along side the KW equivalent transport quantity, obtained by scaling  $A(T) = \Delta\rho/T^2$  by the factor 0.35 and plotting its square-root value.<sup>27</sup> As shown in Fig. 6.14, there is an extraordinary similarity between the temperature dependence of each quantity, within experimental scatter, for the fields available for comparison. Moreover, as shown in Fig. 6.14(c), this quantitative similarity is also observed in the equivalent thermal transport quantity (*i.e.* using  $B(T) = \Delta w_e/T^2$ ), for which the data was scaled by the additional factor  $A/B = 0.47$  in order to account for the (field-independent) proportionality between heat and charge scattering strength (see Section 6.4.1).

These comparisons reveal that at high fields (*e.g.* 8 T), the  $T \rightarrow 0$  ratio of  $\sim 0.35a_0$  appears to persist into the NFL regime at higher temperatures, indicating that the effective mass and scattering cross-section *remain proportional* across the FL-NFL crossover. However, closest to the critical field, it is tempting to conclude that the this ratio is

<sup>27</sup>One must be careful in comparing  $\gamma(T)$  to  $\Delta\rho(T)/T^2$  in this way, since the latter is very sensitive to the choice of  $\rho_0$ , particularly at low temperatures. Furthermore, these data were collected in two different experiments, using samples of different origin, so a closer comparison (*e.g.* plotting the KW ratio directly) is avoided here.

*exceeded*, and that a similar phenomenon that was observed YbRh<sub>2</sub>Si<sub>2</sub> is also occurring in CeCoIn<sub>5</sub>. Since the conclusions [38] stemming from such an observation in YbRh<sub>2</sub>Si<sub>2</sub> depended greatly on the ability to compare the quantities  $A(T)$  and  $\gamma(T)$  to temperatures much lower than 100 mK, it is difficult to conclude on the situation in CeCoIn<sub>5</sub> using the available specific heat data (which has too much scatter below 100 mK).

Hence, although it appears that the nature of the field-induced QCP in CeCoIn<sub>5</sub> may be similar to that of YbRh<sub>2</sub>Si<sub>2</sub>, which was suggested to involve a locally-critical scenario [38] (much like that proposed for CeCu<sub>6-x</sub>Au<sub>x</sub> [51]), a quantitative extraction of *e.g.* the field dependence of the KW ratio at the critical field is lacking. Furthermore, there are some caveats to this comparison, which should also consider the observed transport anisotropy in CeCoIn<sub>5</sub>, which is the subject of the next chapter. **In any case**, the proportionality between thermodynamic and in-plane transport properties in the NFL regime suggests that, for the most part, it is indeed the heavy, in-plane carriers which dominate both quantities, and hence dictate the peculiar NFL properties surrounding the field-induced QCP in CeCoIn<sub>5</sub>.

## 6.5 Conclusions

We have identified the anomalous low-temperature evolution of magnetoresistance in CeCoIn<sub>5</sub> with the field-induced development of a Fermi liquid regime. The critical nature of the field-dependent electron-electron scattering coefficient in this regime, characterized by a divergence that occurs at a critical field  $H^*$ , bears close resemblance to other systems governed by quantum criticality. However, the apparent coincidence of  $H^*$  with the superconducting upper critical field  $H_{c2}$  remains unique to CeCoIn<sub>5</sub>, revealing a new class of quantum criticality in this system.

Some indications of the nature of this remarkable field-induced QCP have been uncovered by our studies of heat and charge transport performed as a function of temperature and magnetic field throughout the  $H$ - $T$  phase diagram. A systematic study of high-temperature charge transport has highlighted the following:

- The crossover from positive to negative magnetoresistance, which extends to very high temperatures, is indicative of a change in character of spin fluctuations with increasing field strength, undoubtedly closely tied to the critical transport behaviour and possibly consequential to the nature of the superconducting state transition as well.

- The crossover from linear to sub-linear power laws observed in the resistivity temperature dependence with increasing field is inconsistent with a single QCP scenario, suggesting that competing energy scales in CeCoIn<sub>5</sub> may arise from the presence of multiple QCPs.
- The anomalous  $T^{2/3}$  dependence of resistivity observed in the high-field non-Fermi-liquid regime - which we show via scaling to be directly linked to the critical point at  $H^*$  - is a key signature of the nature of critical fluctuations arising from the *field-induced* QCP, placing strict constraints on any theory attempting to explain its origin.

A comparison of low-temperature heat and charge transport has further revealed a number of important observations:

- Both heat and charge transport are governed by the same critical exponent as  $H \rightarrow H^*$ , suggesting that critical fluctuations are antiferromagnetic in nature, or at any rate unlikely to be superconducting in origin.
- The Wiedemann-Franz law is satisfied to within 2% as  $H \rightarrow H^*$  for this current-field orientation, ruling out the existence of exotic excitations from the anomalous quantum ground state surrounding the QCP.
- The characteristic energy scale associated with fluctuations is observed to have a minimum value closest to the critical field, and a similarity with the ordered antiferromagnet CeRhIn<sub>5</sub> further suggests fluctuations of an antiferromagnetic nature.

Finally, a comparison between thermodynamic and transport quantities places further constraints on any interpretation of quantum criticality in this system, and suggests that the nature of the field-induced QCP may be similar to that found in other recently investigated systems. The connection between quantum criticality and the onset of superconductivity in CeCoIn<sub>5</sub>, however, remains a fascinating open question, introducing an unexpected departure from the more usual scenario of a weak superconducting order emerging upon suppression of a strong magnetic order [19]. The next chapter, which discusses qualitative anisotropies observed between in-plane and inter-plane transport behaviour, will present additional oddities about this QCP, as well as the effects of band dimensionality in this material.

---

## CeCoIn<sub>5</sub>: MULTI-BAND EFFECTS

---

The electronic structure of CeCoIn<sub>5</sub>, which is heavily influenced by the 4f electrons of the Ce ions, has been well characterized: close agreement has been observed between band structure calculations and experimental measurements of the electronic system. As discussed in Section 3.3, the multi-band nature of CeCoIn<sub>5</sub> includes a combination of light, 3D bands and heavier, quasi-2D bands. Although thermodynamic quantities are expected to be primarily dominated by the bands with heavier effective mass, transport quantities can be strongly influenced by light-mass carriers since their faster Fermi velocities can easily dominate conductivity.

In this chapter, we report a detailed study of heat and charge transport measurements obtained with magnetic fields directed along the c-axis ( $H \parallel [001]$ ), as in the previous chapter, but using a longitudinal configuration with current also directed along the c-axis ( $J \parallel [001]$ ). The behaviour of conductivity in this configuration, which necessarily involves carriers of 3-dimensional nature, is in stark contrast to that reported for in-plane conduction. This contrast is manifested in a number of peculiar observations, such as an *absence of power law evolution* of the resistivity temperature dependence with field, and a field-induced FL regime which *coexists* with NFL behaviour at high fields and low temperatures.

Through these observations, a qualitatively different  $H$ - $T$  phase diagram emerges which reinforces the conclusions about multiple QCPs alluded to previously. A test of the Wiedemann-Franz law, obeyed for  $J \perp [001]$  measurements, reveals a striking contrast in this current configuration, resulting in the most exotic example of anisotropy in the electronic system of CeCoIn<sub>5</sub>. Remarks about the probable relation between the various conduction bands and the non-Fermi liquid behaviour observed throughout the  $H$ - $T$  phase diagram will discuss ideas about the “multi-critical” nature of CeCoIn<sub>5</sub>.

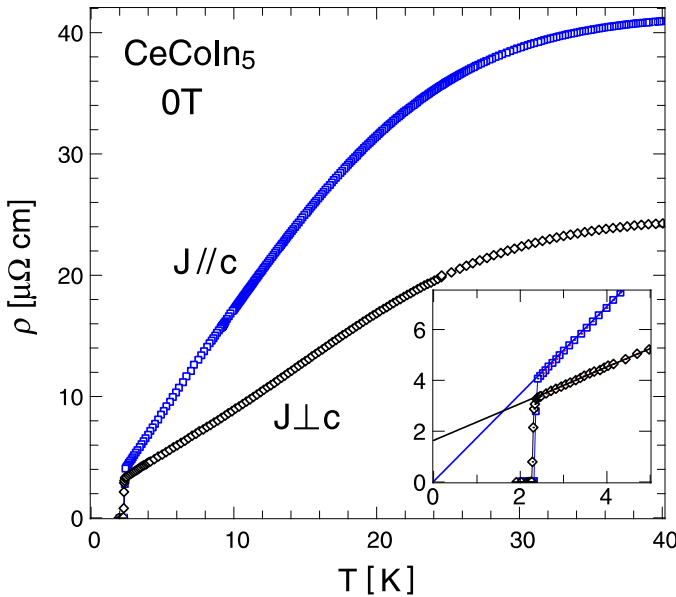


Figure 7.1: Charge transport anisotropy of CeCoIn<sub>5</sub>.

## 7.1 Inter-Plane Charge Transport

We begin with a report of electrical resistivity measurements in the  $J \parallel [001]$  configuration, performed on four separately prepared samples taken from different growth batches. The same behaviour was reproduced in the resistivity of all samples, verifying the intrinsic nature of the anomalous field- and temperature-dependent properties. For convenience, we will refer to charge resistivity measured with in-plane ( $J \perp [001]$ ) current as  $\rho_a$ , and that with inter-plane ( $J \parallel [001]$ ) current as  $\rho_c$ .

As shown in Fig. (7.1), the temperature dependence of  $\rho_c$  upon cooling in zero field is qualitatively similar to that of  $\rho_a$ : a broad maximum near  $T_{coh} \approx 45$  K, followed by  $T$ -linear behaviour below  $\sim 10$  K and a superconducting transition at  $T_c = 2.3$  K. However, there are a number of striking features of ( $J \parallel [001]$ ) charge transport, both in temperature and field dependence, which are to be compared and contrasted with data from Chapter 6. The following sections will focus on each of these separately.

### 7.1.1 Residual Resistivity

There is roughly a factor of  $\sim 2$  anisotropy between  $J \parallel [001]$  and  $J \perp [001]$  conductivity in the temperature range shown in Fig. (7.1).<sup>1</sup> However, this anisotropy is reversed at the lowest temperatures: an extrapolation of the  $T$ -linear portion of resistivity beyond  $T_c$

<sup>1</sup>Note that this is in contrast to that observed in CeRhIn<sub>5</sub> [140], where the anisotropy is reversed - *i.e.* higher inter-plane conductivity.

shows that the putative conductivities cross near 2 K and reverse their hierarchy at lower temperatures, extending to greatly different values. Whereas  $\rho_{0a} = 1.64 \pm 0.1 \mu\Omega \text{ cm}$  (*i.e.*  $\rho_0$  for  $J \perp [001]$ ), the extrapolation<sup>2</sup> of  $\rho_c(T)$  to  $T = 0$  yields a value  $\rho_{0c} = 0.02 \pm 0.02$ ,<sup>3</sup> as shown in the inset of Fig. (7.1). The latter case is highly reminiscent of that observed for *in-plane* transport in both CeIrIn<sub>5</sub> at ambient pressure [103] and CeRhIn<sub>5</sub> at 3.2 GPa applied pressure [183], where an extrapolation of  $\rho(T)$  (linear in  $T$  in both cases) to  $T = 0$  points to nearly no discernible residual resistivity. This is intriguing, since the band structure in both CeCoIn<sub>5</sub> and CeIrIn<sub>5</sub> is thought to be nearly identical [112], whereas that of CeRhIn<sub>5</sub> is somewhat distinct, being more 3-dimensional [110].

Note, however, that it is the large *in-plane* residual resistivity of CeCoIn<sub>5</sub> that is anomalously high, and certainly not representative of the intrinsic impurity-limited values underlying the superconducting state. For example, the extrapolated value of  $\rho_{0a}$  in CeCoIn<sub>5</sub> is much larger than both the field-induced ( $J \perp [001]$ ) normal state value (see Fig. (6.1)) and that observed under applied pressure [163]. The case of pressure-induced superconductivity in CeRhIn<sub>5</sub> is perhaps a more profound example of such anomalous behaviour: the extremely small  $\rho_0$  (see Chapter 5) increases by over 100× under applied pressures that maximize  $T_c$  [102, 183], while higher pressures subsequently return  $\rho_0$  back to much smaller values [183]. Similar behaviour has also been observed in both CeAl<sub>3</sub> [184] and CeCu<sub>5</sub>Au [43] as functions of both pressure and field. Hence, the large value  $\rho_{0a}$  in CeCoIn<sub>5</sub>, which is highly sensitive to pressure, field and current orientation (*i.e.*  $\rho_{0a} \gg \rho_{0c}$ ), may in fact be the consequence of an intrinsic magnetic mechanism tied to quantum criticality [100, 185] and/or Kondo lattice effects [43, 171, 184].<sup>4</sup> In any case, the large value of  $\rho_{0a}$  in CeCoIn<sub>5</sub>, together with the *small* value of  $\rho_{0c}$  provides an important insight into the dimensionality of spin fluctuations responsible for the zero-field NFL properties.

### 7.1.2 Magnetoresistance

The inter-plane MR of CeCoIn<sub>5</sub> is shown in Fig. (7.2), both as a function of temperature ( $\rho_c(T)$ ) and field ( $\rho_c(H)$ ). As can be seen in the  $\rho_c(T)$  curves measured in fields up to

---

<sup>2</sup>Linear fit of data below 10 K.

<sup>3</sup>The error on the value of  $\rho_{0c}$  is dominated by statistical error associated with the linear fit.

<sup>4</sup>Note that in the conventional HF picture, the mass renormalization is not expected to affect the residual resistivity since both the Fermi velocity and relaxation rate are expected to undergo the same mass enhancement [13]. However, in the local QCP picture [51] a change in residual resistivity is expected as a result of the change in volume of the Fermi surface at the QCP [100].

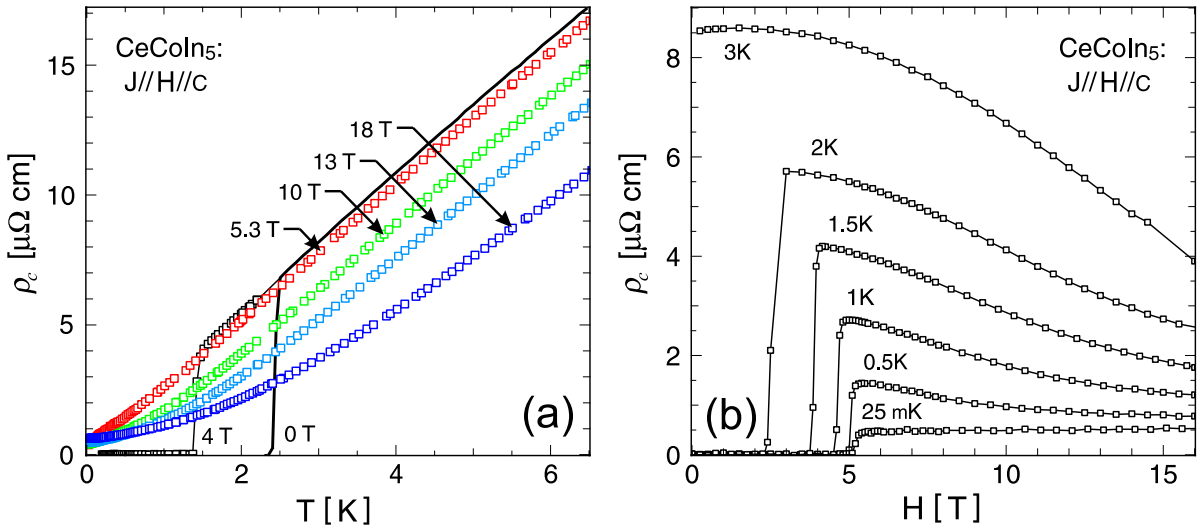


Figure 7.2: Magnetoresistance of CeCoIn<sub>5</sub>( $J \parallel [001]$ ), plotted as a function of (a) temperature and (b) magnetic field.

$H_{c2} = 5$  T, there is essentially *no MR at low fields*. This is more readily observable in the 3 K  $H$ -sweep curve shown in Fig. (7.2)(b), which is relatively flat at low fields. This *absence* of any significant MR at low fields is much different than the behaviour observed in  $\rho_a(H)$ , where a change from positive to negative MR occurs at finite fields, forming a crossover line which holds a significant position in the  $H$ - $T$  phase diagram (see Section 6.3.1). Rather,  $\rho_c(H)$  is *never positive*.<sup>5</sup>

Naively, this qualitative anisotropy could be attributed to the difference between longitudinal and transverse current-field orientations, since a purely longitudinal current is not expected to suffer from normal orbital MR [165]. However, as shown in Fig. (7.3), a comparison of resistivities in both transverse and longitudinal configurations does not support such a simple interpretation. Indeed, there is quite a large difference between longitudinal and transverse MR for  $J \parallel [001]$  currents above  $\sim 1$  K, as shown in Fig. (7.3)(b). But this difference is much less below  $\sim 1$  K, where the transverse resistivity ( $H \perp J \parallel [001]$ ) encounters a dramatic decrease not explainable via orbital effects.<sup>6</sup> Furthermore, the apparent absence of any significant difference between  $\rho_a(T)$  for both  $J \perp [001]$  current orientations shown in Fig. (7.3)(a) suggests that the anisotropy observed in  $H \parallel [001]$  MR is certainly not due to orbital effects, confirming the fact that the anomalous field dependence observed for in-plane currents (*i.e.* Chapter 6) is a consequence of the spin

<sup>5</sup>There is very slight positive MR at very low temperatures and high fields.

<sup>6</sup>Orbital MR is expected to be strongest at the lowest temperatures and highest fields [165], which was indeed observed in the transverse configuration - see Section A.1.

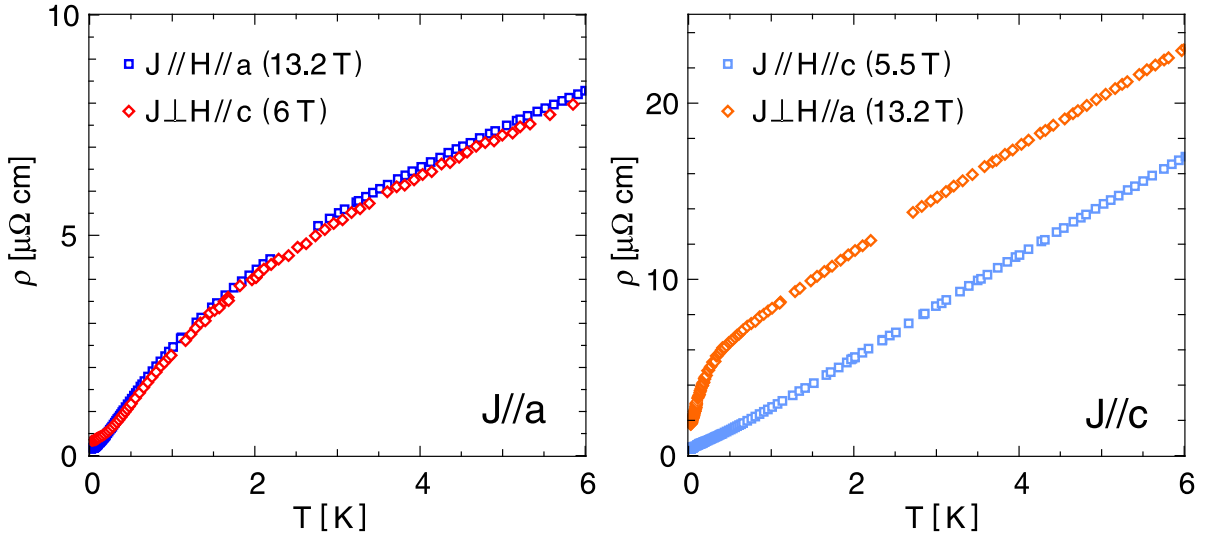


Figure 7.3: Longitudinal ( $J \parallel H$ ) and transverse ( $J \perp H$ ) MR of CeCoIn<sub>5</sub>, for data taken in fields just above  $H_{c2}$  and current orientations (a)  $J \perp [001]$  and (b)  $J \parallel [001]$ .

fluctuation spectrum.

This behaviour - an *absence* of MR up to  $H_{c2}$  - is another similar trait between CeCoIn<sub>5</sub> and CeIrIn<sub>5</sub> [103], suggesting that the carriers in question for both systems may be scattering from similar spin fluctuations. Note that a MR crossover with field is observed in the normal state of CeRhIn<sub>5</sub> (just above  $T_c = 2.2$  K) under a pressure of 2.5 GPa [112], a behaviour very similar to that of CeCoIn<sub>5</sub> for  $J \perp [001]$ . Since a  $T$ -linear dependence of resistivity appears in CeRhIn<sub>5</sub> when the pressure is increased to 3.2 GPa [112], which, moreover, extrapolates to a negligible residual value, it would be interesting to see if the positive MR is removed at this pressure. This would add a third observation of a correlation between  $T$ -linear transport with negligible residual resistivity and the absence of any positive MR.

The absence of MR in  $\rho_c(T)$  up to  $\sim H_{c2}$  results in an extension of its linear  $T$ -dependence down to at least 25 mK in a field of 5.3 T. In CeCoIn<sub>5</sub>, this behaviour spans a temperature range of almost three orders of magnitude; such a large temperature range has also been observed in the YbRh<sub>2</sub>(Si<sub>1-x</sub>Ge<sub>x</sub>)<sub>2</sub> system, where such NFL properties have been associated with the AFM QCP reached at small applied fields [186]. However, the  $T$ -linear behaviour of  $\rho_c(T)$  in CeCoIn<sub>5</sub> near the critical field is in stark contrast to that of  $\rho_a(T)$ . As shown in Section 6.3.2, a combination of anomalous power laws (*i.e.*  $\Delta\rho_a \sim T^{0.45}$  at high temperatures) describes in-plane transport near the critical field, whereas any complicated evolution of power laws with field seems to be absent in  $\rho_c(T)$ .

This suggests that the fluctuations that dominate the scattering of inter-plane carriers have a much weaker field dependence, at least up to  $\sim 5$  T. At fields above  $H_{c2}$ , a notable negative MR develops at higher temperatures in conjunction with a positive curvature in  $\rho_c(T)$  at lower temperatures, which increases with field. However, the linearity of  $\rho_c(T)$  with temperature remains at higher temperatures, which is also in contrast to the behaviour of  $\rho_a(T)$ , where sub- $T$ -linear power laws describe the NFL regime at high fields and temperatures. This “persistent linearity” in the temperature dependence of  $\rho_c(T)$  indicates that there is no notable change in power law with field in the NFL regime, suggesting that the  $H$ - $T$  phase diagram for  $J \parallel [001]$  transport is much simpler and possibly dominated by a *single source* of quantum fluctuations. However, the field-induced FL behaviour of  $\rho_c(T)$  is not so simple, as will be discussed below.

### 7.1.3 Two-Component Conductivity

The development of positive curvature in  $\rho_c(T)$  at low temperatures and high fields, as shown in Fig. (7.2)(a), is highly reminiscent of the behaviour observed in  $\rho_a(T)$ : in the latter case, a small temperature range of  $T^2$  resistivity that grows with field was attributed to a field-induced FL state. However, upon close inspection, the low temperature curvature observed in  $\rho_c(T)$  does not possess a strictly quadratic temperature dependence over any sizable range, even at the highest measured fields of 18 T, as shown in Fig. (7.5). Rather, power law fits (*i.e.*  $\Delta\rho_c \sim T^n$ ) performed on the low temperature portions of the data that possess curvature result in a power law that increases from  $T$ -linear with increasing field, from  $n = 1$  to  $n \simeq 1.5$  for fields from 5.3 T to 18 T, respectively. Furthermore, above the temperature range with curvature,  $T$ -linear resistivity seems to persist to the highest fields. These two facts motivated the use of a *two-component* conductivity model (rather than power law fits) to fit the  $\rho_c(T)$  data, which would capture both aspects - namely, competitive  $T$ -linear and  $T^2$  scattering rates.

Fits were performed using two additive conductivity components (*i.e.*  $\sigma = \sigma_A + \sigma_C$ ), corresponding to a FL component with a standard  $T^2$  scattering rate (*i.e.*  $1/\sigma_A = \rho_A = \rho_{0A} + AT^2$ ) and a NFL component with a  $T$ -linear scattering rate (ie  $1/\sigma_C = \rho_C = \rho_{0C} + CT$ ). Fits using this form were applied to data spanning temperatures between 25 mK and 6.5 K, and indeed result in the best fits to all data up to 18 T.<sup>7</sup>

---

<sup>7</sup>The use of a two-component model returned smaller residual errors on fits spanning larger temperature ranges, as compared to power law fits over a limited range. Although two residual resistivity parameters ( $\rho_{0A}$  and  $\rho_{0C}$ ) were utilized, note that fits were performed equally well assuming one combined residual term, and hence the same number of fit parameters as the power law form.

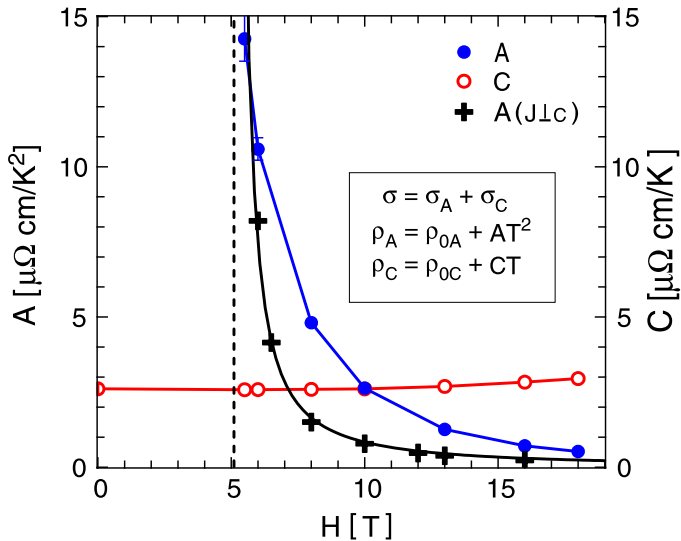


Figure 7.4: Two-component conductivity analysis, showing the field dependence of the FL (solid circles) and NFL (open circles) components of  $J \parallel [001]$  transport. The divergence of the  $J \perp [001] T^2$  coefficient (crosses) is also shown for comparison.

Fig. (7.4) displays the fit results<sup>8</sup> for the temperature coefficients  $A$  and  $C$  extracted from each data set<sup>9</sup> as a function of field. This plot reveals that there is indeed a sizable FL component  $A$  of the conductivity that appears to diverge in a similar manner as found for in-plane conductivity (also shown for comparison), albeit with a somewhat weaker field dependence. Amazingly, the NFL component  $C$  appears to have a very weak, if not *negligible* field dependence over the whole range of study. This feature can in effect be seen directly in the  $\rho_c(T)$  curves (Fig. (7.2)(a)), where the  $T$ -linear slope shows negligible change (above the low temperature curvature) through the whole field range.

This *two-component* interpretation of  $\rho_c(T)$  has very important implications. First, additive conductivities suggest a complete violation of Matthiessen's rule, which asserts that the total scattering rate due to distinct scattering mechanisms is the sum of resistivities due to each mechanism [62]. Additive conductivities, however, imply that the scattering mechanisms responsible for each component act on separate carriers. This can be understood, for instance, within a two-band model in which two separate channels of conduction exist without any inter-band scattering. Second, the greatly contrasting field dependences of each component suggest that the spin fluctuations which scatter each channel are independent, or of a different nature. Third, because this is inter-plane

<sup>8</sup>Note that error bars in Fig. (7.4) only represent the statistical error associated with fitting the data, and do not include error associated with the geometric factor.

<sup>9</sup>Equivalent results were extracted from data for two separate samples.

transport, it must necessarily involve 3D conduction bands. Finally, a divergence of the  $A$  coefficient near the critical field implies that the conductivity of this component becomes negligible as compared to the other, indicating that any transport measurements at this field would necessarily involve only the NFL component. As will be shown below, a comparison of heat and charge transport of this component alone reveals some striking implications for the WF law.

Using this interpretation, one can attempt to compare the field dependence of the coefficients  $A(H)$  and  $C(H)$  of each component, which contain information about the scattering cross-section and hence the effective mass, to the field dependence of the cyclotron masses observed [111] in dHvA measurements for the various bands (as discussed in Section 3.3). In this light, one can associate the divergence of  $A(H)$  at the field-induced QCP with the heavy  $\alpha$  (electron band) and/or  $\beta$  (hole band) orbits, which show a marked increase in cyclotron mass upon decreasing applied fields toward  $H_{c2}$ . Likewise, the field-independent coefficient  $C$  can be associated with the light, 3D  $\epsilon$  (hole band) orbit, which exhibits not only a weak field dependence, but a persistent presence deep into the superconducting state.<sup>10</sup> This latter association is indeed supported by the similarity in transport between CeCoIn<sub>5</sub> ( $J \parallel [001]$ ), CeIrIn<sub>5</sub> ( $J \perp [001]$ ) and CeRhIn<sub>5</sub> ( $J \perp [001]$  under pressure) discussed above, which suggests that the carriers involved in  $T$ -linear transport are associated with similar 3D hole pockets (*i.e.*  $\epsilon$  band) found in each system [112, 116].<sup>11</sup>

Note that a recent dHvA study of CeCoIn<sub>5</sub> by McCollum *et al.* has shown that a marked deviation from conventional Lifshitz-Kosevich behaviour, usually used to extract effective mass values, occurs near the critical field and down to the lowest measured temperatures for the heavy-mass orbits (*e.g.*  $\alpha$  and  $\beta$  orbits) [115]. This behaviour suggests that the field dependence of  $m^*$  observed for each orbit is not simple and may itself contain a complicated multi-component dependence. Nevertheless, the qualitative differences in the field dependence of  $m^*$ 's associated with the various conduction bands suggests *different sources* of mass renormalization - *i.e.* quantum fluctuations that in one case are strongly field-dependent, and in the other case are weak, or field-independent -

---

<sup>10</sup>A separate study of heat and charge transport in the superconducting state of Ce<sub>1-x</sub>La<sub>x</sub>CoIn<sub>5</sub> (as function of La concentration) suggests that carriers associated with this band do not even participate in the superconducting condensate, but rather remain “normal” to very low temperatures [146]. This is strong evidence for a lack of inter-band coupling that could precipitate such two-component behaviour.

<sup>11</sup>It remains an open question as to whether a true relation can be drawn between these carriers and the observed  $\epsilon$  orbits, since dHvA orbits are a consequence of the existence of quasiparticles.

which can only occur if there is little or no communication between conduction bands, as is observed here in transport.

In the spin-density wave picture of QCPs, it has been shown that the combination of 2D spin fluctuations and 3D carriers can account for  $T$ -linear transport, governed by “hot spots” on the Fermi surface where electrons undergo singular scattering with the spin fluctuations [53]. Since the quasiparticle lifetime of the so-called “hot carriers” is less than that of the “cold” carriers (away from the hot spots), it was also recognized that conventional FL behaviour should dominate conduction at the lowest temperatures [53]. However, as pointed out by Paul *et al.*, NFL properties can dominate if there is a large enough hot region (*i.e.* area of the FS) in the system [49], which can also be enhanced by the effects of disorder [50]. Paul *et al.* calculated the lifetimes of hot and cold carriers to have  $1/T$  and  $1/T^2$  dependences, respectively, and parameterized their fraction in the form of a two-component conductivity that is strikingly similar to the form used above to describe the field dependence of  $\rho_c(T)$ . It would be interesting to see whether the model of hot and cold carriers on a single Fermi surface can be extended to a multi-band scenario involving a “hot band” and a “cold band” such as may be the case in CeCoIn<sub>5</sub>.

Another mechanism that has been suggested to lead to multi-band conduction involves the effects of incoherent scattering of electrons from magnetic impurities, or “Kondo holes” in a Kondo lattice system [187]. Although no theoretical treatment of such a scenario has been done, a similar phenomenological treatment of the 115 compounds has been carried out by Nakatsuji *et al.*, which involves a two-fluid description of electrons divided between a condensed “Kondo liquid” and an uncondensed “Kondo gas” of screened Kondo impurity centers [144]. However, the question remains as to how a magnetic field can influence the effect of Kondo impurities on conductivity in either case, although some progress has been made in this area [43].

In regard to this, note that there is indeed a strong effect of impurity concentration on the observed behaviour. As shown in Fig. (7.5), the introduction of La impurities into the system appears to “wash out” the two-component behaviour at high field, resulting in the emergence of a strictly  $T^2$  resistivity with La-doping. Although many scenarios can be imagined (for instance, a similarity between the effects of disorder and magnetic field was recently suggested to occur in nearly magnetic metals [50]), the introduction of impurities may certainly be thought to introduce inter-band scattering that is absent in the pure compound, providing more evidence for the decoupled nature of different carriers in pure CeCoIn<sub>5</sub>.

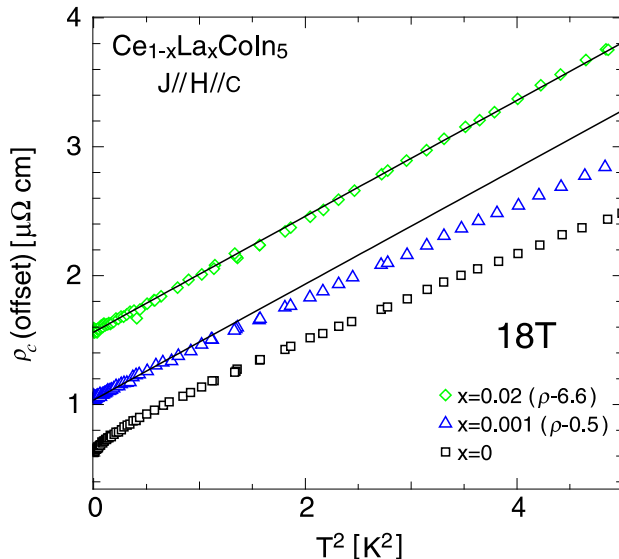


Figure 7.5: Effect of impurities on  $T^2$  component of  $J \parallel [001]$  transport

Whether the two-fluid nature of conductivity in  $J \parallel [001]$  transport, with both field-dependent and field-independent components, can be explained via a hot/cold carrier scenario [49, 50, 53] or a two-fluid Kondo description [144], or whether it involves completely distinct spin fluctuations remains to be seen. This question could be resolved, for instance, with inelastic neutron scattering experiments as a function of field, which can probe the nature of the spin fluctuations in CeCoIn<sub>5</sub> directly. In any case, a comparison of heat and charge transport (as was done in Chapter 5 for CeRhIn<sub>5</sub> and Chapter 6 for CeCoIn<sub>5</sub>) will provide important information on the nature of fluctuations in this current-field orientation, as will be discussed below.

## 7.2 Inter-Plane Thermal Transport

Thermal transport was measured in two of the samples used for resistivity, yielding equivalent results. The similarities between heat and charge transport of these samples, as will be discussed, confirms the intrinsic nature of the measurements reported here, ruling out any spurious effects such as sample inhomogeneity or percolative current paths. We will again use simplified notation to refer to thermal conductivity for heat currents  $J \perp [001]$  as  $\kappa_a$ , and that for currents  $J \parallel [001]$  as  $\kappa_c$ .

As can be seen in Fig. (7.6), the temperature dependence of  $\kappa_c/T$  is very similar to that of  $\kappa_a/T$  (see Fig. (6.9)(a)), showing a divergent behaviour upon decreasing temperature that is reflective of the strong inelastic scattering present in these systems. Although

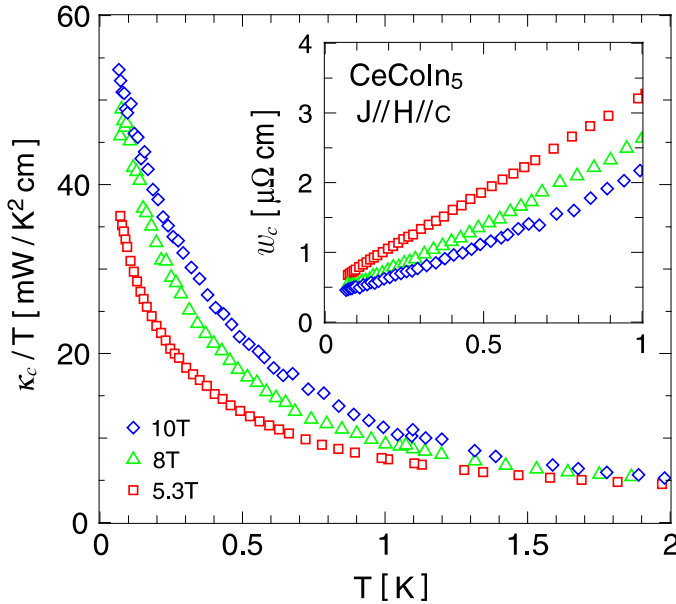


Figure 7.6: Thermal transport of CeCoIn<sub>5</sub> for fields and currents  $H \parallel J \parallel [001]$ . Inset shows the same data plotted as thermal resistivity  $w \equiv L_0 T / \kappa$  for the same fields.

qualitatively the same, plotting the data in this manner does not highlight the important differences between  $\kappa(T)$  in the two current orientations, since any difference in curvatures is hard to observe visually. However, the first peculiarity in  $J \parallel [001]$  transport can be directly observed in the field dependence: whereas  $\kappa_a/T$  clearly decreases with increasing fields in the  $T \rightarrow 0$  limit as shown in Fig. (6.9)(a),  $\kappa_c/T$  seems to *increase* with field up to at least 8 T. This anisotropy is highlighted in a plot of thermal conductivity measured as a function of field-sweeping at a constant average temperature of 60 mK, shown in Fig. (7.7). Although merely an observation at this point, we will show that this odd feature bears important consequences for the  $T \rightarrow 0$  properties near the critical field  $H^*$ .

The second important feature is in regard to the inter-plane thermal resistivity  $w_c \equiv L_0 T / \kappa_c$ , shown in the inset of Fig. (7.6). Amazingly, at a field 5.3 T (closest to  $H^*$ ),  $w_c(T)$  is *linear* in temperature from the lowest measured temperature of 70 mK up to at least 1.2 K.<sup>12</sup> This observation, being the first known occurrence of  $T$ -linear transport observed in the *thermal channel*, suggests that the inelastic scattering mechanism giving rise to  $T$ -linear behaviour acts on both heat and charge carriers in exactly the same manner. Furthermore, the shape of  $w_c(T)$  at higher fields seems to mimic the charge transport data: there is a gradual development of curvature at low temperatures. In order to draw

<sup>12</sup>Above  $\sim 1.2$  K, phonon conductivity becomes significant, causing a decrease in  $w_c(T)$  from the linearity observed at lower temperatures.

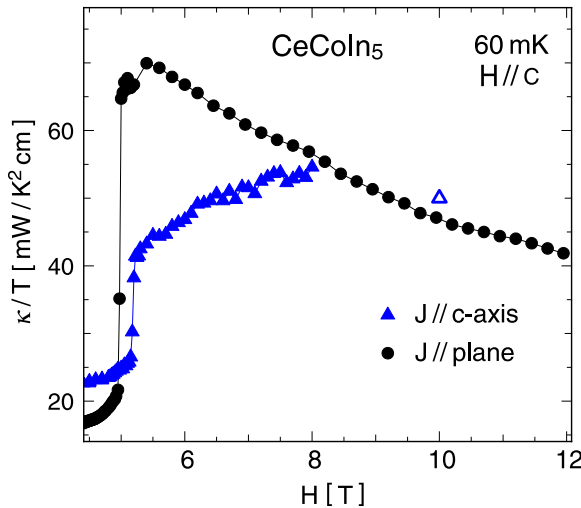


Figure 7.7: Comparison of the field dependence of thermal transport in CeCoIn<sub>5</sub> at 60 mK between currents  $J \perp [001]$  (circles) and  $J \parallel [001]$  (triangles - open triangle indicates data from  $T$ -sweep).

any more conclusions about inter-plane thermal conductivity it is necessary to compare heat and charge transport in detail, which is the topic of the next section.

### 7.2.1 Wiedemann-Franz Law

This section will compare heat and charge conductivity in the  $T \rightarrow 0$  limit, focusing on the validity of the WF law for  $J \parallel [001]$  transport. As shown in Section 6.4.2, a comparison of in-plane ( $J \perp [001]$ ) transport at the critical field reveals that, subsequent to a strong deviation at finite temperatures, the WF law is valid in the  $T \rightarrow 0$  limit. Naively, one would expect that the same should occur for  $J \parallel [001]$  currents, and indeed the inter-plane thermal resistivity  $w_c(T)$ , as mentioned above, has a linear  $T$  dependence at 5.3 T which bears a close resemblance to that of  $\rho_c(T)$ . However, a direct comparison of these two quantities at 5.3 T reveals that their respective residual values  $w_{0c}$  and  $\rho_{0c}$  are not equal: *the WF law appears to be violated in the  $T \rightarrow 0$  limit!*

In Fig. (7.8)(a), we present  $\rho_c(T)$  data, taken from measurements of three independent samples, together with  $w_c(T)$  data measured in two of these in a separate experiment. As shown, the close agreement between measurements of each sample suggests that 1) the absolute values of both  $\rho_c(T)$  and  $w_c(T)$  are correct to well within the  $\sim 10\%$  error associated with determination of the geometric factors for each sample, and 2) that any anomalous properties are not sample-dependent. It is readily apparent that the electrical and thermal resistivities at 5.3 T, when extrapolated to  $T = 0$ , do not point to the same

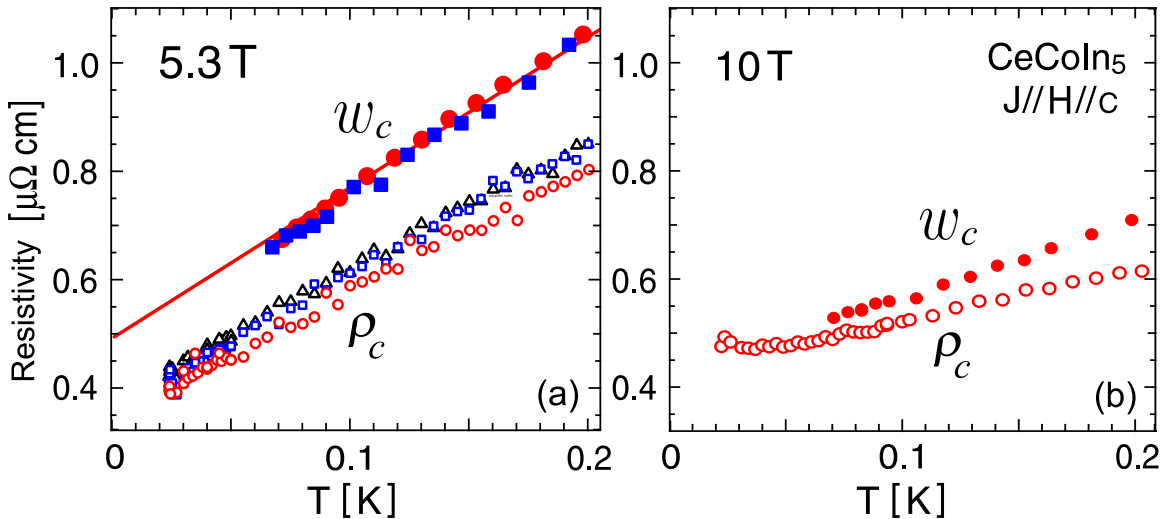


Figure 7.8: Comparison of electrical and thermal resistivities at (a) 5.3 T and (b) 10 T for inter-plane currents ( $J \parallel [001]$ ).

residual values. At this field, linear fits to the charge data (three samples) yield an average residual value of  $\rho_{0c}(5.3 \text{ T}) = 0.354 \pm 0.004 \mu\Omega \text{ cm}$ , and to the thermal data (two of the three samples) yield  $w_{0c}(5.3 \text{ T}) = 0.484 \pm 0.010 \mu\Omega \text{ cm}$ .<sup>13</sup> A comparison of the residual values yields a Lorenz ratio of  $L(0)/L_0 = 0.73 \pm 0.02$ , a violation of 27%.

The most conclusive evidence for the intrinsic nature of this violation is found in the field dependence: as the field is tuned away from  $H^*$ , the WF law is *recovered*. Fig. (7.8)(b) presents data for one sample taken in the same experiment used to measure the 5.3 T data,<sup>14</sup> where only the magnetic field was adjusted to a larger field of 10 T. One can readily see that at this field some curvature appears in both  $\rho_c(T)$  and  $w_c(T)$ , and that both quantities tend toward the same residual value at  $T = 0$ . Power law fits<sup>15</sup> of data for two samples at 10 T yield average residual values of  $\rho_{0c}(10 \text{ T}) = 0.43 \pm 0.01 \mu\Omega \text{ cm}$  and  $w_{0c}(10 \text{ T}) = 0.450 \pm 0.02 \mu\Omega \text{ cm}$ . In this case, the residual values are equal to within error, yielding a Lorenz ratio of  $L(0)/L_0 = 0.96 \pm 0.05$ . This observation strongly suggests that there are no spurious effects causing the apparent WF law violation at 5.3 T: the violation is both intrinsic and *field-tunable*.

A plot of the temperature dependence of the Lorenz ratio  $L/L_0 \equiv \rho(T)/w(T)$  at each

<sup>13</sup>The uncertainties in  $\rho_{0c}$  and  $w_{0c}$  are the calculated errors in the weighted mean of each quantity obtained from linear fits to each data set. These values in fact include errors in the geometric factors for each sample ( $\pm 4, 7$  and  $10\%$ ), but are dominated by statistical error.

<sup>14</sup>This trend was also observed in the other sample for which both heat and charge transport were measured.

<sup>15</sup>The power law fits used to extract residual values are discussed below.

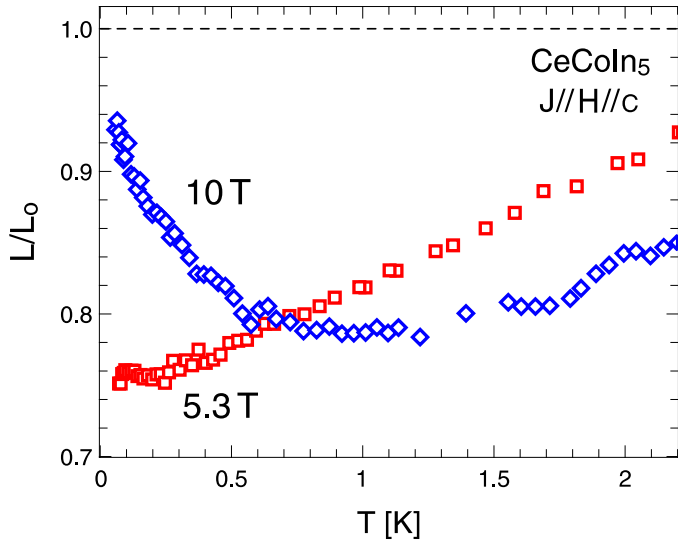


Figure 7.9: Lorenz ratio of heat to charge conductivity in CeCoIn<sub>5</sub> for  $J \parallel [001]$  currents at 5.3 T (squares) and 10 T (diamonds).

field expresses this property in more detail. As shown in Fig. (7.9),  $L/L_0$  decreases with temperature at 5.3 T (in a manner similar to that observed in  $J \perp [001]$  transport) but continues to decrease to the lowest temperatures without any indication of a recovery (increase) toward the WF law expectation of  $L/L_0 = 1$ , while at 10 T a recovery is fully imminent by  $\sim 0.5$  K.

While a plot of  $L/L_0$  at various fields is useful in highlighting the general trend of the WF law violation, it is more instructive to analyze and extrapolate the  $T$ -sweep data (taken at constant fields) of heat and charge transport separately. Fig. (7.10) presents a power law study of the evolution of residual resistivities as a function of field, where the low temperature curvature of both  $\rho_c(T)$  and  $w_c(T)$  was fit using a power law form (*e.g.*  $\rho_0 + AT^n$ ) over the temperature range which showed curvature<sup>16</sup> - *i.e.* up to  $\sim 1$  K for  $w_c(T)$  and  $\sim 2$  K for  $\rho_c(T)$  at all fields. Figs. 7.10(a) and (b) show the fits for charge and heat data, respectively, with the field dependence of the  $T = 0$  extrapolation results shown in Fig. (7.10)(c).<sup>17</sup> The first observation to note is in regard to the field dependence of both quantities near  $H^*$ : while there is little or no change in  $\rho_{0c}$  between 5.3 T and 6 T, which subsequently increases at higher fields,  $w_{0c}$  shows a rather large *decrease*

<sup>16</sup>As stated previously, the best fits of  $\rho_c(T)$  up to 6.5 K were indeed achieved using a two-component conductivity form, but for the purposes of extrapolation to  $T = 0$  power law fits were used to place more weight on the low temperature data.

<sup>17</sup>Note that error bars on values of  $\rho_{0c}$  and  $w_{0c}$  in Fig. (7.10)(c) include uncertainties in geometric factors for the two samples, while those on values of  $L(0)/L_0$  do not.

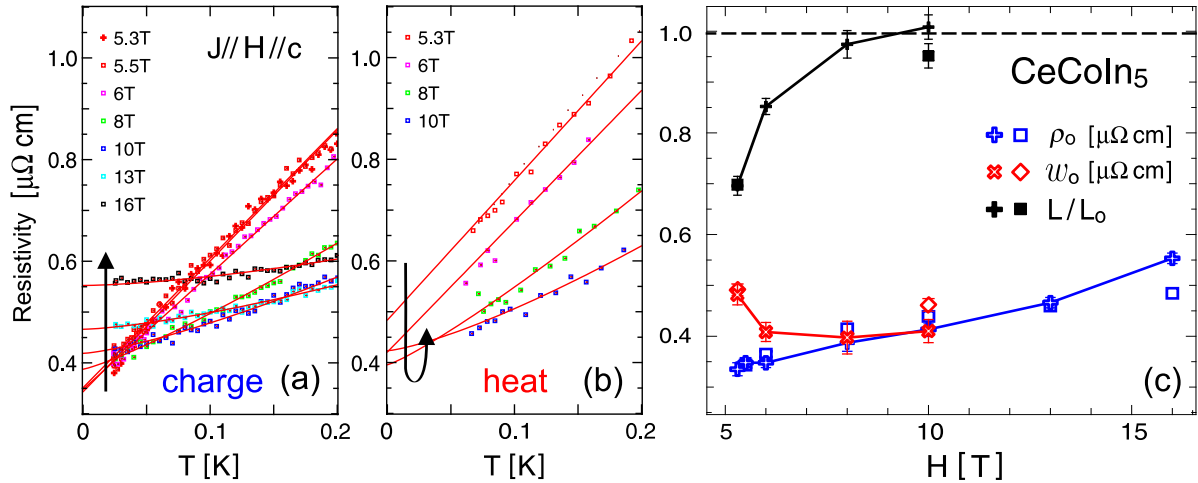


Figure 7.10: Comparison of thermal and electrical residual resistivities in CeCoIn<sub>5</sub> for  $J \parallel [001]$  transport in various fields. Panels (a) and (b) display  $\rho_c(T)$  and  $w_c(T)$  data, respectively, for each field along with power law fits (lines) done up to at least 1 K, as explained in the text. Arrows indicate direction of field increase. (c) Field dependence of residual values extracted from fits, along with corresponding Lorenz ratio (all using the same numerical scale). Data from two samples are plotted for each quantity using different symbols.

immediately upon increasing the field above 5.3 T. As stated previously,  $w_{0c}$  continues to decrease in fields up to at least 8 T, followed by a subsequent increase at higher fields. This stark contrast in field dependence between heat and charge conductivities is qualitatively different than the behaviour observed for in-plane transport, and is at the root of the observed WF law violation in  $J \parallel [001]$  transport.

One may speculate that the observed violation is simply a consequence of finite-temperature measurement - *i.e.* if measurements were taken to lower temperatures, a recovery of the WF law would be observed. This situation is expected [63], for example, in extremely pure materials, where the elastic limit is not reached until extremely low temperatures.<sup>18</sup> However, note that even if  $\rho_c(T)$  were to suddenly saturate below the lowest measured data point at 25 mK (which would be an extreme example of *e.g.* reaching the elastic limit), the extrapolated value of  $w_{0c}$  (determined by a linear fit of  $w_c(T)$  up to 1 K) *would still lie significantly above this value*, as can be seen in Fig. (7.8). This indicates that, were the WF law to recover at lower temperatures, it would have to involve a *drop* in  $w_c(T)$ , or in other words, an *increase* in thermal conductivity.

A decrease in  $w_c(T)$  below 70 mK could occur, for instance, due to a low-lying phase transition. For example, a decrease in resistivity is known to occur at the Néel transition

<sup>18</sup>In an ideally pure system, the Lorenz number never recovers to the Sommerfeld value [63].

of both CeRhIn<sub>5</sub> and YbRh<sub>2</sub>Si<sub>2</sub>, with that of the latter occurring at 70 mK or less.<sup>19</sup> But note that it is hard to conceive of a transition that would not affect both channels of conduction - the transition in CeRhIn<sub>5</sub> imposes sudden decreases at  $T_N$  in both  $\rho(T)$  and  $w(T)$ , as shown in Chapter 5. In any case, the observed behaviour certainly rules out any residual FL behaviour at lower temperatures, which would tend to affect  $\rho(T)$  at a higher temperature than  $w(T)$ , as it does at higher fields (*i.e.*  $T^*$  is higher for charge transport than for thermal transport, as discussed in Chapter 6). Hence, while lower temperature measurements would indeed be useful in further testing the observed violation, any phenomenon responsible for a recovery would have to proceed in an anomalous way, in addition to occurring at an *extremely low* energy scale (*i.e.* below  $\sim 25$  mK), providing theoretical challenges as equally interesting as a  $T = 0$  WF law violation.

While a violation of the WF law is apparent as  $H \rightarrow H^*$  in the  $T \rightarrow 0$ , or so-called elastic limit, it is quite peculiar that *inelastic scattering appears to obey the WF law*. For example, as shown in Figs. 7.10(a) and (b), the linear *slopes* of both  $\rho_c(T)$  and  $w_c(T)$  at 5.3 T are nearly equal. Thus, in addition to a violation of the WF law in the elastic channel, the inelastic scattering channel apparently obeys the WF law - *i.e.*  $\Delta\rho_c/\Delta w_c \simeq 1$  at  $H^*$ . Recall that the latter observation is in contrast to what is expected and observed in a Fermi liquid (where the ratio  $\Delta\rho/\Delta w = A/B$  is less than unity - see Section 2.2.3), whereas it is consistent with behaviour observed in the NFL regime (*i.e.* at higher temperatures - see *e.g.* Fig. (6.10)).

Finally, it should be noted that a disparity also exists in the field dependence of the Lorenz ratio at higher temperatures. Whereas  $L(H)$  exhibits a peak near 2 T for in-plane transport at 3 K, the field dependence of  $L$  for  $J \parallel [001]$  shows a continual decrease with increasing field, much like the MR behaviour at 3 K (see Fig. (7.2)(b)).

### 7.3 Discussion

The observations presented above can be categorized into topics relevant to the interpretations of quantum criticality in CeCoIn<sub>5</sub>. In light of the contrasting behaviour of inter-plane transport reported in Chapter 6, a discussion involving comparisons between the two current orientations and interpretations of these observations is presented below.

---

<sup>19</sup>In YbRh<sub>2</sub>Si<sub>2</sub>,  $T_N$  can be tuned to absolute zero at its field-induced QCP [38].

### 7.3.1 Scattering Anisotropy

The qualitative anisotropy found between in-plane and inter-plane charge transport is a reflection of both the carriers involved in each current and the interaction of those carriers with spin fluctuations. In Chapter 6, it was concluded that the evolution of the  $T$  dependence of resistivity with field in the NFL regime strongly suggests a crossover in energy scales, with zero-field behaviour (*i.e.*  $\Delta\rho \sim T$ ) dictated by a *different* source of NFL scattering than high-field behaviour (*i.e.*  $\Delta\rho \sim T^{2/3}$ ). This evolution appears to be absent for inter-plane transport - where  $T$ -linear resistivity is present across the  $H$ - $T$  plane - suggesting that the NFL behaviour observed under applied fields for  $J \parallel [001]$  transport is representative of the zero-field critical behaviour observed in both cases.

Because this behaviour involves inter-plane transport, one must conclude that 3D carriers are responsible for  $T$ -linear resistivity, while 2D carriers may be associated with the anomalous  $T^{2/3}$  dependence of resistivity at high fields. The fact that one component of  $J \parallel [001]$  conductivity is in fact FL-like may be indicative of the quasi-2D (rather than strictly 2D) nature of the in-plane carriers, which would tend to influence the total in-plane transport much more heavily than the total inter-plane transport. In this case, the larger (extrapolated) residual resistivity for  $J \perp [001]$  transport at  $H = 0$  may be the result of additional scattering of the quasi-2D carriers, which perhaps introduce an added term to the total scattering rate. This would further imply that inter-band scattering is present for  $J \perp [001]$  transport, resulting in additive scattering rates (*i.e.* Matthiessen's rule), whereas it is absent for  $J \parallel [001]$  transport as discussed above. Collectively, such an interpretation is consistent with the absence of large values of  $\rho_0$  in systems more likely to have 3D band structure (*i.e.* CeIrIn<sub>5</sub> and CeRhIn<sub>5</sub>), but such an interpretation must be further tested by examining the anisotropy of low temperature transport in these other systems.

Note that some energy scale appears to be reached near  $H^*$  in both current directions, as reflected by the onset of both negative MR at high temperatures and FL behaviour at low temperatures. To understand this, a scenario can be imagined where the incomplete formation of Kondo singlets *persists* up to  $H^*$  [61], after which the onset of complete Kondo screening of local moments by the quasi-2D carriers (onset of *itinerant* character of  $f$ -electrons hybridized with a particular band) would contribute a channel of conduction, thereby decreasing the total resistivity as the field is increased. Although the agreement between band structure calculations and dHvA measurements suggests an itinerant set

of  $f$ -electrons (see Section 3.3), dHvA experiments are performed under high fields so they do not shed light on the nature of these electrons at or below  $H^*$  (except, of course, in the case of the  $\epsilon$  orbit [111]). Ongoing dHvA experiments [115] near the critical field should hopefully resolve the field-dependent nature of the band structure.

### 7.3.2 Spin fluctuations

Continuing with the assumption of *separate sources* of criticality - *i.e.* both field-dependent and field-independent quantum fluctuations - we can attempt to describe the nature of each quantum phase transition by examining the effect of fluctuations on transport.

#### *Field-Tuned Fluctuations*

We can deduce that the critical spin fluctuations responsible for the *field-induced* QCP at  $H^*$  in CeCoIn<sub>5</sub> are antiferromagnetic in nature, as determined by the parallel divergence of in-plane heat and charge FL coefficients (*i.e.*  $A(H)/B(H) \sim \text{constant}$  - see Section 6.4.1). The true dimensionality of these fluctuations remains a mystery due to the lack of direct experimental studies (*e.g.* inelastic neutron scattering). However, if we assume that the fluctuations in CeCoIn<sub>5</sub> are of the same nature as those in CeRhIn<sub>5</sub> [140], then we can proceed with the notion that they are also 3D. This assumption is corroborated by the fact that in-plane transport is heavily influenced by fields *perpendicular* to the CeIn<sub>3</sub> planes, together with the apparently identical behaviour of magnetoresistance of  $J \perp [001]$  transport for both  $H \parallel [001]$  and  $H \perp [001]$  at  $H_{c2}$  (see Fig. (7.3)).<sup>20</sup> Also, the  $T^{2/3}$  dependence of resistivity which appears in both CeCoIn<sub>5</sub> at high fields and CeRhIn<sub>5</sub> at high pressures suggests that the scatterers are of the same nature in both cases.<sup>21</sup>

As summarized in Section 2.3, the various SDW scenarios predict at best a linear temperature dependence of transport for 3D fluctuations in a strictly 2D system of carriers, while the local QCP scenario is dependent on 2D fluctuations. However, the predictions for a 3D-3D SDW scenario expect a  $T^{3/2}$  behaviour in transport [20]. As shown in Fig. (7.11), transport in CeCoIn<sub>5</sub> close to the critical field does indeed show a small

<sup>20</sup>Further studies are necessary to deduce whether in-plane transport with  $H \parallel [001]$  and  $H \perp [001]$  is similar throughout the  $H$ - $T$  plane, but early indications suggest that it is.

<sup>21</sup>Of course, an essential question remains as to the pressure dependence of the dimensionality of spin fluctuations in CeRhIn<sub>5</sub> - they have been definitively shown [140] to be 3D at ambient pressure, but the pressure evolution of this character is presently unknown.

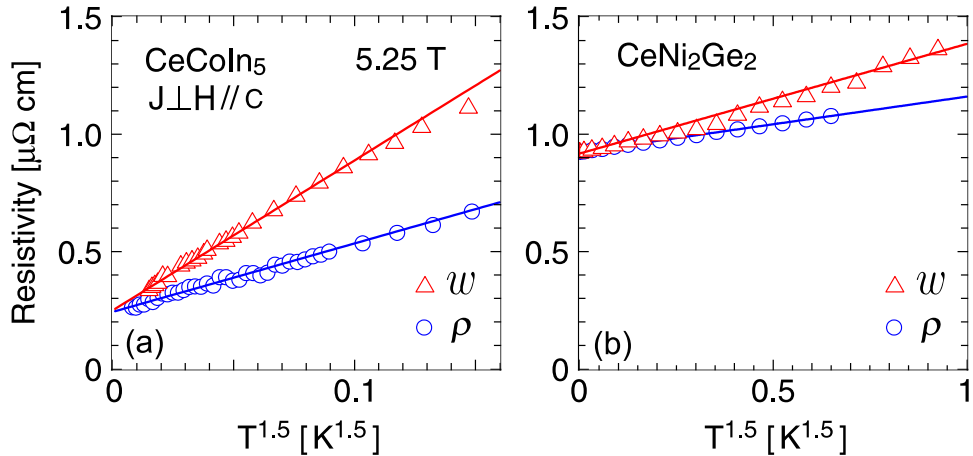


Figure 7.11: Electrical ( $\rho$ ) and thermal ( $w$ ) resistivities of (a) CeCoIn<sub>5</sub> at 5.25 T for  $J \perp [001]$ , and of (b) CeNi<sub>2</sub>Ge<sub>2</sub> at zero field (data from Ref. [56]) plotted vs  $T^{1.5}$ .

range (up to  $\sim 0.3$  K) of  $T^{3/2}$  behaviour,<sup>22</sup> which is comparable to that observed in CeNi<sub>2</sub>Ge<sub>2</sub> [56], a system thought to be well-described by the SDW picture [55, 56]. Furthermore, the behaviour of the electrical [188] and thermal [181] Hall coefficients in the normal state do not show any indication of an oncoming anomaly which would suggest a breakdown of the SDW picture.<sup>23</sup> These observations suggest that the field-tuned QCP in CeCoIn<sub>5</sub> may indeed fit into the SDW scenario, although more detailed comparisons of spin fluctuation theory predictions for susceptibility and specific heat to experimental data at low temperatures near  $H^*$  are required.

#### *Field-Independent Fluctuations*

Again, the equivalent effect of inelastic scattering on both heat and charge transport for  $J \parallel [001]$  (most notably at the critical field, where  $\Delta\rho_c \simeq \Delta w_c \sim T$ ) suggests that antiferromagnetic spin fluctuations are responsible for this NFL behaviour. However, in this case the  $T$ -linear behaviour (associated with 3D carriers) finds many explanations within existing theory. For instance, the SDW scenario predicts  $T$ -linear transport for 2D spin fluctuations coupled to 3D fermions [54]. The same behaviour is also shown by compounds [15, 38] thought to be explained by the local QCP scenario, which also involves strictly 2D fluctuations [51]. A further insight may be made by considering the differences in resistivity observed in  $J \parallel [001]$  transport for  $H \parallel [001]$  and  $H \perp [001]$  at

<sup>22</sup>Note that the same power law is also observed for longitudinal in-plane transport ( $J \parallel H \parallel [100]$ ) in CeCoIn<sub>5</sub>, further suggesting the isotropic nature of spin fluctuations.

<sup>23</sup>Observations of the Hall constant through the critical field at lower temperatures are, of course, complicated by the onset of superconductivity below  $H_{c2}$ .

$H_{c2}$  (see Fig. (7.3)). Unlike the situation for  $J \perp [001]$  transport, the  $J \parallel [001]$  orientation displays a strong dependence on field orientation: when the field is directed along the [001] axis there is little effect on transport, while there is a large increase in resistivity (at high temperatures) when the field is directed in the basal plane. This anisotropy is more akin to the presence of 2D fluctuations which interact with the 3D carriers that dominate inter-plane transport, which is also consistent with the anisotropy in residual resistivity for  $H \parallel [001]$  (*i.e.*  $\rho_{0a} \gg \rho_{0c}$ ).

It is thus tempting to conclude that two types of spin fluctuations exist in CeCoIn<sub>5</sub>: one of a 3D nature interacting primarily with quasi-2D carriers, and one of a 2D nature interacting with 3D carriers. However, without further guidance from theory, the only remaining observations which may be able to scrutinize between the different QCP scenarios are of the WF law, which will be discussed below.

### 7.3.3 WF Law Violation

The observed  $T \rightarrow 0$  violation of the WF law in CeCoIn<sub>5</sub> is unprecedented. Known to hold in such strongly correlated systems as UPt<sub>3</sub> [88], CeAl<sub>3</sub> [87], CeCu<sub>6</sub> [41] and CeNi<sub>2</sub>Ge<sub>2</sub> [56], the WF law is considered one of the most robust physical properties of a Fermi liquid (*i.e.* of a system with quasiparticles). In fact, the only known system to violate the WF law is the electron-doped cuprate superconductor Pr<sub>2-x</sub>Ce<sub>x</sub>CuO<sub>4-y</sub> [96], which exhibits heat transport *in excess* of the WF law in its field-induced normal state.<sup>24</sup>

Although various theoretical ideas on quantum criticality do indeed predict a violation at the QCP, the quantitative aspects of the violation observed in CeCoIn<sub>5</sub> remain anomalous: there is no known theoretical prediction of a WF law violation which involves a *deficiency* in thermal conductivity. For instance, the fractionalized FL scenario examined by Senthil *et al.* predicts that extra exotic Fermionic excitations at the QCP would contribute *additional* thermal conductivity above the WF law expectation in the  $T \rightarrow 0$  limit [57], contrary to what is observed in CeCoIn<sub>5</sub>. Indeed, it is hard to imagine *any type* of spin-charge separation scenario that would result in a smaller residual electronic thermal conductivity than expected by the WF law.

---

<sup>24</sup>Recall (Section 2.2.1) that the reported violation in the  $T \rightarrow 0$  limit - showing less than expected (in fact zero) thermal conductivity - is thought to be an extrinsic effect. See Ref. [97] and Appendix C.2 for details.

### WF law - Inelastic Channel

Recall that the additional peculiarity of the violation in CeCoIn<sub>5</sub> involves the behaviour of inelastic scattering at the QCP: the observation of  $\Delta\rho_c/\Delta w_c \simeq 1$  suggests that agreement with the WF law is observed in the *inelastic* channel of conduction. This is in stark contrast not only to what is expected in a FL (*i.e.* for e-e scattering, where  $\Delta\rho/\Delta w \rightarrow A/B$ ), but also to the observed NFL behaviour both in CeNi<sub>2</sub>Ge<sub>2</sub> and in CeCoIn<sub>5</sub> itself for the  $J \perp [001]$  orientation. This is shown explicitly in Fig. (7.11), where electrical and thermal resistivities of both CeCoIn<sub>5</sub> ( $J \perp [001]$ ,  $H = 5.25$  T) and CeNi<sub>2</sub>Ge<sub>2</sub> ( $J \perp [001]$ ,  $H = 0$ ; taken from Ref. [56]) are plotted as a function of  $T^{1.5}$ . The ratio of the corresponding coefficients of the  $T^{1.5}$  terms of each quantity (*i.e.*  $\Delta\rho/\Delta w$ ) is  $\simeq 0.5$  in both materials, a value that is, incidentally or not, typical of e-e scattering in a metal (see Section 2.2.3).

What is required, then, is a new theoretical perspective which can give rise to a violation in the *elastic* channel while enforcing an agreement with the WF law in the *inelastic* channel. One could argue that, closest to the critical field, the WF law is in fact obeyed in a new sense: the ground state is completely governed by “inelastic” zero-point fluctuations. For instance, if a finite fluctuation frequency exists at  $T = 0$  - *i.e.* no “soft” modes where  $\omega(q) \rightarrow 0$  - then the zero point energy (*i.e.*  $\hbar\omega(q)(n + 1/2)$  at  $n = 0$ ) is always finite, as in an optic phonon mode. Then, as long as  $\omega_0 > 1/\tau_0$ , where  $\tau_0$  is the elastic (*i.e.* impurity) lifetime, the so-called “impurity” limit is never reached, even at  $T = 0$ : the inelastic scattering would virtually dominate transport processes as  $T \rightarrow 0$ , and one would not expect to observe agreement with the WF law. Such a scenario would require the presence of some type of spacially local oscillator which gives rise to the finite zero-point frequency. In this sense, it would be extremely interesting to investigate the consequences of the local QCP picture proposed by Si *et al.* on heat and charge transport, since the spacially local fluctuations responsible for NFL behaviour can presumably be involved in a similar scenario as just described.

### Violation “Anisotropy”

The most intriguing situation to explain regarding this violation involves the available “tuning” parameters. Not only does a violation occur, but it occurs in a very focused region of phase space: starting from  $H = H^*$  and  $J \parallel [001]$ , the WF is restored by changing either magnetic field or current orientation. The first phenomenon is not hard to comprehend at a basic level - magnetic field is the critical tuning parameter, and so

the WF law is restored in the FL regime. However, the second is the most intriguing aspect of this study: why does the same material, under the same conditions, appear to violate the WF law in one current orientation and obey it in another? The only other known study of current orientation anisotropy of the Lorenz ratio near a QCP is that of CeNi<sub>2</sub>Ge<sub>2</sub> [56], where the WF law was observed in the  $T \rightarrow 0$  limit for both  $J \perp [001]$  and  $J \parallel [001]$  currents. This result is not unexpected since CeNi<sub>2</sub>Ge<sub>2</sub> is well-described by the SDW picture, with  $T^{3/2}$  transport in both orientations [55, 56]. In CeCoIn<sub>5</sub>, the situation is quite different: the transport is *qualitatively anisotropic* with respect to current orientation.

The key aspect of the violation in the  $J \parallel [001]$  orientation in CeCoIn<sub>5</sub> lies in the behaviour of the residual thermal scattering term  $w_0(H)$ , shown in Fig. (7.10). Whereas both  $\rho_{0a}$  and  $\rho_{0c}$  show positive MR at all fields above  $H_{c2}$ ,  $w_{0c}$  is qualitatively different than  $w_{0a}$  (and  $\rho_{0a}$  and  $\rho_{0c}$ , for that matter) in that it displays *negative* MR up to at least 8 T: as the field is decreased, the system becomes more thermally resistive than expected by the WF law, and below  $\sim 8$  T the violation occurs. One could argue that this occurs near this field because the FL component (*i.e.*  $\sigma_A$ ) of  $J \parallel [001]$  conductivity becomes much smaller than the NFL component (*i.e.*  $\sigma_C$ ), due to the divergence of the  $A$  coefficient for that component. Consequently, in the absence of the FL component the WF violation would be observed *at all fields* in the normal state. In other words, the “violation anisotropy” may be a reflection of the different conduction bands involved, with FL behaviour found in band(s) that dominate in-plane transport and a breakdown of FL behaviour in band(s) that dominate inter-plane transport.

If the violation of the WF law is truly band-dependent, then one may expect that the introduction of inter-band scattering would cause a recovery of WF law for  $J \parallel [001]$  transport. As discussed in Section 7.1.3, La substitution indeed seems to smear out the two-component nature of conductivity at high fields, and can be thought of as introducing inter-band scatterers. Preliminary studies of  $J \parallel [001]$  heat transport in Ce<sub>0.999</sub>La<sub>0.001</sub>CoIn<sub>5</sub> suggest that the introduction of inter-band scattering does indeed prompt a *recovery of the WF law*. Although further studies are necessary, this observation hints at the fragile nature of this violation and its subtle dependence on the absence of inter-band scattering.

### 7.3.4 Multi-Band Quantum Criticality

The stunning anisotropies observed in the field dependence of cyclotron masses [111], the susceptibility [110, 122] and the current orientation of transport are obvious consequences of the multi-band nature of the electronic structure of CeCoIn<sub>5</sub>. With the added suggestion of the presence of two separate types of spin fluctuations, this brings about the peculiar and strongly unique possibility of different forms of quantum criticality which influence different conduction bands. Although it is difficult to arrive at any strong conclusions, a very simple view can be formed based on the observations of this study. For instance, one could relate the WF agreement observed in  $J \perp [001]$  transport to a SDW QCP scenario where *e.g.* local moments are “quenched” at a finite temperature, leading to a FL ground state. Likewise, the WF violation observed in  $J \parallel [001]$  transport can be associated with a local QCP scenario where local moments remain unscreened at  $T = 0$ . The latter scenario can indeed involve a breakdown of FL theory, as was shown in the case of YbRh<sub>2</sub>Si<sub>2</sub> [38].

Such a picture would be consistent with the existence of two separate kinds of spin fluctuations. However, there is an obvious necessity of further experimental studies in order to resolve the nature of quantum criticality in CeCoIn<sub>5</sub>. Inelastic neutron scattering as a function of field would enable the determination of the nature of spin fluctuations (as was done in CeCu<sub>6-x</sub>Au<sub>x</sub> [15]), while a study of the field dependence of the Hall and Nernst effects (for  $J \parallel [001]$  currents) at low temperatures may enable a critical test of the change in the electronic structure at the critical field [34]. Furthermore, a careful dHvA study of the field dependence of cyclotron masses, which is presently being carried out [115], will aid in identifying the various conduction bands with quantum critical behaviour. Such studies are urgently needed to resolve the complicated story behind NFL behaviour in the 115 system.

## 7.4 Conclusions

This chapter has presented a number of incredible observations of anomalous inter-plane heat and charge transport in CeCoIn<sub>5</sub> which present new and unique challenges to the current understanding of NFL physics. A number of interesting phenomena have been demonstrated in this current orientation which differ in a qualitative way from the in-plane transport phenomena presented in Chapter 6:

- The zero-field resistivity extrapolates to  $\rho_{0c} \simeq 0$ , or a value much less than  $\rho_{0a}$ . This

form of resistivity finds similarities to that of both CeIrIn<sub>5</sub> and CeRhIn<sub>5</sub> under high pressure.

- There is negligible magnetoresistance up to  $H^* = 5$  T, suggesting that some energy scale is reached at this field.
- The  $T$ -linear transport observed in zero field *persists* throughout the  $H$ - $T$  plane, contrary to the  $T^{2/3}$  dependence which develops at high field for  $J \perp [001]$ . At the critical field, the first instance of  $T$ -linear transport in the *thermal channel* of conduction was also observed.
- At high fields and low temperatures, a *two-component* form of conductivity best describes the data, with both FL and NFL contributions present up to at least 18 T. The violation of Matthiessen's rule suggests that there is *no inter-band scattering*, resulting in the coexistence of a *field-dependent* FL component and a *field-independent* NFL component of conduction.

The most striking singularity in this current orientation is revealed in a comparison between heat and charge transport at the critical field: a violation of the WF law is observed in the  $T \rightarrow 0$  limit, stemming from a thermal conductivity that is  $27 \pm 2\%$  less than expected for charge  $e$  fermions in a Fermi liquid. Furthermore, a *recovery* of the WF law occurs above  $\sim 8$  T, indicating that the observed violation is in fact an intrinsic property and is *field-tunable*. The field dependence of the thermal residual resistivity shows a *minimum* near this field, which suggests that it is the thermal channel which is at the root of the observed violation. Finally, the *inelastic* Lorenz number is equal to the (elastic) WF law expectation, in stark contrast to the behavior of  $J \perp [001]$  transport in CeCoIn<sub>5</sub> itself, and observations in other quantum critical systems, suggesting a new type of inelastic scattering mechanism unlike anything previously observed.

The evidence of competing energy scales from  $J \perp [001]$  transport studies presented in Chapter 6 is further elucidated by the behaviour of  $J \parallel [001]$  transport. A comparison of the two data sets has prompted an interpretation involving two distinct kinds of spin fluctuations arising from two distinct quantum phase transitions. These were interpreted as a set of 3D fluctuations interacting with a quasi-2D band of carriers, showing strongly field-dependent character, and a set of 2D fluctuations interacting with a 3D band of carriers, showing field-independent character. Given the currently available theoretical scenarios for quantum criticality, we have assigned the first set to a SDW instability with

a FL ground state, and the second set to a locally-critical scenario which shows signs of an anomalous ground state incompatible with FL theory. Such a scenario, although highly complicated and irregular, is at least consistent with the Wiedemann-Franz law violation anisotropy observed in CeCoIn<sub>5</sub>.

Although suggestions have been made, the definite explanation of the observations reported in this chapter remains elusive, requiring further theoretical and experimental efforts to understand the nature of quantum criticality in CeCoIn<sub>5</sub>. For instance, without a knowledge of the momentum dependence of fluctuations, it is hard to say why inter-band scattering does not occur. In addition to a much needed characterization of spin fluctuations in CeCoIn<sub>5</sub> (as could be done with inelastic neutron scattering), it would be interesting to search for similar transport phenomena in CeIrIn<sub>5</sub>, where *in-plane*  $T$ -linear transport is reportedly very similar to the inter-plane transport of CeCoIn<sub>5</sub> at the critical field.

## CONCLUSIONS

---

---

In this thesis, we have summarized a comprehensive experimental study of normal state heat and charge transport in the heavy fermion superconductor CeCoIn<sub>5</sub>. This study was undertaken in order to explore the non-Fermi liquid properties of this material at extremely low temperatures and high fields, and has resulted in a plethora of unexpected observations. Experiments were conducted on a large number of excellent single-crystal samples provided by Cedomir Petrovic, using a standard four-wire technique for both thermal and electrical conductivity measurements at temperatures down to 25 mK and magnetic fields up to 18 T. In addition to pure CeCoIn<sub>5</sub>, measurements of CeRhIn<sub>5</sub> and Ce<sub>1-x</sub>La<sub>x</sub>CoIn<sub>5</sub> were also performed in order to gain insight into various correlations between the different members of the 115 family of materials.

In order to investigate the nature of spin fluctuations in the 115 system, we began with a transport study of the well-characterized antiferromagnetic material CeRhIn<sub>5</sub> which has provided a number of striking observations. First, a comparison between transport and magnetic entropy has revealed that electron scattering in this system is completely dominated by spin disorder - a characteristic which bears significant importance in understanding the source of scattering in the other members of the 115 family. Second, a comparison between heat and charge transport has allowed 1) a direct measure of the angular distribution of scattering, and 2) the identification of the characteristic energy scale of spin fluctuations, thus providing information on both the momentum and energy dependence of the fluctuations. This introductory study has shown that the comparison of heat and charge transport in these extremely clean materials enables the extraction of much information regarding the scattering mechanisms at play, and has provided an excellent example of the capabilities of this experimental approach.

A comprehensive study of transport in CeCoIn<sub>5</sub> was the main focus of this thesis. We have explored a large portion of the phase space of this system by exploiting the tuning parameters available in our laboratory - namely low temperatures, high magnetic fields

and orientations of the measurement current with respect to the CeIn<sub>3</sub> basal planes. This latter parameter has proven crucial to some of the main conclusions of this study, and has revealed some of the most complicated aspects of the 115 system known to date.

Beginning with in-plane current measurements, we have identified a number of unique and interesting transport properties which have helped to map out the  $H$ - $T$  phase diagram, as well as provide important information on the quantum criticality and non-Fermi liquid behaviour in CeCoIn<sub>5</sub>. As a function of field, this phase diagram includes 1) a crossover in the sign of magnetoresistance which is concomitant with a change in the order of the superconducting transition, 2) a crossover in energy scales, as indicated by a change in transport power laws toward an anomalous  $T^{2/3}$  dependence at high fields, and 3) a Fermi liquid regime which develops beyond the upper critical field of superconductivity. Upon close analysis, a critical divergence in the electron-electron scattering in the Fermi liquid regime has pointed to a quantum critical point which is *field-tuned*, as characterized by a critical field  $H^*$  coincident with the superconducting critical field  $H_{c2}$ .

An in-depth analysis has shown that the presence of this field-induced QCP is further corroborated by the occurrence of  $\Delta H/T$  scaling of resistivity, along with a parallel divergence of electron-electron scattering in the *thermal channel* at  $H^*$ , showing the same critical exponent as in charge conduction. This latter observation has prompted us to conclude that the quantum fluctuations are most likely antiferromagnetic in nature. Finally, a test of the Wiedemann-Franz law for in-plane currents at the field-induced QCP has shown an agreement with Sommerfeld's value for the Lorenz number, suggesting that no obvious breakdown of Fermi liquid theory occurs at this QCP.

A careful preparation of specimens optimized for inter-plane current measurements under longitudinal magnetic fields has enabled the first known measurements of *inter-plane* heat and charge transport in CeCoIn<sub>5</sub>. Contrary to in-plane transport, a quite different story emerges in the  $H$ - $T$  plane for this current orientation. For instance, the  $T$ -linear inter-plane resistivity observed in zero field remains up to high fields, even *coexisting* with the high-field Fermi liquid regime as one part of a two-component conductivity. In addition, this component exhibits an *independence* from any field dependence, providing further evidence for a second type of quantum critical point corresponding to the zero-field non-Fermi liquid properties.

A test of the Wiedemann-Franz law for inter-plane currents has revealed that, contrary to the previous situation, a *violation* is observed in the  $T \rightarrow 0$  limit at the critical field. This observation has given the most exotic known example of anisotropy in the

same system: an orientation-dependent violation of the Wiedemann-Franz law. This phenomenon provides the most convincing evidence for two kinds of quantum fluctuations in CeCoIn<sub>5</sub>, corresponding to a field-induced QCP and a field-independent QCP.

Although this study has revealed a number of fascinating insights into the nature of quantum criticality in the 115 system, much phenomena remains unexplained. For instance, although not originating from superconducting fluctuations, the field-induced QCP remains strongly tied to the upper critical field of the superconducting phase. With the absence of any observable ordered magnetic phase in its vicinity, the origin of this QCP remains unknown. Also, the type of scattering mechanism that can give rise to a sub-linear temperature dependence of transport is another quite elusive aspect of the non-Fermi liquid behaviour in CeCoIn<sub>5</sub>. This, together with the most intriguing anomaly - a violation of the Wiedemann-Franz law - provide condensed matter physicists with a challenging set of phenomena to explain theoretically and further elucidate experimentally.

In conclusion, the fortunate combination of extremely clean crystals with strong inelastic scattering that is tunable with a non-invasive tuning parameter has enabled the fruitful yield of this study. With only a handful of clean, stoichiometric materials in which quantum phase transitions can or have been studied in great detail, the 115 system provides an important example of quantum criticality which is also unique in many aspects.

---

---

# A

---

---

## CeCoIn<sub>5</sub>: ADDITIONAL ANALYSIS

---

---

This Appendix offers additional data and analysis pertinent to the analysis of CeCoIn<sub>5</sub> transport data reported in this study, including explanations of subtleties alluded to in the main text and additional (incomplete) studies which extend the interpretations of the main conclusions.

### A.1 Orbital MR: $\omega_c\tau > 1$ Limit

The *upturn* in  $\rho(T)$  at low temperatures and high fields reported in Section 6.2 is very similar to that observed in the resistivity of UPt<sub>3</sub> in transverse fields, where such a deviation from  $T^2$  behavior at low temperatures is attributed to the realization of the  $\omega_c\tau > 1$  limit [189, 190]. In this limit, the characteristic time of the quasiparticle orbital motion is short compared with the time between collisions, and therefore the Fermi surface topology plays an important role in determining transport properties. This effect can in fact been utilized to study the Fermi surface, as done in the case of UPt<sub>3</sub> [190] and more recently in the cuprate superconductor Tl<sub>2</sub>Ba<sub>2</sub>CuO<sub>6+δ</sub> [191].

In order to confirm that this is indeed the effect responsible for the upturn in CeCoIn<sub>5</sub>, a rotation study was performed on the same sample used for analysis in Section 6.2. Consecutive fridge runs were performed on the same sample after slightly rotating the sample out of its transverse field orientation. As shown in Fig. (A.1), a 5° rotation results in no change in the observed resistivity (as compared to the true transverse orientation) up to fields of  $\sim 10$  T. At higher fields, the slight misalignment starts to *decrease* the magnitude of the upturn. This behaviour becomes more drastic upon a larger rotation - a 30° misalignment results in an almost negligible upturn, even at the highest field of 16 T. This behaviour is conclusive evidence for achievement of the  $\omega_c\tau > 1$  limit in these samples, which would be an interesting regime to further exploit in order to obtain information on the Fermi surface topology.

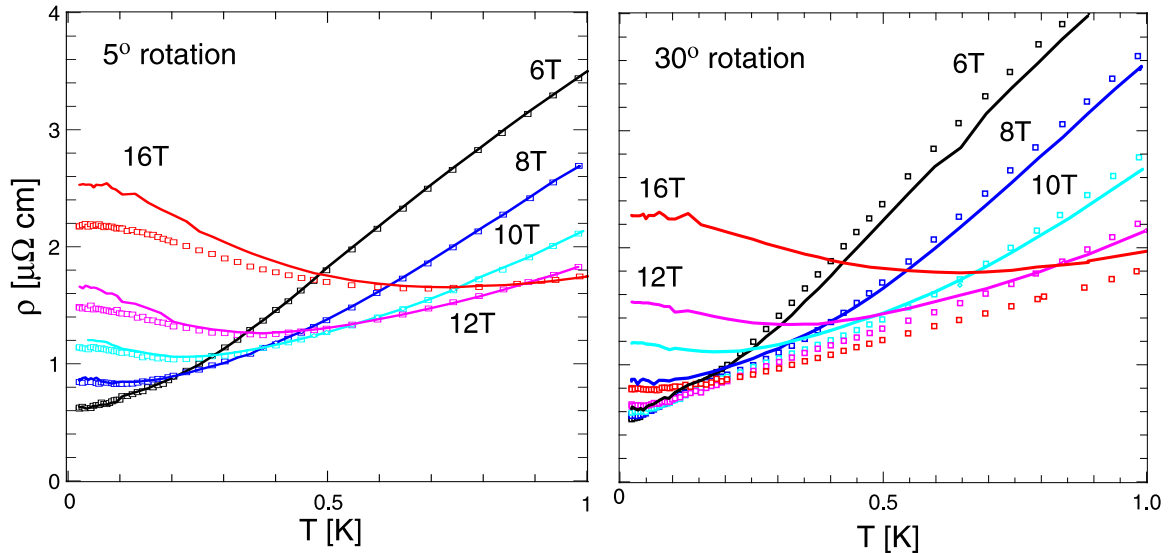


Figure A.1: Orbital magnetoresistance of CeCoIn<sub>5</sub> at low temperatures and high fields. The two panels present resistivity taken from samples with current orientation  $J \perp H$  (solid lines), which were subsequently rotated by small angles and remeasured (squares) for both 5° (left) and 30° (right) misalignments.

## A.2 Breakdown of $\Delta H/T$ Scaling

The observed deviation of  $J \perp [001]$  charge transport from  $\Delta H/T$  scaling, as reported in Section 6.3.3, is quantitatively similar to the phenomenon suggested to occur in the resistivity of nearly AFM metals with finite disorder effects taken into account. Rosch *et al.* calculated the disorder effect on spin fluctuation scattering (in a SDW model [30]) within a semiclassical approach using a Boltzmann equation, and found a breakdown of scaling is expected to occur [50]. Numerical solutions of this model provide quite strong predictions, such as the variation of the resistivity power law as a function of disorder and tuning from the QCP, which are strikingly similar to the behaviour observed in this study. For example, as shown in Fig. A.2, the calculated behaviour of the exponent  $n$  for a system with similar disorder as CeCoIn<sub>5</sub> (*i.e.*  $x = 0.01$  in Ref. [50]) shows a quantitatively similar temperature dependence as observed for CeCoIn<sub>5</sub>. Since this calculation considers magnetic field and the QCP tuning parameter as strictly separate, a comparison to the field-tuned behaviour in CeCoIn<sub>5</sub> may be fortuitous. Furthermore, the influence of superconductivity was also not considered in Rosch's calculations [50]. Nonetheless, this striking similarity deems further investigation.

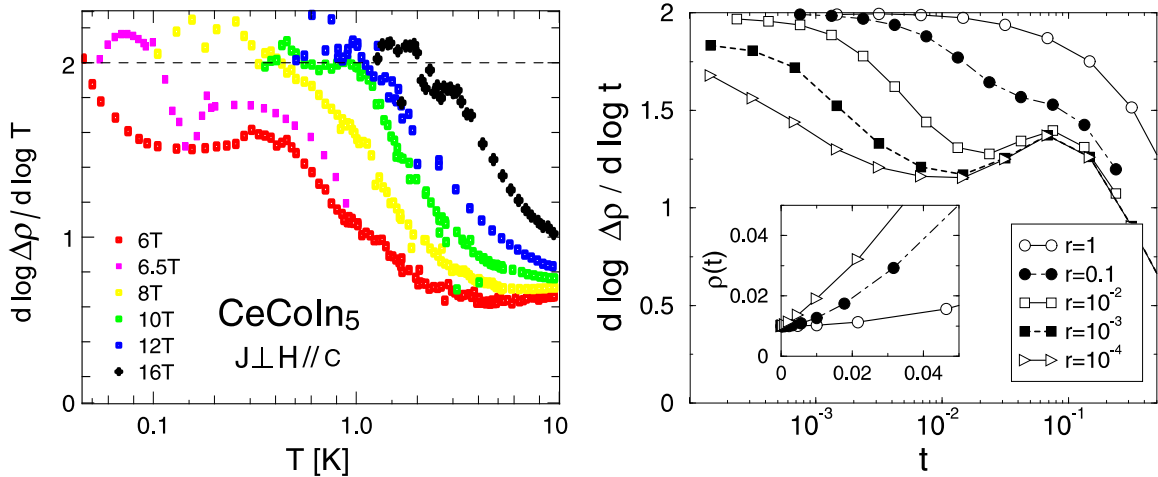


Figure A.2: Comparison between approximate measured resistivity power law (left), as a function of temperature, to the same quantity calculated by Rosch *et al.* to occur for a disorder level  $x = 0.01$  similar to that in CeCoIn<sub>5</sub> ( $x \approx 1/\text{RRR}$ ). Curves in the right figure are for various distances  $r$  to the QCP, plotted as reduced temperature  $t \approx T/T_{\text{coh}}$  (from Ref. [50])

### A.3 Transport in Ce<sub>1-x</sub>La<sub>x</sub>CoIn<sub>5</sub>

Here we report a study of charge transport ( $J \perp H \parallel [001]$ ) in the doped compound Ce<sub>1-x</sub>La<sub>x</sub>CoIn<sub>5</sub>. This series has been studied in some detail [136, 192], but low temperature transport has not been previously reported. Data shown below is for a sample with  $x = 0.10$ , which exhibits behaviour representative of La dopings. This particular level of La doping drastically suppresses the superconducting transition temperature to  $T_c = 1.1$  K, yet only mildly suppresses the upper critical field to  $H_{c2} = 4.2$  T (as compared to  $T_c = 2.3$  K and  $H_{c2} = 5$  T in CeCoIn<sub>5</sub>).

#### A.3.1 Field-Induced QCP in Ce<sub>0.90</sub>La<sub>0.10</sub>CoIn<sub>5</sub>

A study of the evolution of a FL state in Ce<sub>0.90</sub>La<sub>0.10</sub>CoIn<sub>5</sub> with applied field was performed in exactly the same manner as done for pure CeCoIn<sub>5</sub> (see Section 6.2). Fig. (A.3)(a) shows resistivity measured in a series of fields from slightly above  $H_{c2} = 4.2$  T to 16 T, plotted vs.  $T^2$ . As in CeCoIn<sub>5</sub>, the electron-electron scattering strength (slope of  $\rho$  vs.  $T^2$ ) is shown to decrease with increasing field, while the temperature range of  $T^2$  behaviour increases. As shown in Fig. (A.3)(b), the coefficient  $A$  (in  $\Delta\rho = AT^2$ ) appears to diverge in an analogous way to that in the undoped system (Fig. (6.4)(b)). Although attempts to fit the field dependence of  $A$  to a critical form were not successful, the similar increase and magnitude of  $A$  upon approaching  $H_{c2}$  suggest that the phenomenon  $H^* = H_{c2}$  is robust against both the introduction of impurities and the dilution of

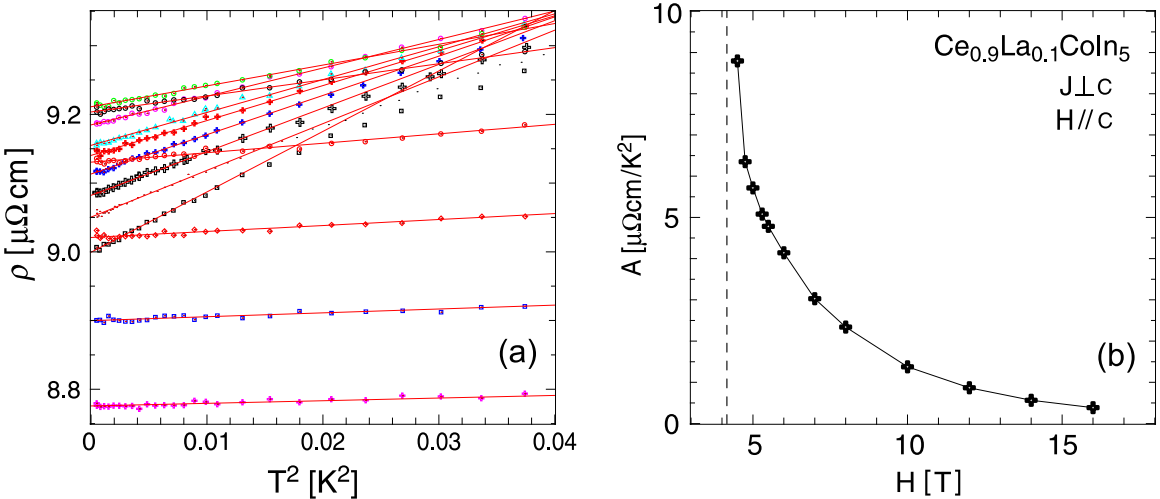


Figure A.3: (a) Resistivity of  $\text{Ce}_{0.90}\text{La}_{0.10}\text{CoIn}_5$  plotted vs.  $T^2$ , with linear fits shown as solid lines through data points for fields 4.5, 4.75, 5, 5.3, 5.5, 6, 7, 8, 10, 12, 14 and 16 T (from highest to lowest slope). (b) Plot of  $T^2$  coefficient vs. field from fits in (a).

the Ce sub-lattice. In other words, *the field-induced QCP in CeCoIn<sub>5</sub> is truly tied to the upper critical field of superconductivity*. At present, this finds no explanation and is a completely new and interesting phenomenon in the study of quantum criticality in HF systems.

The field dependence of resistivity in  $\text{Ce}_{0.90}\text{La}_{0.10}\text{CoIn}_5$  is qualitatively similar to CeCoIn<sub>5</sub>, but with one exception: whereas the *maximum* in MR disappears into the superconducting transition in CeCoIn<sub>5</sub>, it *avoids* the superconducting phase in  $\text{Ce}_{0.90}\text{La}_{0.10}\text{CoIn}_5$ . As indicated by the arrows in Fig. (A.4)(a), a maximum in  $\rho(H)$  is observable in each (constant- $T$ )  $H$ -sweep down to the lowest temperatures, suggesting that the crossover in the sign of MR is observable throughout the  $H$ - $T$  plane. The resultant  $H$ - $T$  phase diagram for  $\text{Ce}_{0.90}\text{La}_{0.10}\text{CoIn}_5$  is plotted in Fig. (A.4)(b), showing the position of the superconducting  $H_{c2}$  from resistivity, the position of the MR crossover and the range of FL ( $\Delta\rho \sim T^2$ ) behaviour. It is strikingly similar to that of CeCoIn<sub>5</sub> (Fig. (6.5)), with the exception of the MR crossover behaviour at low temperatures.

### A.3.2 First-Order Phase Transition

Thermal conductivity studies of the  $\text{Ce}_{1-x}\text{La}_x\text{CoIn}_5$  series have been undertaken in order to investigate the order of the superconducting phase transition in the absence of a direct

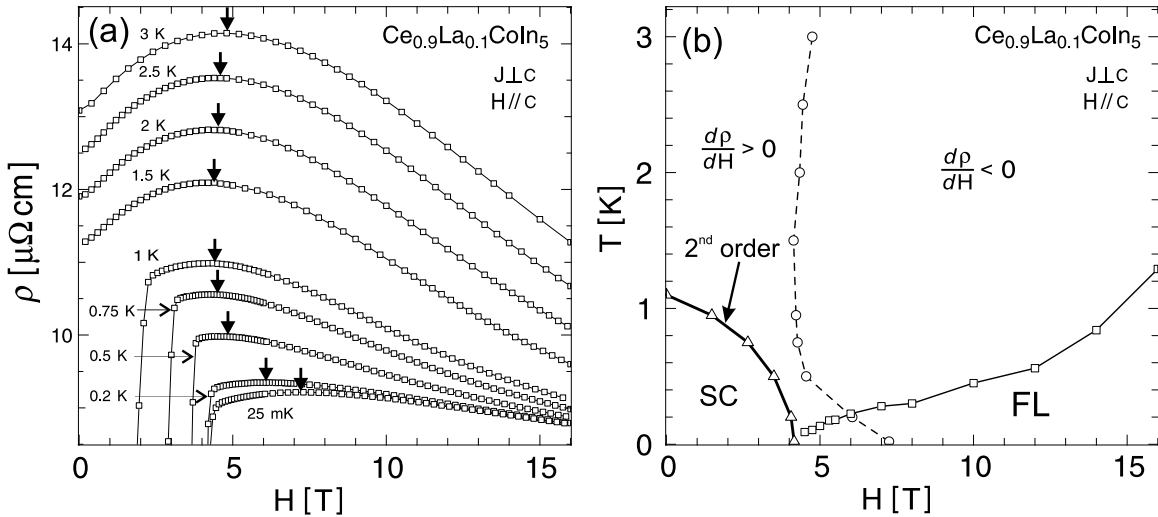


Figure A.4: (a) Magnetoresistance of Ce<sub>0.90</sub>La<sub>0.10</sub>CoIn<sub>5</sub> for various temperatures as shown. Arrows indicate the position of maximum resistivity for each temperature. (b)  $H$ - $T$  phase diagram, showing phase transition (triangles) to superconducting (SC) state, crossover (squares) to field-induced Fermi liquid (FL) state, and position (circles) of magnetoresistance crossover (lines are guides to the eye).

connection to the MR crossover.<sup>1</sup> As shown in Fig. (A.5)(a), the step in  $\kappa(H)$ , which is indicative of a first-order transition in  $H_{c2}$  [125], is still present in  $x = 0.02$  but is not observable at higher La dopings. Amazingly, the doping where the step is no longer discernible ( $x \simeq 0.05$ ) coincides with that where a MR crossover becomes discernible in the residual resistivity, as shown in Fig. (A.5)(b).<sup>2</sup> This coincidence is strong evidence suggesting that the MR crossover is closely tied to the nature of the superconducting transition.

### A.3.3 La-doping Phase Diagram

Finally, the collective normal state transport data of Ce<sub>1-x</sub>La<sub>x</sub>CoIn<sub>5</sub> can be placed in the context of previous studies. Shown in Fig. (A.6) is a schematic illustration of the field dependence of the phenomena discussed above, added onto the previously-constructed  $x$ - $T$  phase diagram [136]. Although our doping studies are currently limited to below  $x = 0.25$ , one can see the emergence of a concise continuation of the superconducting phase to high fields, with character that strongly reflects the behaviour of normal-state

<sup>1</sup>Recall that the MR crossover in CeCoIn<sub>5</sub> appears to impinge the  $H_{c2}$  transition directly at the tricritical point between first- and second-order character (see Fig. (6.5)), as deduced from previous studies [122, 123, 124, 125].

<sup>2</sup>The field dependence of  $\rho(H)$  at 25 mK matches that of  $\rho_0(H)$  extracted from  $T$ -sweep data.

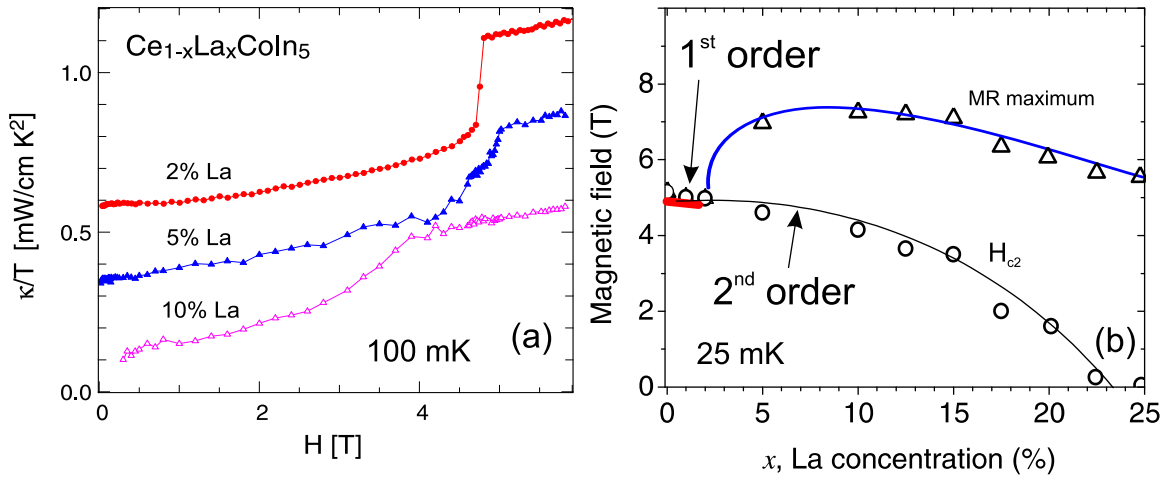


Figure A.5: (a) Field dependence of thermal conductivity  $\kappa(H)$  in  $Ce_{1-x}La_xCoIn_5$  at 100 mK, for  $x = 0.02, 0.05$  and  $0.10$ . (b) Evolution of order of  $H_{c2}$  transition vs.  $x$ , showing field position of MR maximum. The thick (red) line at low  $x$  indicates the dopings where a step in  $\kappa(H)$  is still observable.

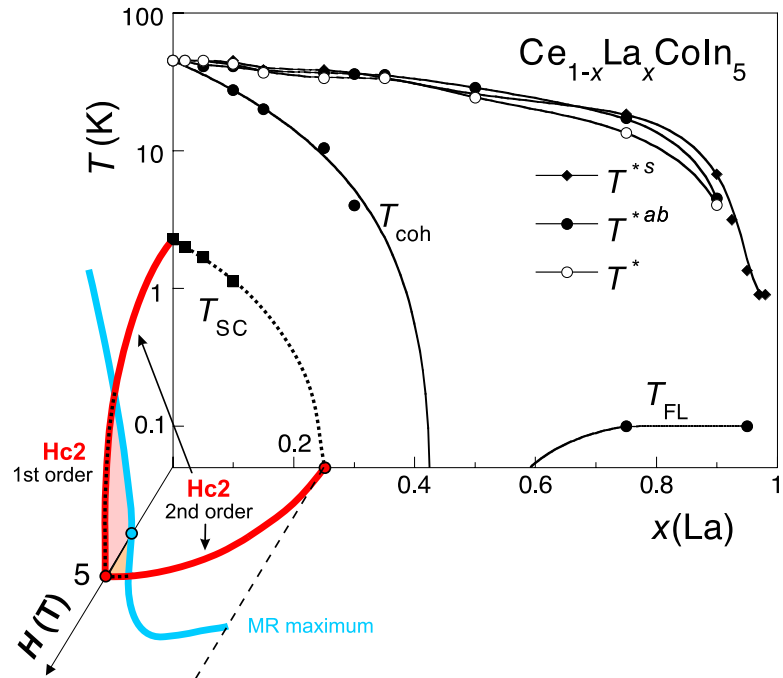


Figure A.6: Schematic  $H$ - $T$ - $x$  phase diagram of  $Ce_{1-x}La_xCoIn_5$ , with evolution of MR crossover superimposed on results from a previous study (see Ref. [136] for details of data in the  $H = 0$  plane).

transport. One could speculate, for instance, that the MR crossover is indicative of a very close magnetic transition which approaches  $T = 0$  slightly within the superconducting phase, but emerges at a finite doping. How the FL phase observed [136] at higher doping evolves with field is an excellent question, requiring further efforts to answer.

---

---

# B

---

---

## CeRhIn<sub>5</sub>: ADDITIONAL ANALYSIS

---

---

This Appendix presents additional data measured in CeRhIn<sub>5</sub> which is not shown in the main text.

### B.1 Low Temperature Magnetoresistance

The magnetoresistance of CeRhIn<sub>5</sub> has been reported previously for fields up to 18 T [164], but only down to temperatures of 1.4 K. Here we report a study of magnetoresistance down to 25 mK with fields applied perpendicular to the basal plane in a transverse configuration. As shown in Fig. B.1,  $\rho(T)$  does not change its qualitative shape in fields up to 16 T, where it appears that the overall  $T$ -dependence is not significantly different than the zero-field shape. However, upon close inspection it can be seen that the  $T$ -dependence of  $\rho$  does undergo a quantitative change in applied field. In contrast to the  $T^2$  dependence of  $\rho(T)$  (see Chapter 5) seen below  $\sim 2$  K in zero applied field,  $\rho(T)$  exhibits a complete saturation below  $\sim 1$  K in fields above  $\sim 5$  T. This saturation characteristic can also be seen in Fig. (B.2), which presents constant-temperature field sweep data: the  $\rho(H)$  curves at 50 mK and 1 K are essentially identical, with negligible differences.

Furthermore, the residual resistivity increases dramatically with field, as seen by the increasing offset of the  $T$ -sweep curves in Fig. B.1. This is highlighted in the constant-temperature field sweeps shown in Fig. B.2. Clearly the saturated resistivity at high fields is not indicative of the impurity-dominated residual resistivity observed in zero field, but it nevertheless remains temperature-independent up to  $\sim 1$  K. The relation between the high-field residual resistivity of CeRhIn<sub>5</sub> and the extrapolated residual resistivity of CeRhIn<sub>5</sub> under pressures which induce superconductivity [102, 183] may be an interesting and important correlation to investigate.

Finally, note that a *linear* MR is observed in CeRhIn<sub>5</sub>, as shown in Fig. (B.2). This is strikingly similar to the behaviour of CeCoIn<sub>5</sub> at the same temperature, as reported in

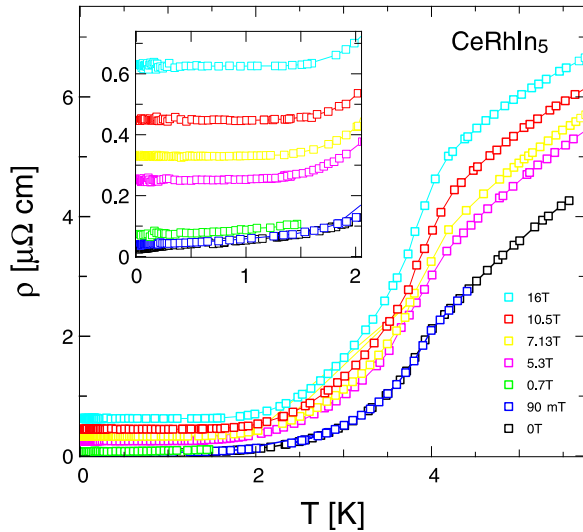


Figure B.1: Resistivity temperature sweeps of CeRhIn<sub>5</sub> taken in constant fields up to 16 T.

Section 6.1. The cause of this field dependence is not clear (as discussed in Section 6.1), but its identical behaviour in both CeRhIn<sub>5</sub> and CeCoIn<sub>5</sub> certainly suggests a similar origin in both systems.

## B.2 Ambient-Pressure Superconductivity

The occurrence of a superconducting transition in CeRhIn<sub>5</sub>, which was observed at  $T_c = 90$  mK in magnetization measurements on a single crystal sample [132], is of extreme importance since the presence of a superconducting ground state *throughout* the phase space of the 115 system (*i.e.* in the alloying series - see Fig. (3.3)) complicates the understanding of the interplay between magnetism and superconductivity. It is widely believed that superconductivity arises in the vicinity of a QCP due to spin fluctuation-mediated pairing, but it is certainly not clear how the robust superconducting state in CeCoIn<sub>5</sub> arises, and whether the superconducting and magnetic ground states in these systems are cooperative or competitive. Although the coexistence of magnetism and superconductivity is certainly supportive of the former, one could argue, for instance, that the similar magnitude of magnetic and superconducting transition temperatures is evidence for the latter.

As shown in Fig. B.3, thermal conductivity measurements reveal a rapid increase in  $\kappa/T$  occurring below  $\sim 200$  mK, which is readily removed with a small applied field of 90 mT. Although a zero-resistance state was not observed, a downward kink in  $\rho(T)$  is

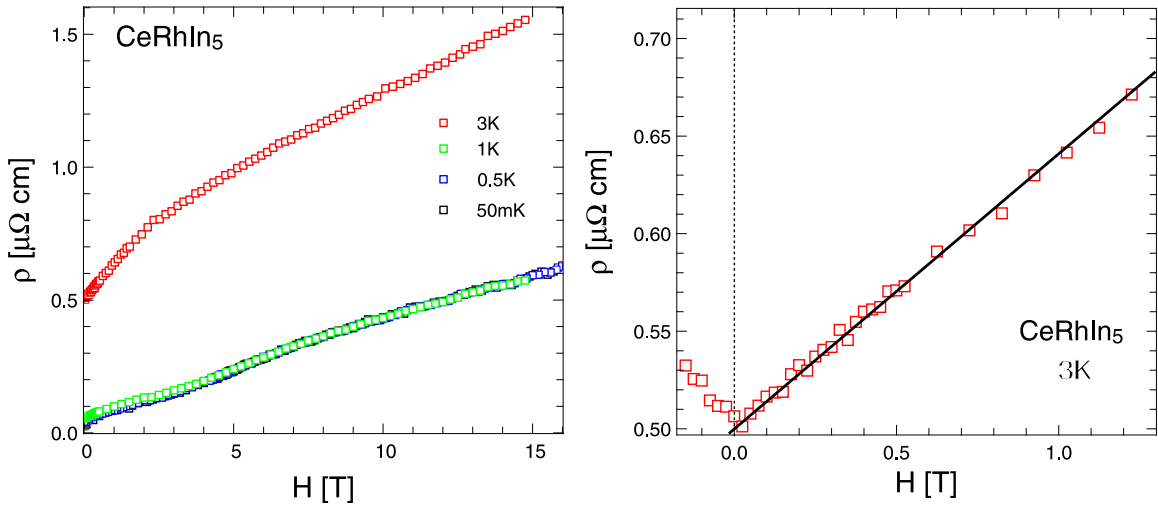


Figure B.2: Left: resistivity of CeRhIn<sub>5</sub> in fields up to 16 T, taken at constant temperatures of 0.05, 0.5, 1 and 3 K. Right: zoom of 3 K data, showing linearity of magnetoresistance at low fields.

indeed seen at the same temperature and is sensitive to the applied measurement current.<sup>1</sup> The sharp anomaly in  $\kappa/T$ , together with the signature in  $\rho(T)$  and the previously observed diamagnetic transition [132], is evidence for a bulk superconducting transition deep within the antiferromagnetic state, at  $T_c \simeq 200$  mK.

The study by Zapf *et al.* included measurements on a powdered sample, presumably from the same growth, which did not show any evidence of a transition at the same temperature as that observed in their single-crystal sample. This was suggested as evidence for either filamentary superconductivity or a strong dependence of  $T_c$  on defects. The higher  $T_c$  observed in this study, as compared to that reported by Zapf *et al.*, may coincide with the apparently higher purity level of the samples used here, supporting the conclusion that the superconductivity is highly sensitive to crystal defects and/or impurities, and that it is indeed a bulk phenomenon. This, together with the surrounding magnetic state, suggests that the superconductivity in CeRhIn<sub>5</sub> is unconventional in nature, possibly arising from a magnetically-mediated interaction. Furthermore, the apparent sensitivity to impurities or defects is in contrast to the relatively insensitive dependence of  $T_c$  on doping in CeCoIn<sub>5</sub> [192], suggesting that the relation between the superconducting states found in each system is at the very least not a simple one.

<sup>1</sup>Due to the high conductivity of these samples, it was difficult to obtain a reasonable signal-to-noise ratio using excitation currents below  $\sim 0.1$  mA and hence difficult to search for a true zero-resistance state. It should be possible to prepare a sample with a better geometry (*i.e.* higher resistance) in order to check for this.

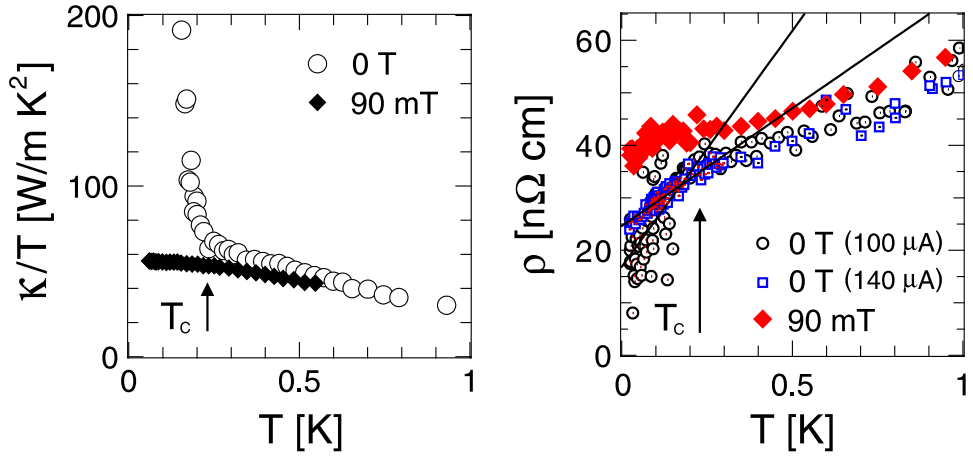


Figure B.3: Superconducting transition in CeRhIn<sub>5</sub> as observed in thermal conductivity (left) and resistivity (right) measurements.

What remains anomalous is the fact that  $\kappa/T$  *increases* below the transition: in contrast to the sudden increase observed just below  $T_N$  (and similarly in CeCoIn<sub>5</sub> just below  $T_c$ ), which can be explained by a sudden decrease in spin fluctuations [137, 156], the explanation of such an increase at temperatures  $T \ll T_N$  is difficult to explain in the same way. In any case, magnetic spin fluctuations play an important role in shaping the properties of CeRhIn<sub>5</sub>, and a careful characterization of their role in a possible ambient-pressure superconducting state is essential.

---

## THERMAL CONDUCTIVITY: CONSIDERATIONS

---

This Appendix includes some additional considerations in analyzing thermal conductivity measurements, including a discussion of the methods used to extract a phonon contribution and a summary of the effects of electron-phonon decoupling in low temperature measurements.

### C.1 Phonon Conductivity

In any conductive material,  $\kappa$  is the sum of an electronic ( $\kappa_e$ ) and a phononic ( $\kappa_{ph}$ ) contribution, but in highly conductive metals  $\kappa_e$  is generally much greater than  $\kappa_{ph}$  so the contribution from the latter can be neglected at very low temperatures. This is indeed the case for both CeRhIn<sub>5</sub> and CeCoIn<sub>5</sub>, which both display very low residual resistivities. However, a small but finite phonon contribution to  $\kappa$  does appear at temperatures above  $\sim 1$  K, so a method by which  $\kappa_{ph}$  can be subtracted from the measured thermal conductivity to obtain  $\kappa_e$  is required in order to make proper comparisons (*e.g.* to extract the electronic Lorenz ratio) at higher temperatures, as discussed in Chapter 5 for CeRhIn<sub>5</sub> and Chapter 6 for CeCoIn<sub>5</sub>.

The best means to estimate  $\kappa_{ph}$  is to measure a structurally-equivalent material which has no electronic conduction - *i.e.* an insulator. Since all members of the 115 series are highly conductive this is not possible, so the next best approach is to study a structurally-equivalent material which has a low, but well-understood electronic conductivity. This was done by measuring  $\kappa(T)$  in the isostructural and closely related material Ce<sub>1-x</sub>La<sub>x</sub>CoIn<sub>5</sub>, where the introduction of La impurities *increases* the elastic impurity scattering so that it dominates over the intrinsic inelastic scattering. In such a case,  $\kappa_e$  may be obtained from the Wiedemann-Franz law ( $\kappa_e(T) = L_0 T / \rho(T)$ ), so that the phonon contribution can be estimated as  $\kappa_{ph}(T) \simeq \kappa(T) - L_0 T / \rho(T)$ .

Fig. (C.1) shows the results of such a study on Ce<sub>0.98</sub>La<sub>0.02</sub>CoIn<sub>5</sub>, in which the introduction of 2% La increases the residual resistivity to  $\rho_0 = 2.6 \mu\Omega \text{ cm}$  (at 5 T), or

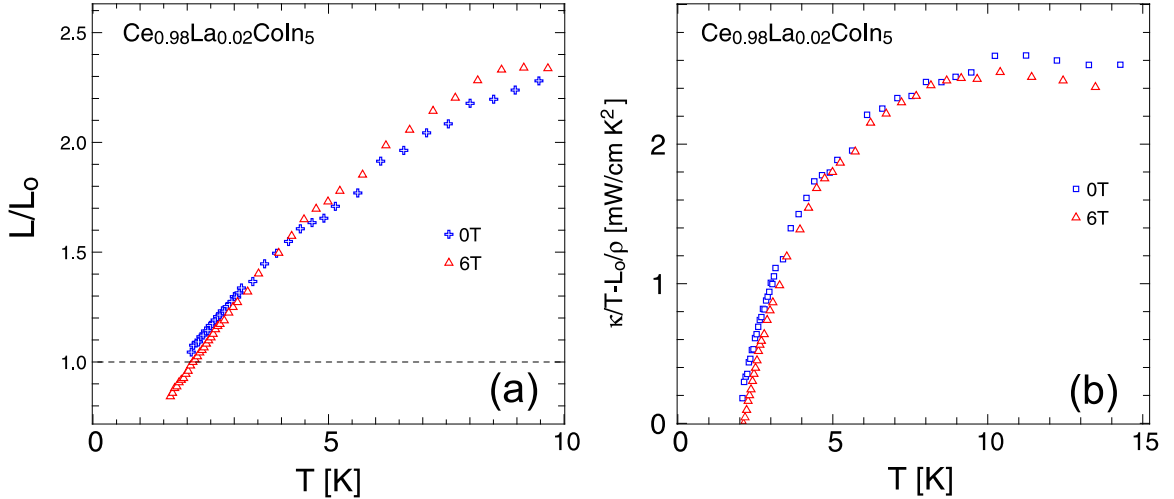


Figure C.1: (a) Lorenz ratio of  $\text{Ce}_{0.98}\text{La}_{0.02}\text{CoIn}_5$  in zero and applied field. (b) Estimate of phonon contribution to thermal conductivity.

approximately  $10\times$  larger than in pure  $\text{CeCoIn}_5$ . As shown, there is a large increase of the Lorenz ratio above the WF expectation at higher temperatures which can be attributed to additional thermal conductivity from  $\kappa_{ph}$ . A plot of  $\kappa/T - L_0/\rho$  vs.  $T$  (Fig. (C.1)(b)) shows the temperature dependence of  $\kappa_{ph}/T$ , which rises approximately linearly with  $T$  but encounters a maximum near 10 K: this is reminiscent of the behaviour expected of phonon conductivity in a solid.<sup>1</sup> Furthermore, the negligible change of  $L/L_0$  and  $\kappa/T - L_0/\rho$  with applied field strongly supports the notion that the additional conductivity is truly phononic, which should not depend directly on field.

Note, however, that at lower temperatures there is still a signature of strong inelastic scattering in  $\text{Ce}_{0.98}\text{La}_{0.02}\text{CoIn}_5$ , since the Lorenz ratio tends toward a value less than unity below  $\sim 2$  K. To ensure that the estimate  $\kappa_{ph}(T) \simeq \kappa(T) - L_0 T / \rho(T)$  is reasonable, and to confirm that  $\kappa_{ph}$  in  $\text{Ce}_{0.98}\text{La}_{0.02}\text{CoIn}_5$  is truly representative of that in the undoped 115 compounds, we have performed the same study on  $\text{Ce}_{0.90}\text{La}_{0.10}\text{CoIn}_5$ , where  $\rho_0 = 9.0 \mu\Omega \text{ cm}$  (at 5 T) is further increased. As shown in Fig. (C.2), the same behaviour is observed in  $\text{Ce}_{0.90}\text{La}_{0.10}\text{CoIn}_5$  but with a Lorenz ratio that steadily decreases toward the WF expectation as  $T \rightarrow 0$ . Also, the estimation of  $\kappa_{ph}/T$  shown in Fig. (C.2)(b)

<sup>1</sup>The thermal conductivity of phonons  $\kappa_{ph}$  can be influenced by a number of scattering mechanisms [63]. As discussed in Section 2.1.2, the scattering of phonons from conduction electrons is expected to result in  $\kappa_{ph} \sim T^2$  [63] if it is the dominant mechanism. But once  $\kappa_{ph}$  is of a substantial magnitude this is no longer the case, and mechanisms such as Umklapp scattering will influence the phonon conductivity at higher temperatures. For instance, non-conductive materials generally show a *maximum* in phonon conductivity between 10 and 20 K, where a crossover occurs between boundary scattering and Umklapp or impurity scattering [63].

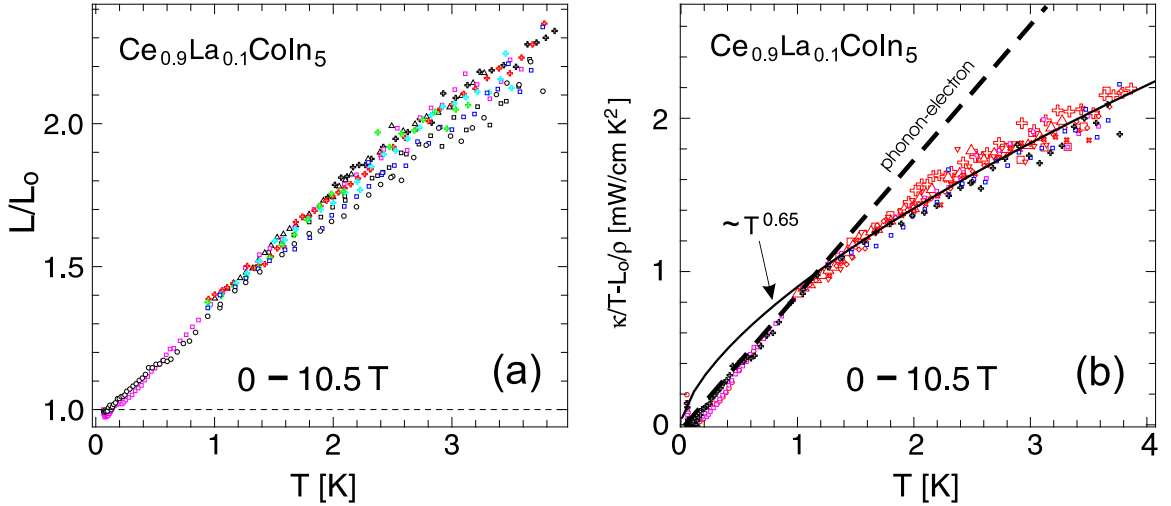


Figure C.2: (a) Lorenz ratio of  $Ce_{0.90}La_{0.10}CoIn_5$  in zero and applied fields up to 10.5 T. (b) Estimate of phonon contribution to thermal conductivity.

rises smoothly and linearly from zero up to  $\sim 1$  K, followed signs of saturation at higher temperatures. Hence,  $\kappa_{ph}$  has an approximate  $T^2$  dependence at low temperatures (shown by the dashed line in Fig. (C.2)(b)), as expected for phonon-electron scattering, and signs of a maximum at higher temperatures. The purely phononic nature of this contribution is again confirmed by the comparison of data through a large range of fields, showing negligible field dependence. Moreover, the magnitude of  $\kappa_{ph}$  (*i.e.* near  $\sim 4$  K) appears to be very similar in both  $Ce_{0.98}La_{0.02}CoIn_5$  and  $Ce_{0.90}La_{0.10}CoIn_5$ , suggesting that the use of this magnitude as an estimate of  $\kappa_{ph}$  in both  $CeRhIn_5$  and  $CeCoIn_5$  is a reasonable assumption.

In order to apply the phonon subtraction to both  $CeRhIn_5$  and  $CeCoIn_5$  data, a fit to the temperature dependence of  $\kappa_{ph}(T)$  thus obtained is shown as a solid line in Fig. (C.2)(b).<sup>2</sup> The resulting electronic conductivity of  $CeRhIn_5$ , defined as  $\kappa_e \equiv \kappa - \kappa_{ph}$ , deviates from the measured  $\kappa$  only slightly (by approximately 10% at  $T_N$ ), as shown in Chapter 5 (see Fig. (5.1)).

<sup>2</sup>Note that a slightly smaller power law was utilized to better fit the true  $T$  dependence of  $\kappa_{ph}$ , which is very similar in both La-doped compounds. Although the fit is not very good below  $\sim 1$  K, the magnitude of  $\kappa_{ph}$  becomes negligible as compared to  $\kappa_e$  at these temperatures in both  $CeCoIn_5$  and  $CeRhIn_5$ .

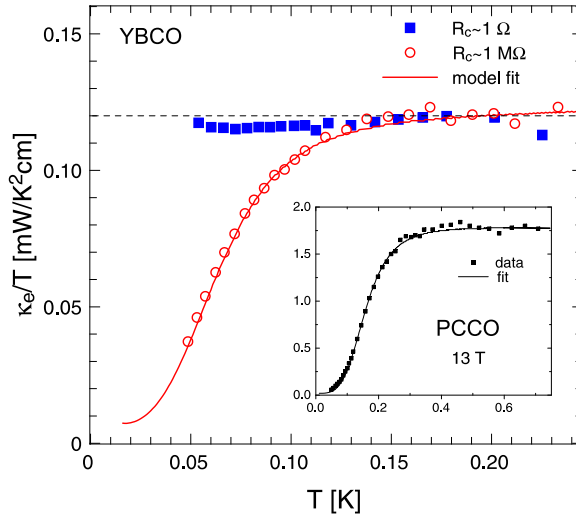


Figure C.3: Main panel: Electronic contribution to the thermal conductivity for a single sample of  $\text{YBa}_2\text{Cu}_3\text{O}_{6.95}$  in the superconducting state, measured using both standard, conductive contacts (open circles), and highly resistive contacts (solid squares). The dashed line is the expected [75] value of the electronic conductivity in the superconducting state. Inset: The electronic thermal conductivity of  $\text{Pr}_{2-x}\text{Ce}_x\text{CuO}_{7-\delta}$  in the field-induced normal state (from Ref. [96]). The solid line is a fit to the model discussed in the text.

## C.2 Contact Considerations

In this section we present data from an experiment designed to test the effects of varying the electrical contact resistance (between measurement wires and sample) on the measurement of low temperature thermal conductivity, as well as a numerical simulation used to model the temperature dependence of electron-phonon coupling.

### C.2.1 Test Experiment

A sample of optimally-doped  $\text{YBa}_2\text{Cu}_3\text{O}_{6.95}$  (YBCO) was chosen as the test specimen, since it's low temperature thermal conductivity is well-characterized [75] and the quasiparticle heat conductivity ( $\alpha T$ ) displays universal behavior [193]. Furthermore, the boundary scattering regime, where the phonon conductivity has a  $T^3$  dependence, can be readily achieved in such samples, making it easy to distinguish between the electronic ( $\alpha T$ ) and phononic ( $\beta T^3$ ) contributions in *e.g.* a plot of  $\kappa/T = \alpha + \beta T^2$ . Hence, there is no ambiguity in deciding on the intrinsic low temperature behaviour of  $\kappa$ , and any *extrinsic* effect from high contact resistance can be readily determined.

In Fig. (C.3) the electronic thermal conductivity  $\kappa_e/T \equiv \alpha$  of YBCO, obtained by subtracting the boundary-scattered phonon contribution  $\beta = 3.2 \text{ mW/K}^4\text{cm}$  (typical of this size specimen), is plotted versus  $T$  in order to enable the direct observation of

the behaviour of the quasiparticle conductivity  $\alpha T$  as a function of contact resistance. This plot shows two sets of data obtained from experiments using the same sample: 1) using standard, conductive contacts ( $< 1 \Omega$  resistance) between the sample and heat current leads (made with Ag Epoxy as described elsewhere [75]), and 2) using highly resistive contacts made with Ag paint, resulting in measured contact resistances of order  $\sim 1 M\Omega$ . For the first case, the data show an electronic term  $\alpha = 0.12 \text{ mW/K}^2\text{cm}$  which is independent of temperature throughout the boundary scattering regime and reproduces the value measured previously [75]. For the second case, the data show the same electronic term down to  $\sim 150 \text{ mK}$ . Below this temperature, a downturn in  $\kappa_e/T$  is evident, departing ever more drastically from the constant high- $T$  value as the temperature is decreased.

This behaviour is compared to measurements of  $\text{Pr}_{2-x}\text{Ce}_x\text{CuO}_{7-\delta}$  (PCCO) in the normal state (as obtained in a magnetic field of 13T applied perpendicular to the  $\text{CuO}_2$  planes), where the apparent  $T = 0$  WF law violation was associated with a dramatic decrease in  $\kappa_e/T$  toward a negligible value as  $T \rightarrow 0$  [96]. As shown in the inset of Fig. (C.3), the electronic<sup>3</sup> contribution  $\kappa_e/T$  to the thermal conductivity of PCCO is also independent of  $T$  above  $\sim 300 \text{ mK}$ , below which it exhibits a downturn strikingly similar to that observed in the YBCO experiment with highly resistive contacts. In this experiment, the lowest contact resistances were typically  $\sim 1\Omega$ .

### C.2.2 Coupled Resistor Model

A thermal resistor model was constructed to simulate the behaviour of two separate electronic and phononic heat current paths through a material, coupled by a thermal resistance  $R_{el-ph}$  containing all of the physics describing the electron-phonon interaction (a simplified version of the full model is shown in Fig. (C.4)). In this model, two resistors, labelled  $R_{ph}$  and  $R_{el}$ , are associated with the sample's resistance to phonon and quasiparticle heat currents, respectively. These are related to the values of  $\alpha$  and  $\beta$  and the measured dimensions of the sample according to

$$\begin{aligned} R_{ph}^{-1} &= \beta T^3 \frac{A}{L} \\ R_{el}^{-1} &= \alpha T \frac{A}{L} \end{aligned} \tag{C.1}$$

---

<sup>3</sup>The phonon subtraction for PCCO is discussed in Ref. [96].

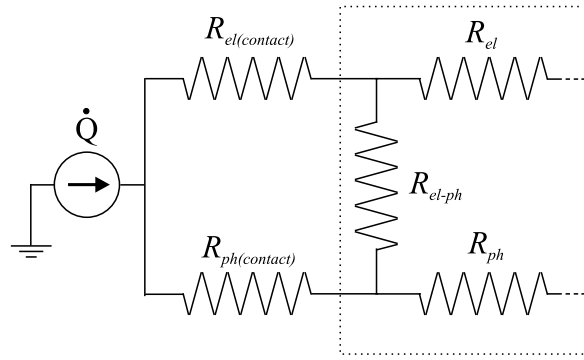


Figure C.4: The coupled thermal-resistors in the model used to analyze the low-T thermal conductivity data. The thermal resistance of the sample for phonons ( $R_{ph}$ ) and quasiparticles ( $R_{el}$ ), along with the corresponding resistance of the current contacts are shown. The dotted line represents the sample's boundary. The temperature-dependence of the quasiparticle-phonon thermal resistance of the sample,  $R_{el-ph}$ , gives rise to the observed downturn.

where  $A$  and  $L$  are the cross-sectional area of the sample and the distance between the voltage contacts, respectively. For each of the leads and contacts in the experimental configuration we associated two additional resistors (for the resistance to phonon heat current and to quasiparticle heat current). Of these, the resistors pertinent to this discussion are those of the current contacts that are labelled  $R_{el(c)}$  and  $R_{ph(c)}$ . Similar temperature dependences were assigned to each contact resistance - *i.e.*  $R_{el(c)}^{-1}$  and  $R_{ph(c)}^{-1}$  were taken to be proportional to  $T$  and  $T^3$ , respectively - and the coefficients of each were determined from measurement of both the electrical and thermal resistance across each contact. An additional resistor,  $R_{el-ph}$  that coupled the parallel channels of electron and phonon heat transport, was used to represent electron-phonon heat exchange. It was assumed to have a resistance given by  $R_{el-ph}^{-1} = \Sigma T^n$ , with the values of  $\Sigma$  and  $n$  taken as free parameters.

The thermal conductance of the coupled-resistor system was computed numerically using common circuit simulation software (PSPICE), fitting the temperature dependence of the observed downturns in YBCO and PCCO by using the coefficient  $\Sigma$  and exponent  $n$  as free parameters (and fixing all other parameters to measured values - *i.e.* sample/contact electrical and thermal resistances and geometries).

The result of the model fit to the YBCO data with highly resistive contacts is shown as the solid line in Fig. (C.3). The simulation of the low-temperature downturn matches the behaviour of the experimental data and is due entirely to the temperature dependence of  $R_{el-ph}$ , as obtained using a  $T^5$  dependence. When the simulation was performed using the same fit parameters for  $R_{el-ph}$ , but with resistance values of the highly con-

ductive contacts, the experimentally observed behavior ( $T$ -independent  $\kappa_e/T$ ) was again reproduced (not shown): lowering the contact resistance values decreases the magnitude of the downturn in the simulation until it is completely absent. This ability to tune the presence of the downturn by changing only contact resistance values, both numerically and experimentally, is strong evidence that this low temperature effect is entirely dictated by the coupling strength (*i.e.*  $\Sigma$ ) and temperature dependence (*i.e.*  $T^n$ ) of the electron-phonon interaction.

The normal state PCCO data was also fit by using measured parameter values and varying the magnitude and  $T$ -dependence of  $R_{el-ph}$ . As shown by the solid line in the inset of Fig. (C.3), the downturn in the PCCO data can also be fit, resulting in a  $T^5$  dependence of  $R_{el-ph}$  (exponents ranging from 4.5 to 5 give a good fit to the data). In PCCO, the best achievable contact resistances ( $> 1 \Omega$ ) are not significantly higher than those of the YBCO sample with conductive contacts (and, for that matter, typical values in many heat conductivity experiments), and yet the downturn is still significant. In this model, a number of other factors, including sample conductance and geometry can play a significant role in determining such behaviour. Furthermore, as will be discussed in the next section, the coupling strength (*e.g.*  $\Sigma$ ) can vary greatly between different materials: although the fit value of  $n$  for PCCO is approximately the same as that in YBCO, the coefficient  $\Sigma$  is an order of magnitude larger, suggesting that lower contact resistances would decrease the magnitude of the downturn effect in PCCO as it does for YBCO.

We found  $R_{el-ph}$  to be proportional to  $T^{-5}$ , which implies that the temperature variation of  $R_{el-ph}$  is more rapid than that of any of the other resistors. At high temperature  $R_{el-ph}$  is small, so the quasiparticles and phonons can efficiently exchange heat. The heat current,  $\dot{Q}$  is divided between the phonon and quasiparticles in the sample according to the relative size of  $R_{el}$  and  $R_{ph}$ . At low temperature,  $R_{el-ph}$  is very large, and the quasiparticle and phonon channels of heat transport become decoupled. The division of the heat current between the phonons and quasiparticles in the sample is then determined by the relative size of  $R_{el} + R_{el(c)}$  and  $R_{ph} + R_{ph(c)}$ . At intermediate temperatures the division of the heat current depends on  $R_{el-ph}$ , which gives an additional temperature dependence to the overall conductivity. Note that the power law ( $T^5$ ) extracted from this numerical work agrees extremely well with a recent calculation of the electron-phonon heat transfer rate [97], and the magnitude of the coupling parameter ( $\Sigma$ ) also agrees with calculation to within an order of magnitude.

The case applicable to the downturn in the data of Fig. (C.3) is for intermediate

temperatures and contact resistances such that  $R_{el(c)} \gg R_{ph(c)}$  (recall that we used measured values of these contact resistances). Since the heat current is provided mainly by phonons, as the temperature decreases and the phonons and quasiparticles become thermally decoupled, the current through  $R_{el}$  becomes very small. This results in a measured electronic contribution to the thermal conductivity that appears negligible at the lowest temperatures. Thus the observed downturn (especially in the case of PCCO) of the data for  $\kappa/T$  versus  $T$  appears to approach zero as  $T \rightarrow 0$ .

The value of  $R_{el-ph}$  has been measured for several metals in experiments done on thin films at milliKelvin temperatures. For pure copper films,  $R_{el-ph}$  has been found to vary as  $T^{-4}$ , in agreement with predictions for metals in which the mean free path of electrons is much longer than the wavelength of phonons (as was known to be the case in these experiments) [194], [195]. Similar measurements have been carried out on thin, disordered-metal films, in which the phonon wavelength was significantly shorter than the electron mean free path, and the predicted  $T^{-5}$  variation of  $R_{el-ph}$  has been observed [196]. We determined the magnitude of the electron-phonon heat transfer rate (*i.e.*  $\Sigma$ ) for a given volume, temperature and temperature-difference for the cuprate data shown above and found that it is the same, to within a factor of ten, as that reported for the disordered metal films (using a  $T^5$  dependence). The magnitude of the same quantity for the pure copper films at 50mK (a typical temperature within our experimental range) is larger by more than an order of magnitude than for the disordered metal films or cuprate samples.

### C.2.3 Contact Effects in CeCoIn<sub>5</sub>

Finally, a similar test was performed by varying the contact resistance on a sample of CeCoIn<sub>5</sub>. This was done by preparing contacts in various ways, resulting in contact resistances varying from  $R_c \simeq 5$  mΩ for soldered contacts, to  $R_c \simeq 0.5\text{-}1$  Ω for other methods as discussed in Section 4.1.2. In Fig. (C.5), we compare  $\kappa$  measurements in the normal state ( $H > H_{c2}$ ) on two samples: one with soldered contacts and one with contacts prepared by evaporating gold and attaching wires with silver paint, for which  $R_c \simeq 0.5\text{-}1$  Ω. Also plotted is the Wiedemann-Franz law expectation for the thermal conductivity as obtained from resistivity measurements on the same samples.

As can be seen, it is quite evident that for the soldered contacts we see a steadily increasing value of  $\kappa/T$  as  $T$  is decreased, but the WF law is also observed to hold at the lowest temperatures. On the other hand, the sample with more resistive contacts shows

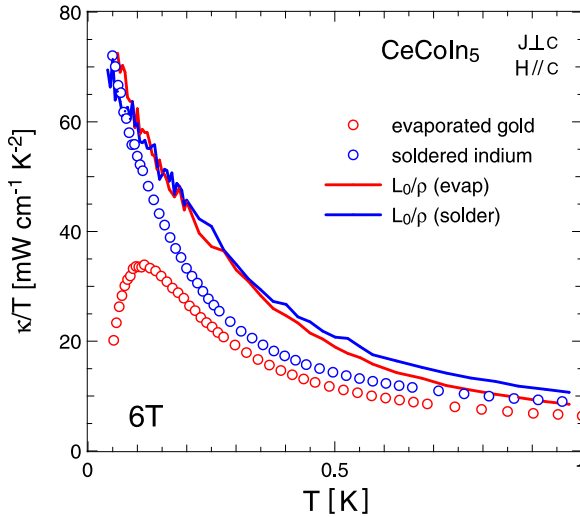


Figure C.5: Effect of contact resistance on  $\kappa$  measurements in CeCoIn<sub>5</sub>.

a sudden overturn near  $\sim 100$  mK, with a subsequently increasing *violation* of the WF law upon decreasing temperature further. Because this is the normal state, there is no doubt that the massive violation of the WF law can be attributed to electron-phonon decoupling in the same manner as described above for YBCO and PCCO. (In this case, the thermal conductivity is not of a conventional nature so no attempt at simulating this downturn effect was made using the model described above.)

---

---

## BIBLIOGRAPHY

---

---

- [1] G. Wiedemann and R. Franz. Ueber die wärme-leitungsfähigkeit der metalle. *Annals of Physics*, 89:497, 1853. 1, 21
- [2] J. Bardeen, L. N. Cooper, and J. R. Schrieffer. Theory of superconductivity. *Physical Review*, 108:1175–1204, 1957. 2
- [3] L.D. Landau. The theory of a Fermi liquid. *Soviet Physics. JETP*, 3:920, 1957. 2
- [4] D. Pines and P. Nozières. *Theory of Quantum Liquids*. Addison-Wesley, 1995. 2
- [5] A. A. Abrikosov. *Introduction to the Theory of Normal Metals*, volume 12 of *Solid State Physics*. Academic Press, New York, 1972. 2, 17, 18
- [6] R. B. Laughlin. *The Quantum Hall Effect*, chapter 7, pages 233–301. Graduate Texts in Contemporary Physics. Springer-Verlag, New York, second edition, 1990. 2
- [7] C.M. Varma, Z. Nussinov, and W. van Saarloos. Singular or non-Fermi liquids. *Physics Reports*, 361:267–417, 2002. 2, 4, 11, 85
- [8] J. G. Bednorz and K. A. Müller. Possible high  $T_c$  superconductivity in the Ba-La-Cu-O system. *Zeitschrift für Physik B*, 64(2):189–193, 1986. 2
- [9] Z. Fisk, D.W. Hess, C.J. Pethick, D. Pines, J.L. Smith, J.D. Thompson, and J.O. Willis. Heavy-electron metals: new highly correlated states of matter. *Science*, 239(4835), 1988. 3, 4, 5
- [10] G. R. Stewart. Heavy-fermion systems. *Reviews of Modern Physics*, 56(4):755–787, 1984. 3, 75

- [11] K. Andres, J. E. Graebner, and H. R. Ott. *4f*-virtual-bound-state formation in CeAl<sub>3</sub> at low temperatures. *Physical Review Letters*, 35(26):1779–1782, 1975. 4, 7, 19, 70
- [12] A. C. Hewson. *The Kondo problem to heavy fermions*. Cambridge University Press, New York, 1993. 4, 5, 18
- [13] P. Coleman. *Local moment physics in heavy electron systems*, volume 629 of *Lectures on the Physics of Highly Correlated Electron Systems VI*. American Institute of Physics, 2001. 4, 11, 103
- [14] S. Doniach. The Kondo lattice and weak antiferromagnetism. *Physica B*, 91:231, 1977. 4, 13
- [15] A. Schröder, G. Aeppli, R. Coldea, M. Adams, O. Stockert, H.v. Löhneysen, E. Bucher, R. Ramazashvili, and P. Coleman. Onset of antiferromagnetism in heavy-fermion metals. *Nature*, 407:351, 2000. 4, 10, 13, 119, 123
- [16] A. A. Abrikosov and L. P. Gorkov. Contribution to the theory of superconducting alloys with paramagnetic impurities. *Soviet Physics. JETP*, 12(6):1243–1253, 1961. 5
- [17] F. Steglich, J. Aarts, C. D. Bredl, W. Lieke, D. Meschede, W. Franz, and H. Schäfer. Superconductivity in the presence of strong pauli paramagnetism: CeCu<sub>2</sub>Si<sub>2</sub>. *Physical Review Letters*, 43(25):1892–1896, 1979. 5
- [18] R. Joynt and L. Taillefer. The superconducting phases of UPt<sub>3</sub>. *Reviews of Modern Physics*, 74(1):235–294, January 2002. 5
- [19] N. D. Mathur, F. M. Grosche, S. R. Julian, I. R. Walker, D. M. Freye, R. K. W. Haselwimmer, and G. G. Lonzarich. Magnetically mediated superconductivity in heavy fermion compounds. *Nature*, 394:39–43, 1998. 5, 6, 12, 29, 30, 83, 84, 100
- [20] G. R. Stewart. Non-fermi-liquid behavior in *d*- and *f*-electron metals. *Reviews of Modern Physics*, 73(4):797–855, 2001. 6, 7, 8, 10, 11, 12, 27, 38, 75, 77, 83, 118
- [21] C. L. Seaman, M. B. Maple, B. W. Lee, S. Ghamaty, M. S. Torikachvili, J. S. Kang, L. Z. Liu, J. W. Allen, and D. L. Cox. Evidence for non-Fermi liquid behavior in the Kondo alloy Y<sub>1-x</sub>U<sub>x</sub>Pd<sub>3</sub>. *Physical Review Letters*, 67(20):2882, 1991. 6

- [22] M. B. Maple, C. L. Seaman, D. A. Gajewski, Y. Dalichaouch, V. B. Barbutta, M. C. Deandrade, H. A. Mook, H. G. Lukefahr, O. O. Bernal, and D. E. MacLaughlin. Non Fermi-liquid behavior in strongly correlated *f*-electron materials. *Journal of Low Temperature Physics*, 95(1–2):225, 1994. 6
- [23] M. B. Maple, M. C. Deandrade, J. Herrmann, Y. Dalichaouch, D. A. Gajewski, C. L. Seaman, R. Chau, R. Movshovich, M. C. Aronson, and R. Osborn. Non Fermi-liquid ground-states in strongly correlated *f*-electron materials. *Journal of Low Temperature Physics*, 99(3–4):223, 1995. 6
- [24] M. C. Aronson, R. Osborn, R. A. Robinson, J. W. Lynn, R. Chau, C. L. Seaman, and M. B. Maple. Non-Fermi-liquid scaling of the magnetic response in  $\text{UCu}_{5-x}\text{Pd}_x$  ( $x = 1, 1.5$ ). *Physical Review Letters*, 75(4):725, 1995. 7
- [25] P. Noziéres and A. Blandin. Kondo effect in real metals. *Journal de Physique*, 41(3):193, 1980. 7
- [26] D. L. Cox and A. Zawadowski. Exotic Kondo effects in metals: magnetic ions in a crystalline electric field and tunnelling centres. *Advances in Physics*, 47(5):599, 1998. 7
- [27] O. O. Bernal, D. E. MacLaughlin, H. G. Lukefahr, and B. Andraka. Copper NMR and thermodynamics of  $\text{UCu}_{5-x}\text{Pd}_x$ : evidence for Kondo disorder. *Physical Review Letters*, 75(10):2023, 1995. 8
- [28] E. Miranda, V. Dobrosavljevic, and G. Kotliar. Kondo disorder: a possible route towards non-Fermi-liquid behaviour. *Journal of Physics: Condensed Matter*, 8:9871–9900, 1996. 8
- [29] L. D. Landau and E. M. Lifshitz. *Statistical Physics Part 1*, volume 5 of *Course of Theoretical Physics*. Pergamon Press Ltd., London, 1959. 9
- [30] J. A. Hertz. Quantum critical phenomena. *Physical Review B*, 14(3):1165, 1976. 9, 11, 27, 84, 130
- [31] S. Sachdev. *Quantum Phase Transitions*. Cambridge University Press, Cambridge, 1999. 9

- [32] T. Vojta. *Quantum Phase Transitions*. Computational Statistical Physics. Springer, Berlin, 2002. 9
- [33] N. Goldenfeld. *Lectures on Phase Transitions and the Renormalization Group*. Frontiers in Physics. Addison-Wesley, Reading, MA, 1992. 9
- [34] P. Coleman, C. Pépin, Q. Si, and R. Ramazashvili. How do Fermi liquids get heavy and die? *Journal of Physics: Condensed Matter*, 13:R723–R738, 2001. 9, 11, 14, 15, 23, 75, 123
- [35] S. Süllow, M.C. Aronson, B. D. Rainford, and P. Haen. Doniach phase diagram revisited: From ferromagnet to Fermi liquid in pressurized CeRu<sub>2</sub>Ge<sub>2</sub>. *Physical Review Letters*, 82(14):2963, 1999. 10
- [36] H. Kadowaki, M. Sato, and S. Kawarazaki. Spin fluctuation in heavy fermion CeRu<sub>2</sub>Si<sub>2</sub>. *Physical Review Letters*, 92(9):097204, 2004. 10, 12
- [37] H. Kadowaki, B. Fk, T. Fukuhara, K. Maezawa, K. Nakajima, M. A. Adams, S. Raymond, and J. Flouquet. Spin fluctuations and non-Fermi-liquid behavior of CeNi<sub>2</sub>Ge<sub>2</sub>. *Physical Review B*, 68(14):140402, 2003. 10, 12
- [38] J. Custers, P. Gegenwart, H. Wilhelm, K. Neumaier, Y. Tokiwa, O. Trovarelli, C. Geibel, F. Steglich, C. Pépin, and P. Coleman. The break-up of heavy electrons at a quantum critical point. *Nature*, 424:524, 2003. 10, 11, 13, 83, 87, 97, 98, 99, 116, 119, 123
- [39] H. von Löhneysen. Non-Fermi-liquid behaviour in the heavy-fermion system CeCu<sub>6-x</sub>Au<sub>x</sub>. *Journal of Physics: Condensed Matter*, 8(48):9689, 1996. 10, 97
- [40] H. v. Löhneysen, C. Pfleiderer, T. Pietrus, O. Stockert, and B. Will. Pressure versus magnetic-field tuning of a magnetic quantum phase transition. *Physical Review B*, 63(13):134411, 2001. 10
- [41] A. Amato, D. Jaccard, J. Flouquet, F. LaPierre, J. L. Tholence, R. A. Fisher, S. E. Lacy, J. A. Olsen, and N. E. Phillips. Thermodynamic and transport properties of CeCu<sub>6</sub>. *Journal of Low Temperature Physics*, 68(5–6):371, 1987. 10, 22, 97, 120

- [42] H. Sato, J. Zhao, W. P. Pratt, Y. Onuki, and T. Komatsubara. Transport properties of the heavy-fermion compound CeCu<sub>6</sub> down to 14 mK. *Physical Review B*, 36(16):8841, 1987. 10, 97
- [43] H. Wilhelm, S. Raymond, D. Jaccard, O. Stockert, H. von Löhneysen, and A. Rosch. Pressure-induced residual resistivity anomaly in CeCu<sub>5</sub>Au. *Journal of Physics: Condensed Matter*, 13(17):L329, 1987. 10, 103, 109
- [44] P. Gegenwart, J. Custers, C. Geibel, K. Neumaier, T. Tayama, K. Tenya, O. Trovarelli, and F. Steglich. Magnetic-field induced quantum critical point in YbRh<sub>2</sub>Si<sub>2</sub>. *Physical Review Letters*, 89(5):056402, 2002. 11, 78, 80, 81
- [45] A. M. Tsvelik and M. Reiser. Phenomenological theory of non-Fermi-liquid heavy-fermion alloys. *Physical Review B*, 48(13):9887, 1993. 11
- [46] P. Coleman. Theories of non-Fermi liquid behavior in heavy fermions. *Physica B*, 259–261:353, 1999. 11
- [47] P. Coleman and C. Pépin. Heavy electron quantum criticality. *Acta Physica Polonica B*, 34(2), 2003. 11, 14, 97
- [48] A. J. Millis. Effect of a nonzero temperature on quantum critical points in itinerant fermion systems. *Physical Review B*, 48(10):7183, 1993. 11, 27, 84
- [49] I. Paul and G. Kotliar. Thermoelectric behavior near the magnetic quantum critical point. *Physical Review B*, 64(18):184414, 2001. 11, 12, 27, 84, 109, 110
- [50] A. Rosch. Magnetotransport in nearly antiferromagnetic metals. *Physical Review B*, 62(8):4945, 2000. 11, 12, 27, 78, 83, 84, 109, 110, 130, 131
- [51] Q. Si, S. Rabello, K. Ingersent, and J. L. Smith. Locally critical quantum phase transitions in strongly correlated metals. *Nature*, 413:804, 2001. 12, 13, 14, 99, 103, 119
- [52] T. Moriya. *Spin Fluctuations in Itinerant Electron Magnetism*. Springer-Verlag, Berlin, 1985. 12, 27, 84
- [53] R. Hlubina and T. M. Rice. Resistivity as a function of temperature for models with hot spots on the Fermi surface. *Physical Review B*, 51(14):9253, 1995. 12, 27, 109, 110

- [54] A. Rosch. Interplay of disorder and spin fluctuations in the resistivity near a quantum critical point. *Physical Review Letters*, 82(21):4280, 1999. 12, 27, 84, 119
- [55] P. Gegenwart, J. Custers, T. Tayama, K. Tenya, C. Geibel, G. Sparn, N. Harrison, P. Kerschl, D. Eckert, K. H. Müller, and F. Steglich. Tuning heavy fermion systems into quantum criticality by magnetic field. *Journal of Low Temperature Physics*, 133:3, 2003. 12, 119, 122
- [56] S. Kambe, H. Suderow, T. Fukuhara, J. Flouquet, and T. Takimoto. Spin-fluctuation mediated thermal conductivity around the magnetic instability of CeNi<sub>2</sub>Ge<sub>2</sub>. *Journal of Low Temperature Physics*, 117(1–2):101, 1999. 12, 22, 28, 96, 119, 120, 121, 122
- [57] T. Senthil, M. Vojta, and S. Sachdev. Weak magnetism and non-Fermi liquids near heavy-fermion critical points. *Physical Review B*, 69(3):035111, 2004. 14, 23, 28, 91, 120
- [58] P. Coleman and C. Pépin. What is the fate of the heavy electron at a quantum critical point? *Physica B*, 312–313:383–389, 2002. 14
- [59] T. Senthil and M. P. A. Fisher. *Physical Review B*, 62:7850, 2000. 14, 23
- [60] C. Pépin and P. Coleman. Breakdown of the Fermi liquid theory in heavy fermion compounds. cond-mat/0211284, 2002. 14
- [61] C. Pépin. The fate of Kondo resonances in certain Kondo lattices: a “poor woman’s” scaling analysis. cond-mat/0402447, 2004. 14, 117
- [62] Neil W. Ashcroft and N. David Mermin. *Solid State Physics*. W. B. Saunders Company, 1976. 17, 18, 22, 23, 25, 40, 107
- [63] H. M. Rosenberg. *Low Temperature Solid State Physics*. Oxford University Press, London, 1963. 18, 20, 21, 23, 115, 141
- [64] J. M. Ziman. *Principles of the Theory of Solids*. Cambridge University Press, 1964. 18, 23, 90
- [65] A. H. Wilson. *The Theory of Metals*. Cambridge University Press, London, 2nd edition, 1965. 18, 23

- [66] A.J. Bennett and M.J. Rice. Exact solutions of Boltzmann's equation for combined electron-electron electron-impurity scattering. *Physical Review*, 185(3):968, 1969. 18, 26
- [67] D. K. Wagner, J. C. Garland, and R. Bowers. Low-temperature electrical and thermal resistivities of Tungsten. *Physical Review B*, 3(10):3141, 1971. 18, 22, 26
- [68] G. K. White and R. J. Tainsh. Electron scattering in nickel at low temperatures. *Physical Review Letters*, 19(4):165, 1967. 18, 22, 26
- [69] J. T. Schriempf, A. I. Schindler, and D. L. Mills. Effect of electron-electron scattering on the low-temperature Lorenz numbers of dilute Pd-Ni alloys. *Physical Review*, 187(3):959, 1969. 18, 19, 22, 24, 25, 26, 68, 71
- [70] M. J. Rice. Electron scattering in transition metals. *Physical Review Letters*, 20(25):1439, 1968. 18, 19
- [71] A. I. Schindler and M. J. Rice. s-electron-paramagnon scattering in dilute Pd-Ni alloys: Theory and experiment. *Physical Review*, 164(2):759, 1967. 19
- [72] A. B. Kaiser. Localized spin fluctuations in nearly-magnetic dilute alloys: thermal resistivity and Lorenz number. *Physical Review B*, 3(9):3040, 1971. 19, 25, 68, 69, 71, 94, 95
- [73] K. Kadowaki and S. B. Woods. Universal relationship of the resistivity and specific-heat in heavy-fermion compounds. *Solid State Communications*, 58(8):507, 1986. 19, 71, 97
- [74] C. Hess, B. Buchner, U. Ammerahl, L. Colonescu, F. Heidrich-Meisner, W. Brenig, and A. Revcolevschi. Magnon heat transport in doped  $\text{La}_2\text{CuO}_4$ . *Physical Review Letters*, 90(19):197002, 2003. 19
- [75] M. Sutherland, D. G. Hawthorn, R. W. Hill, F. Ronning, S. Wakimoto, H. Zhang, C. Proust, E. Boaknin, C. Lupien, L. Taillefer, R. Liang, D. A. Bonn, W. N. Hardy, R. Gagnon, N. E. Hussey, T. Kimura, M. Nohara, and H. Takagi. Thermal conductivity across the phase diagram of cuprates: Low-energy quasiparticles and doping dependence of the superconducting gap. *Physical Review B*, 67(17):174520, 2003. 20, 42, 67, 143, 144

- [76] Etienne Boaknin. *Thermal conduction in the vortex state of unconventional superconductors*. PhD thesis, University of Toronto, Toronto, Canada, 2003. 21, 43, 48, 54, 59, 60, 61, 63, 64
- [77] G. V. Chester and A. Thellung. Law of Wiedemann and Franz. *Proceedings of the Physical Society of London*, 77:1005, 1961. 22
- [78] L. Smrcka and P. Streda. Transport coefficients in strong magnetic fields. *Journal of Physics C*, 10:2153, 1977. 22
- [79] M. J. Kearney and P. N. Butcher. Thermal transport in disordered systems. *Journal of Physics C*, 21:L265, 1988. 22
- [80] C. Castellani, C. DiCastro, G. Kotliar, and P. A. Lee. Thermal conductivity in disordered interacting-electron systems. *Physical Review Letters*, 59:477, 1987. 22
- [81] G. K. White and R. J. Tainsh. Lorenz number for high-purity copper. *Physical Review*, 119(6):1869, 1960. 22
- [82] E. R. Rumbo. Transport properties of very pure copper and silver below 8.5 K. *Journal of Physics F: Metal Physics*, 6:85, 1976. 22
- [83] W. D. Jung, F. A. Schmidt, and G. C. Danielson. Thermal conductivity of high-purity vanadium. *Physical Review B*, 15(2):659, 1977. 22, 24
- [84] A. C. Anderson, R. E. Peterson, and J. E. Robichaux. Thermal and electrical conductivity of Ag and Pt below 1 K. *Physical Review Letters*, 20(9):459, 1968. 22
- [85] D. Jha, M. H. Jericho, and P. L. Taylor. Lorenz number of dilute Ag alloys. *Physical Review B*, 1(4):1870, 1970. 22
- [86] E. Boaknin, R. W. Hill, C. Proust, L. Taillefer, and P. C. Canfield. Highly anisotropic gap function in borocarbide superconductor LuNi<sub>2</sub>B<sub>2</sub>C. *Physical Review Letters*, 87:237001, 2001. 22, 64
- [87] H. R. Ott, O. Marti, and F. Hulliger. Low temperature thermal conductivity of CeAl<sub>3</sub>. *Solid State Communications*, 49:1129, 1984. 22, 120

- [88] H. Suderow, J. P. Brison, A. Huxley, and J. Flouquet. Thermal conductivity and gap structure of the superconducting phases of UPt<sub>3</sub>. *Journal of Low Temperature Physics*, 108:11, 1997. 22, 120
- [89] A. Bernasconi, M. Mombelli, Z. Fisk, and H. R. Ott. Low-temperature transport properties of UCu<sub>5</sub>. *Zeitschrift für Physik B*, 94(4):423, 1994. 22
- [90] M. A. Tanatar, S. Nagai, Z. Q. Mao, Y. Maeno, and T. Ishiguro. Thermal conductivity of superconducting Sr<sub>2</sub>RuO<sub>4</sub> in oriented magnetic fields. *Physical Review B*, 63:064505, 2001. 22
- [91] E. Boaknin, M. A. Tanatar, J. Paglione, D. Hawthorn, F. Ronning, R. W. Hill, M. Sutherland, L. Taillefer, J. Sonier, S. M. Hayden, and J. W. Brill. Heat conduction in the vortex state of NbSe<sub>2</sub>: Evidence for multiband superconductivity. *Physical Review Letters*, 90:117003, 2003. 22, 64
- [92] S. Y. Li, L. Taillefer, D. G. Hawthorn, M. A. Tanatar, J. Paglione, M. Sutherland, R. W. Hill, C. H. Wang, and X. H. Chen. Giant electron-electron scattering in the fermi-liquid state of na<sub>0.7</sub>co<sub>2</sub>. *Physical Review Letters*, 93(5):056401, 2004. 22, 64
- [93] C. Proust, E. Boaknin, R. W. Hill, L. Taillefer, and A. P. Mackenzie. Heat transport in a strongly overdoped cuprate: Fermi liquid and a pure d-wave BCS superconductor. *Physical Review Letters*, 89(14):147003, 2002. 22, 64
- [94] S. Nakamae, K. Behnia, N. Mangkorntong, M. Nohara, H. Takagi, S. J. C. Yates, and N. E. Hussey. Electronic ground state of heavily overdoped nonsuperconducting La<sub>2-x</sub>Sr<sub>x</sub>CuO<sub>4</sub>. *Physical Review B*, 68(10):100502, 2003. 22, 23
- [95] R. Bel, K. Behnia, C. Proust, P. van der Linden, D. Maude, and S. I. Vedeneev. Test of the Wiedemann-Franz law in an optimally doped cuprate. *Physical Review Letters*, 92(17):177003, 2004. 22
- [96] R. W. Hill, C. Proust, L. Taillefer, P. Fournier, and R. L. Greene. Breakdown of Fermi-liquid theory in a copper-oxide superconductor. *Nature*, 414:711, 2001. 22, 42, 120, 143, 144
- [97] M. F. Smith, M.B. Walker, J. Paglione, and L. Taillefer. The origin of low temperature downturns in the thermal conductivity of the cuprates. unpublished, 2004. 23, 42, 120, 146

- [98] C. Herring. Simple property of electron-electron collisions in transition metals. *Physical Review Letters*, 19(4):167, 1967. 26
- [99] Benoit Lussier. *Heat Conduction in Unconventional Superconductors*. PhD thesis, McGill University, Montréal, Canada, 1996. 26
- [100] Q. Si, S. Rabello, K. Ingersent, and J. L. Smith. Local fluctuations in quantum critical metals. *Physical Review B*, 68(11):115103, 2003. 27, 103
- [101] I. R. Walker, F. M. Grosche, D. M. Freye, and G. G. Lonzarich. The normal and superconducting states of CeIn<sub>3</sub> near the border of antiferromagnetic order. *Physica C*, 282–287:303–306, 1997. 29
- [102] H. Hegger, C. Petrovic, E. G. Moshopoulou, M. F. Hundley, J. L. Sarrao, Z. Fisk, and J. D. Thompson. Pressure-induced superconductivity in quasi-2D CeRhIn<sub>5</sub>. *Physical Review Letters*, 84:4986, 2000. 29, 38, 41, 65, 67, 68, 83, 85, 103, 136
- [103] C. Petrovic, R. Movshovich, M. Jaime, P. G. Pagliuso, M. F. Hundley, J. L. Sarrao, Z. Fisk, and J. D. Thompson. A new heavy-fermion superconductor CeIrIn<sub>5</sub>: A relative of the cuprates? *Europhysics Letters*, 53(3):354–359, 2001. 29, 36, 38, 76, 103, 105
- [104] C. Petrovic, P. G. Pagliuso, M. F. Hundley, R. Movshovich, J. L. Sarrao, J. D. Thompson, Z. Fisk, and P. Monthoux. Heavy-fermion superconductivity in CeCoIn<sub>5</sub> at 2.3 K. *Journal of Physics: Condensed Matter*, 13(17):L337–L342, 2001. 30, 43, 65, 74, 75
- [105] J. L. Sarrao, L. A. Morales, J. D. Thompson, B. L. Scott, G. R. Stewart, F. Wastin, J. Rebizant, P. Boulet, E. Colineau, and G. H. Lander. Plutonium-based superconductivity with a transition temperature above 18 K. *Nature*, 420:297–299, 2002. 30
- [106] P. G. Pagliuso, R. Movshovich, A.D. Bianchi, M. Nicklas, N. O. Moreno, J. D. Thompson, M. F. Hundley, J. L. Sarrao, and Z. Fisk. Multiple phase transitions in Ce(Rh,Ir,Co)In<sub>5</sub>. *Physica B*, 312–313:129–131, 2002. 30, 32
- [107] E.G. Moshopoulou, J.L. Sarrao, P.G. Pagliuso, N.O.Moreno, J.D. Thompson, Z. Fisk, and R.M. Ibberson. Comparison of the crystal structure of the heavy-

- fermion materials CeCoIn<sub>5</sub>, CeRhIn<sub>5</sub> and CeIrIn<sub>5</sub>. *Applied Physics A*, 74:S895–S897, 2002. 30
- [108] P. G. Pagliuso, N. J. Curro, N. O. Moreno, M. F. Hundley, J. D. Thompson, J. L. Sarrao, and Z. Fisk. Structurally tuned superconductivity in heavy-fermion CeMIn<sub>5</sub> (M=Co, Ir, Rh). *Physica B*, 320:370–375, 2002. 31
- [109] R. S. Kumar, H. Kohlmann, B. E. Light, A. L. Cornelius, V. Raghavan, T. W. Darling, and J. L. Sarrao. Anisotropic elastic properties of CeRhIn<sub>5</sub>. *Physical Review B*, 69:014515, 2004. 31
- [110] H. Shishido, R. Settai, D. Aoki, S. Ikeda, H. Nakawaki, N. Nakamura, T. Iizuka, Y. Inada, K. Sugiyama, T. Takeuchi, K. Kindo, T.C. Kobayashi, Y. Haga, H. Harima, Y. Aoki, T. Namiki, H. Sato, and Y. Ōnuki. Fermi surface, magnetic and superconducting properties of LaRhIn<sub>5</sub> and CeTIn<sub>5</sub> (T = Ir and Co). *Journal of the Physical Society of Japan*, 71(1):162–173, 2002. 33, 34, 35, 36, 38, 40, 66, 74, 103, 123
- [111] R. Settai, H. Shishido, S. Ikeda, Y. Murakawa, M. Nakashima, D. Aoki, Y. Haga, H. Harima, and Y. Ōnuki. Quasi-two-dimensional Fermi surfaces and the de Haas-van Alphen oscillation in both the normal and superconducting mixed states of CeCoIn<sub>5</sub>. *Journal of Physics: Condensed Matter*, 13(27):L627–L634, 2001. 33, 34, 108, 118, 123
- [112] T. Maehira, T. Hotta, K. Ueda, and A. Hasegawa. Relativistic band-structure calculations for CeTIn<sub>5</sub> (T = Ir and Co) and analysis of the energy bands by using tight-binding method. *Journal of the Physical Society of Japan*, 72(4):854–864, 2003. 33, 103, 105, 108
- [113] Y. Haga, Y. Inada, H. Harima, K. Oikawa, M. Murakawa, H. Nakawaki, Y. Tokiwa, D. Aoki, H. Shishido, S. Ikeda, N. Watanabe, and Y. Ōnuki. Quasi-two-dimensional Fermi surfaces of the heavy fermion superconductor CeIrIn<sub>5</sub>. *Physical Review B*, 63:060503(R), 2001. 33
- [114] T. J, B, M, C Janssen, S Haworth, M, P. Meeson Hayden, M. Springford, and A. Wasserman. Quantitative investigation of the de Haas-van Alphen effect in the superconducting state. *Physical Review B*, 57(18):11698, 1998. 34

- [115] A. McCollam, S. R. Julian, D. Aoki, and J. Flouquet. Anomalous de Haas-van Alphen oscillations in CeCoIn<sub>5</sub>. presented at APS March Meeting, session [H20.010], 2004. 34, 108, 118, 123
- [116] D. Hall, E. C. Palm, T. P. Murphy, S. W. Tozer, C. Petrovic, E. Miller-Ricci, L. Peabody, C. Q. H. Li, U. Alver, R. G. Goodrich, J. L. Sarrao, P. G. Pagliuso, J. M. Wills, and Z. Fisk. Electronic structure of CeRhIn<sub>5</sub>: de Haas-van Alphen and energy band calculations. *Physical Review B*, 64(6):064506, 2001. 34, 71, 108
- [117] T. Ito, P.A. Rayjada, N. Kamakura, Y. Takata, T. Yokoya, A. Chainani, S. Shin, M. Nohara, and H. Takagi. Soft x-ray energy-dependent angle-resolved photoemission study of CeIrIn<sub>5</sub>. *Journal of Physics: Condensed Matter*, 15(28):S2149–S2152, 2003. 34
- [118] S.I. Fujimori, T. Okane, J. Okamoto, K. Mamiya, Y. Muramatsu, A. Fujimori, T. Narimura, K. Kobayashi, K. Shimada, H. Namatame, M. Taniguchi, H. Harima, D. Aoki, S. Ikeda, H. Shishido, Y. Tokiwa, Y. Haga, and Y. Ōnuki. Photoemission study of CeMIn<sub>5</sub> (M=Rh,Ir): nearly localized nature of f electrons. *Physica B*, 329–333:547–548, 2003. 34
- [119] J. L. Wang, Z. Zeng, Q. Q. Zheng, and H. Q. Lin. Electronic structure of heavy fermion superconductor CeMIn<sub>5</sub> (M=Rh,Ir). *Journal of Applied Physics*, 93(10):6891–6893, 2002. 34
- [120] U. Alver, R. G. Goodrich, N. Harrison, D. W. Hall, E. C. Palm, T. P. Murphy, S. W. Tozer, P. G. Pagliuso, N. O. Moreno, J. L. Sarrao, and Z. Fisk. Localized f electrons in Ce<sub>x</sub>La<sub>1-x</sub>RhIn<sub>5</sub>: de Haas-van Alphen measurements. *Physical Review B*, 64:180402, October 2001. 34
- [121] H. Shishido, R. Settai, S. Araki, T. Ueda, Y. Inada, T.C. Kobayashi, T. Muramatsu, Y. Haga, and Y. Ōnuki. Evolution of pressure-induced heavy fermion state and superconductivity in CeRhIn<sub>5</sub>: A high-pressure Fermi surface study. *Physical Review B*, 66:214510, 2002. 35
- [122] T. Tayama, A. Harita, T. Sakakibara, Y. Haga, H. Shishido, R. Settai, and Y. Onuki. Unconventional heavy-fermion superconductor CeCoIn<sub>5</sub>: dc magnetization study at temperatures down to 50 mk. *Physical Review B*, 65(18):180504, 2002. 35, 36, 38, 81, 82, 123, 133

- [123] T. P. Murphy, Donavan Hall, E. C. Palm, S. W. Tozer, C. Petrovic, Z. Fisk, R. G. Goodrich, P. G. Pagliuso, J. L. Sarrao, and J. D. Thompson. Anomalous superconductivity and field-induced magnetism in CeCoIn<sub>5</sub>. *Physical Review B*, 65(10):100514, 2002. 35, 36, 81, 82, 133
- [124] A. Bianchi, R. Movshovich, N. Oeschler, P. Gegenwart, F. Steglich, J. D. Thompson, P. G. Pagliuso, and J. L. Sarrao. First-order superconducting phase transition in CeCoIn<sub>5</sub>. *Physical Review Letters*, 89(13):137002, 2002. 35, 81, 133
- [125] K. Izawa, H. Yamaguchi, Yuji Matsuda, H. Shishido, R. Settai, and Y. Onuki. Angular position of nodes in the superconducting gap of quasi-2D heavy-fermion superconductor CeCoIn<sub>5</sub>. *Physical Review Letters*, 87(5):057002, 2001. 36, 41, 42, 81, 133
- [126] A. Bianchi, R. Movshovich, C. Capan, P. G. Pagliuso, and J. L. Sarrao. Possible Fulde-Ferrell-Larkin-Ovchinnikov superconducting state in CeCoIn<sub>5</sub>. *Physical Review Letters*, 91(18):187004, 2003. 36
- [127] H. A. Radovan, N. A. Fortune, T. P. Murphy, S. T. Hannahs, E. C. Palm, S. W. Tozer, and D. Hall. Magnetic enhancement of superconductivity from electron spin domains. *Nature*, 425:51–55, 2003. 36, 81
- [128] R. Borth, E. Lengyel, P.G. Pagliuso, J.L. Sarrao, G. Sparn, F. Steglich, and J.D. Thompson. Heat capacity of the heavy fermion superconductor CeIrIn<sub>5</sub> under hydrostatic pressure. *Physica B*, 312–313:136, 2002. 36
- [129] S. Kos, I. Martin, and C. M. Varma. Specific heat at the transition in a superconductor with fluctuating magnetic moments. *Physical Review B*, 68(5):052507, 2003. 36
- [130] R. Movshovich, M. Jaime, J. D. Thompson, C. Petrovic, Z. Fisk, P. G. Pagliuso, and J. L. Sarrao. Unconventional superconductivity in CeIrIn<sub>5</sub> and CeCoIn<sub>5</sub>: Specific heat and thermal conductivity studies. *Physical Review Letters*, 86(22):5152–5155, 2001. 36, 41, 42, 67
- [131] P. G. Pagliuso, C. Petrovic, R. Movshovich, D. Hall, M. F. Hundley, J. L. Sarrao, J. D. Thompson, and Z. Fisk. Coexistence of magnetism and superconductivity in CeRh<sub>1-x</sub>Ir<sub>x</sub>In<sub>5</sub>. *Physical Review B*, 64:R100503, 2001. 37

- [132] V. S. Zapf, E. J. Freeman, E. D. Bauer, J. Petricka, C. Sirvent, N. A. Frederick, R. P. Dickey, and M. B. Maple. Coexistence of superconductivity and magnetism in  $\text{CeRh}_{1-x}\text{Co}_x\text{In}_5$ . *Physical Review B*, 65:014506, 2001. 37, 137, 138
- [133] R. A. Fisher, F. Bouquet, N. E. Phillips, M. F. Hundley, P. G. Pagliuso, J. L. Sarrao, Z. Fisk, and J. D. Thompson. Specific heat of  $\text{CeRhIn}_5$ : Pressure-driven evolution of the ground state from antiferromagnetism to superconductivity. *Physical Review B*, 65:224509, 2002. 37
- [134] T. Takeuchi, T. Inoue, K. Sugiyama, D. Aoki, Y. Tokiwa, Y. Haga, K. Kindo, and Y. Onuki. Magnetic and thermal properties of  $\text{CeIrIn}_5$  and  $\text{CeCoIn}_5$ . *Journal of the Physical Society of Japan*, 70(3):877, 2001. 38, 39
- [135] J. S. Kim, J. Alwood, G. R. Stewart, J. L. Sarrao, and J. D. Thompson. Specific heat in high magnetic fields and non-fermi-liquid behavior in  $\text{CeMIn}_5$  ( $M = \text{Ir}, \text{Co}$ ). *Physical Review B*, 64(13):134524, 2001. 38, 74
- [136] S. Nakatsuji, S. Yeo, L. Balicas, Z. Fisk, P. Schlottmann, P. G. Pagliuso, N. O. Moreno, J. L. Sarrao, and J. D. Thompson. Intersite coupling effects in a kondo lattice. *Physical Review Letters*, 89(10):106402, 2002. 38, 41, 74, 131, 133, 134, 135
- [137] N. J. Curro, B. Simovic, P. C. Hammel, P. G. Pagliuso, J. L. Sarrao, J. D. Thompson, and G. B. Martins. Anomalous NMR magnetic shifts in  $\text{CeCoIn}_5$ . *Physical Review B*, 64(18):180514, 2001. 39, 67, 72, 139
- [138] Y. Kawasaki, S. Kawasaki, M. Yashima, T. Mito, G. Zheng, Y. Kitaoka, H. Shishido, R. Settai, Y. Haga, and Y. Onuki. Anisotropic spin fluctuations in heavy-fermion superconductor  $\text{CeCoIn}_5$ : In-NQR and Co-NMR Studies. *Journal of the Physical Society of Japan*, 72(9):2308, 2003. 39, 78
- [139] N. J. Curro, P. C. Hammel, P. G. Pagliuso, J. L. Sarrao, J. D. Thompson, and Z. Fisk. Evidence for spiral magnetic order in the heavy fermion material  $\text{CeRhIn}_5$ . *Physical Review B*, 62(10):R6100, 2000. 39, 72
- [140] W. Bao, G. Aeppli, J. W. Lynn, P. G. Pagliuso, J. L. Sarrao, M. F. Hundley, J. D. Thompson, and Z. Fisk. Anisotropic three-dimensional magnetic fluctuations in heavy fermion  $\text{CeRhIn}_5$ . *Physical Review B*, 65:100505, February 2002. 39, 65, 67, 69, 72, 102, 118

- [141] A. Llobet, J. S. Gardner, E. G. Moshopoulou, J.-M. Mignot, M. Nicklas, W. Bao, N. O. Moreno, P. G. Pagliuso, I. N. Goncharenko, J. L. Sarrao, and J. D. Thompson. Magnetic structure of CeRhIn<sub>5</sub> as a function of pressure and temperature. *Physical Review B*, 69(2):024403, 2004. 39, 85
- [142] W. Bao, P. G. Pagliuso, J. L. Sarrao, J. D. Thompson, Z. Fisk, and J. W. Lynn. Magnetic structure of heavy-fermion Ce<sub>2</sub>RhIn<sub>8</sub>. *Physical Review B*, 64(2):020401, 2001. 39
- [143] A. L. Cornelius, P. G. Pagliuso, M. F. Hundley, and J. L. Sarrao. Field-induced magnetic transitions in the quasi-two-dimensional heavy-fermion antiferromagnets Ce<sub>n</sub>RhIn<sub>3n+2</sub> (n = 1 or 2). *Physical Review B*, 64(14):144411, 2001. 40, 70, 71, 72
- [144] S. Nakatsuji, D. Pines, and Z. Fisk. Two fluid description of the kondo lattice. *Physical Review Letters*, 92(1):016401, 2004. 41, 109, 110
- [145] H. Aoki, T. Sakakibara, H. Shishido, R. Settai, Y. Onuki, P. Miranović, and K. Machida. Field-angle dependence of the zero-energy density of states in the unconventional heavy-fermion superconductor CeCoIn<sub>5</sub>. *Journal of Physics: Condensed Matter*, 16:L13, 2004. 41
- [146] M.A. Tanatar, J. Paglione, D.G. Hawthorn, E. Boaknin, R.W. Hill, F. Ronning, M. Sutherland, L. Taillefer, C. Petrovic, and P.C. Canfield. Unpaired electrons in the superconducting state of heavy-fermion CeCoIn<sub>5</sub>. unpublished, 2004. 42, 108
- [147] Christian Lupien. *Ultrasound attenuation in the unconventional superconductor Sr<sub>2</sub>RuO<sub>4</sub>*. PhD thesis, University of Toronto, Toronto, Canada, 2002. 43, 48, 50, 51
- [148] Robert C. Richardson and Eric N. Smith, editors. *Experimental Techniques in Condensed Matter Physics at Low Temperatures*. Frontiers in Physics. Addison-Wesley, Redwood City, CA, 1988. 48
- [149] O. V. Lounasmaa. *Experimental Principles and Methods Below 1 K*. Academic Press, London, 1974. 48, 50, 52
- [150] F. Pobell. *Matter and Methods at Low Temperatures*. Springer-Verlag, Berlin, second edition, 1996. 48

- [151] G. K. White. *Experimental Techniques in Low-Temperature Physics*. Monographs on the Physics And Chemistry of Materials. Oxford University Press, Oxford, third edition, 1979. 48
- [152] E.T. Swartz. Efficient  $^4\text{He}$  cryostats for storage dewars. *Review of Scientific Instruments*, 57:2848, 1986. 48
- [153] W. A. Little. The transport of heat between dissimilar solids at low temperatures. *Canadian Journal of Physics*, 37(3):334–349, 1959. 56
- [154] D. G. Hawthorn, R. W. Hill, C. Proust, F. Ronning, M. Sutherland, E. Boaknin, C. Lupien, M. A. Tanatar, J. Paglione, S. Wakimoto, H. Zhang, L. Taillefer, T. Kimura, M. Nohara, H. Takagi, and N. E. Hussey. Field-induced thermal metal-to-insulator transition in underdoped  $\text{La}_{2-x}\text{Sr}_x\text{CuO}_{4+\delta}$ . *Physical Review Letters*, 90(19):197004, 2003. 63
- [155] Y. Kohori, Y. Yamato, Y. Iwamoto, T. Kohara, E. D. Bauer, M. B. Maple, and J. L. Sarrao. NMR and NQR studies of the heavy fermion superconductors  $\text{CeTIn}_5$  ( $T = \text{Co}$  and  $\text{Ir}$ ). *Physical Review B*, 64(13):134526, 2001. 67, 74
- [156] P. J. Hirschfeld and W. O. Putikka. Theory of thermal conductivity in  $\text{YBa}_2\text{Cu}_3\text{O}_{7-\delta}$ . *Physical Review Letters*, 77(18):3909, 1996. 67, 139
- [157] M. E. Fisher and J. S. Langer. Resistive anomalies at magnetic critical points. *Physical Review Letters*, 20(13):665, 1968. 67
- [158] K. N. Lee, R. Bachmann, W. W. Hansen, T. H. Geballe, and J. P. Maita. Magnetic ordering in prb6. *Physical Review B*, 2(11):4580, 1970. 67
- [159] W. Higemoto, A. Koda, R. Kadono, Y. Kawasaki, Y. Haga, D. Aoki, R. Settai, H. Shishido, and Y. Onuki.  $\mu\text{SR}$  studies on heavy fermion superconductors  $\text{CeIrIn}_5$  and  $\text{CeCoIn}_5$ . *Journal of the Physical Society of Japan*, 71(4):1023–1026, 2002. 74, 78
- [160] S. Ikeda, H. Shishido, M. Nakashima, R. Settai, D. Aoki, Y. Haga, H. Harima, Y. Aoki, T. Namiki, H. Sato, and Y. Onuki. Unconventional superconductivity in cecoin<sub>5</sub> studied by the specific heat and magnetization measurements. *Journal of the Physical Society of Japan*, 70(10):3187, 2001. 74

- [161] A. Bianchi, R. Movshovich, I. Vekhter, P. G. Pagliuso, and J. L. Sarrao. Avoided antiferromagnetic order and quantum critical point in CeCoIn<sub>5</sub>. *Physical Review Letters*, 91(25):257001, 2003. 74, 87, 88, 97, 98
- [162] S. Özcan, D. M. Broun, B. Morgan, R. Haselwimmer, J. L. Sarrao, S. Kamal, C. P. Bidinosti, P. J. Turner, M. Raudsepp, and J. R. Waldram. London penetration depth measurements of the heavy-fermion superconductor CeCoIn<sub>5</sub> near a magnetic quantum critical point. *Europhysics Letters*, 62(3):412–418, 2002. 74
- [163] V. A. Sidorov, M. Nicklas, P. G. Pagliuso, J. L. Sarrao, Y. Bang, A. V. Balatsky, and J. D. Thompson. Superconductivity and quantum criticality in CeCoIn<sub>5</sub>. *Physical Review Letters*, 89(15):157004, 2002. 76, 103
- [164] A. D. Christianson, A. H. Lacerda, M. F. Hundley, P. G. Pagliuso, and J. L. Sarrao. Magnetotransport of CeRhIn<sub>5</sub>. *Physical Review B*, 2002. 77, 78, 136
- [165] A. B. Pippard. *Magnetoresistance in Metals*, volume 2 of *Cambridge Studies in Low Temperature Physics*. Cambridge University Press, Cambridge, 1989. 77, 78, 104
- [166] H. Rohrer. Magnetoresistance of dilute alloys. *Physical Review*, 174(2):583, 1968. 78
- [167] U. Rauchschwalbe, F. Steglich, and H. Rietschel. Magneto-resistance of heavy-fermion compounds. *Physica B*, 148:33, 1987. 78
- [168] K. Ishida, K. Okamoto, Y. Kawasaki, Y. Kitaoka, O. Trovarelli, C. Geibel, and F. Steglich. YbRh<sub>2</sub>Si<sub>2</sub>: Spin fluctuations in the vicinity of a quantum critical point at low magnetic field. *Physical Review Letters*, 89(10):107202, 2002. 78
- [169] W. Bao, A. Llobet, G. Aeppli, J.L. Sarrao, P.G. Pagliuso, N.O. Moreno, and K. Prokes. Magnetic field induced ferromagnetism in heavy fermion superconductor CeCoIn<sub>5</sub>. presented at APS March Meeting, session [S32.013], 2003. 78, 96
- [170] A. A. Abrikosov. Quantum linear magnetoresistance. *Europhysics Letters*, 49(6):789, 2000. 78

- [171] F. Ohkawa. Magnetoresistance of Kondo lattices. *Physical Review Letters*, 64(19):2300, 1990. 78, 103
- [172] R. P. Dickey, M. C. de Andrade, J. Herrmann, M. B. Maple, F. G. Aliev, and R. Villar. Crossover from non-Fermi-liquid to Fermi-liquid behavior in the magnetoresistivity of  $U_{0.9}Th_{0.1}Be_{13}$ . *Physical Review B*, 56(17):11169, 1997. 79, 80
- [173] U. Rauchschwalbe, F. Steglich, and H. Rietschel. Itinerant metamagnetism of  $CeRu_2Si_2$ : bringing out the dead. Comparison with the new  $Sr_3Ru_2O_7$  case. *Physica B*, 319(1–4), 2002. 80
- [174] N. Doiron-Leyraud, I. R. Walker, L. Taillefer, M. J. Steiner, S. R. Julian, and G. G. Lonzarich. Fermi-liquid breakdown in the paramagnetic phase of a pure metal. *Nature*, 425:595, 2003. 83, 84
- [175] O. Trovarelli, C. Geibel, S. Mederle, C. Langhammer, F. M. Grosche, P. Gegenwart, M. Lang, G. Sparn, , and F. Steglich.  $YbRh_2Si_2$ : Pronounced non-Fermi-liquid effects above a low-lying magnetic phase transition. *Physical Review Letters*, 85(3):626, 2000. 83, 84
- [176] H. Q. Yuan, F. M. Grosche, M. Deppe, C. Geibel, G. Sparn, and F. Steglich. Observation of two distinct superconducting phases in  $CeCu_2Si_2$ . *Science*, 302:2104, 2003. 84
- [177] K. H. Kim, N. Harrison, M. Jaime, G. S. Boebinger, and J. A. Mydosh. Magnetic-field-induced quantum critical point and competing order parameters in  $URu_2Si_2$ . *Physical Review Letters*, 91(25):256401, 2003. 84
- [178] S. L. Bud'ko, E. Morosan, and P. C. Canfield. Magnetic field induced non-Fermi-liquid behavior in  $YbAgGe$  single crystals. *Physical Review B*, 69(1):014415, 2004. 84
- [179] M. Brühwiler, B. Batlogg, S. M. Kazakov, and J. Karpinski. Evidence for two electronic components in  $Na_xCoO_2$  ( $x = 0.7\text{-}0.75$ ). cond-mat/0309311, 2003. 84, 85
- [180] W. Metzner, D. Rohe, and S. Andergassen. Soft Fermi surfaces and breakdown of Fermi-liquid behavior. *Physical Review Letters*, 91(6):066402, 2003. 85

- [181] R. Bel, K. Behnia, Y. Nakajima, K. Izawa, Y. Matsuda, H. Shishido, R. Settai, and Y. Onuki. Giant nernst effect in CeCoIn<sub>5</sub>. *Physical Review Letters*, 92(21):217002, 2004. 96, 119
- [182] N. Tsujii, K. Yoshimura, and K. Kosuge. Deviation from the Kadowaki-Woods relation in Yb-based intermediate-valence systems. *Journal of Physics: Condensed Matter*, 15:1993, 2003. 97
- [183] T. Muramatsu, N. Tateiwa, T. C. Kobayashi, K. Shimizu, K. Amaya, D. Aoki, H. Shishido, Y. Haga, and Y. Onuki. Superconductivity of CeRhIn<sub>5</sub> under high pressure. *Journal of the Physical Society of Japan*, 70(11):3362, 2001. 103, 136
- [184] J. Flouquet, P. Haen, F. LaPierre, C. Fierz, A. Amato, and D. Jaccard. Residual resistivity in cerium heavy fermion compounds. *Journal of Magnetism and Magnetic Materials*, 76–77:285, 1988. 103
- [185] Y. B. Kim and A. J. Millis. Residual resistivity near a two-dimensional metamagnetic quantum critical point. *Physical Review B*, 67(8):085102, 2003. 103
- [186] J. Custers, P. Gegenwart, K. Neumaier, H. Wilhelm, N. Oeschler, K. Ishida, Y. Kitakoa, C. Geibel, and F. Steglich. Quantum criticality in YbRh<sub>2</sub>Si<sub>2</sub>. *Journal of Physics: Condensed Matter*, 15:S2047, 2003. 105
- [187] S. Kambe and J. Flouquet. Kondo impurity scattering and the magnetic quantum critical transition. *Solid State Communications*, 103(10):551, 1997. 109
- [188] Y. Nakajima, K. Izawa, Y. Matsuda, S. Uji, T. Terashima, H. Shishido, R. Settai, Y. Onuki, and H. Kontani. Normal-state Hall angle and magnetoresistance in quasi-2D heavy fermion CeCoIn<sub>5</sub> near a quantum critical point. *Journal of the Physical Society of Japan*, 73(1):5, 2004. 119
- [189] L. Taillefer, F. Piquemal, and J. Flouquet. The anisotropic magnetoresistance of UPt<sub>3</sub> at low temperatures. *Physica C*, 153(1):451, 1988. 129
- [190] L. Taillefer, J. Flouquet, and W. Joss. High field magnetoresistance of UPt<sub>3</sub>. *Journal of Magnetism and Magnetic Materials*, 76–77:218, 1988. 129

- [191] N. E. Hussey, M. Abdel-Jawad, A. Carrington, A. P. Mackenzie, and L. Balicas. A coherent three-dimensional fermi surface in a high-transition-temperature superconductor. *Nature*, 425(6960):814, 2003. 129
- [192] C. Petrovic, S. L. Bud'ko, V. G. Kogan, and P. C. Canfield. Effect of La substitution on the superconducting state of CeCoIn<sub>5</sub>. *Physical Review B*, 66:054534, 2002. 131, 138
- [193] L. Taillefer, B. Lussier, R. Gagnon, K. Behnia, and H. Aubin. Universal heat conduction in YBa<sub>2</sub>Cu<sub>3</sub>O<sub>6.9</sub>. *Physical Review Letters*, 79(3):483, 1997. 143
- [194] A. C. Anderson and R. E. Peterson. thermal resistance between electrons and phonons in copper. *Physics Letters A*, 38:519, 1972. 147
- [195] M. L. Roukes, M. R. Freeman, R. S. Germain, and R. C. Richardson. hot-electrons and energy-transport in metals at millikelvin temperatures. *Physical Review Letters*, 55:422, 1985. 147
- [196] M. E. Gershenson, D. Gong, T. Sato, B. S. Karasik, and A. V. Sergeev. Millisecond electron-phonon relaxation in ultrathin disordered metal films at millikelvin temperatures. *Applied Physics Letters*, 79:2040, 2001. 147